EXPANDING THE METALLOMICS TOOLBOX:

DEVELOPMENT OF CHEMICAL AND BIOLOGICAL METHODS

IN UNDERSTANDING COPPER BIOCHEMISTRY

A Dissertation
Presented to
The Academic Faculty

by

Pritha Bagchi

In Partial Fulfillment
of the Requirements for the Degree
Doctor of Philosophy in the
School of Chemistry and Biochemistry

Georgia Institute of Technology
August 2013

EXPANDING THE METALLOMICS TOOLBOX:

DEVELOPMENT OF CHEMICAL AND BIOLOGICAL METHODS

IN UNDERSTANDING COPPER BIOCHEMISTRY

Approved by:

Dr. Christoph J. Fahrni, Advisor
School of Chemistry & Biochemistry
Georgia Institute of Technology

Dr. Loren D. Williams
School of Chemistry & Biochemistry
Georgia Institute of Technology

Dr. Wendy L. Kelly
School of Chemistry & Biochemistry
Georgia Institute of Technology

Dr. Melissa L. Kemp
Department of Biomedical Engineering
Georgia Institute of Technology

Dr. Raquel Lieberman
School of Chemistry & Biochemistry
Georgia Institute of Technology

Date Approved: April 29, 2013

To my husband and my parents

ACKNOWLEDGEMENTS

This journey began with a bus ride in 1998 in Kolkata, India, when I looked through the window and saw the colossal gates of the Science College of the University of Calcutta. Since then I had pursued my dream to get a doctorate degree and finally reached the moment for which I lived for the last fifteen years. I could not have dared to dream without my parents, could not have made the journey without my husband, and could not have reached the goal without my advisor.

I would like to thank my advisor, Dr. Christoph Fahrni, for sparking my interest in copper biochemistry and mentoring me through my graduate studies. Dr. Fahrni has allowed me to develop this dissertation work as well as explore other areas outside of copper biology. I would also like to express my sincere gratitude towards him for believing in me through a very difficult time of my personal life. I would also like to thank my committee members: Dr. Wendy Kelly, Dr. Melissa Kemp, Dr. Raquel Lieberman, and Dr. Loren Williams for their guidance throughout these years.

I would like to thank fellow graduate student Dr. M. Thomas Morgan, whose work has had a significant impact on my dissertation. Not only did he synthesize all the compounds that I have used in my work, but I strongly feel that my learning in graduate school would not have been complete without the numerous hours we spent together discussing our research. I would also like to thank Dr. Reagan McRae and Dr. Karl Huettinger, who helped me through my initial months in the Fahrni laboratory. I got invaluable support from Dr. Susan Orwig and Dr. Derrick Watkins who shared their

experiences in protein expression and purification with me and always extended their helping hands.

I cannot thank Dr. Hally Shaffer enough for her assistance; there was one time when without her help in transportation, I literally could not have done any research. I will always cherish my friendship with Dr. S. Sumalekshmy (Suma), Dr. Anna Duraj-Thatte, and Daisy Bourassa with whom I made a special bond during these years.

I could not have achieved my goal without the love and support of my husband, Dr. Aniruddha Bagchi, who shared my dream as one of his own. He always walked by my side even in the darkest days of my life. I am very fortunate to get the love and blessings of my in-laws, Mr. Dipak Bagchi and Ms. Mamata Bagchi, who truly consider me as their daughter, not merely their daughter-in-law. The phrase "Thank You" cannot capture my feelings towards my parents, Mr. Chandan Maitra and Ms. Sangita Maitra, who sacrificed everything to give me the best possible education and always inspired me to aim high. I would like to take this opportunity to thank my cousins Arpita and Shuvasree and my lifelong friends Ayesha and Dipyaman for their unwavering support and unconditional friendship.

TABLE OF CONTENTS

LIST OF TABLES

LIST OF FIGURES

LIST OF SCHEMES

LIST OF ABBREVIATIONS

AAS	Atomic absorption spectrometry
AE	Anion exchange
ALS	Amyotrophic lateral sclerosis
APP	Amyloid precursor protein
Atox1	Antioxidant 1
ATP	Adenosine triphosphate
BCA	Bicinchoninic acid
BCS	Bathocuproinedisulfonic acid
BIAM	Biotin-conjugated iodoacetamide
BME	B-mercaptoethanol
BN-PAGE	Blue-native polyacrylamide gel electrophoresis
CCO	Cytochrome c oxidase
CCS	Copper chaperone for superoxide dismutase
CE	Capillary electrophoresis
COMMD1	Copper metabolism gene MURR1 domain
Cox	Cytochrome c oxidase
CTR	Copper transporter
CV	Cyclic voltammetry
DBH	Dopamine β-hydroxylase
DETC	Diethyldithiocarbamic acid
DLS	Dynamic light scattering
DTT	Dithiothreitol
EPXMA	Electron probe X-ray microanalysis
ESI-MS	Electrospray ionization mass spectrometry

ESPT	Excited-state proton transfer
GSH	Glutathione
HPLC	High-performance liquid chromatography
HSAB	Hard and soft acids and bases
IAM	Iodoacetamide
ICAT	Isotope coded affinity tag
ICP-MS	Inductively coupled plasma mass spectrometry
IE	Ion-exchange
IMAC	Immobilized-metal affinity chromatography
IMS	Inter-membrane space
ITC	Isothermal titration calorimetry
LA-ICPMS	Laser ablation inductively coupled plasma mass spectrometry
MALDI-MS	Matrix-assisted laser-desorption ionization-mass spectrometry
MRE	Metal responsive elements
MT	Metallothionein
MTF	Metal transcription factor
NEM	N-ethyl maleimide
PAGE	Polyacrylamide gel electrophoresis
PAM	Peptidylglycine-α-amidating mono-oxygenase
PAR	4-pyridylazaresorcinol
PDB	Protein data bank
PET	Photoinduced electron transfer
PIXE	Proton or particle induced X-ray emission
RP-HPLC	Reversed-phase high-performance liquid chromatography
Sco	Synthesis of cytochrome c oxidase
SEC	Size exclusion chromatography

SELDI	Surface enhanced laser desorption ionization
SIMS	Secondary ion mass spectrometry
SOD	Superoxide dismutase
SXRF	Synchrotron X-ray fluorescence
TBP	Tributylphosphine
TCEP	Tris(2-carboxyethyl) phosphine
XANES	X-ray absorption near-edge structure
XRF	X-ray fluorescence

SUMMARY

Copper is an essential trace element that is important for a broad range of biological processes. Increasing evidence links impaired copper homeostasis to a variety of diseases, including Menkes disease, Wilson's disease, Parkinson's disease, Alzheimer's disease, amyotrophic lateral sclerosis (ALS), and more recently to cancer, diabetes, cardiovascular disease, and atherosclerosis. Despite the significant progress has been made in characterizing the copper trafficking pathways, the overall understanding of copper metabolism is still incomplete particularly in relation to the subcellular distribution and storage of the kinetically labile copper pool. Copper is predominantly present in its monovalent oxidation state in the reducing intracellular environment and consequently Cu(I)-selective fluorescent probes are useful for the detection of exchangeable copper(I) ions in biological systems. One of the objectives of this dissertation is, therefore, characterization of the coordination properties of Cu(I) sensors in order to apply them for cellular imaging and other biochemical applications. Furthermore, inconsistent data on the Cu(I)-stability constants of proteins in the literature limit our knowledge regarding the thermodynamics of copper binding to proteins *in vivo*. Cu(I)-binding affinities of proteins are often determined by the competition titrations using Cu(I) affinity standards, however, the binding affinity values of these standards are discordant owing to the redox instability of the aquated Cu^{+} ions and the formation of ternary complexes between Cu(I)-ligands and proteins. Therefore, the second objective of this work is to determine the binding affinities of a set of copper(I) chelators unequivocally as these well-characterized Cu(I) ligands will be instrumental as affinity standards to study copper biochemistry of proteins. The final objective of this dissertation is to develop detection methods to selectively identify copper proteins from cellular extract which will be useful in identifying putative copper binding proteins.

Chapter 1 summarizes the current knowledge regarding mammalian copper homeostasis and coordination chemistry of endogenous copper proteins. This chapter also discusses the pathways in copper metabolism that are yet to be deciphered.

Chapter 2 begins with a detailed discussion about various thermodynamic aspects of copper(I)-ligand binding which is a prerequisite to understand different methods that can be employed to measure Cu(I) binding affinity of a ligand. In this chapter, we characterized a set of affinity standards including three new sulfonated thioether-based ligands that form colorless, water-soluble, and air-stable copper(I) complexes and three previously reported Cu(I) chelators. Together these compounds constitute a web of accurately cross-verified Cu(I) affinities which will be useful in determining binding affinities of copper proteins unequivocally as exemplified with a bacterial copper chaperone CusF.

Chapter 3 first gives an introduction about the analytical techniques available for in situ detection of copper in biological samples including total and kinetically labile cellular copper and protein-bound copper ions. The introductory section also presents the photophysical concepts behind the fluorescence turn-on probes based on photoinduced electron transfer (PET). Coordination properties of a water soluble, high contrast Cu(I)-selective fluorescent probe CTAP-2 were determined in this chapter. The anticipated formation of nanoparticles of several previously published poorly water soluble Cu(I)-selective fluorescence turn-on probes was first time confirmed by dynamic light scattering in this work. CTAP-2 was also applied to develop a novel analytical method featuring in-gel detection of a copper chaperone containing an accessible Cu(I) site under non-denaturing condition.

Chapter 4 starts with the discussion on a ligand design that evolved in the Fahrni laboratory resulting in a methanolic Cu(I)-selective fluorescent probe with an astonishingly

high fluorescence contrast ratio and quantum yield. Integration of this ligand design with the original solubilizing framework of CTAP-2 was expected to improve the fluorescence properties of CTAP-2, however, the fluorescence contrast ratio and quantum yield of the new probe **4.3** did not improve over CTAP-2. Further thermodynamic and photophysical studies uncovered two separate factors responsible for the low fluorescence quantum yield and contrast ratio: one was the incomplete Cu(I)-N coordination in the copper bound probes and the other was the two distinct excited-state proton transfer (ESPT) pathways in neutral and acidic solutions.

Chapter 5 first discusses the available protein separation methods in relation to copper proteome and highlights the limitations of these techniques in preserving the native copper-protein interactions which is crucial to identify the copper proteins from cellular extract by the available microanalytical techniques as described in chapter 3. In this work, several "metal free" techniques were developed which did not require the imaging of protein bound copper ions but rather involved in translating the copper binding to a protein into a measurable and quantifiable signal. While some methods suffered from poor resolution of proteins and insurmountable technical difficulties, two of the newly developed methods, including copper-dependent labeling of cysteines with heavy and light isotopes and difference gel electrophoresis with Cy3 and Cy5 meleimide dyes, were able to differentiate between apo and copper-bound form of known copper-proteins. Therefore, these methods showed potentials for future applications in identifying copper-binding proteins from a complex cellular extract.

CHAPTER 1

INTRODUCTION

Copper is an essential trace element and is required for various biological processes such as cellular respiration, connective tissue cross-linking, pigment formation, and antioxidant defense (1). Table 1.1 gives examples of human copper binding proteins and their physiological roles. Despite the utility of copper in diverse biological functions, free copper ions, either Cu(I) or Cu(II), are highly toxic and hence copper has to be tightly regulated in living cells. In order to achieve the proper intracellular balance of copper, nature has evolved sophisticated homeostatic machinery in all forms of life (2). Accordingly, disruptions in copper homeostasis are implicated in numerous diseases, including Menkes disease, Wilson's disease, Parkinson's disease, Alzheimer's disease, and amyotrophic lateral sclerosis (ALS) (3).

Table 1.1. *Examples of Copper Binding Proteins in Human*

Protein[a]	**Function**
Amyloid precursor protein (APP)	Involved in copper homeostasis in neurons presumably through copper ion reduction; proteolytic cleavage leads to generation of Aβ peptide that aggregates in amyloid plaques associated with Alzheimer's disease
Atox1	Copper chaperone that delivers Cu(I) to ATP7A and ATP7B
ATP7A	Cu(I)-transporting P-type ATPase expressed in all tissues except liver, delivers copper to proteins during biosynthesis, mediates excretion of excess intracellular copper

Table 1.1. *Continued*

Protein[a]	Function
ATP7B	Cu(I)-transporting P-type ATPase expressed primarily in the liver, supplies copper in biosynthetic pathways, responsible for biliary excretion of excess copper
Ceruloplasmin	Major copper-carrying protein in the blood, functions as a ferroxidase in iron metabolism which oxidizes Fe^{2+} into Fe^{3+} for subsequent incorporation into transferrin
CCS	Copper chaperone that delivers Cu(I) to Cu/Zn superoxide dismutase (SOD)
COMMD1	Primary function is down-regulation of NF-kappa-B activity and a possible role in regulation of copper metabolism
Cox11	Metallate Cu_B site into subunit I of cytochrome c oxidase in mitochondria
Cox17	Copper chaperone that transfers Cu(I) to Sco1 and Cox11 for incorporating Cu(I) into cytochrome c oxidase in mitochondria
CTR1	High affinity Cu(I) transporter involved in cellular copper uptake
CTR2	Probable low affinity Cu(I) transporter involved in cellular copper uptake
Cu/Zn SOD	Antioxidant enzyme that catalyzes the disproportionation of superoxide to hydrogen peroxide and oxygen
Cytochrome c oxidase (CCO)	Terminal enzyme in the mitochondrial respiratory chain that catalyzes the reduction of dioxygen to water
Dopamine β-hydroxylase (DBH)	Oxygenase that converts dopamine to norepinephrine

Table 1.1. *Continued*

Protein[a]	Function
Hephaestin	Implicated in iron and copper homeostasis
Lysyl Oxidase	Catalyzes formation of aldehydes from lysine residues in collagen and elastin precursors for connective tissue cross-linking
Metallothionein	Cysteine-rich protein presumably involved in copper storage
Peptidylglycine-α-amidating mono-oxygenase (PAM)	Catalyzes conversion of peptidylglycine substrates into α-amidated products; an important step for biological activities of neuropeptides
Prion protein	This protein binds Cu via the N-terminal octapeptide repeats; misfolding of the protein is associated with neurodegenerative disorders
Sco1/ Sco2	Metallate Cu_A site into subunit II of cytochrome c oxidase in mitochondria
Steap proteins	Family of metalloreductases involved in Fe^{3+} and Cu^{2+} reduction
Tyrosinase	Oxidase that functions in the synthesis of pigments such as melanins

[a] List compiled from the UniProtKB/Swiss-Prot database

1.1. Interconnected Pathways in Mammalian Copper Homeostasis

In biological systems, several copper binding proteins are integral parts of copper homeostatic machinery and work in conjunction to regulate cellular copper uptake, distribution, and excretion (4). Knowledge of the copper coordination sites, the mode of interaction among protein partners, and the thermodynamic and kinetic parameters of copper-protein binding can be integrated to understand the factors determining copper

transport processes, their selectivity and specificity. Significant progress has been made in characterizing the copper trafficking pathways in mammalian cells and this subsection will review the key components (Figure 1.1).

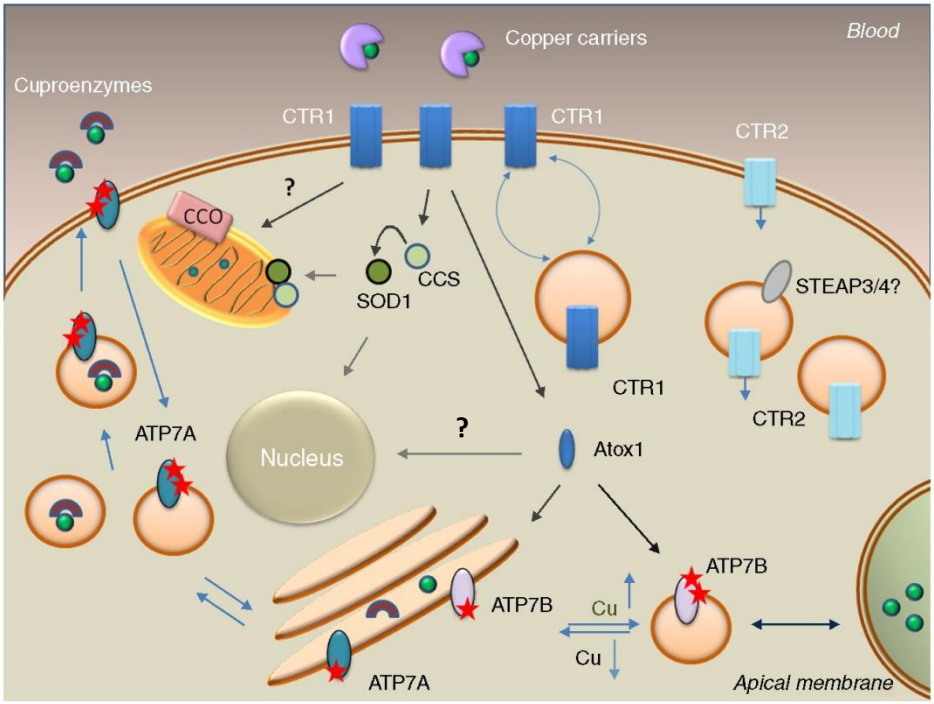

Figure 1.1. *Copper Distribution Pathways in a Generalized Mammalian Cell.* CTR1 accepts cooper from the extracellular copper carriers and transfers copper into cytosol; changes in copper levels induce reversible trafficking of CTR1 between the plasma membrane and intracellular vesicles. CTR2 is predominantly intracellular but can be found at the plasma membrane. Entering copper is escorted by copper chaperones to multiple destinations; CCS distributes copper to SOD1 in cytosol and mitochondria, while Atox1 transfers copper to Cu-ATPases in the secretory pathway. An ensemble of proteins regulates copper delivery to cytochrome c oxidase (CCO) in mitochindria. Cu-ATPases transport copper to the secretory pathways for incorporation into cuproenzumes and mediate copper excretion by sequestering excess copper in vesicles. The trafficking of Cu-ATPases between these two locations is associated with phosphorylation by a kinase (indicated by stars), which increases in response to copper elevation. Reproduced with permission from Reference (4), © 2010, Elsevier.

1.1.1. Copper Import into the Cytosol

Under physiological conditions, Cu ions can exist in two oxidation states: the reduced form is Cu(I) and the oxidized form is Cu(II). This redox activity has been harnessed by cuproenzymes where copper acts as a redox cofactor and thus not surprisingly 93% of the enzymes that use copper are oxidoreductases (EC 1) (5). The dietary copper predominantly exists in its oxidized form (Cu^{2+}), but inside the reducing cytosolic environment (-260 mV) (6), copper is primarily present in form of Cu(I). Therefore, prior to import across the plasma membrane, extracellular Cu^{2+} has to be reduced by reductases in membrane. Although these cupric reductases have not yet been identified definitively, the Steap proteins, a family of metalloreductases in humans, are one of the prominent candidates for this role (7).

Copper enters the cell via a high affinity membrane permease copper transporter 1 (CTR1) which is present as a homotrimer in the membrane (8-10). A single CTR1 polypeptide contains three transmembrane domains: a methionine-rich N terminus, a cysteine-histidine cluster in the C terminus and an MX_3M motif in the second transmembrane domain which is essential for copper import. The trimer forms a channel-like permeation pathway for copper (11, 12). The transcriptional regulation of CTR1 was shown by Song et al. where human CTR1 (hCTR1) mRNA level was up-regulated under copper-depleted conditions and down-regulated under copper-replete conditions (13). They have also shown that expression of exogenous hCTR1 is accompanied by the down-regulation of the endogenous hCTR1 mRNA. The modulation of CTR1 activity also occurs by the intracellular distribution of the protein. CTR1 is present at the plasma membrane during cellular demand for Cu, whereas elevation of extracellular copper induces endocytosis of CTR1 to vesicles and thus decreasing copper uptake across the membrane (14, 15). Moreover, elevated Cu levels have been shown to increase CTR1 protein degradation (16) which is considered as one of the mechanisms to control cellular copper influx.

A second transporter protein, structurally related to CTR1, has also been identified in mammals and designated as CTR2. The occurrence of this low-affinity copper transporter is largely intracellular and may function to release copper from intracellular vesicles into the cytosol (17). Moreover, a small fraction of CTR2 is detected at the plasma membrane (18), but the biological role of the protein at this location remains to be explored.

1.1.2. Copper Chaperones

Once inside the cell, copper binds to cytosolic copper chaperones which then transfer copper to specific cellular destinations. CCS (copper chaperone for superoxide dismutase) activates cytosolic Cu/Zn superoxide dismutase (SOD1), facilitating both Cu(I) transfer and disulfide bond formation; while Atox1 transfers copper to the copper-transporting ATPases in the secretory pathway. A low molecular weight carrier or a yet-to-be characterized protein initiates a series of transfer reactions that result in copper delivery to cytochrome c oxidase (CCO) in mitochondria.

a) Metallation of Cu/Zn SOD

Copper chaperone for superoxide dismutase (CCS) has three structural domains (19). Domain II structurally resembles Cu/Zn SOD and is engaged in the CCS-SOD1 interactions, but the copper is not bound in this site. Domains I and III have CXXC and CXC Cu^{+} binding motifs, respectively. Heterodimerization between a monomer of Cu-bound CCS and Zn-loaded SOD1 results in the transfer of Cu onto SOD1, where four histidine ligands coordinate the copper ion in square pyramidal geometry with water as the fifth ligand (20). In the process, Cu-CCS catalyzes the oxygen-dependent formation of an intramolecular disulfide bond in SOD1 which is required for its catalytic activity (21). Additionally, both CCS and Cu/Zn SOD are localized to the inter-membrane space of mitochondria (IMS), where active Cu/Zn SOD is thought to protect cells from

superoxide generated from the incomplete reduction of oxygen during mitochondrial electron transport (22).

Cellular Cu status regulates CCS at a post translational level through protein degradation, resulting in high CCS levels during Cu deficiency and low protein levels during times of elevated intracellular Cu (23-25). Although alterations in CCS expression do not affect SOD1 protein levels, the activity of the enzyme changes as a function of CCS and thus the copper levels (26). Mutant forms of SOD1 protein aggregate in the motor neurons of a familial form of amyotrophic lateral sclerosis (ALS) patients (27-29). Given that the posttranslational modifications of SOD1, including copper/zinc binding and disulfide formation, generally increase protein structural stability, it is expected that the immature mutant forms, which is devoid of metals and the disulfide bond, are more prone to unfolding and aggregation, underscoring the importance of this enzyme (30, 31).

b) Copper Delivery to Secretory Compartments

Several Cu-containing proteins travel through the secretory pathway for the metal incorporation during their biosynthesis where copper is supplied by Cu-transporting ATPases, ATP7A and ATP7B. The ATPases are transmembrane proteins in the Golgi network which acquire copper from cytosolic chaperone Atox1. A βαββαβ ferredoxin fold is the key structural feature of Atox1 which coordinates to a solvent-exposed Cu^{+} ion by a CXXC motif (32). Cu is transferred from Atox1 to a metal binding domain, MTCXXC, in the N terminus of the ATPases, ATP7A and ATP7B (33). This transfer occurs via a series of inter-protein ligand exchange reactions (34, 35), ultimately leading to the movement of Cu(I) across the membrane of the secretory compartment utilizing the energy released from ATP hydrolysis (36).

In addition to its role in delivering copper to ATPases, it has been suggested that Atox1 can also function as a transcription factor, which translocates into the nucleus under conditions of high Cu and stimulates the expression of the gene encoding

extracellular SOD3 as well as other genes involved in cell proliferation such as cyclin D1 (37, 38). However, the mechanisms that govern the translocation of Atox1 from cytosol to the nucleus are yet to be deciphered.

c) Copper Insertion into Cytochrome c Oxidase

Unlike Atox1 and CCS which escort copper directly to their targets, copper insertion into cytochrome c oxidase (CCO) is mediated by the concerted action of several Cu-binding proteins, Cox17, Cox 11, Sco1 and Sco2. In the IMS, copper chaperone Cox17 escorts copper to Sco1 and Cox11, which are implicated in the sequential transfer of the metal to Cu_A site on the Cox2 subunit and Cu_B site of the Cox1 subunit of CCO respectively. Although a basic understanding of the key steps of copper insertion in CCO is developing (39), it is currently unclear how Cu travels from the site of import at the plasma membrane to the mitochondria. Cobine et al. have purified a not yet fully characterized nonproteinaceous ligand that is present in the cytosol and mitochondrial matrix and may function in mitochondrial Cu delivery (40, 41). Sco2 is structurally similar to Sco1 and both of them are essential for CCO assembly (42), yet the physiological role of Sco2 has not been fully elucidated.

1.1.3. Cellular Copper Storage

The wide range of catalytic functions performed by copper-binding enzymes is attributed to the ability of copper to cycle between the oxidized Cu(II) and reduced Cu(I) forms making it a suitable redox cofactor. The same redox activity is paradoxically responsible for cellular oxidative damage mediated by "free" aqueous copper ion. Therefore, one essential component in copper regulation is the cell's ability to store excess Cu and to mobilize Cu reserves during times of cellular need. Metallothionein and glutathione are examples of ligands that are presumably involved in copper storage in order to protect cells from excess toxic copper.

Mammalian metallothioneins (MT) are small cysteine-rich polypeptides that bind up to 12 Cu^{+} ions through cysteine thiols. MT expression is regulated at the transcription level by MTF1 (metal transcription factor 1), which in response to elevated Cu levels binds to the metal responsive elements (MRE) in the promoter regions of its target genes (43). It has also been proposed that MT may act as a copper storage protein that could be mobilized during cellular demand of Cu. In support of this hypothesis, it has been shown that mouse embryonic fibroblasts lacking MT have reduced viability under Cu limiting conditions (44).

Copper bound to glutathione (GSH), a low molecular weight cysteine containing tripeptide present at millimolar concentrations in the cytosol, represents a potential pool of exchangeable Cu. Although affinity of GSH is too weak to compete for Cu(I) binding with endogenous copper chaperone proteins (45), it has been proposed that GSH might be involved in complexing the copper ions soon after its import in the cytosol. The complexed metal is then transferred to MT where it is stored and mobilzed during cellular need (46).

1.1.4. Copper Efflux

The two mammalian Cu-transporting ATPases, ATP7A and ATP7B, are responsible for the speciation of Cu into the lumen of the secretory compartment for its insertion into Cu-dependent enzymes such as ceruloplasmin, tyrosinase, and lysyl oxidase. Moreover, ATP7A and ATP7B play key roles in exporting excess Cu from cells by primarily engaging in a copper-dependent trafficking. Although there are divergent explanations in the literature delineating the actual mechanism of copper efflux by ATPases, the general picture is that the Cu-ATPases undergo a post-translational kinase-mediated phosphorylation in response to elevated copper. The copper-loaded phosphorylated proteins then relocalize to vesicles which are then transported towards

cellular membrane. Copper is subsequently excreted by fusion of these vesicles with the membrane (4).

Mutations in the *ATP7A* gene result in Menkes disease, characterized by a defect in the mobilization of copper from intestine resulting in peripheral Cu deficiency and inadequate metal supply to Cu-dependent enzymes. Mutations in the *ATP7B* gene cause Wilson's disease, characterized by excessive accumulation of Cu in hepatic and neuronal tissues. Both copper homeostasis disorders present with severe neurological, developmental, and cognitive defects, in addition to hypopigmentation, skin laxity, and kinky hair for Menkes disease, and hepatitis and liver cirrhosis for Wilson's disease patients.

1.2. Metal Coordination in Copper Homeostatic Proteins

The elemental composition, number, and geometry of the ligands in copper coordination in proteins provide information about their selectivity towards Cu(I) or Cu(II) ions and the relative thermodynamic stabilities of the resulting complexes. Following the principles of hard and soft acids and bases (HSAB) theory (47), Cu(I) can be assigned as a soft Lewis acid and therefore is expected to bind to soft ligand like sulfur, whereas Cu(II) is a borderline Lewis acid and thus favors hard Lewis base like carboxylate oxygen and borderline base like imidazole nitrogen. A bioinformatics study with the copper-proteins in Protein Data Bank (PDB) (48) showed that Cu(I) binding sites in nature are indeed dominated by Cys residues, 74% of all Cu(I) sites in various proteins contain cysteine followed by 16% methionine and 10% histidine. The amino acid cysteine is especially abundant in copper transport proteins where 97% of these proteins bind Cu(I) with this ligand. In contrast, the major amino acid in the Cu(II)-binding sites is histidine (78%), other ligands include aspartate (11%) and tyrosine (11%).

Table 1.2. *Copper Binding Sites in Homeostatic Proteins*

Organism	Protein	Binding Site	Cellular Location
Human	Atox1	MXCXXC	Cytosol
	ATP7A	MXCXXC	trans-Golgi membrane
	ATP7B	MXCXXC	trans-Golgi membrane
	CCS	Domain 1: MXCXXC Domain 3: CXC	Cytosol
	Cox 11	CXC	Mitochondrial inter-membrane space (IMS)
	Cox 17	CC	Mitochondrial inter-membrane space (IMS)
	Cu/Zn superoxide dismutase (SOD1)	Four His ligands plus a water molecule	Cytosol
	Sco1/ Sco2	CPDVC sequence plus a histidine	Mitochondrial inter-membrane space (IMS)
E. coli	CusF	Met_2His plus π-interaction from tryptophan	Periplasm
	DR1885	Met_3His	Periplasm

Although HSAB theory acts as a guideline in understanding copper coordination in biology, the redox potential of the cellular compartment and electrostatic contribution of the ligands are major factors determining which side chain is employed in a biological copper binding site. For instance, cysteine and methionine are both sulfur-containing ligands that preferentially bind Cu(I), but cysteine is more prevalent in a reducing

environment as in the cytosol, whereas methionine is common in an oxidizing environment as in the periplasm of Gram-negative bacteria. This is because cysteine thiol sulfur is susceptible to oxidation and the oxidized disulfide form is incapable to bind Cu(I).

The nature of the copper binding site also gives an indication about the specific role of these proteins in regulating copper inside the cell. For example, surface-exposed Cu(I)-binding site is a general feature of copper chaperones to ensure facile metal transfer to the partner proteins. This is indeed the case for Atox1-like copper chaperones and their target ATPases. These proteins contain highly conserved solvent-exposed CXXC motifs where two cysteines bind Cu(I) in a linear geometry (32). Such protein conformation allows for flexible coordination chemistry, and thus a third ligand can be accommodated during the copper transfer process resulting in heterodimeric complexes of chaperones and their targets (33, 34). It is also worth noting that in some of the copper chaperones, such as Atox1 and Cox17, a conserved lysine residue is located close to the copper center, most likely stabilizing the overall negative charge of the $[Cu(I)(Cys)_2]^{-1}$ complex.

Periplasmic copper-trafficking proteins in Gram-negative bacteria contain methionine residue in the surface-exposed Cu(I)-binding site. The methionine thioether is more difficult to oxidize than cysteine thiol in oxidizing environment like periplasm. Another difference between these two ligands is that the methionine thioether group lacks the electrostatic component of the cysteine thiolate ligand and is expected to have weaker Cu(I) affinities. Therefore, methionine usually forms high-coordinate Cu(I)-complexes (three or four coordinate) to compensate for this lower Cu(I) affinity. Met_2His binding site is found in the periplasmic copper chaperone CusF, with an unusual contribution from a strong cation-pi interaction with a tryptophan residue in copper recognition (49). Similarly, in mitochondrial inter-membrane space (IMS) which is more oxidizing than the cytosol, a third ligand is present in the Cu(I)-binding site where the metal is bound by cysteine containing motif, as in Sco1 and Sco2 where a histidine serves the purpose (50).

In the enzymes where copper is used as a redox cofactor, the binding sites are usually buried in the protein and can adopt various geometries according to the copper oxidation state. For example, in the active site of Cu/Zn superoxide dismutase (SOD1), one Cu ion is ligated by three histidines in a trigonal planar geometry when in the reduced state and one Zn ion is ligated by one aspartic acid and three histidines. One of the histidine ligands of the Zn ion also ligates the Cu ion when in the oxidized state and thus has been termed the bridging histidine. The Cu(II) ion is additionally coordinated by a water molecule and thus forms a five coordinate square pyramidal geometry (51, 52). These conformational changes especially the bridging histidine plays an important role in the disproportionation of superoxide.

Table 1.2 shows that there are a limited number of structural motifs associated with Cu(I)-binding sites in proteins. Different coordination motifs also seem to be tailored to different functional properties of proteins and their cellular localizations with an ultimate goal to stabilize the copper ion in a biological environment. Therefore, the structural patterns in conjunction with information on the cellular compartmentalization of the proteins can be used to understand the molecular components of copper management.

1.3. Understanding Copper Biochemistry: Bridging the Gaps

Copper is essential as a cofactor for many proteins and enzymes involved in key biological processes as compiled in Table 1.1. Given the importance of copper in human physiology and the potential toxicity of the free metal ion, malfunction in copper regulatory mechanisms is typically associated with severe pathological conditions. Defective copper transport is directly responsible for genetic diseases, such as Menkes disease, Wilson's disease, and cytochrome c oxidase deficiency (42, 53). Copper has also been implicated, though not causally associated, to neurological diseases such as Alzheimer's disease, Parkinson's disease, amyotrophic lateral sclerosis, and prion disease

(54). Moreover, copper-trafficking proteins are also considered as critical components in cancer cell proliferation (55), host-pathogen interactions in infectious diseases (56), and resistance to chemotherapeutic drugs (57). Accordingly, it is important to understand the cellular components involved in Cu homeostasis which is critical to prevent diseases related to copper imbalance. Significant research efforts have been made in elucidating structure, function, interaction partners of several copper proteins, however many fundamental questions about copper biochemistry still remain unanswered, particularly with regard to storage, mobilization, and subcellular distribution.

Based on the binding affinity of superoxide dismutase (SOD1), Rae et al. estimated that under normal growth conditions the concentration of cytosolic free copper to be less than 10^{-18} M, corresponding to one free copper atom per cell (58). This proposition can be perceived in the light of redox lability of copper ions. Aqueous Cu(I) ion is highly reactive toward molecular oxygen. For example, in air-saturated water at 25°C , Cu(I) is rapidly oxidized to Cu(II) with a half-life in millisecond time scale (59). Moreover, at micromolar concentrations aqueous Cu(I) would either disproportionate into Cu(II) and Cu(s) at acidic pH, or precipitate as Cu_2O under neutral or basic conditions. As a consequence of its redox activity, "free" aquated Cu^+ ion is toxic in the cellular environment because of its capability to induce oxidative damages through different mechanisms. For instance, both aerial oxidation of intracellular Cu^+ (aq) ion to Cu^{2+} (aq) ion and the reverse reduction by glutathione are very rapid (60); they occur in the millisecond range. This redox shuttling will eventually deplete the cellular reservoir of glutathione and other reductants such as ascorbic acid. Additionally, Cu^+ ion can participate in Fenton-type chemistry with H_2O_2, leading to the generation of highly reactive free radicals which can cause damage to a wide variety of biomolecules, including lipids, proteins, and DNA (61, 62). Furthermore, Cu(II) is located at the top of the Irving-Williams series which means Cu(II)-complexes are relatively more stable than other divalent metals, thus Cu(II) ions have the potential to displace native metal ions

from endogenous metalloproteins. Consequently, free copper ions, either Cu(I) or Cu(II), can exert detrimental effects in living organisms. For all of these reasons, it is not surprising that cellular copper pool is buffered at a low concentration by coordination to endogenous ligands. Metallothionein and glutathione in the cytosol are possible candidates to serve this purpose; however, there is a lack of compelling evidence to support this conjecture. In addition to the cytosolic copper reservoirs, Cobine et al. isolated a small ligand in the mitochondrial matrix of yeast and human cells which binds Cu(I) in an anionic complex, but its chemical nature has yet to be elucidated (40, 41).

Contrary to the notion of low cytosolic free copper content, literature evidence supports the existence of a kinetically labile intracellular copper pool. Herd et al. showed rapid uptake and release of radioactive copper, ^{64}Cu, from mammalian cells depending on the copper concentration of the surrounding medium (63). However, with the exception of the small ligand purified by Cobine et al. from the mitochondrial matrix whose chemical identity and functions are yet to be investigated (40, 41), little is currently known about the chemical nature and the subcellular localization of this labile copper pool.

Although a multitude of genes and proteins associated with copper homeostasis were identified, many pathways are yet to be deciphered with respect to the intracellular copper distribution (1). Among them, the copper delivery to mitochondria and nucleus are the most intriguing ones. The copper chaperone Cox17, which is required for CCO assembly, was initially thought to deliver cytosolic copper to mitochondria based on its presence in both the cytosol and IMS (64). However, yeast cells lacking Cox17 retain wild type mitochondrial copper levels (40). In addition, tethering Cox17 to the mitochondrial inner membrane resulted in its exclusive localization within the organelle, and CCO assembly was not interrupted (65). These studies thus refute the proposition that Cox17 functions as copper chaperone for mitochondrial copper, rather transportation of Cu(I) to the mitochondria is mediated by another metallochaperone or transport

pathway. Cobine et al. suggested the possible role of the small molecule ligand discussed in the preceding paragraph as a copper transporter to mitochondria based on the localization of the apo-ligand in the cytosol (41). It has been proposed in this study that Cu(I) binding to the ligand within the cytosol initiates the translocation of the copper-bound ligand to the mitochondria for storage and subsequent use in insertion of the metal in CCO.

Accumulating literature evidence suggests that copper plays a fundamental role in regulating cell proliferation critical in physiological repair processes such as wound healing and angiogenesis as well as in various pathophysiologies including tumor growth, atherosclerosis, and neuron degenerative diseases (66-74). Synchrotron X-ray fluorescence (SXRF) images showed presence of copper in the nucleus of a mammalian cell (75) and a recent study by SXRF revealed marked redistribution of Cu and Zn ions during mitosis (76), thus emphasizing an essential role of copper in cell growth and proliferation. Nevertheless, little is known about the underlying molecular mechanisms of copper-regulated cell growth as well as the mode of transportation and storage of copper inside the nucleus. In the latter context, Hamza et al. provided the first clue when they demonstrated that the copper chaperone protein Atox1 is distributed throughout the cytosol and nucleus of a mammalian cell (77). In agreement with this observation, further studies indicate that Atox1 may function as a copper-responsive transcription factor regulating cell proliferation (by cyclin D1 expression) and oxidative stress (by SOD3 expression) (38, 78, 79). However, Atox1-deficient fibroblast cells ($Atox1^{-/-}$) showed an elevated nuclear Cu content compared to wild-type ($Atox1^{+/+}$) cells contradicting the potential role of the protein as nuclear copper transporter (80). Consequently, identifying the pathway of translocation of copper into the nucleus still remains a fascinating area for future research.

There are additional reasons that support the presence of copper-containing proteins inside the nucleus. In *Saccharomyces cerevisiae* (baker's yeast), Mac1 and Ace1

activate transcription in response to low and high intracellular concentrations of copper respectively (81, 82). Both of these proteins bind Cu^{+} ion tightly, K_d being 9.7 x 10^{-20} M for Mac1 and 4.7 x 10^{-18} for Ace1 (83). One striking feature of transcriptional regulation of copper in yeast is the complementarities of Ace1 and Mac1 in gene activation. Specifically, the apo form of Ace1 has a low affinity for DNA, but upon copper binding, Ace1 binds to a specific promoter DNA activating copper-detoxification genes (84). In contrast, Mac1 activates the expression of high affinity copper uptake genes in its metal-free apo form and the copper-bound form is inactive (85). The reversible Cu(I)-binding in Ace1 and Mac1 induces conformational changes, which are pivotal in regulation of gene expression. Intuitively, this might appear paradoxical in the light of high binding affinities of Ace1 and Mac1 as metal dissociation from such binding sites are expected to be very slow, however, the metal exchange reaction can also occur by associative mechanism whose rate is independent of the metal dissociation kinetics. In fact, copper chaperones insert the metal ions into target proteins by such associative mechanism (20, 33, 34). Similar to the yeast cell, a host of proteins controlling the translocation, storage, and utilization of copper in the nuclei of mammalian cells seems highly plausible.

In order to shed new light on these poorly understood fundamental processes of copper homeostasis, the author of this dissertation created valuable chemical and biological tools for investigating copper biochemistry by combining the coordination chemistry, cellular imaging, and proteomics. This work included (i) development of robust Cu(I) affinity standards to understand the thermodynamics of copper-protein binding, (ii) characterization of Cu(I)-selective fluorescent sensors to probe the subcelllular localization of kinetically labile copper, (iii) in-gel detection of copper chaperones under non-denaturing condition creating a novel role for water soluble Cu(I)-sensors, and (iv) selective detection of copper-binding proteins exploiting the differential reactivity of thiol functional groups in cysteines with respect to copper availability.

1.4. References

1. Kim BE, Nevitt T, & Thiele DJ (2008) Mechanisms for copper acquisition, distribution and regulation. *Nature Chemical Biology* 4(3):176-185.

2. Nevitt T, Ohrvik H, & Thiele DJ (2012) Charting the travels of copper in eukaryotes from yeast to mammals. *Biochimica Et Biophysica Acta-Molecular Cell Research* 1823(9):1580-1593.

3. Kozlowski H, Janicka-Klos A, Brasun J, Gaggelli E, Valensin D, & Valensin G (2009) Copper, iron, and zinc ions homeostasis and their role in neurodegenerative disorders (metal uptake, transport, distribution and regulation). *Coordination Chemistry Reviews* 253(21-22):2665-2685.

4. Lutsenko S (2010) Human copper homeostasis: a network of interconnected pathways. *Current Opinion in Chemical Biology* 14(2):211-217.

5. Waldron KJ, Rutherford JC, Ford D, & Robinson NJ (2009) Metalloproteins and metal sensing. *Nature* 460(7257):823-830.

6. Go YM & Jones DP (2008) Redox compartmentalization in eukaryotic cells. *Biochimica Et Biophysica Acta-General Subjects* 1780(11):1271-1290.

7. Ohgami RS, Campagna DR, McDonald A, & Fleming MD (2006) The Steap proteins are metalloreductases. *Blood* 108(4):1388-1394.

8. Eisses JF & Kaplan JH (2002) Molecular characterization of hCTR1, the human copper uptake protein. *Journal of Biological Chemistry* 277(32):29162-29171.

9. Lee J, Pena MMO, Nose Y, & Thiele DJ (2002) Biochemical characterization of the human copper transporter CTR1. *Journal of Biological Chemistry* 277(6):4380-4387.

10. Eisses JF & Kaplan JH (2005) The mechanism of copper uptake mediated by human CTR1 - A mutational analysis. *Journal of Biological Chemistry* 280(44):37159-37168.

11. Aller SG & Unger VM (2006) Projection structure of the human copper transporter CTR1 at 6-angstroms resolution reveals a compact trimer with a novel channel-like architecture. *Proceedings of the National Academy of Sciences of the United States of America* 103(10):3627-3632.

12. De Feo CJ, Aller SG, Siluvai GS, Blackburn NJ, & Unger VM (2009) Three-dimensional structure of the human copper transporter hCTR1. *Proceedings of the National Academy of Sciences of the United States of America* 106(11):4237-4242.

13. Song IS, Chen HHW, Aiba I, Hossain A, Liang ZD, Klomp LWJ, & Kuo MT (2008) Transcription factor Sp1 plays an important role in the regulation of copper homeostasis in mammalian cells. *Molecular Pharmacology* 74(3):705-713.

14. Guo Y, Smith K, Lee J, Thiele DJ, & Petris MJ (2004) Identification of methionine-rich clusters that regulate copper-stimulated endocytosis of the human CTR1 copper transporter. *Journal of Biological Chemistry* 279(17):17428-17433.

15. Molloy SA & Kaplan JH (2009) Copper-dependent recycling of hCTR1, the human high affinity copper transporter. *Journal of Biological Chemistry* 284(43):29704-29713.

16. Petris MJ, Smith K, Lee J, & Thiele DJ (2003) Copper-stimulated endocytosis and degradation of the human copper transporter, hCTR1. *Journal of Biological Chemistry* 278(11):9639-9646.

17. Van den Berghe PVE, Folmer DE, Malingre HEM, Van Beurden E, Klomp AEM, De Sluis BV, Merkx M, Berger R, & Klomp LWJ (2007) Human copper transporter 2 is localized in late endosomes and lysosomes and facilitates cellular copper uptake. *Biochemical Journal* 407:49-59.

18. Bertinato J, Swist E, Plouffe LJ, Brooks SPJ, & L'Abbe MR (2008) CTR2 is partially localized to the plasma membrane and stimulates copper uptake in COS-7 cells. *Biochemical Journal* 409:731-740.

19. Schmidt PJ, Rae TD, Pufahl RA, Hamma T, Strain J, O'Halloran TV, & Culotta VC (1999) Multiple protein domains contribute to the action of the copper chaperone for superoxide dismutase. *Journal of Biological Chemistry* 274(34):23719-23725.

20. Lamb AL, Torres AS, O'Halloran TV, & Rosenzweig AC (2001) Heterodimeric structure of superoxide dismutase in complex with its metallochaperone. *Nature Structural Biology* 8(9):751-755.

21. Furukawa Y, Torres AS, & O'Halloran TV (2004) Oxygen-induced maturation of SOD1: a key role for disulfide formation by the copper chaperone CCS. *Embo Journal* 23(14):2872-2881.

22. Okado-Matsumoto A & Fridovich I (2001) Subcellular distribution of superoxide dismutases (SOD) in rat liver - Cu,Zn-SOD in mitochondria. *Journal of Biological Chemistry* 276(42):38388-38393.

23. Prohaska JR, Broderius M, & Brokate B (2003) Metallochaperone for Cu,Zn-superoxide dismutase (CCS) protein but not mRNA is higher in organs from copper-deficient mice and rats. *Archives of Biochemistry and Biophysics* 417(2):227-234.

24. Bertinato J & L'Abbe MR (2003) Copper modulates the degradation of copper chaperone for Cu,Zn superoxide dismutase by the 26 S proteosome. *Journal of Biological Chemistry* 278(37):35071-35078.

25. Caruano-Yzermans AL, Bartnikas TB, & Gitlin JD (2006) Mechanisms of the copper-dependent turnover of the copper chaperone for superoxide dismutase. *Journal of Biological Chemistry* 281(19):13581-13587.

26. Prohaska JR, Geissler J, Brokate B, & Broderius M (2003) Copper,zinc-superoxide dismutase protein but not mRNA is lower in copper-deficient mice and mice lacking the copper chaperone for superoxide dismutase. *Experimental Biology and Medicine* 228(8):959-966.

27. Shibata N, Hirano A, Kobayashi M, Sasaki S, Kato T, Matsumoto S, Shiozawa Z, Komori T, Ikemoto A, Umahara T, & Asayama K (1994) Cu/Zn Superoxide dismutase-like immunoreactivity in lewy body-like inclusions of sporadic amyotrophic-lateral-sclerosis. *Neuroscience Letters* 179(1-2):149-152.

28. Shibata N, Hirano A, Yamamoto T, Kato Y, & Kobayashi M (2000) Superoxide dismutase-1 mutation-related neurotoxicity in familial amyotrophic lateral sclerosis. *Amyotrophic Lateral Sclerosis and Other Motor Neuron Disorders* 1(3):143-161.

29. Shibata N & Kobayashi M (1997) Familial amyotrophic lateral sclerosis and Cu/Zn superoxide dismutase mutation. *Neuropathology* 17(4):255-262.

30. Furukawa Y & O'Halloran TV (2005) Amyotrophic lateral sclerosis mutations have the greatest destabilizing effect on the apo- and reduced form of SOD1, leading to unfolding and oxidative aggregation. *Journal of Biological Chemistry* 280(17):17266-17274.

31. Rakhit R, Cunningham P, Furtos-Matei A, Dahan S, Qi XF, Crow JP, Cashman NR, Kondejewski LH, & Chakrabartty A (2002) Oxidation-induced misfolding and agagaregation of superoxide dismutase and its implications for amyotrophic lateral sclerosis. *Journal of Biological Chemistry* 277(49):47551-47556.

32. Anastassopoulou I, Banci L, Bertini I, Cantini F, Katsari E, & Rosato A (2004) Solution structure of the apo and copper(I)-loaded human metallochaperone HAH1. *Biochemistry* 43(41):13046-13053.

33. Wernimont AK, Huffman DL, Lamb AL, O'Halloran TV, & Rosenzweig AC (2000) Structural basis for copper transfer by the metallochaperone for the Menkes/Wilson disease proteins. *Nature Structural Biology* 7(9):766-771.

34. Pufahl RA, Singer CP, Peariso KL, Lin SJ, Schmidt PJ, Fahrni CJ, Culotta VC, PennerHahn JE, & Ohalloran TV (1997) Metal ion chaperone function of the soluble Cu(I) receptor Atx1. *Science* 278(5339):853-856.

35. Bancl L, Bertini I, Chasapis CT, Rosato A, & Tenori L (2007) Interaction of the two soluble metal-binding domains of yeast Ccc2 with copper(I)-Atx1. *Biochemical and Biophysical Research Communications* 364(3):645-649.

36. La Fontaine S & Mercer JFB (2007) Trafficking of the copper-ATPases, ATP7A and ATP7B: Role in copper homeostasis. *Archives of Biochemistry and Biophysics* 463(2):149-167.

37. Itoh S, Ozumi K, Kim HW, Nakagawa O, McKinney RD, Folz RJ, Zelko IN, Ushio-Fukai M, & Fukai T (2009) Novel mechanism for regulation of extracellular SOD transcription and activity by copper: Role of antioxidant-1. *Free Radical Biology and Medicine* 46(1):95-104.

38. Itoh S, Kim HW, Nakagawa O, Ozumi K, Lessner SM, Aoki H, Akram K, McKinney RD, Ushio-Fukai M, & Fukai T (2008) Novel role of antioxidant-1 (Atox1) as a copper-dependent transcription factor involved in cell proliferation. *Journal of Biological Chemistry* 283(14):9157-9167.

39. Cobine PA, Pierrel F, & Winge DR (2006) Copper trafficking to the mitochondrion and assembly of copper metalloenzymes. *Biochimica Et Biophysica Acta-Molecular Cell Research* 1763(7):759-772.

40. Cobine PA, Ojeda LD, Rigby KM, & Winge DR (2004) Yeast contain a non-proteinaceous pool of copper in the mitochondrial matrix. *Journal of Biological Chemistry* 279(14):14447-14455.

41. Cobine PA, Pierrel F, Bestwick ML, & Winge DR (2006) Mitochondrial matrix copper complex used in metallation of cytochrome oxidase and superoxide dismutase. *Journal of Biological Chemistry* 281(48):36552-36559.

42. Shoubridge EA (2001) Cytochrome c oxidase deficiency. *American Journal of Medical Genetics* 106(1):46-52.

43. Heuchel R, Radtke F, Georgiev O, Stark G, Aguet M, & Schaffner W (1994) The transcription factor MTF-1 is essential for basal and heavy metal-induced metallothionein gene-expression *Embo Journal* 13(12):2870-2875.

44. Ogra Y, Aoyama M, & Suzuki KT (2006) Protective role of metallothionein against copper depletion. *Archives of Biochemistry and Biophysics* 451(2):112-118.

45. Xiao ZG, Brose J, Schimo S, Ackland SM, La Fontaine S, & Wedd AG (2011) Unification of the copper(I) binding affinities of the metallo-chaperones Atx1, Atox1, and related proteins. Detection probes and affinity standards. *Journal of Biological Chemistry* 286(13):11047-11055.

46. Freedman JH, Ciriolo MR, & Peisach J (1989) The role of glutathione in copper-metabolism and toxicity. *Journal of Biological Chemistry* 264(10):5598-5605.

47. Pearson RG (1963) Hard and soft acids and bases. *Journal of the American Chemical Society* 85(22):3533-&.

48. Bertini I, Cavallaro G, & McGreevy KS (2010) Cellular copper management-a draft user's guide. *Coordination Chemistry Reviews* 254(5-6):506-524.

49. Xue Y, Davis AV, Balakrishnan G, Stasser JP, Staehlin BM, Focia P, Spiro TG, Penner-Hahn JE, & O'Halloran TV (2008) Cu(I) recognition via cation-pi and methionine interactions in CusF. *Nature Chemical Biology* 4(2):107-109.

50. Banci L, Bertini I, Calderone V, Ciofi-Baffoni S, Mangani S, Martinelli M, Palumaa P, & Wang SL (2006) A hint for the function of human Sco1 from different structures. *Proceedings of the National Academy of Sciences of the United States of America* 103(23):8595-8600.

51. Strange RW, Antonyuk SV, Hough MA, Doucette PA, Valentine JS, & Hasnain SS (2006) Variable metallation of human superoxide dismutase: Atomic resolution crystal structures of Cu-Zn, Zn-Zn and as-isolated wild-type enzymes. *Journal of Molecular Biology* 356(5):1152-1162.

52. Murphy LM, Strange RW, & Hasnain SS (1997) A critical assessment of the evidence from XAFS and crystallography for the breakage of the imidazolate bridge during catalysis in Cu/Zn superoxide dismutase. *Structure* 5(3):371-379.

53. de Bie P, Muller P, Wijmenga C, & Klomp LWJ (2007) Molecular pathogenesis of Wilson and Menkes disease: correlation of mutations with molecular defects and disease phenotypes. *Journal of Medical Genetics* 44(11):673-688.

54. Gaggelli E, Kozlowski H, Valensin D, & Valensin G (2006) Copper homeostasis and neurodegenerative disorders (Alzheimer's, prion, and Parkinson's diseases and amyotrophic lateral sclerosis). *Chemical Reviews* 106(6):1995-2044.

55. Merlot AM, Kalinowski DS, & Richardson DR (2013) Novel chelators for cancer treatment: Where are we now? *Antioxidants & Redox Signaling* 18(8):973-1006.

56. Hodgkinson V & Petris MJ (2012) Copper homeostasis at the host-pathogen interface. *Journal of Biological Chemistry* 287(17):13549-13555.

57. Casini A & Reedijk J (2012) Interactions of anticancer Pt compounds with proteins: an overlooked topic in medicinal inorganic chemistry? *Chemical Science* 3(11):3135-3144.

58. Rae TD, Schmidt PJ, Pufahl RA, Culotta VC, & O'Halloran TV (1999) Undetectable intracellular free copper: The requirement of a copper chaperone for superoxide dismutase. *Science* 284(5415):805-808.

59. Morgan MT, Bagchi P, & Fahrni CJ (2013) Fluorescent probes for monovalent copper. *Encyclopedia of Inorganic and Bioinorganic Chemistry*, (John Wiley & Sons, in press).

60. Gorren ACF, Schrammel A, Schmidt K, & Mayer B (1996) Decomposition of S-nitrosoglutathione in the presence of copper ions and glutathione. *Archives of Biochemistry and Biophysics* 330(2):219-228.

61. Burkitt MJ (2001) A critical overview of the chemistry of copper-dependent low density lipoprotein oxidation: Roles of lipid hydroperoxides, alpha-tocopherol, thiols, and ceruloplasmin. *Archives of Biochemistry and Biophysics* 394(1):117-135.

62. Jomova K & Valko M (2011) Advances in metal-induced oxidative stress and human disease. *Toxicology* 283(2-3):65-87.

63. Herd SM, Camakaris J, Christofferson R, Wookey P, & Danks DM (1987) Uptake and efflux of copper-64 in Menkes-disease and normal continuous lymphoid-cell lines. *Biochemical Journal* 247(2):341-347.

64. Beers J, Glerum DM, & Tzagoloff A (1997) Purification, characterization, and localization of yeast Cox17p, a mitochondrial copper shuttle. *Journal of Biological Chemistry* 272(52):33191-33196.

65. Maxfield AB, Heaton DN, & Winge DR (2004) Cox17 is functional when tethered to the mitochondrial inner membrane. *Journal of Biological Chemistry* 279(7):5072-5080.

66. Hu GF (1998) Copper stimulates proliferation of human endothelial cells under culture. *Journal of Cellular Biochemistry* 69(3):326-335.

67. McAuslan BR & Gole GA (1980) Cellular and molecular mechanisms in angiogenesis. *Transactions of the Ophthalmological Societies of the United Kingdom* 100(SEP):354-358.

68. Sen CK, Khanna S, Venojarvi M, Trikha P, Ellison EC, Hunt TK, & Roy S (2002) Copper-induced vascular endothelial growth factor expression and wound healing. *American Journal of Physiology-Heart and Circulatory Physiology* 282(5):H1821-H1827.

69. Volker W, Dorszewski A, Unruh V, Robenek H, Breithardt G, & Buddecke E (1997) Copper-induced inflammatory reactions of rat carotid arteries mimic restenosis/arteriosclerosis-like neointima formation. *Atherosclerosis* 130(1-2):29-36.

70. Birkaya B & Aletta JM (2005) NGF promotes copper accumulation required for optimum neurite outgrowth and protein methylation. *Journal of Neurobiology* 63(1):49-61.

71. Brewer GJ (2005) Copper lowering therapy with tetrathiomolybdate as an Antiangiogenic strategy in cancer. *Current Cancer Drug Targets* 5(3):195-202.

72. Goodman VL, Brewer GJ, & Merajver SD (2004) Copper deficiency as an anti-cancer strategy. *Endocrine-Related Cancer* 11(2):255-263.

73. Harris ED (2004) A requirement for copper in angiogenesis. *Nutrition Reviews* 62(2):60-64.

74. Mandinov L, Mandinova A, Kyurkchiev S, Kyurkchiev D, Kehayov I, Kolev V, Soldi R, Bagala C, de Muinck ED, Lindner V, Post MJ, Simons M, Bellum S, Prudovsky I, & Maciag T (2003) Copper chelation represses the vascular response to injury. *Proceedings of the National Academy of Sciences of the United States of America* 100(11):6700-6705.

75. Yang LC, McRae R, Henary MM, Patel R, Lai B, Vogt S, & Fahrni CJ (2005) Imaging of the intracellular topography of copper with a fluorescent sensor and by synchrotron x-ray fluorescence microscopy. *Proceedings of the National Academy of Sciences of the United States of America* 102(32):11179-11184.

76. McRae R, Lai B, & Fahrni CJ (2013) Subcellular redistribution and mitotic inheritance of transition metals in proliferating mouse fibroblast cells. *Metallomics* 5(1):52-61.

77. Hamza I, Schaefer M, Klomp LWJ, & Gitlin JD (1999) Interaction of the copper chaperone HAH1 with the Wilson disease protein is essential for copper homeostasis. *Proceedings of the National Academy of Sciences of the United States of America* 96(23):13363-13368.

78. Jeney V, Itoh S, Wendt M, Gradek Q, Ushio-Fukai M, Harrison DG, & Fukai T (2005) Role of antioxidant-1 in extracellular superoxide dismutase function and expression. *Circulation Research* 96(7):723-729.

79. Muller PAJ & Klomp LWJ (2009) ATOX1: A novel copper-responsive transcription factor in mammals? *International Journal of Biochemistry & Cell Biology* 41(6):1233-1236.

80. McRae R, Lai B, & Fahrni CJ (2010) Copper redistribution in Atox1-deficient mouse fibroblast cells. *Journal of Biological Inorganic Chemistry* 15(1):99-105.

81. Keller G, Bird A, & Winge DR (2005) Independent metalloregulation of Ace1 and Mac1 in *Saccharomyces cerevisiae*. *Eukaryotic Cell* 4(11):1863-1871.

82. Gross C, Kelleher M, Iyer VR, Brown PO, & Winge DR (2000) Identification of the copper regulon in Saccharomyces cerevisiae by DNA microarrays. *Journal of Biological Chemistry* 275(41):32310-32316.

83. Wegner SV, Sun F, Hernandez N, & He C (2011) The tightly regulated copper window in yeast. *Chemical Communications* 47(9):2571-2573.

84. Dobi A, Dameron CT, Hu S, Hamer D, & Winge DR (1995) Distinct regions of Cu(I)-center-dot-Ace1 contact 2 spatially-resolved DNA major groove sites. *Journal of Biological Chemistry* 270(17):10171-10178.

85. Joshi A, Serpe M, & Kosman DJ (1999) Evidence for (Mac1p)(2)center dot DNA ternary complex formation in Mac1p-dependent transactivation at the CTR1 promoter. *Journal of Biological Chemistry* 274(1):218-226.

CHAPTER 2

COORDINATION CHEMISTRY OF MONOVALENT COPPER LIGANDS: A NEW SET OF COLORLESS, WATER-SOLUBLE, AND AIR-STABLE AFFINITY STANDARDS

Copper(I) binding affinities of small molecules and proteins reported in the literature are largely inconsistent and thus incomparable. This is primarily because of a lack of unified affinity standards. In this chapter, Cu(I) stability constants of several monovalent ligands were determined unequivocally and a new set of sulfonated thioether-based ligands were developed that form colorless, water-soluble, and air-stable copper complexes. These robust Cu(I) affinity standards were then applied to measure stability constants of other Cu(I)-ligands or proteins.

2.1. Background

The major challenge of copper homeostasis is to strike a balance between maintaining bioavailability of copper and controlling free intracellular copper concentration. Numerous copper binding proteins are critical components of this homeostatic machinery. They function in unification to buffer the cellular copper pool such that to ensure the accessibility of the metal ion for the intended cellular functions while protecting the cells from copper toxicity (1). In order to understand the mechanism of copper transport through these interconnected pathways at the molecular level, knowledge about the Cu(I)-binding affinities of these proteins is crucial. This section will discuss different aspects of metal-ligand equilibrium encountered in binding affinity measurements of copper(I) complexes.

.

2.1.1. Metal Affinity of a Ligand

The experimental determination of binding affinity of a ligand L (or protein) to a metal ion (M) with 1:1 stoichiometry relies on the equilibrium description according to eqn. (2.1):

$$M + L \rightleftharpoons ML \; ; \qquad K_c = \frac{[ML]}{[M][L]} \tag{2.1}$$

where K_c refers to the stoichiometric equilibrium constant. Binding affinity of a ligand can also be described as stability constant or formation constant. On the other hand, the metal binding affinity of a protein is often expressed in terms of dissociation constant which can be defined by eqn. (2.2):

$$K_d = {}^{1}/_{K_c} = \frac{[M][L]}{[ML]} \tag{2.2}$$

Similar to eqn. (2.1), binding interaction for a 1:2 complex formation is given by eqn. (2.3),

$$M + 2L \rightleftharpoons ML_2 \; ; \qquad \beta_2 = \frac{[ML_2]}{[M][L]^2} \tag{2.3}$$

where β_2 is known as the overall stability constant. Eqn. (2.3) can also be written in terms of stepwise equilibrium constants (K_1 and K_2) according to eqn. (2.6):

$$M + L \rightleftharpoons ML \; ; \qquad K_1 = \frac{[ML]}{[M][L]} \tag{2.4}$$

$$ML + L \rightleftharpoons ML_2 \; ; \qquad K_2 = \frac{[ML_2]}{[ML][L]} \tag{2.5}$$

The overall stability constant, β_2, is obtained by multiplying equations (2.4) and (2.5):

$$\beta_2 = K_1 \times K_2 = \frac{[ML_2]}{[M][L]^2} \tag{2.6}$$

2.1.2. Ionic Strength Dependence of Binding Affinity

In Section 2.1.1, binding affinity (K_c) was defined as stoichiometric stability constant where all species in the equilibrium were expressed in terms of molar concentrations. However, the position of most solution equilibria involving ions is dependent on the concentrations and the charges of the electrolytes present in the medium. This electrolyte effect results from the attractive and repulsive electrostatic forces that exist between the ions of an electrolyte and the ions involved in a metal-binding equilibrium. To account for the effects of electrolytes on chemical equilibria, binding affinities should ideally be expressed as thermodynamic stability constants ($K°$) by eqn. (2.7),

$$K^\circ = \frac{a_{ML}}{a_M \times a_L} \tag{2.7}$$

where a_x represents the activity of each species.

The activity, or effective concentration, of a species X is defined by eqn. (2.8),

$$a_x = [X] \,.\, \gamma_x \tag{2.8}$$

where [X] is the molar concentration of X and γ_x is the activity coefficient. The activity coefficient and thus the activity of X depend on the ionic strength of the medium according to the Debye Huckel equation (2.9) (2):

$$-\log \gamma_x = \frac{A\, z_x^2 \sqrt{\mu}}{1 + B\, \alpha_x \sqrt{\mu}} \tag{2.9}$$

where z_x = charge of the species X; α_x = effective diameter of the hydrated ion X in angstrom; μ = ionic strength of the solution; A and B = constants which are the functions of the temperature and the dielectric constant of a solvent. A and B adopt the values of 0.51 and 0.33 , respectively at 25 °C in aqueous solution (3). The ionic strength of a solution is defined by eqn. (2.10),

$$\mu = \frac{1}{2}\sum_{i=1}^{n} c_i \, z_i^2 \qquad (2.10)$$

where c_i = molar concentration of ion i, z_i = charge of that ion, and the sum is taken over all ions in the solution.

By substituting eqn. (2.8) in eqn. (2.7), $K°$ can be written as:

$$K^{\circ} = \frac{[ML]}{[M][L]} \times \frac{\gamma_{ML}}{\gamma_M \ \gamma_L} \qquad (2.11)$$

Combining equations (2.1) and (2.11), $K°$ and K_c can be related by eqn. (2.12).

$$K^{\circ} = K_c \times \frac{\gamma_{ML}}{\gamma_M \ \gamma_L} \qquad (2.12)$$

Theoretically, $K°$ for a metal-ligand equilibrium can be calculated from the knowledge of K_c and the activity coefficients of the species in equilibrium. In order to determine K_c, molar concentrations of the species present in a metal-binding equilibrium can be measured conveniently by most analytical methods. However, their activity coefficients cannot be computed reliably using the Debye Huckel equation (Eqn. (2.9)), partly because of the uncertainty in the extrapolation of the experimental parameters to infinite dilution, which is necessary for the measurements of the activity coefficients, and partly because of the inconsistencies in determining the effective diameter values (α_x) (4,

5). For these reasons, stoichiometric stability constants (K_c) are used instead of thermodynamic stability constants ($K°$) for binding affinity measurements.

It can be followed from eqn. (2.9) that at very dilute solution, when $\mu \rightarrow 0$, $\gamma_x \rightarrow 1$, hence under this condition $K°$ is equal to K_c, but for all practical purposes, $K° \neq K_c$. Under such conditions, where μ is a non-zero number, activity coefficient (γ_x) has a negative correlation with the ionic strength (μ) of the medium. Nevertheless, γ_x is constant at a given μ and consequently the degree of deviation of $K°$ from K_c does not vary when the ionic strength remains unchanged. Experimentally, this condition can be achieved by using a large excess of an inert background electrolyte that does not chemically interact with any of the species in equilibrium. Moreover, different electrolytes composed of ions of the same charge have same ionic strength at a given concentration, but their activity coefficients will vary due to different effective diameters. Therefore, it is utmost important to specify the concentration and the nature of the electrolyte while reporting binding affinity values such that the data acquired under the same conditions can be compared directly.

2.1.3. Concept of Apparent Stability Constant: pH-dependence of Binding Affinity

The binding affinity of a ligand as defined by eqn. (2.1) is the simplest representation of a metal-ligand equilibrium. Usually, there are at least two other competing equilibria associated with metal coordination in aqueous solution; one is the hydrolysis of the aquated metal ion (2.13) and the other is the protonation of the ligand (2.14). The charges associated with metal complexes and protonated ligands are ignored in the following equations for the sake of convenience.

$$M(H_2O)_x + H_2O \rightleftharpoons M(OH)(H_2O)_{x-1} + H_3O^+ \quad (2.13)$$

$$L + nH_3O^+ \rightleftharpoons LH_n + nH_2O \quad (2.14)$$

In order to simplify the measurement of stability constants in presence of these competing equilibria, Gerold Schwarzenbach introduced the concept of apparent or conditional stability constants (6). Metal-ligand equilibrium for a 1:1 complex defined in terms of apparent binding affinity takes the form of eqn (2.15).

$$K' = \frac{[ML]}{[M'][L']} \tag{2.15}$$

Here, M′ refers to all metal ion species that are not complexed by the ligand L, i.e.,

$$[M'] = [M] + [MA] + [MA_2] + \ldots\ldots + [MA_n] = \alpha_M\,[M] \tag{2.16}$$

where, A refers to any auxiliary complexing agent including H_2O as in eqn. (2.13). Similarly, L′ refers to all forms of ligands that are not bound to the metal ion. i.e.,

$$[L'] = [L] + [LH] + [LH_2] + \ldots\ldots + [LH_n] = \alpha_L\,[L] \tag{2.17}$$

According to Schwarzenbach's definition, stoichiometric (as expressed by eqn. (2.1)) and conditional stability constants of a metal-ligand complex are related by eqn. (2.18).

$$K' = \frac{[ML]}{\alpha_M[M] \times \alpha_M[L]} = \frac{K_c}{\alpha_M\,\alpha_L} \tag{2.18}$$

Based on eqn. (2.16), we can write

$$\alpha_M = \frac{[M']}{[M]} = \frac{[M] + [MA] + [MA_2] + \ldots\ldots + [MA_n]}{[M]}$$

or,

$$\alpha_M = 1 + \frac{[MA]}{[M]} + \frac{[MA_2]}{[M]} + \ldots\ldots + \frac{[MA_n]}{[M]} \tag{2.19}$$

For metal-induced hydrolysis (eqn. (2.13)), equilibrium constant K_M is given by

$$K_M = \frac{[M(OH)(H_2O)_{x-1}]\,[(H_3O)^+]}{[M(H_2O)_x]} \tag{2.20}$$

Thus, for a metal hydrolysis equilibrium, it can be written from eqn. (2.19),

$$\alpha_M = 1 + \frac{[M(OH)(H_2O)_{x-1}]}{[M(H_2O)_x]} = 1 + \frac{K_M}{[(H_3O)^+]} \tag{2.21}$$

Alternatively,

$$\alpha_M = 1 + 10^{(pH - pK_M)} \tag{2.22}$$

where, $pH = -\log[H_3O^+]$ and $pK_M = -\log K_M$.

Similarly, for a ligand with two protonation sites, eqn. (2.14) can be written by,

$$\begin{aligned} L + H_3O^+ &\rightleftharpoons LH + H_2O \\ L + 2H_3O^+ &\rightleftharpoons LH_2 + 2H_2O \end{aligned} \tag{2.23}$$

Now, from eqn. (2.17),

$$\alpha_L = \frac{[L']}{[L]} = \frac{[L] + [LH] + [LH_2]}{[L]} = 1 + \frac{[LH]}{[L]} + \frac{[LH_2]}{[L]} \tag{2.24}$$

or,

$$\alpha_L = 1 + \frac{[H_3O^+]}{K_{H1}} + \frac{[H_3O^+]^2}{K_{H1}K_{H2}} \tag{2.25}$$

where, K_{H1}, K_{H2} are the acid dissociation constants for the first and second protons , respectively.

Alternatively,

$$\alpha_L = 1 + 10^{(pK_1 - pH)} + 10^{(pK_1 + pK_2 - 2pH)} \quad (2.26)$$

where, $pK_1 = -\log K_{H1}$ and $pK_2 = -\log K_{H2}$

Substituting equations (2.22) and (2.26) in eqn. (2.18), the correlation between stoichiometric and conditional stability constants yields,

$$K' = \frac{K_c}{[1 + 10^{(pH - pK_M)}][1 + 10^{(pK_1 - pH)} + 10^{(pK_1 + pK_2 - 2pH)}]} \quad (2.27)$$

The effect of pH on the apparent affinity of a ligand can be evaluated on the basis of eqn. (2.26) and (2.27). In an experiment, when the pK_a of a ligand is higher than the pH of the medium, $\alpha_L >> 1$, hence $K' << K_c$. On the other hand, for a ligand whose pK_a is lower than the pH, $\alpha_L \sim 1$, so $K' \sim K_c$, thus under this condition the effect of pH is negligible.

2.1.4. Challenges in Determination of Cu(I) Stability Constants

The major challenge in measurement of Cu(I) affinity is the redox lability of aqueous Cu^+ ions which is not only susceptible towards oxidation but also towards disproportionation into Cu^{2+} (aq) and Cu^0 (s) at acidic pH or precipitation as Cu_2O at neutral or basic pH (7). However, Cu^+ ions can be stabilized in aqueous solution in presence of ligands that favor Cu(I)-complexes by shifting the reduction potentials of ligand bound Cu(II/I) towards more positive values (8). This is indeed the case under the physiological condition where several high-affinity Cu(I) ligands (or proteins) sequester the copper ions resulting in a very low intracellular free Cu^+ (aq) concentration in eukaryotic cells (9).

Another challenge is that the binding affinities of the majority of biologically relevant Cu(I)-complexes are in the range of 10^{12} M^{-1} or higher (10, 11); which means

for a 1:1 copper-ligand complex with binding affinity of 10^{12} M^{-1}, 50% of the ligand is metal bound at 10^{-12} M concentration of the copper ions. However, sensitivity of common detection methods is usually in the micromolar (10^{-6} M) range. At such high concentrations, the fractional saturation of ligands with high affinities is near unity, but the accurate determination of stability constants requires a fractional saturation range of 0.2-0.8, fractional saturation being defined as the ratio of metal-complex to added metal ion (12). Therefore, the instability of redox active Cu^{+} (aq) ions and often the high affinity of ligands preclude direct measurements of stability constants of Cu(I)-complexes by simply titrating the Cu^{+} ions with the ligands.

One of the solutions to the problems outlined above is determination of the Cu(I)-stability constant of the ligand under study in presence of a competing ligand (affinity standard) whose Cu(I) affinity is comparable to that of the ligand being measured. This strategy can shift the position of the original complexation equilibrium towards a reliable fractional saturation window. Additionally, under this condition, the equilibrium concentration of free Cu^{+} (aq) is usually very low such that neither disproportionation nor oxidation is thermodynamically favorable. This method relies on the accurate stability constant data of the affinity standard. The major pitfall of this method is ternary complex formation where the copper ion is simultaneously bound to both ligands.

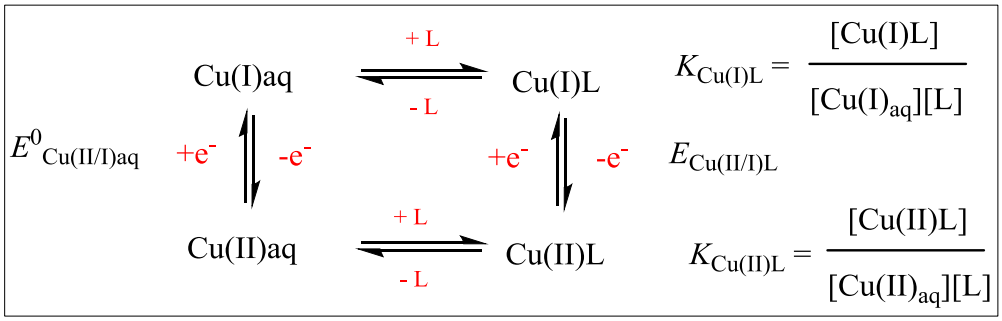

Scheme 2.1: *Thermodynamic Cycle*

Alternatively, the Cu(I) stability constant of a ligand can be determined indirectly from its Cu(II)-complexation equilibrium, which is the most common approach found in the literature. This method takes advantage of the thermodynamic cycle as described in Scheme 2.1, where Cu(I) affinities are calculated from the experimentally determined Cu(II) stability constants and the formal potentials of the ligand-bound Cu(II/I) redox couples according to eqn. (2.28).

For a thermodynamic cycle as depicted in Scheme 2.1, the free energy change of Cu(I)-complexation equilibrium takes the form of eqn. (2.28) by utilizing the Nernst relationship for a one electron redox process,

$$-RT\ln K_{\mathrm{Cu(I)L}} = FE^{0}_{\mathrm{Cu(II/I)aq}} - RT\ln K_{\mathrm{Cu(II)L}} - FE_{\mathrm{Cu(II/I)L}}$$

or,

$$E_{\mathrm{Cu(II/I)L}} = E^{0}_{\mathrm{Cu(II/I)aq}} - \frac{2.303\,RT}{F}\log\frac{K_{\mathrm{Cu(II)L}}}{K_{\mathrm{Cu(I)L}}} \qquad (2.28)$$

where $E_{\mathrm{Cu(II/I)L}}$ = formal potential of ligand bound Cu(II/I) couple; $E^{0}_{\mathrm{Cu(II/I)aq}}$ = standard reduction potential of the aqueous Cu(II/I) couple; F = Faraday constant; R = universal gas constant; T = temperature in Kelvin.

This method is only applicable for complexes with thermodynamically reversible redox potential. Although Cu(II) affinities and $E_{\mathrm{Cu(II/I)L}}$ values can be determined conveniently, there is a discrepancy in the literature regarding the value of $E^{0}_{\mathrm{Cu(II/I)aq}}$. In a recent publication, Xiao et al. (10) referred to a value of 0.164 V (13), whereas Bernardo et al. (14) calculated this value to be 0.13 V by correcting another literature value of this redox potential (0.153 V) (15) with the activity coefficients as described below. Depending on the literature value used for $E^{0}_{\mathrm{Cu(II/I)aq}}$, the resultant Cu(I) stability constant of a particular ligand can vary by a factor of 4 or $\Delta\log K_{\mathrm{Cu(I)L}} = 0.6$.

At 25 °C, for the redox process,

$$Cu^{2+}\,(aq) + e \rightleftharpoons Cu^{+}\,(aq)$$

the half-cell potential can be written as:

$$E = E^0_a - 0.059\ \log\frac{a_{Cu^+}}{a_{Cu^{2+}}} \tag{2.29}$$

where E^0_a = standard reduction potential defined by the value of E at infinite dilution when the ionic strength of the medium practically equals to zero and the activity coefficients of the ions are unity according to the IUPAC convention (16). In order to apply the reduction potential E^0_a in a solution of 0.1 M ionic strength, Bernardo et al. proposed the following conversion of the standard reduction potential (E^0_a) to the "concentration potential".

Substituting eqn. (2.8) into eqn (2.29),

$$E = E^0_a - 0.059\ \log\frac{[Cu^+]\gamma_{Cu^+}}{[Cu^{2+}]\gamma_{Cu^{2+}}}$$

or,

$$E = E^0_a - 0.059\ \log\frac{\gamma_{Cu^+}}{\gamma_{Cu^{2+}}} - 0.059\ \log\frac{[Cu^+]}{[Cu^{2+}]}$$

or,

$$E = E^0_c - 0.059\ \log\frac{[Cu^+]}{[Cu^{2+}]} \tag{2.30}$$

where $E^0_c = E^0_a - 0.059\ \log\frac{\gamma_{Cu^+}}{\gamma_{Cu^{2+}}}$ = "concentration potential".

Theoretically, the activity coefficients of ions in aqueous solution can be determined by the Debye-Huckel equation (eqn. (2.9)); however, the validity of the

Debye-Huckel theory is limited to the completely dissociated electrolytes, a condition that can only be achieved at infinite dilution. Therefore, C.W. Davies recommended a correction of the original Debye-Huckel equation in order to include ion-association commonly present at concentrations used for any practical measurement of activity coefficient (17). The proposed equation for an aqueous solution at 25 °C is given by,

$$-\log \gamma_x = 0.5\, z_x^2 \left(\frac{\sqrt{\mu}}{1+\sqrt{\mu}} - 0.2\, \mu \right) \tag{2.31}$$

Calculating from eqn. (2.31), $\gamma_{Cu}{}^{+}$ becomes 0.78 and $\gamma_{Cu}{}^{2+}$ equals to 0.36 at 0.1 M ionic strength. Therefore, under this condition, following eqn. (2.30) the "concentration potential" (E^0_c) becomes 0.13 V by subtracting 0.02 V from the standard reduction potential (E^0_a).

Table 2.1. *Apparent Affinities of Selected Human Cu(I)-Binding Proteins*

Protein	**Experimental Method**	**Competing Ligand**	**pH**	**Binding Affinity (M^{-1})**	**Ref.**
CCS	ESI-MS	DTT	7.5	4.2×10^{14}	(18)
WT- CCS	UV-vis spectroscopy	BCA	6.5	1.1×10^{17}	(19)
	UV-vis spectroscopy	BCS	7.5	5.5×10^{17}	(19)
			6.5	4.4×10^{16}	(19)
CCS –	UV-vis spectroscopy	BCS	7.5	5.5×10^{17}	(19)
Domain1			6.5	5.6×10^{16}	(19)
CCS –	UV-vis spectroscopy	BCA	7.5	6.4×10^{16}	(19)
Domain 3			6.5	4.2×10^{15}	(19)
SOD1	ESI-MS	DETC	7.5	4.3×10^{15}	(18)
SOD1	UV-vis spectroscopy	PAR	7.4	1.7×10^{17}	(20)

Table 2.1. *Continued*

Protein	Experimental Method	Competing Ligand	pH	Binding Affinity (M^{-1})	Ref.
Atox1 or Hah1	UV-vis spectroscopy	BCS	7.0	5.6×10^{17}	(21)
			7.0	2.5×10^{17}	(11)
	ESI-MS	DTT	7.5	6.0×10^{13}	(18)
	UV-vis spectroscopy	BCA	7.5	3.5×10^{10}	(22)
	ITC		6.5	2.5×10^{5}	(23)
ATP7A	UV-vis spectroscopy	BCS	7.0	3.6×10^{17}	(21)
(MBD-1)	ESI-MS	DTT	7.5	4.0×10^{14}	(18)
	Equilibrium dialysis against Cu(I)		7.4	2.6×10^{4}	(24)
ATP7A (MBD-2, 5, 6)	ESI-MS	DTT	7.5	7.7×10^{13} – 3.8×10^{14}	(18)
ATP7A (MBD-3)	ESI-MS	DTT	7.5	9.6×10^{12}	(18)
ATP7B (MBD 1-6)	UV-vis spectroscopy	BCA	7.5	2.2×10^{10} – 6.3×10^{10}	(22)
	ITC		6.5	2.1×10^{5} – 4.7×10^{6}	(23)
ATP7B (MBD 5-6)	UV-vis spectroscopy	BCS	7.0	4.0×10^{17}	(10)
Cox 17	ESI-MS	DTT	7.5	5.7×10^{13}	(18)
Sco1	ESI-MS	DTT	7.5	3.2×10^{14}	(18)
Sco2	ESI-MS	DTT	7.5	2.7×10^{14}	(18)

In addition to ternary complex formation during competition experiments and anomalous $E^{0}_{Cu(II/I)aq}$ values in the literature, reliable determination of binding affinity also suffers from other factors, including the lack of effective competition equilibrium, change of pH during measurement, aerial oxidation of Cu^{+} ions and binding sites, and

incorrect analysis of the experimental data. Therfore, it is not surprising that there is a lack of consensus in the literature regarding the binding affinities of Cu(I) ligands (and proteins). A compilation of apparent stability constants of Cu(I)-proteins in Table 2.1 shows as large as 12-13 orders of magnitude difference in the values for some proteins such as Atox1. These discrepancies are too large to be explained by the differences in the pH values of the measurements and are much more dependent on the methods of determination. In this context, the reliability of the Cu(I) ligands used as affinity standards in the equilibrium competitions are of major contributing factors.

Monodentate ligands such as cyanide (25) or thiourea (26) bind copper ions strongly but with multiple coordination stoichiometry. Although these ligands are employed as Cu(I) affinity standards, they are prone to ternary complex formation during competition experiments with ligands under study, especially in presence of vacant Cu(I) coordination sites as Cu(I) can adopt a coordination number of up to four (27). In fact, Cu(I) in low-coordinate protein complexes has been shown to form heterodimers in biology (28, 29). Dithiothreitol (DTT), typically employed as a reducing agent for protein disulfides, has also been utilized as a competing ligand in determining Cu(I)-binding affinities of proteins (Table 2.1). However, due to its high reactivity with oxygen and variable coordination stoichiometry, the utility of this ligand is dubious (10).

It is evident from Table 2.1 that BCS and BCA are widely used as competing ligands. These ligands form colored 2:1 Cu(I)-complexes and the complexation can be easily followed by increase in the absorbance at 483 nm for BCS and at 562 nm for BCA, a wavelength region where most Cu(I)-ligands including proteins do not absorb. However, reported log β_2 values for 2:1 complex formation with these ligands rarely converge to a consensus value (Table 2.2). Evidently use of these divergent values of affinity standards to determine the stability constants of other ligands (and proteins) results in a progression of errors in the literature. Furthermore, these bidentate chelators, though more sterically restricted than small monodentate ligands such as cyanide and

thiourea, are still likely to form ternary complex, especially with other ligands that form low-coordinate complexes. As previously mentioned by Xiao et al. (10), this was presumably a source of error in an earlier attempt to determine the Cu(I)-affinity of BCS by competition with cyanide (30).

In order to address these problems, we characterized the thermodynamic properties of a set of copper chelators featuring a wide range of affinities which can be reliably used as Cu(I) affinity standards. In this work, three new monovalent copper ligands were developed which form air-stable, water soluble Cu(I)-complexes with 1:1 metal-ligand stoichiometry that do not absorb in the near-UV and visible range. Their Cu(I) stability constants together with three other copper chelators from the literature, including PEMEA, BCA, and BCS, were determined reliably by independent titrations and cross-verifications with other ligands. The consolidated stability constants of these ligands encompass an affinity range over seven orders of magnitude. This will allow us to use this set of robust affinity standards to determine stability constants of a wide array of new ligands including proteins.

Table 2.2. *Previously Reported Stability Constants of Selected Cu(I) Affinity Standards*

Ligand	**Experimental Method**	**log β_2**	**Ref.**
BCA	ITC	14.7	(22)
	Direct titration with Cu(I)	11.4	(30)
	Indirect competition with BCS	16.7	(31)
		17.2	(32)
		17.3	(10)
BCS	Bjerrum's method	19.5	(13)
		19.8	(33)
		19.9	(10)
	Competition with cyanide (CN^-)	22.5	(30)

2.2. Results and Discussion

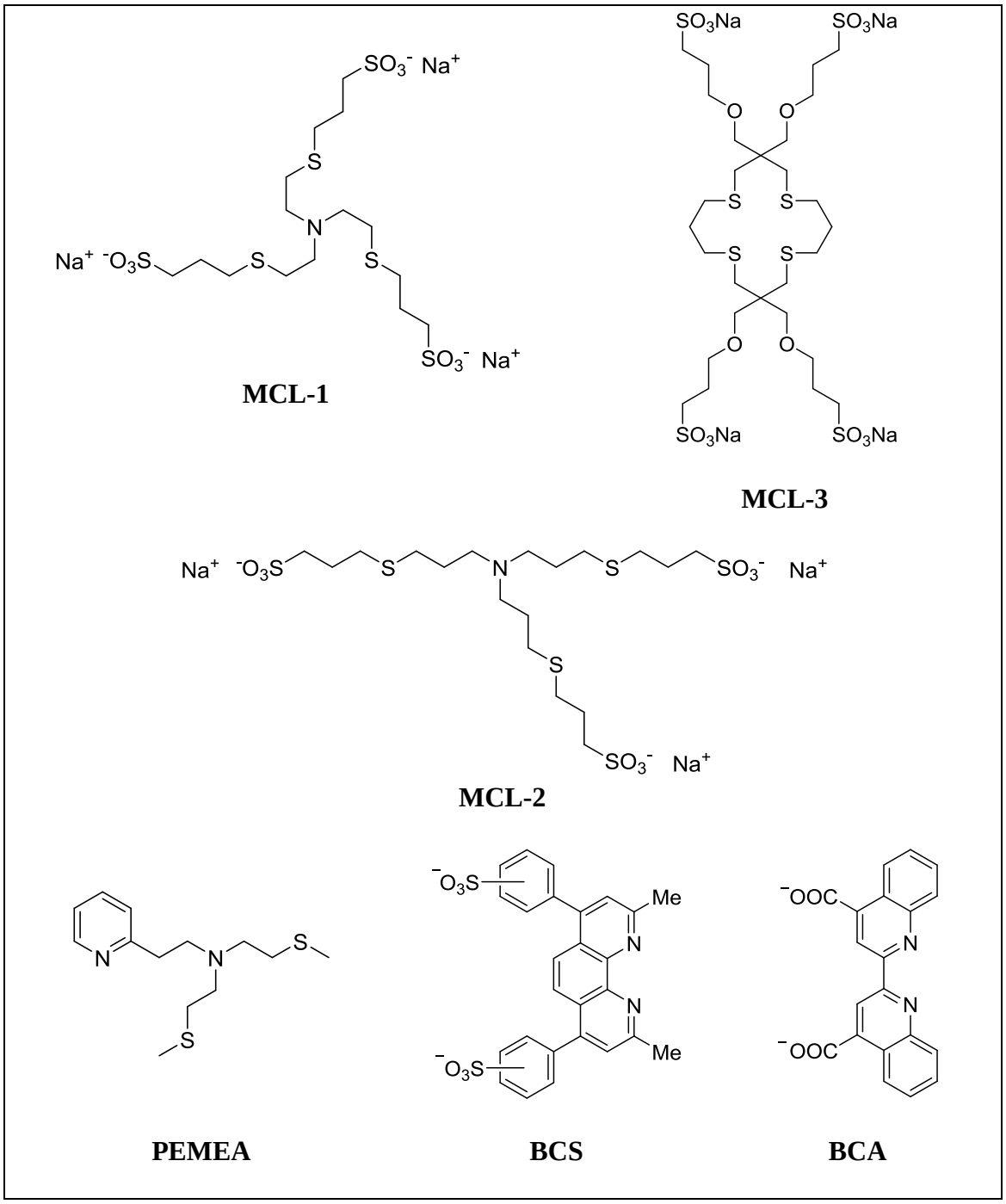

Figure 2.1. *Molecular Structures of Copper(I) Affinity Standards*

The copper(I) ligands studied in this work are shown in Figure 2.1. Three new ligands, MCL-1, MCL-2, and MCL-3, were synthesized by Dr. M. T. Morgan along with the literature compounds PEMEA and DHEAMP. The ligands BCA and BCS are commercially available.

The thermodynamic properties of copper complexes with tetradentate sulfur-rich ligands, including tripodal thioether-amines (8) and thiocrown macrocycles (34), have been extensively evaluated by Rorabacher and coworkers. These ligands often form air-stable Cu(I) complexes with 1:1 metal-ligand stoichiometry. By saturating the Cu(I) coordination sphere, these tetradentate chelators are expected to provide greater resistance to ternary complex formation than monodentate ligands, which is a prerequisite during competition experiments in determining stability constants of Cu(I)-complexes. Moreover, these ligands often exhibit a directly measurable low to moderate Cu(II)-binding affinities and electrochemically reversible redox cycling between Cu(II) and Cu(I) complexes, allowing the relatively high Cu(I)-binding affinity to be calculated from the thermodynamic cycle (eqn. (2.28)). Furthermore, the Cu(I)-complexes of aliphatic polythioethers are typically colorless (8), and hence these chelators can be potentially used as affinity standards in spectrophotometric competition titrations where the copper complex formation of the ligand under study can be monitored in the near-UV and visible range without any interference from the standards. Despite of these favorable properties of the thioether-rich tetradentate Cu(I)-ligands previously characterized by Rorabacher et al., these compounds, being poorly water soluble, have limited applicability as affinity standards particularly in aqueous solution. In order to design water soluble polythioether-based Cu(I) ligands, Dr. M. T. Morgan in the Fahrni lab introduced solubilizing groups by modifying the lipophilic ligand frameworks previously published in the literature. For example, TMMEA and TEMEA (8) were used as starting points for the design of MCL-1, while [16]aneS_4 was a precursor for MCL-3 ligand (34).

Protonation Constant of MCL-1

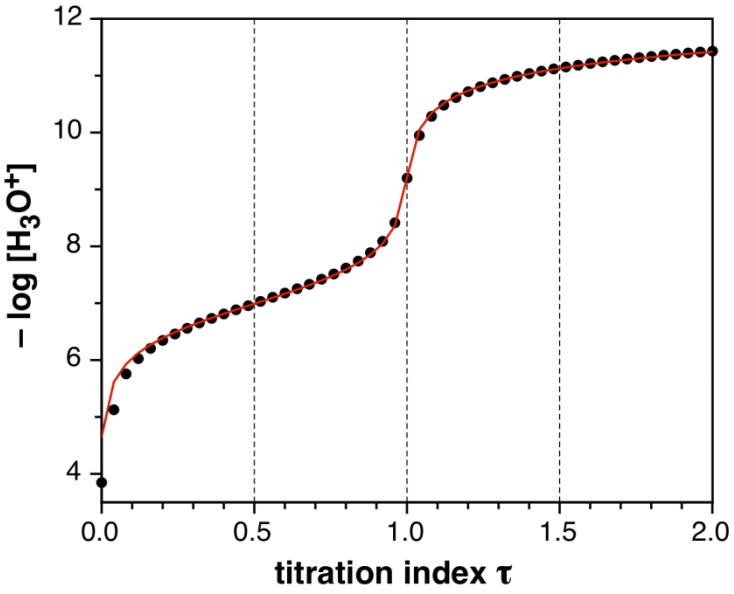

Protonation Constant of MCL-2

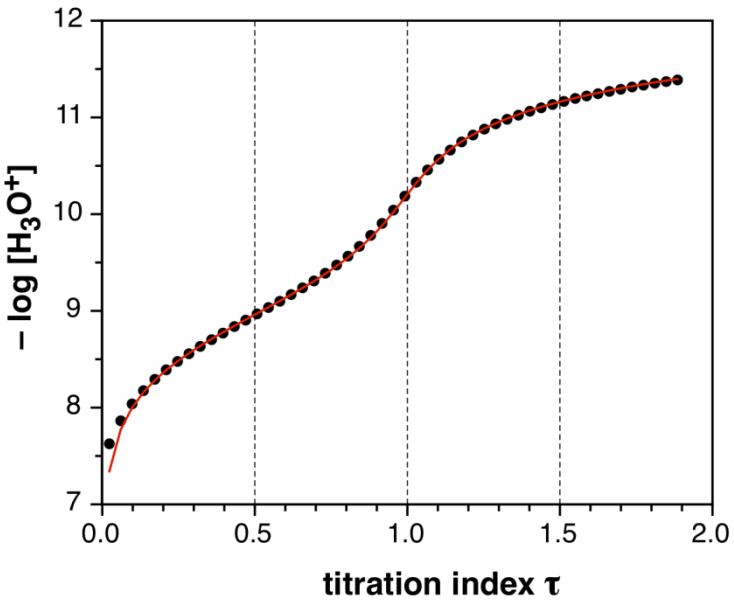

Figure 2.2. *Protonation Constants of MCL-1 and MCL-2 Determined by Acid-Base Titrations.* Fully protonated ligands (5 mM; 0.1 M KCl as an ionic background) were titrated with a standardized solution of 0.1 M KOH. Protonation constants were then determined from the potentiometric data using the Hyperquad software package (35), which yielded logK_{H1} values of 7.00±0.02 and 8.98±0.01 for MCL-1 and MCL-2, respectively.

Protonation Constant of DHEAMP

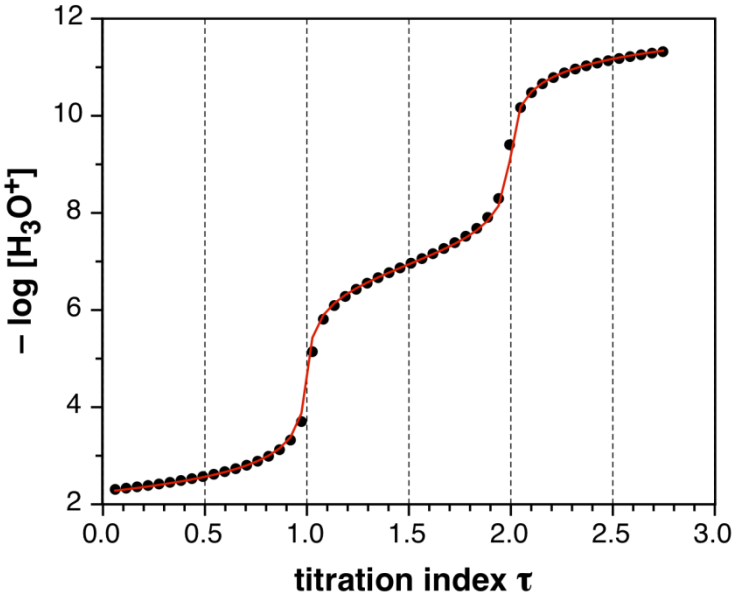

Protonation Constant of BCS

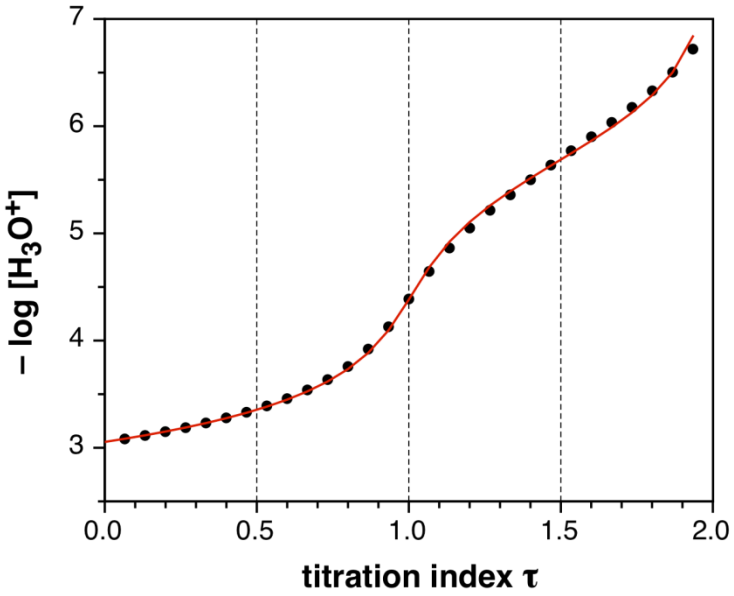

Figure 2.3. *Protonation Constants of DHEAMP and BCS Determined by Acid-Base Titrations.* Fully protonated ligands (5 mM for DHEAMP and 1 mM for BCS; 0.1 M KCl as an ionic background) were titrated with a standardized solution of 0.1 M KOH. Protonation constants were then determined from the potentiometric data using the Hyperquad software package (35), which yielded logK_{H1} values of 6.94±0.01 and 5.70±0.02 for DHEAMP and BCS, respectively.

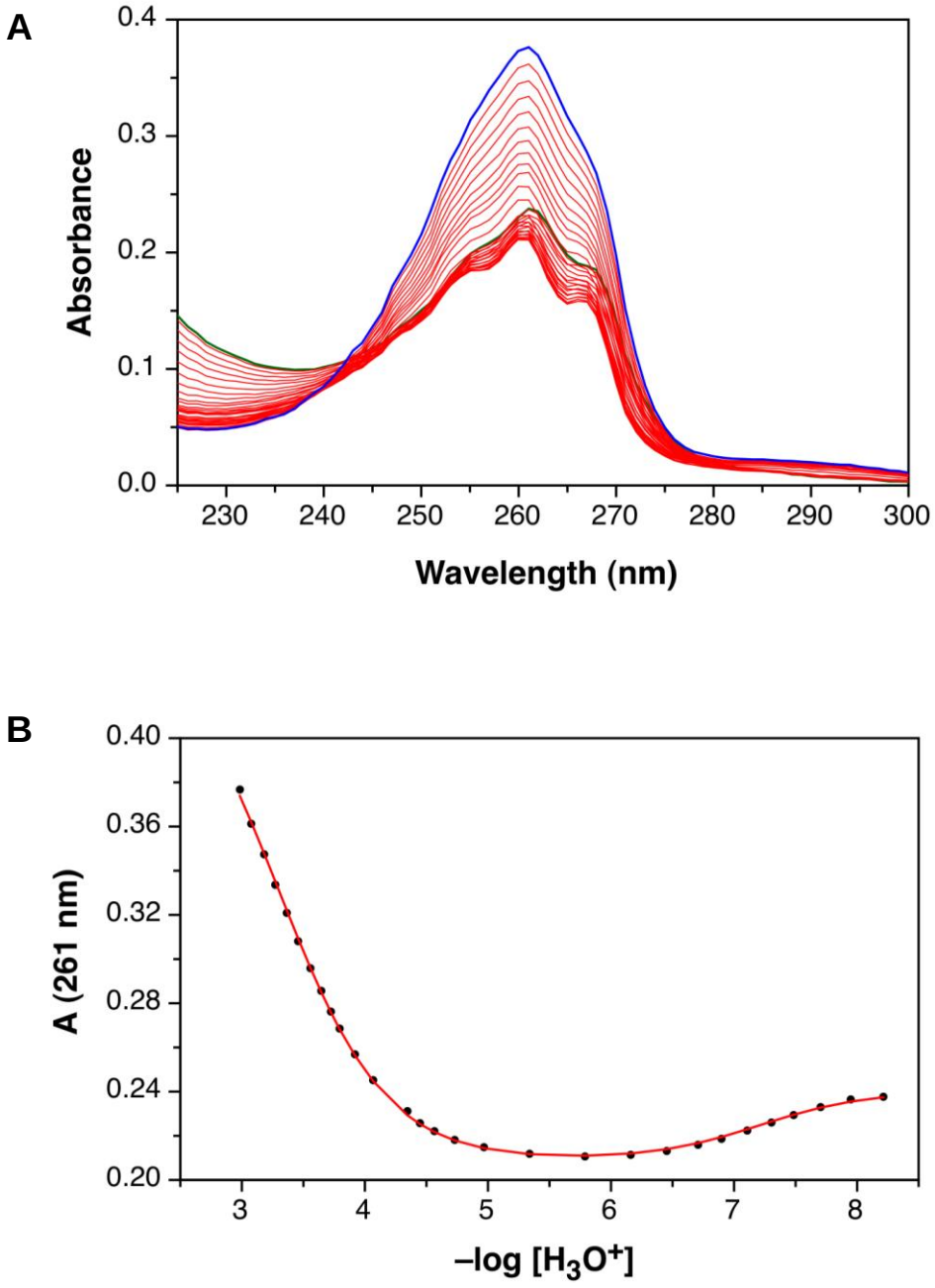

Figure 2.4. *Protonation Constant of PEMEA Determined by UV-Vis Spectroscopy*. **A.** Green trace and blue trace correspond to the UV-visible spectra at $-\log[H_3O^+]$ = 8.2 and 3, respectively. **B.** Absorbance change (black points) and curve fit (solid trace) for the titration. Spectrophotometric titrations with PEMEA (55 μM; 0.1 M KCl as an ionic background) were carried out by varying $-\log[H_3O^+]$ from 4 to 3 with the addition of HCl and from 4 to 8.2 with the addition of KOH. Protonation constants of PEMEA were then determined by non-linear least-squares fitting over the entire spectral range using the SPECFIT software package (36). Average fitted values: $\log K_{H1}$ = 7.24±0.03 and $\log K_{H2}$ = 3.23±0.04.

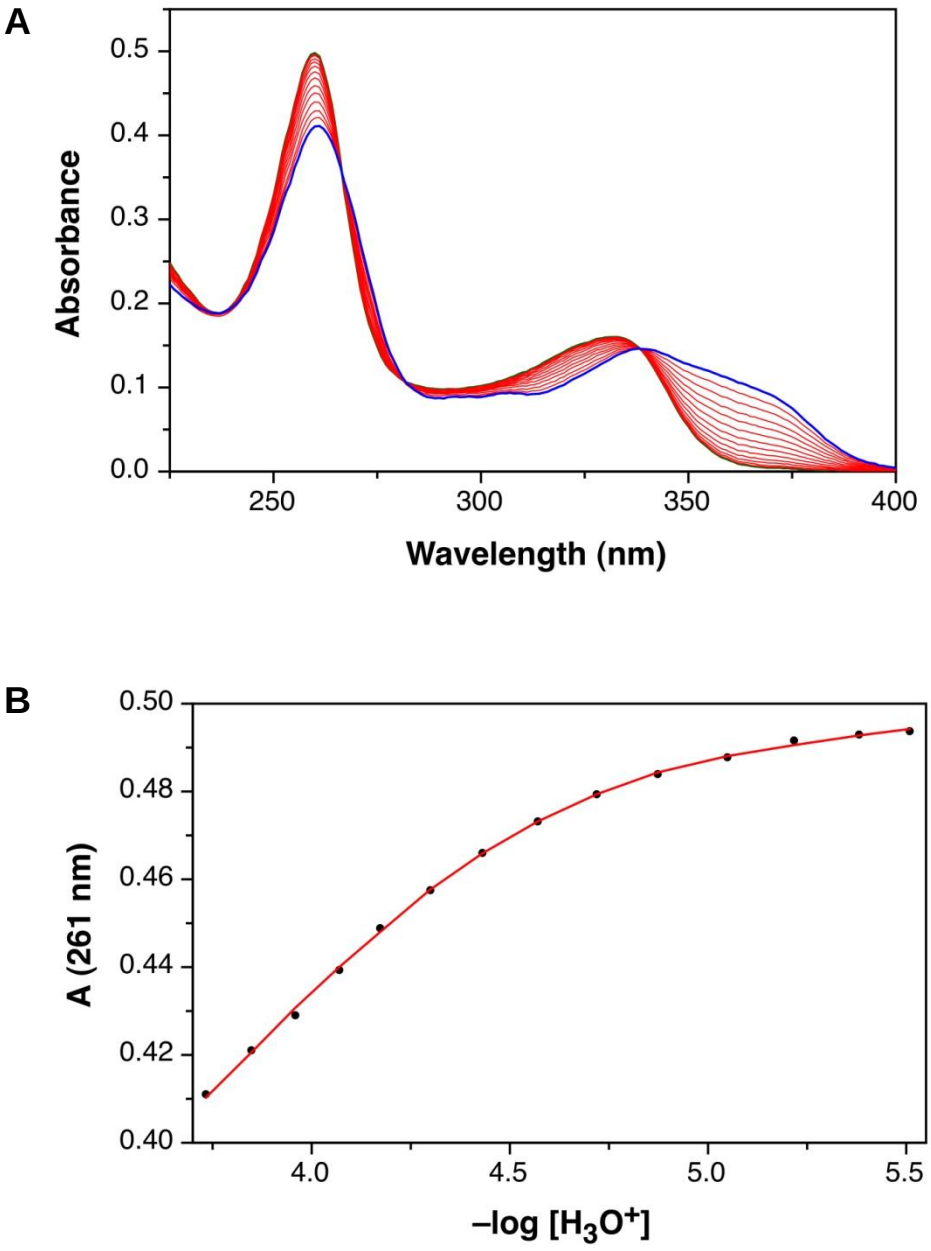

Figure 2.5. *Protonation Constant of BCA Determined by UV-Vis Spectroscopy.* **A.** Green trace and blue trace correspond to the UV-visible spectra at $-\log[H_3O^+]$ = 5.5 and 3.7, respectively. **B.** Absorbance change (black points) and curve fit (solid trace) for the titration. Spectrophotometric titrations with BCA (10 μM; 0.1 M KCl as an ionic background) were carried out by varying $-\log[H_3O^+]$ from 5.5 to 3.7 with the addition of HCl. Protonation constant of BCA was then determined by non-linear least-squares fitting over the entire spectral range using the SPECFIT software package (36). Average fitted value: $\log K_{H1} = 3.80 \pm 0.02$

Table 2.3. *Protonation Constants of the Monovalent Copper Ligands in Aqueous Solution at 25 ºC, 0.1 M KCl*

Ligand	logK_{H1}	logK_{H2}	Ref.[d]
PEMEA	7.24 (3)[a]	3.23 (4)	
	7.33 (15)[b]	3.26 (8)[b]	(8)
MCL-1	7.00 (2)		
BCA	3.80 (2)		
	3.74 (4)[c]		(37)
MCL-2	8.98 (1)		
DHEAMP	6.94 (1)		
	6.92 (1)	1.16 (9)	(38)
BCS	5.70 (2)		
	5.7		(10)

[a] The standard deviation of the mean is listed in parentheses next to the value as referenced to the last digits reported (e.g., 3.23 (4) means 3.23 ± 0.04). [b] These values were reported as mixed-mode values (See text). [c] Experiment was conducted at 0.2 M ionic strength. [d] Values stated without reference are from this work.

2.2.1. Protonation Constants

As discussed in section 2.1.3, Cu(I) stability constants of ligands with one or more basic donor atoms are pH dependent, and hence the protonation constants (logK_{Hn}) of the monovalent copper ligands were determined in this work using potentiometric titrations. With the exception of PEMEA and BCA, the fully protonated ligands were titrated with standardized KOH solutions, and logK_{Hn} values were determined from the half-neutralization points of the acid-base titration curves (Figure 2.2 and Figure 2.3). This method often requires millimolar concentrations of compounds, for example, ligand concentrations used in this work were 1 mM for BCS and 5 mM for MCL-1, MCL-2, and

DHEAMP. However, PEMEA and BCA were not soluble at millimolar concentrations in aqueous solution; therefore, the protonation constants of these ligands were determined by spectrophotometric titrations where the changes in the UV-visible spectrum were monitored as a function of $-\log[H_3O^+]$ (Figure 2.4 and Figure 2.5). Low micromolar concentrations of compounds were sufficient to obtain a measurable UV-vis response, for example, measurements were conducted at a concentration of 55 μM for PEMEA and 10 μM for BCA, and thus circumventing the solubility problems of BCA and PEMEA.

The protonation constants for all copper ligands are tabulated in Table 2.3. The $\log K_{Hn}$ values in this work are reported as concentration constants where all species present in the protonation equilibria are expressed in molar concentrations. As described in sections 2.1.2 and 2.1.3, measurements of binding affinities require a chemically inert ionic background and pH buffered at a given value. However, in the laboratory, pH's of buffer solutions are determined by pH-meter which records the activity of hydronium ion in the buffer. Such measurement of pH is influenced by the hydronium ion concentration as well as the ionic strength of the solution. Therefore, as Martell and Smith (39) suggested, at 0.1 M ionic strength, protonation constants that are based on $[H_3O^+]$ (concentration constants, $\log K_{Hn}$) must be corrected upward by 0.11 (eqn.2.32) to mixed-mode protonation constants ($\log K^{m}_{Hn}$) where hydronium ion is expressed in terms of activity and all other species in terms of molar concentrations. This correction factor is based on Debye-Huckel equation (eqn. (2.9)) as described below.

For the protonation of a ligand,

$$H_{n-1}L + H_3O^+ \rightleftharpoons H_nL + H_2O$$

the mixed-mode equilibrium constant, K^{m}_{Hn} (where n= 1,2,3,4), is given by,

$$K^{m}_{Hn} = \frac{[H_nL]}{[H_{n-1}L]\, a_{H_3O^+}}$$

or,

$$\log K_{Hn}^{m} = \log\left(\frac{[H_nL]}{[H_{n-1}L]}\right) - \log a_{H_3O^+}$$

By applying eqn. (2.8),

$$\log K_{Hn}^{m} = \log\left(\frac{[H_nL]}{[H_{n-1}L]}\right) - \log[H_3O^+] - \log(\gamma_{H_3O^+})$$

Calculating from eqn. (2.31), $-\log \gamma_{H_3O^+}$ is equal to 0.11 at 0.1 M ionic strength. Thus,

$$\log K_{Hn}^{m} = \log K_{Hn} + 0.11 \qquad (2.32)$$

where, $K_{Hn} = \frac{[H_nL]}{[H_{n-1}L][H^+]}$

Direct potentiometric titrations at 0.1 M ionic strength yielded protonation constant of 7.00±0.02 for the amine nitrogen of MCL-1. Conversion of this value which was derived from the measurement of $-\log[H_3O^+]$ to mixed-mode constant yielded a value of 7.11 for ligand MCL-1**.** This value is substantially lower than the mixed-mode protonation constants of 8.36 and 8.32 reported for the analogous ligands TMMEA and TEMEA, respectively, which were measured in aqueous solution at 0.1 M ionic strength (8). Cooper et al. also measured the protonation constant of TEMEA in 80% methanol which yielded a value of 6.34 (40). Interestingly, the authors of this paper extrapolated this value to the aqueous solution and predicted a mixed mode protonation constant of 7.1 which was identical to the value we obtained for MCL-1. Additionally, previously reported literature values of $\log K_{Hn}$ for BCS ($\log K_{H1}$ = 5.7) (10), BCA ($\log K_{H1}$ = 3.74 at 0.2 M ionic strength) (37), and PEMEA ($\log K_{H1}^{m}$ = 7.33 and $\log K_{H2}^{m}$ = 3.26) corroborated well with the values determined in this work.

Table 2.4. *Formal Potentials for the Ligand bound Cu(II/I) Redox Couples and the Stability Constants for the Cu(II) and Cu(I) Complexes in Aqueous Solution (25 °C, 0.1 M $KClO_4$).*

Ligand	$E_{1/2}$ vs. SHE $E_{Cu(II/I)L}$ [V]	Competing Ligand	Copper Source	log$K_{Cu(II)L}$	log$K_{Cu(I)L}$ from Eqn. (2.28)	log$K_{Cu(I)L}$ from Competition Titration	Eqm. No.	Ref.
PEMEA	0.595 (2)	–	$CuSO_4$	7.85 (8)	15.71 (8)	–	*r1*	
	0.595			7.89 (4)	15.76			(8)
		Acetonitrile	$[Cu(I)(CH_3CN)_4]PF_6$	–	–	15.71 (2)	*e1*	
MCL-1	0.716 (1)	–	$CuSO_4$	6.42 (2)	16.33 (2)	–	*r2*	
		PEMEA	Cu(I)-MCL-1	–	–	16.33 (7)	*e2*	
BCA	Irreversible	MCL-1	Cu(I)-MCL-1	–	–	17.67 (3)	*e3*	
		PEMEA	$[Cu(I)(CH_3CN)_4]PF_6$	–	–	17.63 (5)	*e4*	
						17.3		(10)
MCL-2	Irreversible	BCA	Cu(I)-MCL-2	–	–	13.08 (13)	*e5*	

Table 2.4 (*Continued)*

Ligand	$E_{1/2}$ vs. SHE $E_{Cu(II/I)L}$ [V]	Competing Ligand	Copper Source	log$K_{Cu(II)L}$	log$K_{Cu(I)L}$ from Eqn. (2.28)	log$K_{Cu(I)L}$ from Competition Titration	Eqm. No.	Ref.
DHEAMP	–	–	$CuSO_4$	9.21 (1)	–	–	*e6*	
				9.2 (1)				(38)
BCS	0.626 (1)	DHEAMP	$CuSO_4$	12.42 (7)	20.81 (8)	–	*r3*	
				11.8	19.9			(10)
		MCL-1	Cu(I)-MCL-1	–	–	20.80 (3)	*e7*	
			Cu(I)-MCL-2	–	–	20.81 (4)	*e7*	
MCL-3	0.729 (3)	–	$CuSO_4$	3.47 (4)			*r4*	
		BCS	Cu(I)-MCL-3	–	–	13.80 (4)	*e8*	
		BCA	Cu(I)-MCL-3	–	–	13.78 (6)	*e9*	

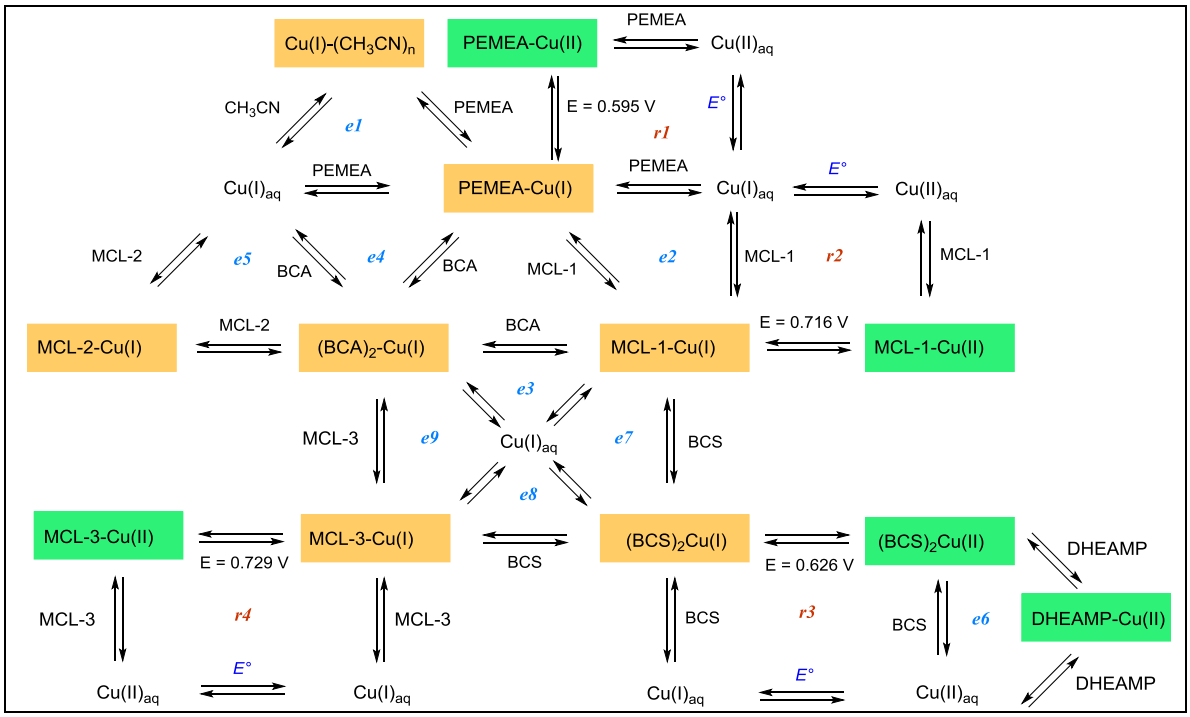

Scheme 2.2. *Schematic Representation of Thermodynamic Equilibria to Determine Stability Constants of Copper(I) Ligands.* **Orange** and **green** boxes depict Cu(I)- and Cu(II)-binding to the ligands, respectively. Stability constants derived from thermodynamic cycle are represented by equlibria ***r1-4*** and those derived from competition titrations are shown in equlibria ***e1-9***.

2.2.2. Stability Constants of Copper(I) Ligands

The thermodynamic equilibria studied in this work to determine binding affinities of copper(I) ligands are represented in Scheme 2.2. For ligands where Cu(II) and Cu(I) complexes are mutually electrochemically reversible, copper(I) stability constants were determined from the thermodynamic cycle using the Cu(II)-affinities of the ligands and formal potentials of the ligand-bound Cu(II/I) reversible redox couples. The affinity values derived this way were then verified with the ones obtained from competition titrations where two ligands competed for the Cu^{+} (aq) ions. For ligands where the redox cycling between Cu(II) and Cu(I) complexes are electrochemically irreversible, the stability constants were derived from two independent competition titrations involving two different competing ligands. A comprehensive summary of the formal potentials and

stability constants for all copper ligands determined by individual equilibrium is given in Table 2.4.

It is often difficult to compare relative binding affinities between complexes with different metal-ligand stoichiometry, e.g., 1:1 and 1:2 metal-ligand complexes. Table 2.5 describes the Cu(I) binding affinities of different ligands in terms of pCu which is equal to $-\log[Cu(I)]_{free}$ in a solution containing 10 μM ligand and 1 μM Cu(I) at pH 7. This concept was introduced by Raymond and coworkers who utilized pM values to compare the affinities of various iron-binding siderophores (41). pCu values will enable us to compare directly the binding affinities of different ligands with 1:1 and 1:2 metal-ligand stoichiometry. As an example, the absolute affinity of MCL-1 is 4.48 units lower than BCS on a logarithmic scale, but its pCu value is higher by 0.3 units. Therefore, under the same experimental conditions MCL-1 binds Cu^{+} ions more tightly than BCS, however, this conclusion cannot be drawn based on absolute affinities of these ligands.

Table 2.5. *Cu(I) and Cu(II) Stability Constants of the Copper(I) Ligands in Aqueous Solution (25 ºC, 0.1 M $KClO_4$)*

Ligand	**log$K_{Cu(II)L}$**	**log$K_{Cu(I)L}$**[a]	**log$K'_{Cu(I)L}$ at pH 7**	**pCu**[b]
PEMEA	7.85	15.71	15.20	16.2
MCL-1	6.42	16.33	15.97	16.9
BCA	-	17.66[c]	17.66	13.5
MCL-2	-	13.08	10.99	11.9
BCS	12.42	20.81[c]	20.76	16.6
MCL-3	3.47	13.80	13.80	14.8

[a] These values correspond to the mean values obtained by taking average of $\log K_{Cu(I)L}$ values weighted by the standard deviations of individual methods (Table 2.4) [b] $pCu = -\log[Cu(I)]_{free}$ for a solution containing 10 μM ligand and 1 μM Cu(I) at pH = 7; calculated by the software Hyss (42). [c] $\log\beta_2^{Cu(I)}$.

2.2.2.1. Stability Constant of PEMEA

PEMEA was first characterized by Ambundo et al. (8) who calculated the Cu(I) stability constant solely based on a thermodynamic cycle. PEMEA was chosen as a compound of interest for this work because (a) this compound forms Cu(I) and Cu(II) complexes with 1:1 stoichiometry, (b) both Cu(I) and Cu(II) complex formation can be followed by UV-vis spectroscopy, and (c) the ligand has two protonation sites. The apparent binding affinities (or conditional stability constants; Section 2.1.3) of PEMEA at different pH can be varied over a broad range because of its two substantially different protonation constant values ($\log K_{H1}$ = 7.24 and $\log K_{H2}$ = 3.23), thus making it useful as a competing ligand in determining stability constants of other ligands with a wide range of affinities.

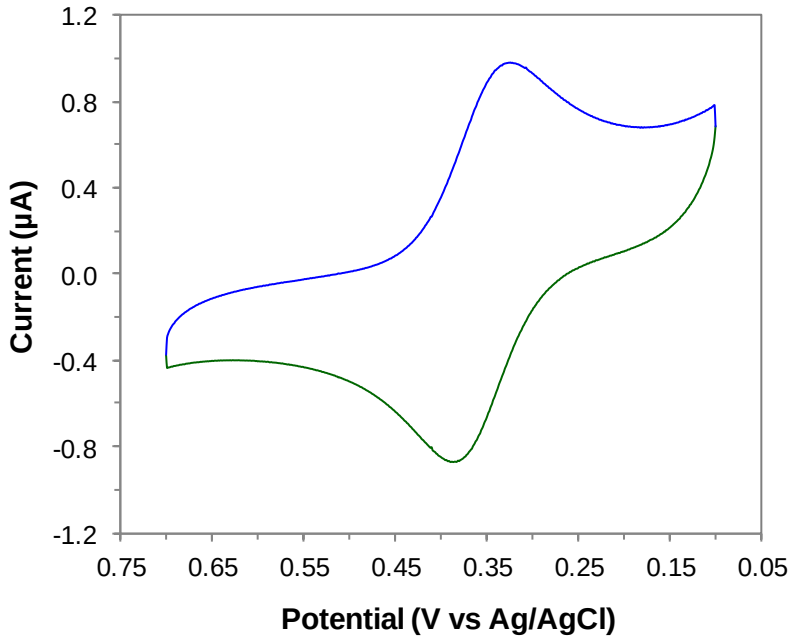

Figure 2.6. *Determination of Formal Potential of PEMEA.* Cyclic Voltammogram of PEMEA (150 µM) in presence of $CuSO_4$ (1 mM) at pH 5 (10 mM PIPBS, 0.1 M $KClO_4$); scan rate 20 mV s^{-1}. Green and blue traces correspond to the forward and the backward sweep, respectively.

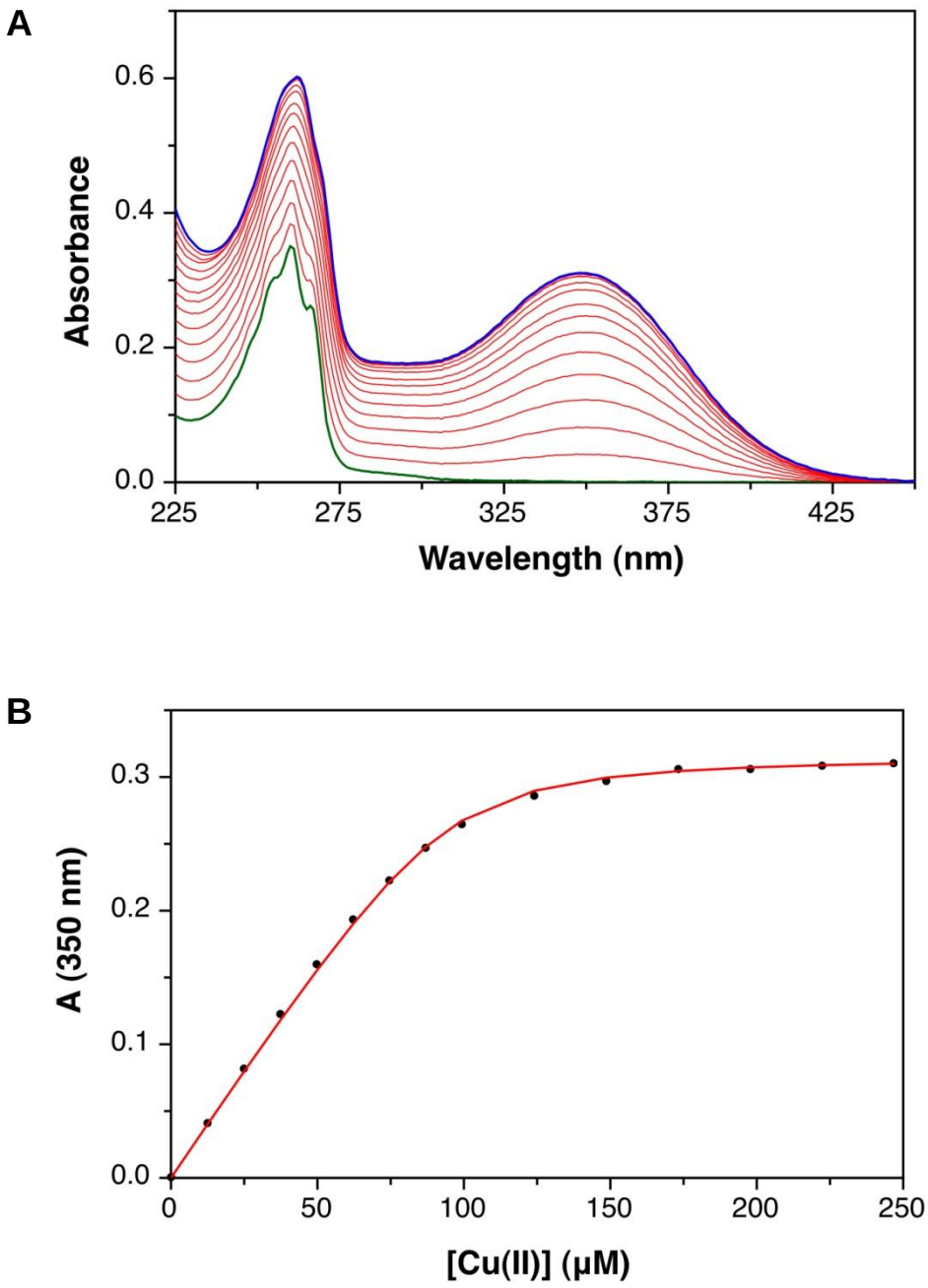

Figure 2.7. *Determination of Cu(II) Stability Constant of PEMEA: Titration of PEMEA with $CuSO_4$.* **A.** Green trace and blue trace correspond to the UV-visible spectra at [Cu(II)] = 0 and 247 μM, respectively. **B.** Absorbance change (black points) and curve fit (solid trace) for the titration. PEMEA (96 μM) was titrated with $CuSO_4$ at pH 5 (10 mM PIPBS, 0.1 M $KClO_4$, 25 °C). Cu(II) stability constant value was then determined by non-linear least-squares fitting over the spectral range 300-450 nm using the SPECFIT software package (36). Average fitted value: $\log K_{Cu(II)L} = 7.85 \pm 0.08$.

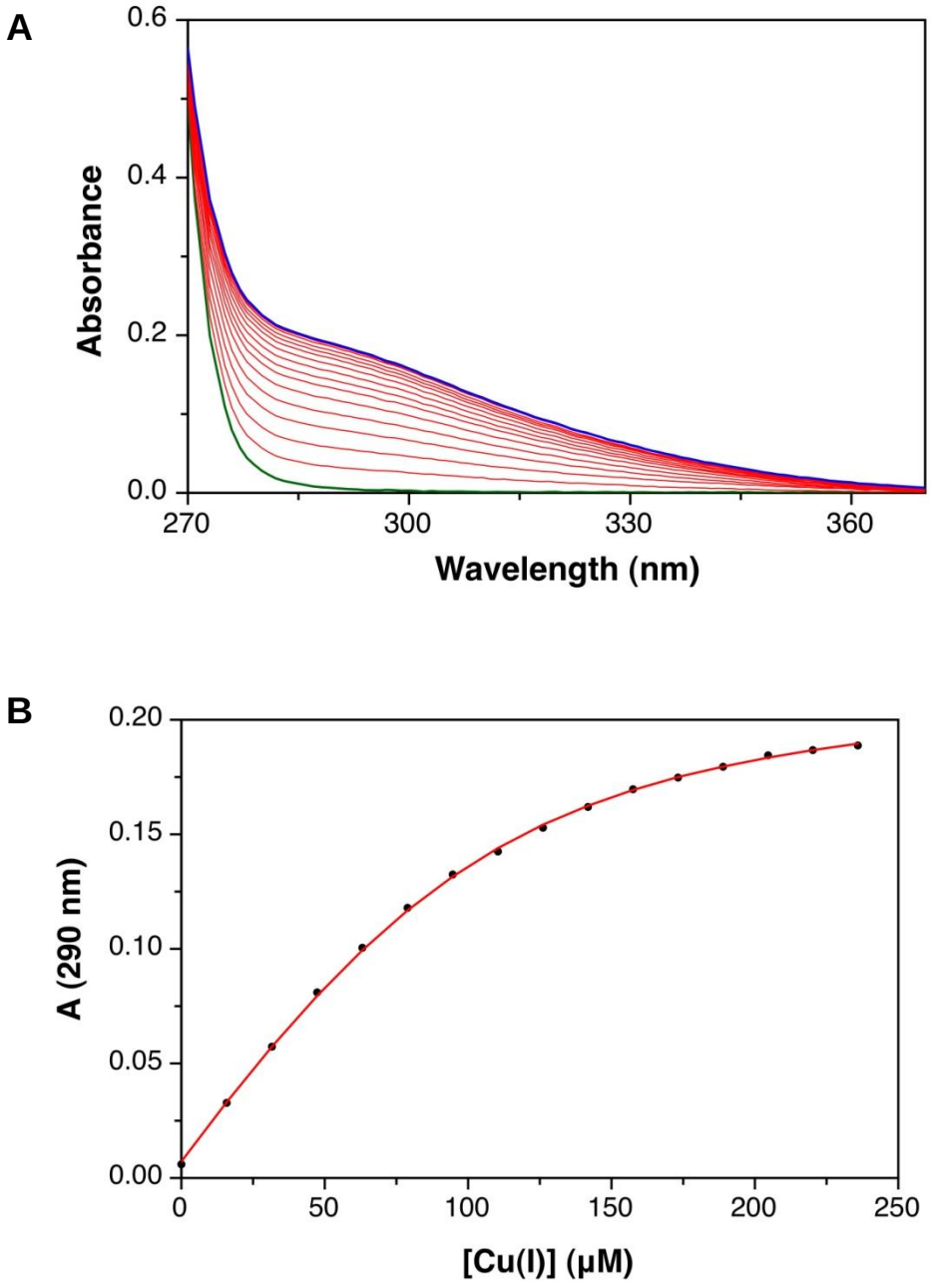

Figure 2.8. *Determination of Cu(I) Stability Constant of PEMEA: Titration of PEMEA with Cu(I) in the Presence of Acetonitrile.* **A.** Green trace and blue trace correspond to the UV-visible spectra at [Cu(I)] = 0 and 236 µM, respectively. **B.** Absorbance change (black points) and curve fit (solid trace) for the titration. PEMEA (100 µM) was titrated with $[Cu(I)(CH_3CN)_4]PF_6$ in the presence of 958 mM acetonitrile acting as a competing ligand at pH 2 (14 mM $HClO_4$, 0.1 M $KClO_4$, 25 °C, in the presence of 100 µM sodium ascorbate). Cu(I) stability constant value of PEMEA was then determined by non-linear least-squares fitting over the entire spectral range using the SPECFIT software package (36). Average fitted value: $\log K_{Cu(I)L} = 15.71 \pm 0.02$.

a) Cu(I) Affinity of PEMEA from Thermodynamic Cycle (r1)

PEMEA showed a quasi-reversible one-electron redox process with a half-wave potential of 0.595±0.002 V vs SHE in the presence of $CuSO_4$ (Figure 2.6). The Cu(II)-complex of PEMEA has an absorption maximum at 350 nm (Figure 2.7). UV-vis titrations of PEMEA with Cu^{2+} (aq) yielded a $\log K_{Cu(II)L}$ of 7.85±0.08; using these data, we obtained a $\log K_{Cu(I)L}$ value of 15.71 from eqn. (2.28). The previously published formal potential ($E_{Cu(II/I)L}$ = 0.595) and stability constant values ($\log K_{Cu(II)L}$ = 7.89 and $\log K_{Cu(I)L}$ = 15.76) of PEMEA (8) corroborated well with our data.

b) Cu(I) Affinity of PEMEA from Competition with Acetonitrile (e1)

As discussed in section 2.1.4, Cu(I) stability constant determined from the thermodynamic cycle depends on the $E^0_{Cu(II/I)aq}$ value. Therefore, we sought to verify the Cu(I)-stability constant value of PEMEA using an independent method. Acetonitrile has the ability to stabilize Cu(I) ions upon complexation towards oxidation and disproportionation. The ligand binds Cu(I) with 1:1, 2:1, and 3:1 ligand-metal stoichiometry with stability constants of $\log\beta_1$ = 2.63, $\log\beta_2$ = 4.02, and $\log\beta_3$ = 4.29 (27), respectively. These values were directly determined previously by Kamau et al. using a method based on the kinetics of Cu(I)-oxidation by Co(III) complexes, which did not require the measurement of Cu(II)/Cu(I) reduction potential and therefore acetonitrile could be used as a competing ligand to cross-validate the $\log K_{Cu(I)L}$ value of PEMEA. Although the absolute binding affinity of PEMEA is much higher for an effective competition experiment with acetonitrile, its apparent affinity at pH 2 ($\log K'_{Cu(I)L}$ = 9.0) is much lower due to the presence of two protonation sites in PEMEA. Therefore, at pH 2, PEMEA can compete with acetonitrile ligand for the Cu^+ (aq) ions (Figure 2.8). The stability constant of PEMEA determined by this competition method ($\log K_{Cu(I)L}$ = 15.71±0.02) is exactly the same as obtained from eqn. (2.28).

2.2.2.2. Stability Constant of MCL-1

MCL-1 is one of the two water soluble tripodal ligands synthesized for this work where three sulfur donor atoms are connected to a central amine nitrogen through thiaether linkages. These tripodal ligands form 1:1 Cu(I)- complexes which are spectroscopically silent in the near-UV and visible region. Therefore, they can be used as competing ligands where the second ligand forms a colored complex or absorbs in near-UV as a result of complexation with Cu(I).

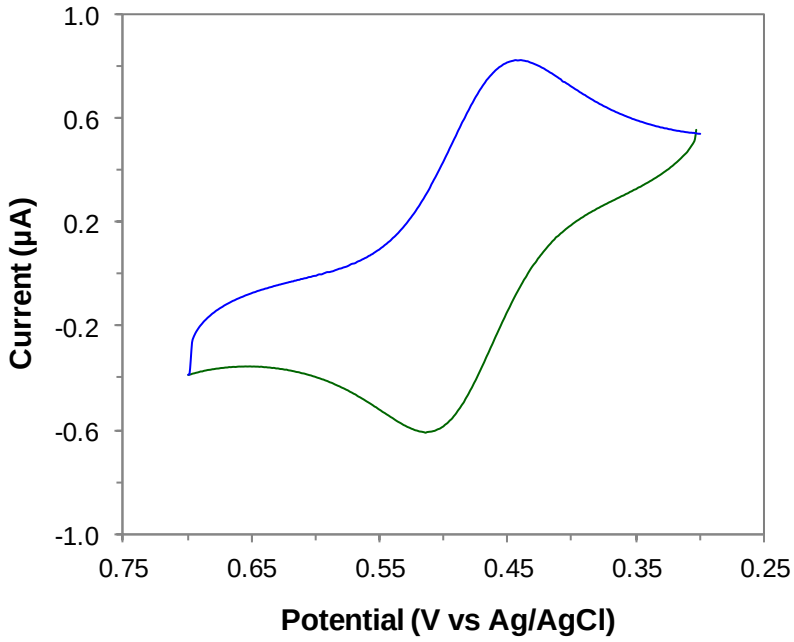

Figure 2.9. *Determination of Formal Potential of MCL-1*. Cyclic Voltammogram of MCL-1 (150 µM) in presence of $CuSO_4$ (1 mM) at pH 5 (10 mM PIPBS, 0.1 M $KClO_4$); scan rate 20 mV s^{-1}. Green and blue traces correspond to the forward and the backward sweep, respectively.

a) Cu(I) Affinity of MCL-1 from Thermodynamic Cycle (r2)

In the presence of $CuSO_4$, MCL-1 showed a quasi-reversible one-electron redox process with a half-wave potential of 0.716±0.001 V vs SHE (Figure 2.9). UV-vis titrations of the ligand with Cu^{2+} (aq) can be followed by the change in the absorption maximum of the Cu(II)-complex at 374 nm (Figure 2.10). This experiment yielded a $\log K_{Cu(II)L}$ of 6.42±0.02 which subsequently gave a calculated $\log K_{Cu(I)L}$ = 16.33 for the ligand.

b) Cu(I) Affinity of MCL-1 from Competition with PEMEA (e2)

In this competition titration, the Cu(I) complex of MCL-1, isolated as Cu(I)-MCL-1, was used as the copper source. Since free aqueous Cu^+ ions are unstable towards oxidation and disproportionation, this is a convenient method of supplying Cu(I) for the titration. Usually Cu(I)-acetonitrile complex is used in the literature as a copper metallation reagent. Salts of Cu(I)-acetonitrile complexes, e.g., $[Cu(I)(CH_3CN)_4]PF_6$, $[Cu(I)(CH_3CN)_4]BF_4$, are very stable when dissolved in acetonitrile, but aqueous solution of these salts are not stable towards oxidation. Therefore, to prevent aqueous Cu^+ ions from oxidation, a considerable amount of acetonitrile has to be present in the titration medium as a Cu(I) stabilizing agent. In order to avoid introduction of another competing ligand (acetonitrile) besides the ligands of interest, we used pre-formed Cu(I) complex of one of the ligands in the competition titrations wherever applicable. At pH 5, PEMEA ligand competes with MCL-1 for Cu^+ ions and from this competing equilibrium a $\log K_{Cu(I)L}$ = 16.33±0.07 was obtained for MCL-1 (Figure 2.11).

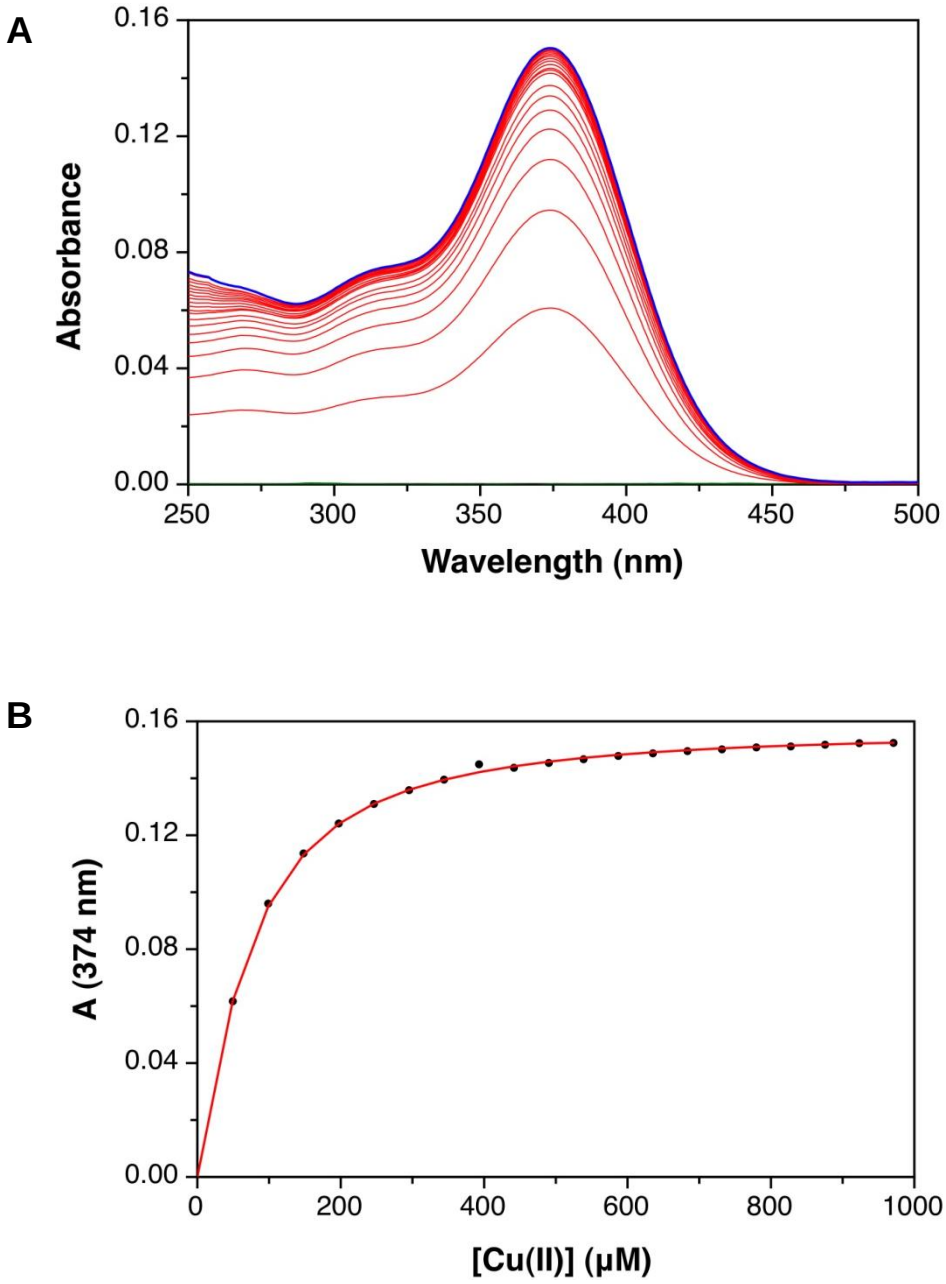

Figure 2.10. *Determination of Cu(II) Stability Constant of MCL-1: Titration of MCL-1 with $CuSO_4$.* **A.** Green trace and blue trace correspond to the UV-visible spectra at [Cu(II)] = 0 and 971 μM, respectively. **B.** Absorbance change (black points) and curve fit (solid trace) for the titration. MCL-1 (50 μM) was titrated with $CuSO_4$ at pH 5 (10 mM PIPBS, 0.1 M $KClO_4$, 25 °C). Cu(II) stability constant value was then determined by non-linear least-squares fitting over the spectral range 300-450 nm using the SPECFIT software package (36). Average fitted value: $\log K_{Cu(II)L} = 6.42 \pm 0.02$.

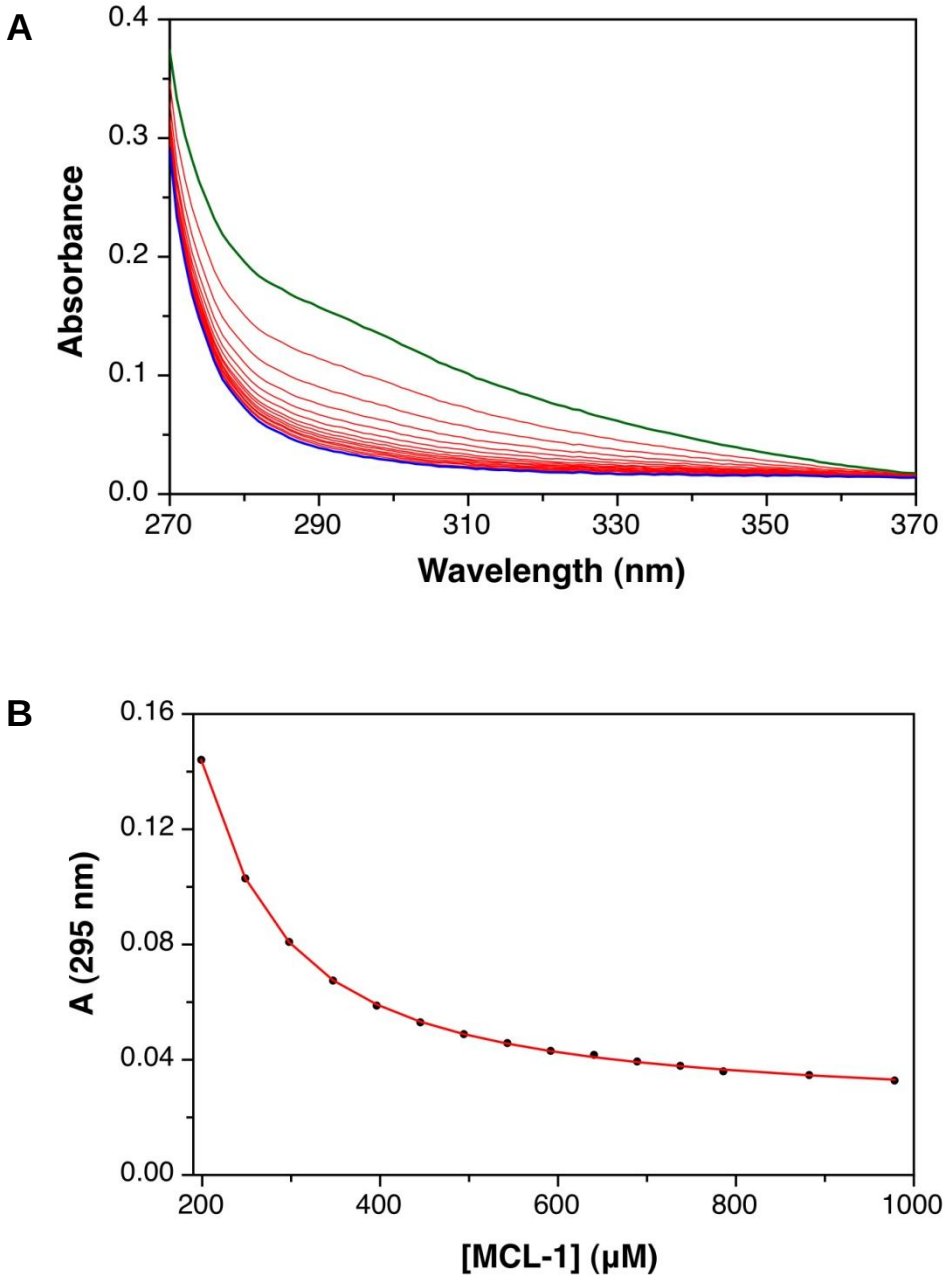

Figure 2.11. *Determination of Cu(I) Stability Constant of MCL-1: Titration of Cu(I)-complex of PEMEA with MCL-1.* **A.** Green trace and blue trace correspond to the UV-visible spectra at [MCL-1] = 200 and 978 µM, respectively. **B.** Absorbance change (black points) and curve fit (solid trace) for the titration. Cu(I)-complex of PEMEA was initially formed by the addition of 200 µM Cu-MCL-1 wherein Cu(I) ions would be distributed between 200 µM of MCL-1 and 96 µM of PEMEA acting as a competing ligand. Cu(I)-complex of PEMEA was then titrated with MCL-1 at pH 5 (10 mM PIPBS, 0.1 M $KClO_4$, 25 °C). Finally, Cu(I) stability constant value of MCL-1 was determined by non-linear least-squares fitting over the entire spectral range using the SPECFIT software package (36). Average fitted value: $\log K_{Cu(I)L} = 16.33 \pm 0.07$.

2.2.2.3. Stability Constant of BCA

2,2′-Bicinchoninic acid (BCA) is a copper(I) chelator used in the measurement of protein concentration commonly known as BCA assay (43). Cu(I)-complex of BCA is purple in color and has a 1:2 metal-ligand stoichiometry. The redox process of BCA is irreversible, thus preventing determination of its stability constant value from the thermodynamic cycle. In this case, we employed two competition experiments, one with PEMEA and another with MCL-1, to obtain a reliable stability constant value of BCA.

a) Cu(I) Affinity of BCA from Competition with MCL-1 (e3).

As discussed in section 2.2.2.2, MCL-1 is a useful ligand to compete with BCA for Cu^{+} ions since Cu(I)-MCL-1 does not absorb at 562 nm where $[Cu(I)(BCA)_2]$ complex absorbs. In this titration pre-formed Cu(I) complex of MCL-1 is used to metallate BCA. When BCA and Cu(I)-MCL-1 were mixed in equimolar ratio, 50% of BCA was metallated, thus assuring the formation of only 2:1 complex of BCA throughout the titration. Under this condition, UV-vis titration with MCL-1 ligand provided a stability constant value of 17.67±0.03 (Figure 2.12).

b) Cu(I) Affinity of BCA from Competition with PEMEA (e4).

The Cu(I)-complex of PEMEA absorbs below 400 nm, thus rendering it suitable as a competing ligand to the determine binding affinity of $[Cu(I)(BCA)_2]$ complex, which absorbs at λ_{max} = 562 nm. $[Cu(I)(BCA)_2]$ complex was formed by the addition of $[Cu(I)(CH_3CN)_4]PF_6$ to excess BCA (molar ratio BCA:Cu(I) = 2.5) to ensure the exclusive presence of a 1:2 metal-ligand complex. Spectrophotometric titrations were performed by monitoring the change in absorption at 562 nm by the addition of PEMEA (Figure 2.13). The value obtained by fitting the titration data over the entire spectral range using the least square method was 17.63±0.05.

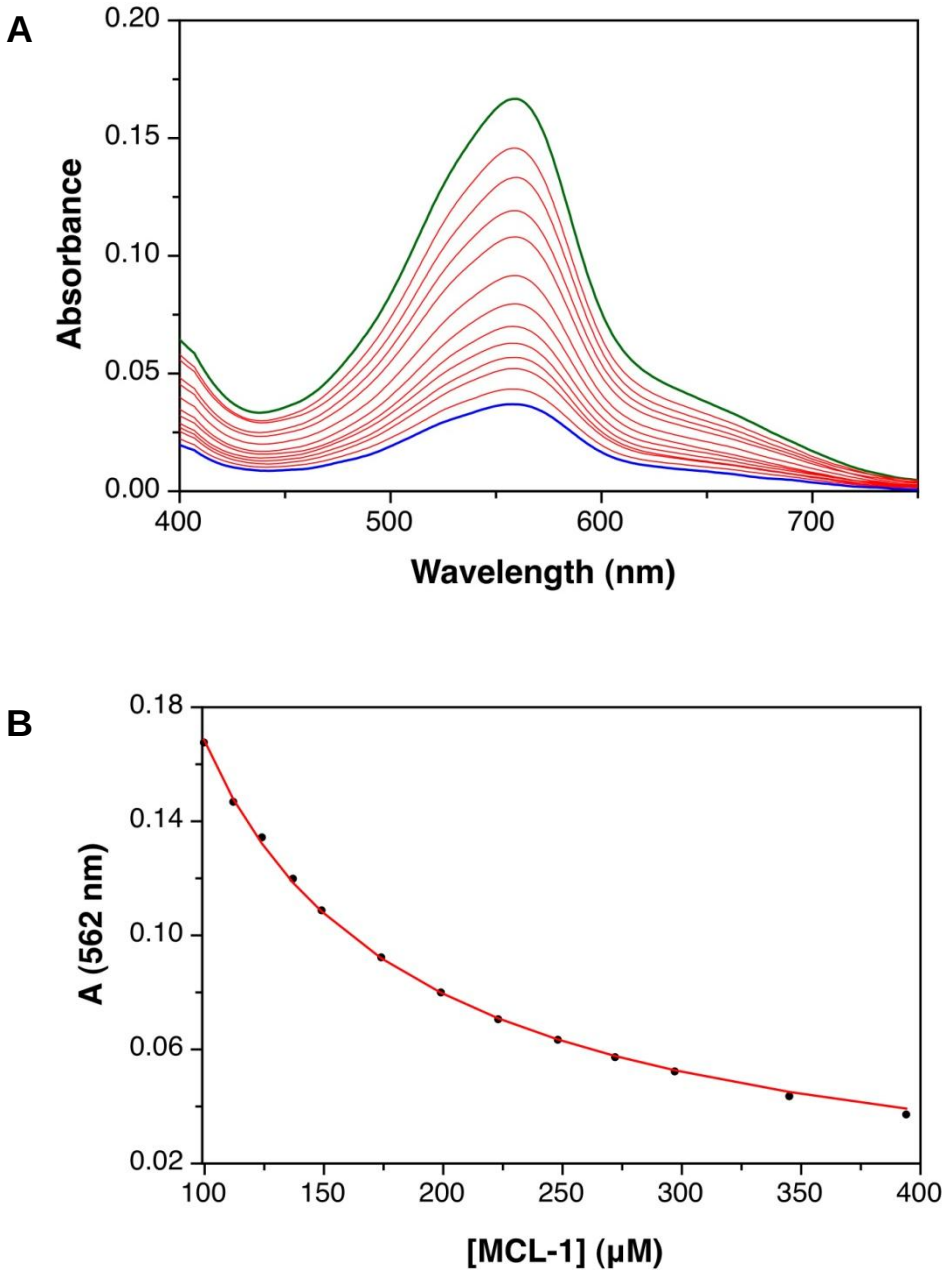

Figure 2.12. *Determination of Cu(I) Stability Constant of BCA: Titration of Cu(I)-complex of BCA with MCL-1*. **A.** Green trace and blue trace correspond to the UV-visible spectra at [MCL-1] = 100 and 394 μM, respectively. **B.** Absorbance change (black points) and curve fit (solid trace) for the titration. Cu(I)-complex of BCA was initially formed by the addition of 100 μM Cu-MCL-1 wherein Cu(I) ions would be distributed between 100 μM of BCA and 100 μM of MCL-1 acting as a competing ligand. Cu(I)-complex of BCA was then titrated with MCL-1 at pH 5 (10 mM PIPBS, 0.1 M $KClO_4$, 25 °C). Finally, Cu(I) stability constant value of MCL-1 was determined by non-linear least-squares fitting over the spectral range 450-700 nm using the SPECFIT software package (36). Average fitted value: $\log\beta_2^{Cu(I)} = 17.67 \pm 0.03$.

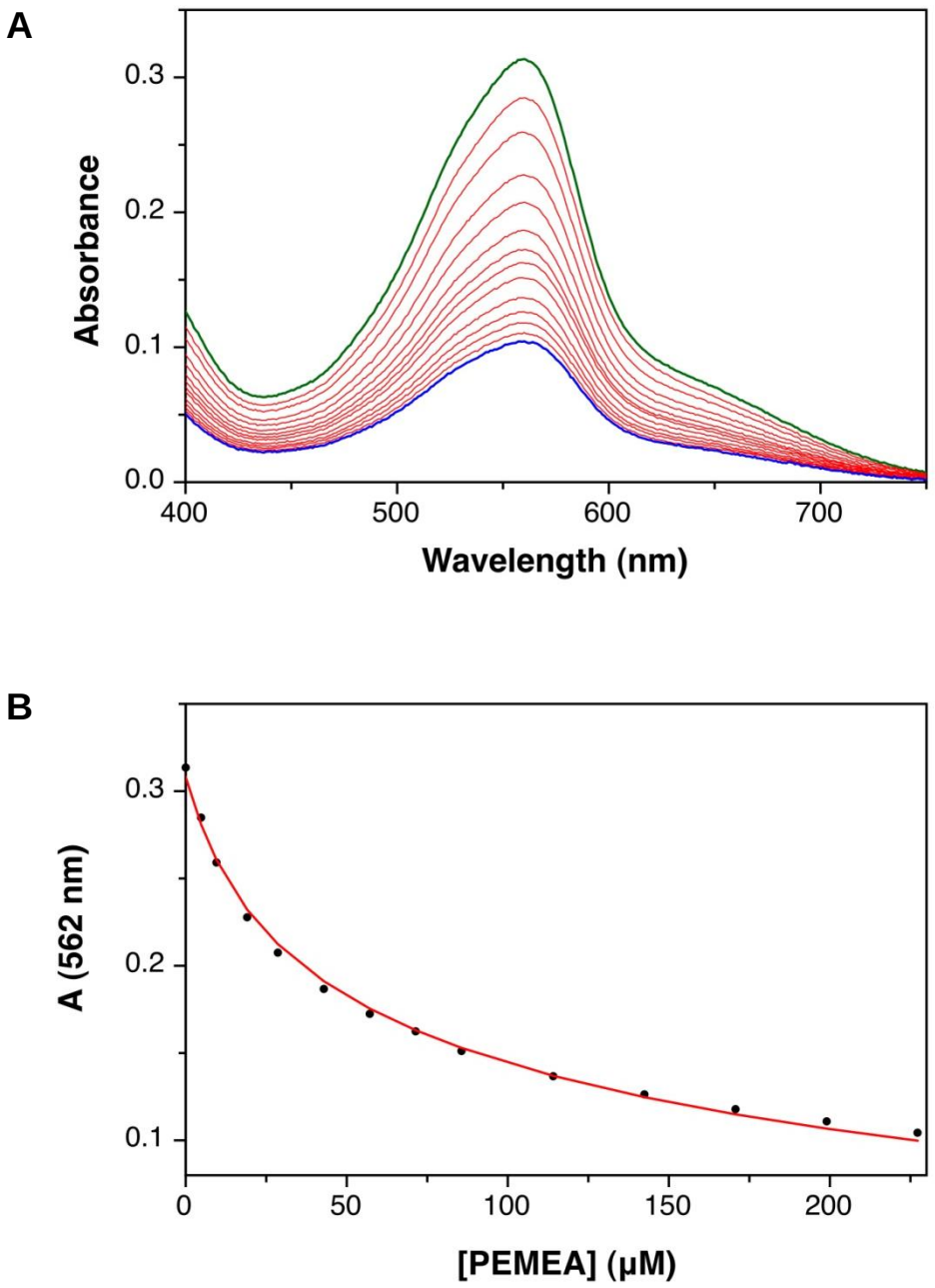

Figure 2.13. *Determination of Stability Constant of BCA: Titration of Cu(I)-complex of BCA with PEMEA.* **A.** Green trace and blue trace correspond to the UV-visible spectra at [PEMEA] = 0 and 227 µM , respectively. **B.** Absorbance change (black points) and curve fit (solid trace) for the titration. Cu(I)-complex of BCA was initially formed by the addition of 40 µM $[Cu(I)(CH_3CN)_4]PF_6$ to 100 µM of BCA. Cu(I)-complex of BCA was then titrated with the competing ligand MCL-1 at pH 5 (10 mM PIPBS, 0.1 M $KClO_4$, 25 °C). Finally, Cu(I) stability constant value of BCA was determined by non-linear least-squares fitting over the spectral range 450-700 nm using the SPECFIT software package (36). Average fitted value: $\log\beta_2^{Cu(I)} = 17.63 \pm 0.05$.

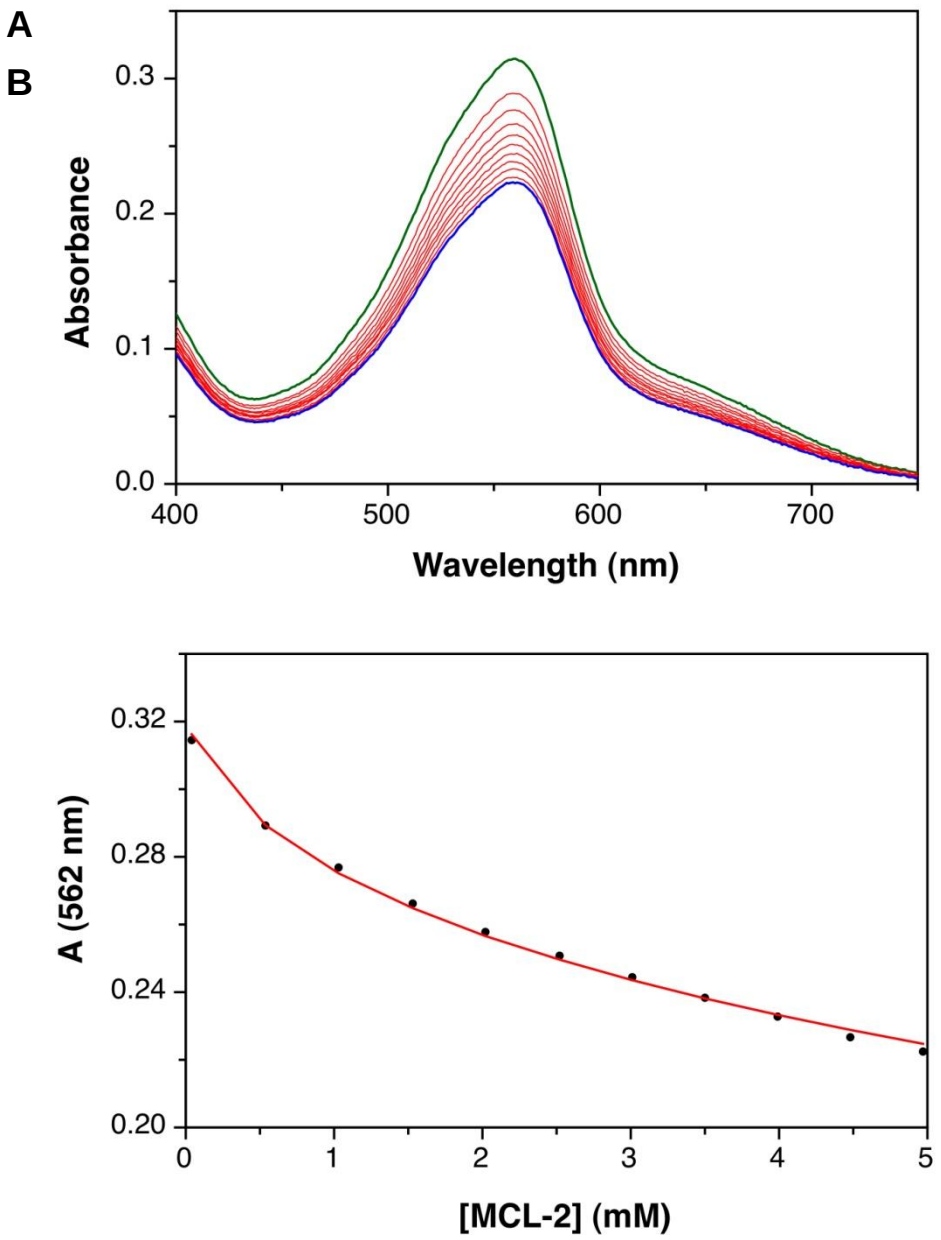

Figure 2.14. *Determination of Cu(I) Stability Constant of MCL-2: Titration of Cu(I)-complex of BCA with MCL-2.* **A.** Green trace and blue trace correspond to the UV-visible spectra at [MCL-2] = 0.04 and 4.97 mM, respectively. **B.** Absorbance change (black points) and curve fit (solid trace) for the titration. Cu(I)-complex of BCA was initially formed by the addition of 40 µM Cu-MCL-2 wherein Cu(I) ions would be distributed between 40 µM of MCL-2 and 100 µM of BCA acting as a competing ligand. Cu(I)-complex of BCA was then titrated with MCL-2 at pH 7 (50 mM PIPES, 60 mM $KClO_4$, 25 °C). Finally, Cu(I) stability constant value of MCL-2 was determined by non-linear least-squares fitting over the spectral range 450-700 nm using the SPECFIT software package (36). Average fitted value: $\log K_{Cu(I)L} = 13.08 \pm 0.13$.

The measured stability constant of BCA is different from a recently published data ($\log\beta_2^{Cu(I)}$ = 17.3) where the binding affinity of BCA was indirectly derived from another copper chelator BCS (10). As a general description of this method, Cu(I) stability constant of a Cu(I)-binding protein was determined by competition with BCS, this value was subsequently used to obtain $\log\beta_2^{Cu(I)}$ value of BCA from a separate competition experiment between the protein and BCA under the same experimental condition. Therefore, the literature value of BCA depends on accurate determination of the stability constants of BCS and the protein involved in the study. On the contrary, we determined the stability constants of BCA using two different copper sources (Cu-MCL-1 and $[Cu(I)(CH_3CN)_4]PF_6$) and two different ligands (MCL-1 and PEMEA) by direct competition experiments. The stability constant values of BCA generated from these two independent experiments are reasonably close to each other. Based on these experiments, we derived an average $\log\beta_2^{Cu(I)}$ value of 17.66 for BCA, weighted by the standard deviations of the individual methods.

2.2.2.4. Stability Constant of MCL-2 *(e5)*

MCL-2 is a water-soluble ligand and is based on a similar tripodal architecture comparable to MCL-1. This ligand showed a completely irreversible redox process suggesting large structural changes associated with the conversion from Cu(I) to Cu(II). Direct titration of the ligand with aqueous Cu^+ ions was not possible because of the susceptibility of Cu^+ ions towards oxidation and the lack of spectroscopic characteristics of Cu(I)-MCL-2 complex in the measurable window of UV-vis spectrum. Therefore, the binding affinity of this ligand was determined from a competition experiment with BCA for the Cu^+ ions (Figure 2.14). Pre-formed Cu(I) complex of MCL-2 was used in this experiment as the copper source. MCL-2 indeed forms a weaker complex with Cu(I) ($\log K_{Cu(I)L}$ = 13.08±0.13) compared to other ligands characterized in this study. Moreover, potentiometric titrations showed that MCL-2 ($\log K_{H1}$ = 8.98) is much more

basic than MCL-1 ($\log K_{H1}$ = 7.00) resulting in a much lower apparent affinity at biologically relevant pH ($\log K'_{Cu(I)L}$ = 10.99 at pH 7). Therefore, this ligand can be used as a copper source to metallate other ligands and proteins. Aqueous solution of Cu(I)-MCL-2 is much more stable towards oxidation and disproportionation compared to Cu(I)-acetonitrile complex dissolved in pure water. Although Cu(I)-acetonitrile complex is very stable in acetonitrile-water mixture, presence of acetonitrile can alter the metal binding property of a protein by destabilizing its tertiary structure (44, 45).

2.2.2.5. Stability Constant of BCS

The use of bathocuproine as a copper(I) chelator can be dated back to 1950's (46). Bathocuproinedisulfonic acid (BCS) is a water soluble analog of bathocuproine (47). BCS is a high-affinity ligand which binds copper with 1:2 metal-ligand stoichiometry. The resultant Cu(I) complex has an absorption maximum at 483 nm, hence the binding of Cu(I) to BCS can be easily monitored by UV-vis spectroscopy. BCS binds both Cu(I) and Cu(II) with high affinities and thus precludes the measurement of both affinities by direct titration of the ligand with either Cu(I) or Cu(II) ions (see section 2.1.4). In a recent publication, Xiao et al. (10) determined the Cu(II) binding affinity of BCS at 3-4 mM concentration by Bjerrum's method (48), where they followed the competition between Cu^{2+} ions and protons for BCS ligand by potentiometric titration. One of the major limitations of this approach is that at such high concentration of BCS, the potentials of reference electrodes typically used in potentiometry, silver chloride (Ag/AgCl) or calomel (Hg/Hg_2Cl_2), will fluctuate as BCS is capable of stable complex formation with both silver and mercury ions (49-52). In our laboratory, attempt to measure the protonation constant of BCS above 1 mM concentration was unsuccessful due to destabilization of the electrode potential. Moreover, BCS has been shown to undergo self-association at concentrations above about 1 mM (53), hence at that concentration the self-association equilibrium will also compete with the metal-binding equilibrium.

Therefore, Bjerrum's method is not a proper choice to measure Cu(II)-stability constant of BCS, as a high concentration of the ligand is required for this method.

In the current study, we determined the Cu(II) affinity of BCS from a direct competition titration with DHEAMP by spectrophotometric titration. Low millimolar concentration of BCS (0.3 mM) is sufficient for this method and thus the problem of aggregation can be avoided.

a) Competition with DHEAMP: Cu(I) Affinity of BCS from Thermodynamic Cycle (r3)

DHEAMP was first characterized by Damu et al. (38) as part of a series of metal complexation agents that bind to various metal ions (Figure 2.15). The first protonation constant ($\log K_{H1}$ = 6.94±0.01; Figure 2.3) and Cu(II) binding affinity ($\log K_{Cu(II)L}$ = 9.21±0.01; Figure 2.16) of this ligand were verified in the current study and they agreed very well with the literature values ($\log K_{H1}$ = 6.92 and $\log K_{Cu(II)L}$ = 9.2). The second protonation constant of DHEAMP was not determined in this work because of its very low value ($\log K_{H2}$ = 1.16 as determined in ref. (38)). Such a low $\log K_{H}$ value cannot be determined precisely and hence $\log K_{H2}$ of DHEAMP was not included in our SPECFIT model to calculate the Cu(II) binding affinity of the ligand. Moreover, buffer pH used in the titrations with DHEAMP was at least one log unit higher than the second protonation constant value, thus our stability constant values were not expected to change much with the omission of this protonation constant.

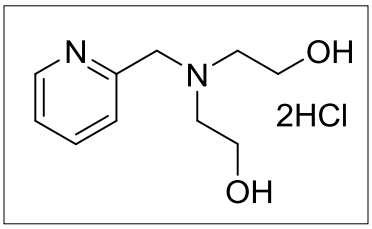

Figure 2.15. *Molecular Structure of DHEAMP.*

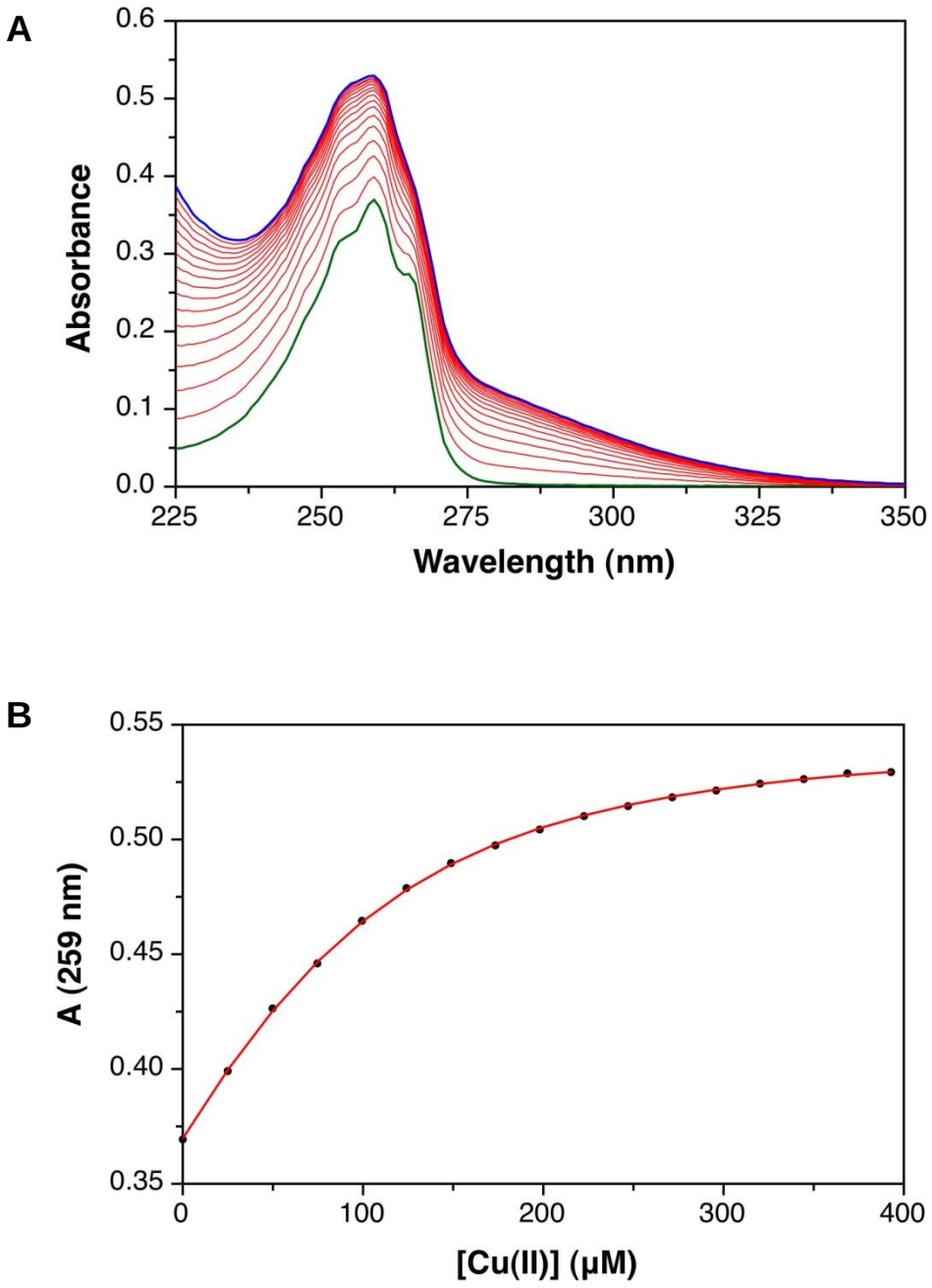

Figure 2.16. *Determination of Cu(II) Stability Constant of DHEAMP: Titration of DHEAMP with $CuSO_4$.* **A.** Green trace and blue trace correspond to the UV-visible spectra at [Cu(II)] = 0 and 393 μM, respectively. **B.** Absorbance change (black points) and curve fit (solid trace) for the titration. DHEAMP (100 μM) was titrated with $CuSO_4$ at pH 2.11 (10 mM $HClO_4$, 0.1 M $KClO_4$, 25 °C). Cu(II) stability constant value was then determined by non-linear least-squares fitting over the entire spectral range using the SPECFIT software package (36). Average fitted value: $\log K_{Cu(II)L} = 9.21 \pm 0.01$.

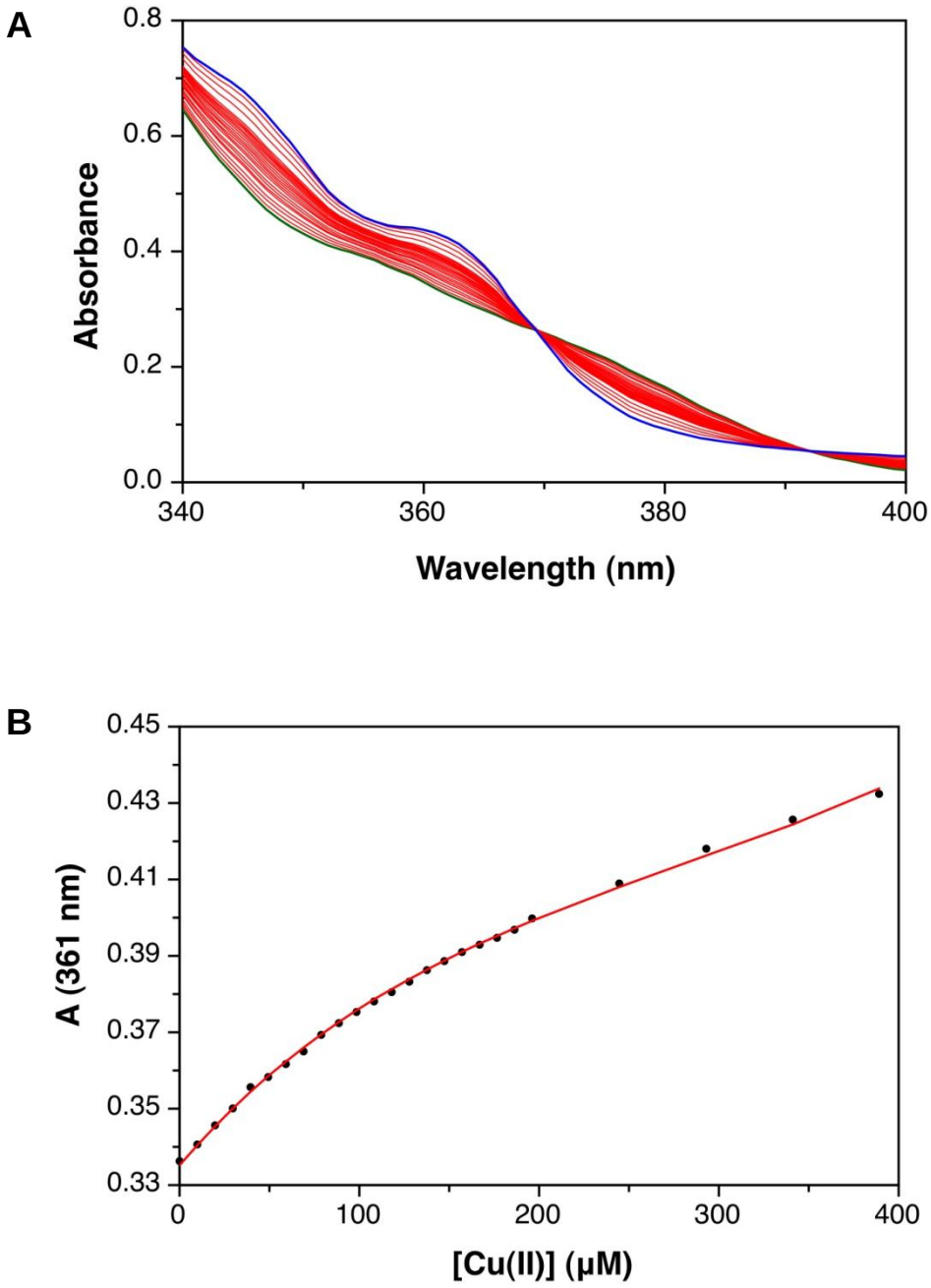

Figure 2.17. *Determination of Cu(II) Stability Constant of BCS: Titration of BCS with $CuSO_4$ in presence of DHEAMP*. **A.** Green trace and blue trace correspond to the UV-visible spectra at [Cu(II)] = 0 and 390 µM, respectively. **B.** Absorbance change (black points) and curve fit (solid trace) for the titration. BCS (300 µM) was titrated with $CuSO_4$ in the presence of 300 µM DHEAMP acting as a competing ligand at pH 6 (10 mM MES, 0.1 M $KClO_4$, 25 °C). Cu(II) stability constant value of BCS was then determined by non-linear least-squares fitting over the entire spectral range using the SPECFIT software package (36). Average fitted value: $\log\beta_2^{Cu(II)} = 12.42 \pm 0.07$.

The competition titration between BCS and DHEAMP for Cu^{2+} ion yielded $\log\beta_2^{Cu(II)}$ = 12.42±0.07 for BCS (Figure 2.17). Copper bound to BCS showed a reversible redox process with a half-wave potential of 0.626±0.001 V vs. SHE (Figure 2.18). Based on this data we obtained a value of $\log\beta_2^{Cu(I)}$ = 20.81 for $[Cu(I)(BCS)_2]$ complex from eqn. (2.28). Although our $\log\beta_2^{Cu(II)}$ of BCS differs by 0.6 log units compared to the value in ref. (10) ($\log\beta_2^{Cu(II)}$ = 11.8), the calculated Cu(I) stability constant is one log unit higher than the previously published value ($\log\beta_2^{Cu(I)}$ = 19.9). As discussed in section 2.1.4, this additional discrepancy is due to the different $E^0_{Cu(II/I)aq}$ values used in eqn. (2.28). While we used 0.13 V as suggested by Bernardo et al. (14), Xiao et al. adopted the value 0.164 V from a different literature (13). This difference in $E^0_{Cu(II/I)aq}$ values changes the calculated Cu(I)-binding affinity by 0.6 log units.

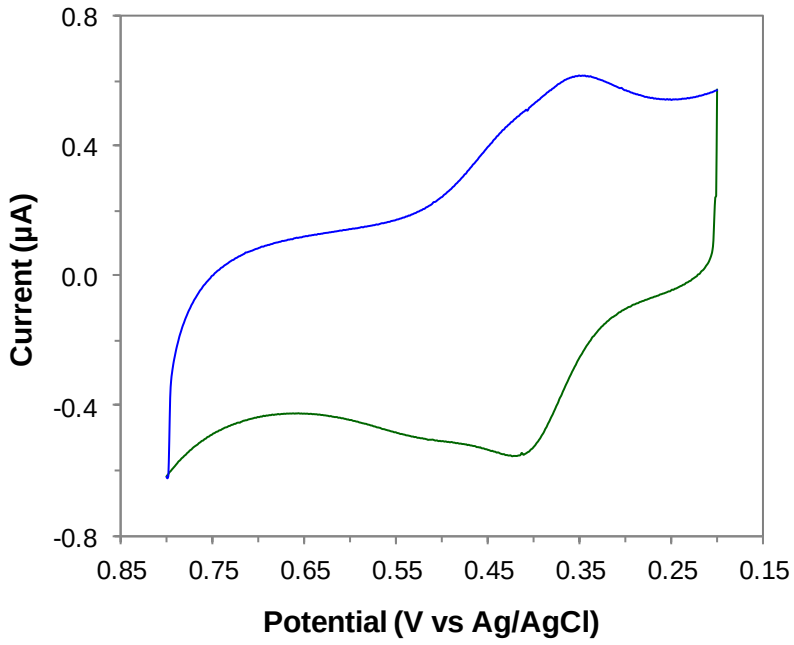

Figure 2.18. *Determination of Formal Potential of BCS.* Cyclic Voltammogram of BCS (150 µM) in presence of $CuSO_4$ (50 µM) at pH 5 (10 mM PIPBS, 0.1 M $KClO_4$); scan rate 50 mV s^{-1}. Green and blue traces correspond to the forward and the backward sweep, respectively.

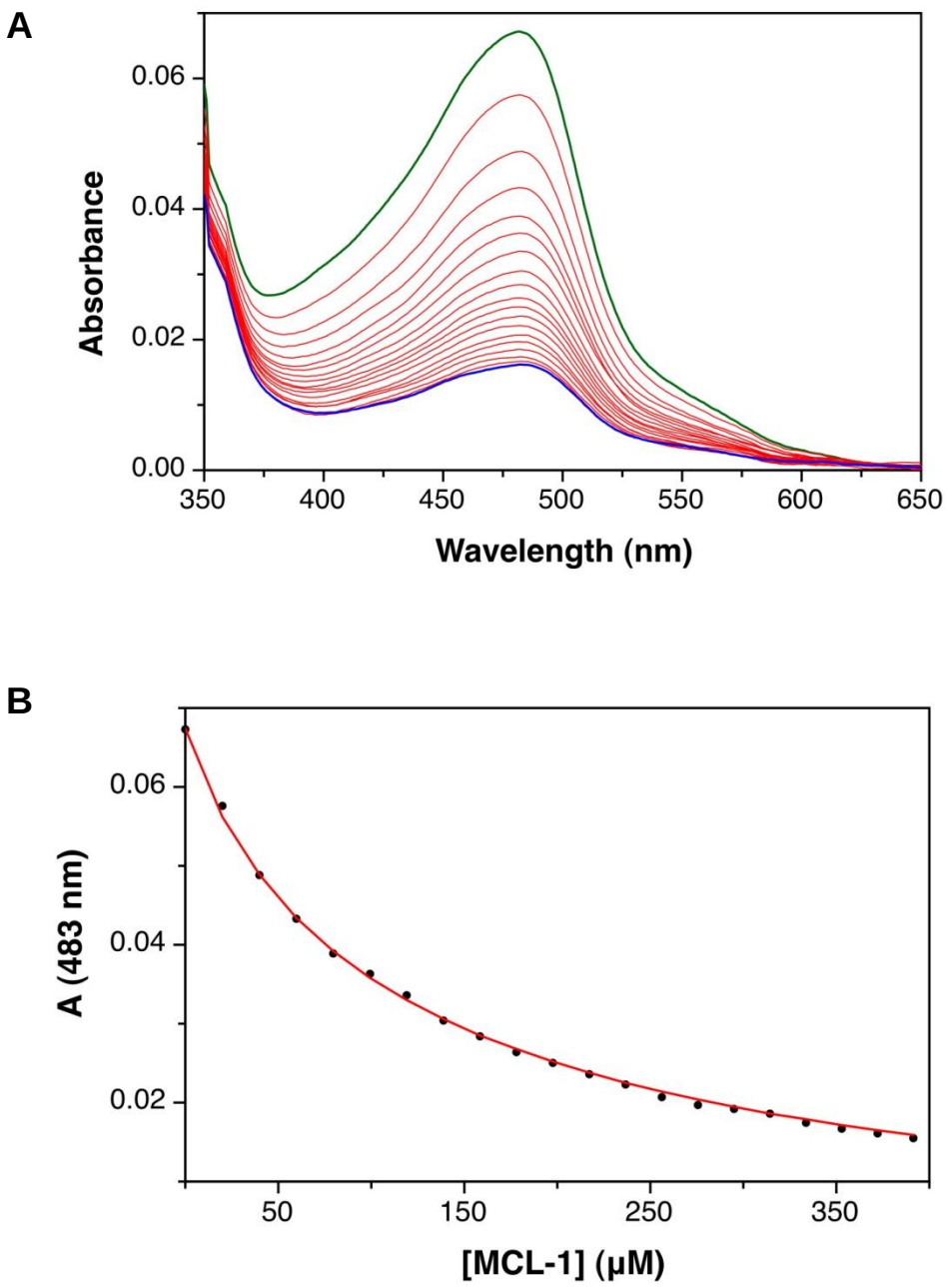

Figure 2.19. *Determination of Cu(I) Stability Constant of BCS: Titration of Cu(I)-complex of BCS with MCL-1*. **A.** Green trace and blue trace correspond to the UV-visible spectra at [MCL-1] = 0 and 391 μM, respectively. **B.** Absorbance change (black points) and curve fit (solid trace) for the titration. Cu(I)-complex of BCS was initially formed by the addition of 5 μM Cu(I)-MCL-2 to 50 μM of BCS. Cu(I)-complex of BCS was then titrated with the competing ligand MCL-1 at pH 7 (10 mM PIPES, 0.1 M $KClO_4$, 25 °C). Finally, Cu(I) stability constant value of BCS was determined by non-linear least-squares fitting over the spectral range 400-600 nm using the SPECFIT software package (36). Average fitted value: $\log\beta_2^{Cu(I)} = 20.81 \pm 0.04$.

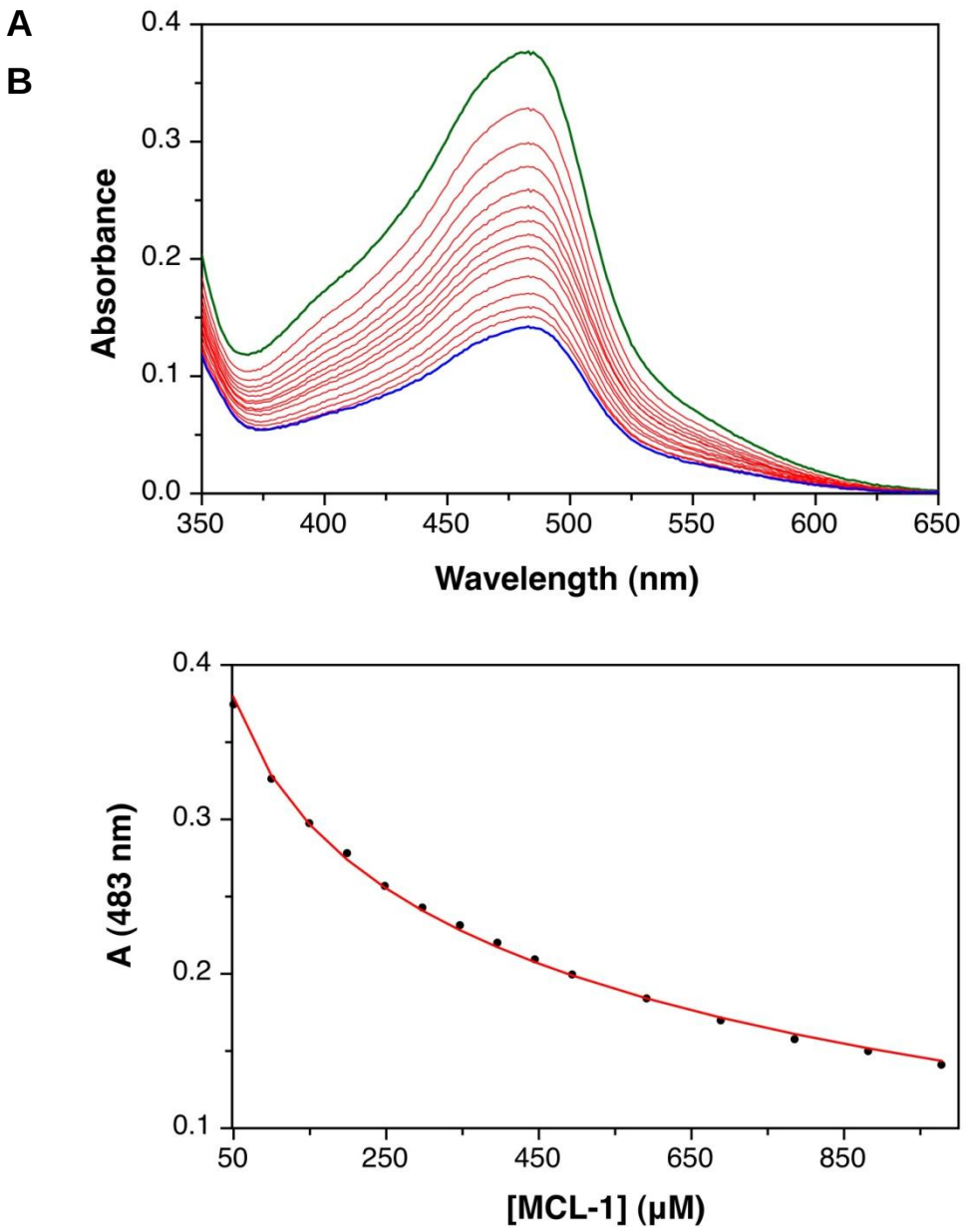

Figure 2.20. *Determination of Cu(I) Stability Constant of BCS: Titration of Cu(I)-complex of BCS with MCL-1.* **A.** Green trace and blue trace correspond to the UV-visible spectra at [MCL-1] = 50 and 978 μM, respectively. **B.** Absorbance change (black points) and curve fit (solid trace) for the titration. Cu(I)-complex of BCS was initially formed by the addition of 50 μM Cu-MCL-1 wherein Cu(I) ions would be distributed between 100 μM of BCS and 50 μM of MCL-1 acting as a competing ligand. Cu(I)-complex of BCS was then titrated with MCL-1 at pH 7 (10 mM PIPES, 0.1 M $KClO_4$, 25 °C). Finally, Cu(I) stability constant value of BCS was determined by non-linear least-squares fitting over the spectral range 400-600 nm using the SPECFIT software package (36). Average fitted value: $\log\beta_2^{Cu(I)} = 20.80\pm0.03$.

b) Cu(I) Affinity of BCS from Competition with MCL-1 (e7).

The stability constant of $[Cu(I)(BCS)_2]$ complex was cross-verified from a competition titration with MCL-1 for Cu^+ ions. In this method, $[Cu(I)(BCS)_2]$ complex was titrated with MCL-1 which was monitored by decrease in the absorbance at 483 nm (λ_{max} of Cu(I) complex of BCS). Two different copper sources, pre-formed Cu(I)-MCL-2 (Figure 2.19) and Cu(I)-MCL-1 (Figure 2.20), were used in these titrations to compare the stability constant values of BCS. Under both experimental conditions there were negligible concentrations of free Cu^+ (aq) present as the Cu^+ ions were either exclusively bound to BCS when Cu(I)-MCL-2 was used, or it was partitioned between BCS and MCL-1 in addition of Cu(I)-MCL-1. In both cases, spectrophotometric titrations revealed stability constant values ($\log\beta_2^{Cu(I)}$ = 20.81±0.04 for Cu(I)-MCL-2 and 20.80±0.03 for Cu(I)-MCL-1) which matched exactly with that obtained from the thermodynamic cycle ($\log\beta_2^{Cu(I)}$ = 20.81±0.08).

2.2.2.6. Stability Constant of MCL-3

MCL-3 is a water-soluble copper chelator, which is based on a 16-membered macrocycle with four sulfur donor atoms. The copper binding moiety of this ligand has no ionizable group, thus it has an unique advantage as an affinity standard as the Cu(I)-binding affinity of MCL-3 is independent of the pH of the medium.

a) Cu(I) Affinity of MCL-3 from Thermodynamic Cycle (r4)

Titration of MCL-3 with Cu^{2+} (aq) at pH 5 gave us a stability constant value $\log K_{Cu(II)L}$ of 3.47±0.04 (Figure 2.22). However, cyclic voltammetry of Cu(I)/Cu(II)-MCL-3 revealed a one-electron irreversible redox process with a large peak separation of 90 mV (at 20 mV s^{-1} scan rate) and a $E_{1/2}$ value of 0.729±0.003 V vs SHE (Figure 2.21). Given this large peak separation, the measured potential is not suitable to determine a reliable Cu(I) affinity based on thermodynamic cycle and the experimental Cu(II)

stability constant. Instead, Cu(I) affinity of MCL-3 was determined from two separate competition titrations with BCA and BCS as competing ligands.

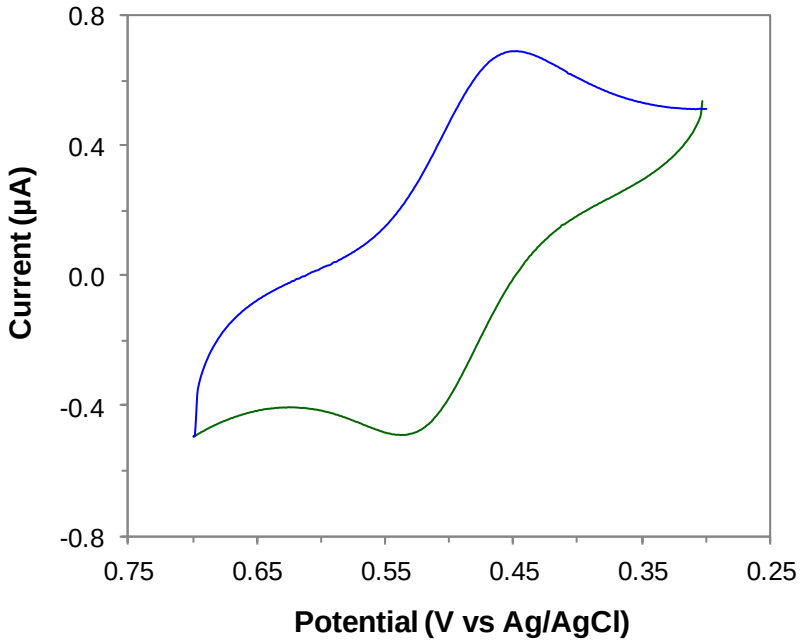

Figure 2.21. *Determination of Formal Potential of MCL-3.* Cyclic Voltammogram of MCL-3 (150 µM) in presence of $CuSO_4$ (1 mM) at pH 5 (10 mM PIPBS, 0.1 M $KClO_4$); scan rate 20 mV s^{-1}. Green and blue traces correspond to the forward and the backward sweep, respectively.

b) Cu(I) Affinity of MCL-3 from Competition with BCS (e8) or BCA (e9)

Derivation of Cu(I)-affinities of MCL-3 in competition with BCA or BCS for Cu^+ ion are based on the same general method. In both experiments, pre-formed Cu(I)-MCL-3 was used to metallate the competing ligands (BCA or BCS). Titration of these copper complexes with MCL-3 was monitored by the change in absorbance either at 562 nm for BCA (Figure 2.23) or at 483 nm for BCS (Figure 2.24), where the free ligands do not absorb. The stability constant values obtained from both sets of data converged at $\log K_{Cu(I)L} = 13.80 \pm 0.03$.

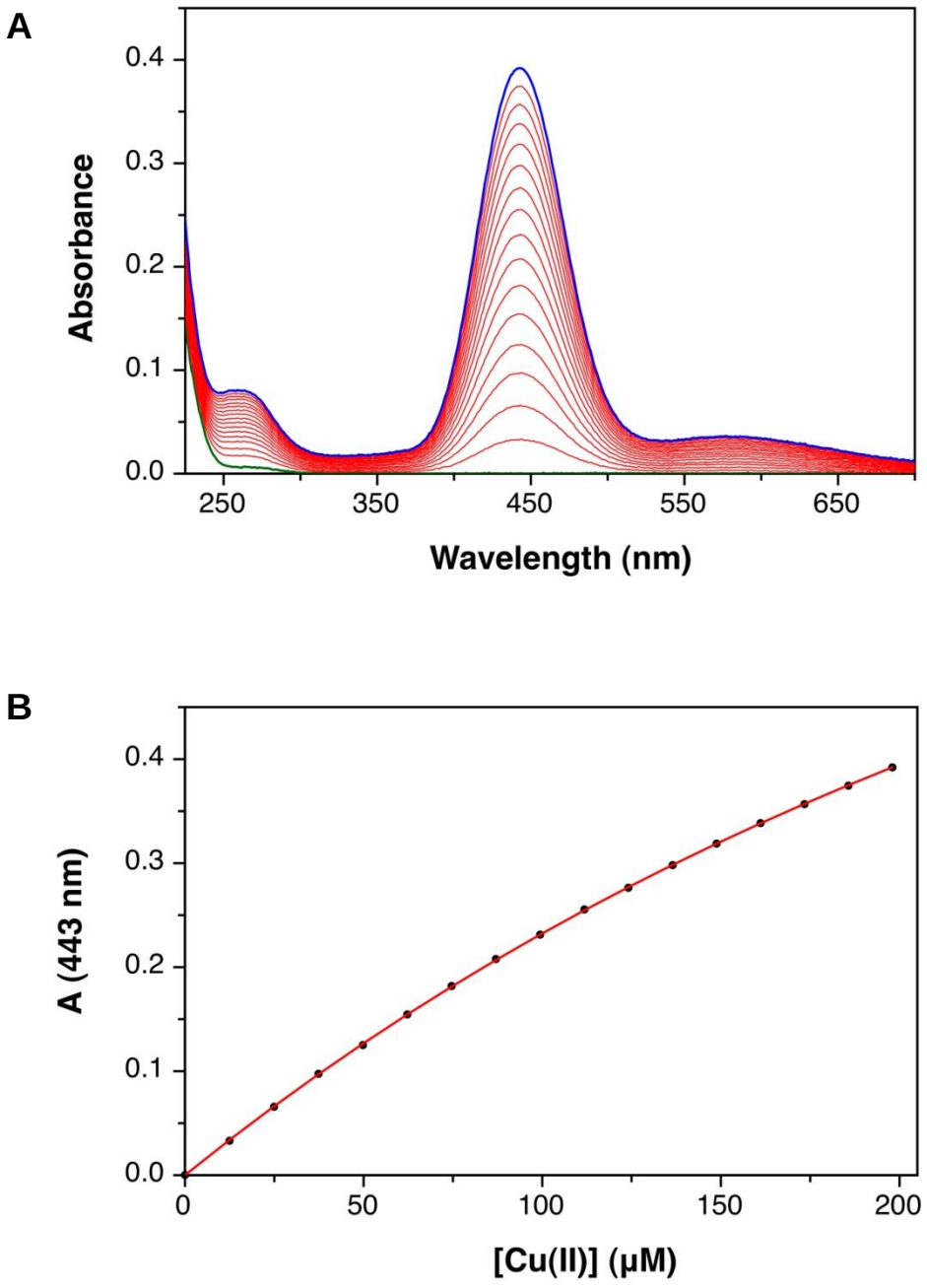

Figure 2.22. *Determination of Cu(II) Stability Constant of MCL-3: Titration of MCL-3 with $CuSO_4$.* **A.** Green trace and blue trace correspond to the UV-visible spectra at [Cu(II)] = 0 and 198 μM, respectively. **B.** Absorbance change (black points) and curve fit (solid trace) for the titration. MCL-3 (100 μM) was titrated with $CuSO_4$ at pH 5 (10 mM PIPBS, 0.1 M $KClO_4$, 25 °C). Cu(II) stability constant value was then determined by non-linear least-squares fitting over the spectral range 300-700 nm using the SPECFIT software package (36). Average fitted value: $\log K_{Cu(II)L} = 3.47 \pm 0.04$.

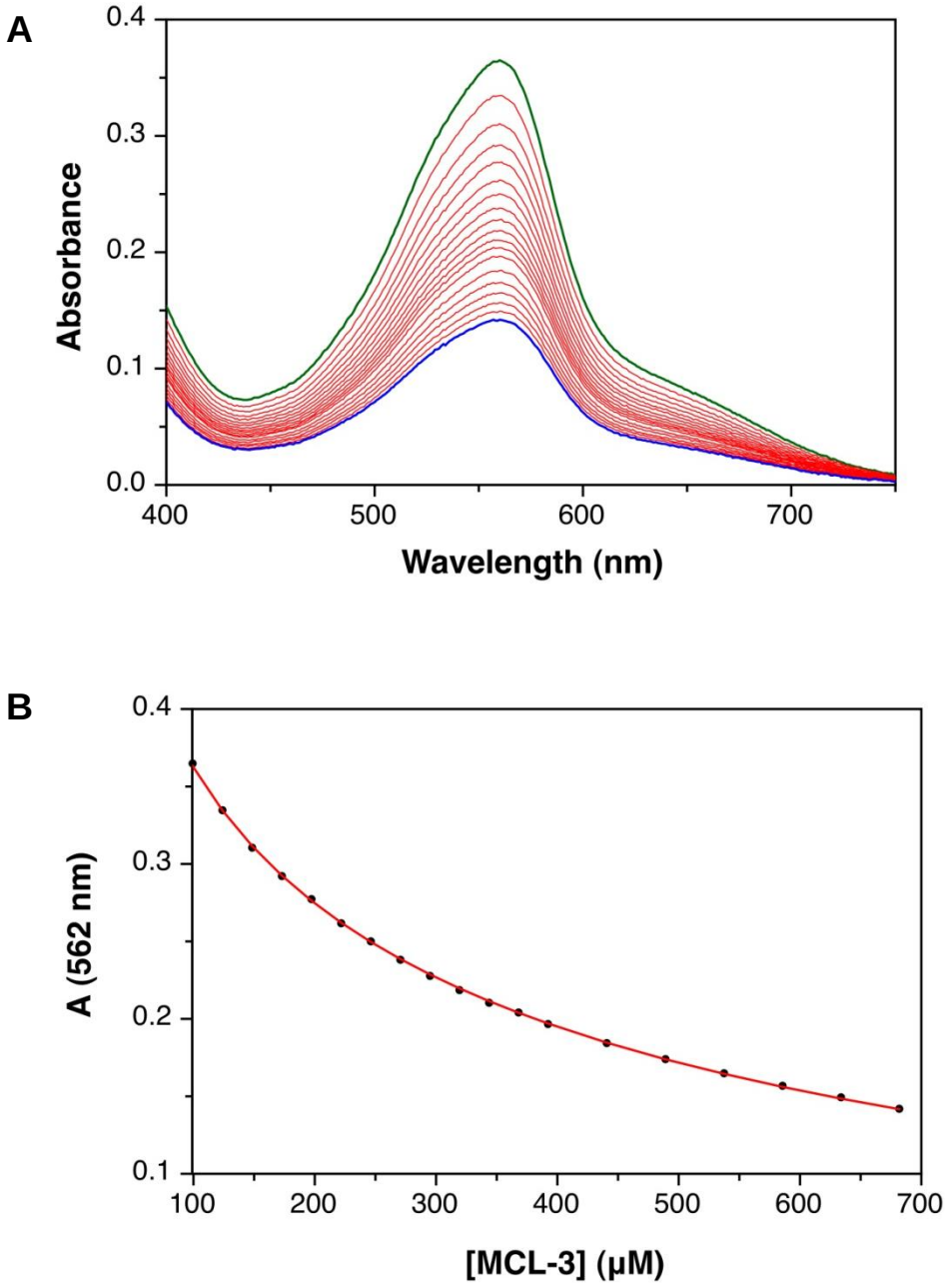

Figure 2.23. *Determination of Cu(I) Stability Constant of MCL-3: Titration of Cu(I)-complex of BCA with MCL-3.* **A.** Green trace and blue trace correspond to the UV-visible spectra at [MCL-3] = 100 and 682 µM, respectively. **B.** Absorbance change (black points) and curve fit (solid trace) for the titration. Cu(I)-complex of BCA was initially formed by the addition of 100 µM Cu-MCL-3 wherein Cu(I) ions would be distributed between 100 µM of MCL-3 and 200 µM of BCA acting as a competing ligand. Cu(I)-complex of BCA was then titrated with MCL-3 at pH 5 (10 mM PIPBS, 0.1 M $KClO_4$, 25 °C). Finally, Cu(I) stability constant value of MCL-3 was determined by non-linear least-squares fitting over the spectral range 450-700 nm using the SPECFIT software package (36). Average fitted value: $\log K_{Cu(I)L} = 13.78 \pm 0.06$.

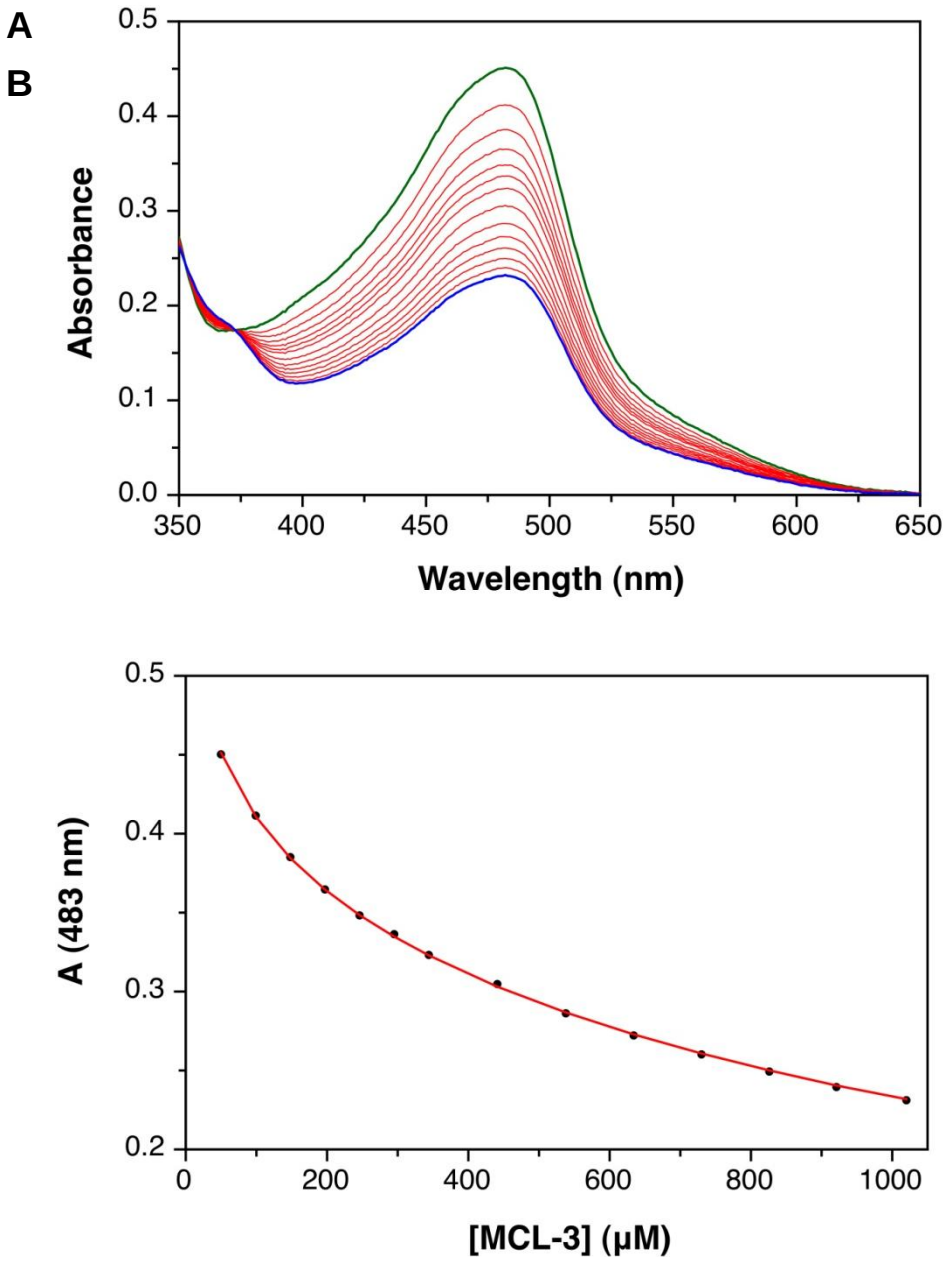

Figure 2.24. *Determination of Cu(I) Stability Constant of MCL-3: Titration of Cu(I)-complex of BCS with MCL-3.* **A.** Green trace and blue trace correspond to the UV-visible spectra at [MCL-3] = 50 and 1020 µM, respectively. **B.** Absorbance change (black points) and curve fit (solid trace) for the titration. Cu(I)-complex of BCS was initially formed by the addition of 50 µM Cu-MCL-3 wherein Cu(I) ions would be distributed between 50 µM of MCL-3 and 100 µM of BCS acting as a competing ligand. Cu(I)-complex of BCS was then titrated with MCL-3 at pH 5 (10 mM PIPBS, 0.1 M $KClO_4$, 25 °C). Finally, Cu(I) stability constant value of MCL-3 was determined by non-linear least-squares fitting over the spectral range 420-600 nm using the SPECFIT software package (36). Average fitted value: $\log K_{Cu(I)L} = 13.80 \pm 0.04$.

2.2.3. Determination of Cu(I) Affinity of a Protein using Copper Ligands

Accurate measurement of Cu(I) affinities of proteins is pivotal to understand the rationale behind the exchange of copper between protein partners leading to the distribution of cellular copper. However, determination of metal binding affinities of copper proteins encounter similar challenges as discussed in section 2.1.4 including redox lability of aqueous Cu^{+} ions and usually high Cu(I) affinities of proteins inhibiting direct estimation of stability constants. Cu(I) binding sites in proteins are more susceptible towards oxidation as cysteine is the preferred ligand for Cu(I) among biomolecules (54). Additionally, precise estimation of protein concentrations is not trivial especially for proteins lacking tryptophan residue, such as hAtox1, Atx1, Copz, where concentration cannot be measured by absorbance of protein at 280 nm (55). Consequently, as discussed in section 2.1.4, the reported stability constants of copper proteins are largely controversial (Table 2.1). These values were often determined using competing ligands with divergent published Cu(I) affinities (Table 2.2). Therefore, the binding affinities of copper proteins found in the literature are not comparable, thus impeding the understanding of the molecular mechanism of copper homeostasis. The set of affinity standards thoroughly characterized in this work covers a broad range of stability constants ($10^{13} – 10^{21}$) and hence they can be utilized to study Cu(I) binding of a wide array of proteins. The binding affinity of a copper chaperone, CusF, was determined in this work as a first example.

CusF is a periplasmic copper chaperone protein found in *Escherichia coli*. In this protein, Cu(I) is bound by Met_2His motif, which is typical in oxidizing environments including the periplasm (56). A tryptophan residue in the vicinity of the Cu(I) binding site is also shown to stabilize the metal binding via a strong cation-π interaction (57, 58) (Figure 2.25).

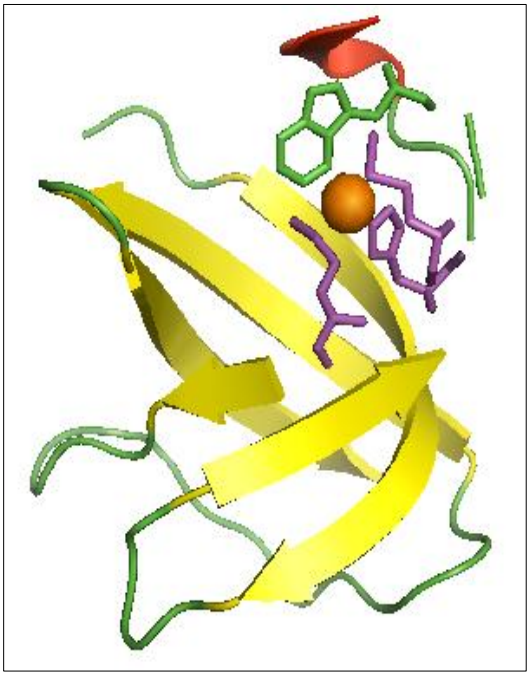

Figure 2.25. *Crystal Structure of CusF* (PDB Code: 2VB2 (57))

Table 2.6. *Stability Constants of CusF*

Competing Ligand	**Experimental Method**	**pH**	**Binding Affinity (M^{-1})**	**Ref.**[b]
MCL-3	Fluorescence	7.0	1.95×10^{14}	
BCA	UV-vis Spectroscopy	7.0	1.62×10^{14}	
		7.0	6.31×10^{13}[a]	(57)
		7.5	1.1×10^{8} – 2.2×10^{11}	(58)
-	ITC	7.0	2.72×10^{6}	(59)

[a] This value was published as $K_d \times \beta_2 = 7.3 \times 10^3$, where K_d is the dissociation constant of the protein and β_2 is the overall stability constant of $Cu(I)(BCA)_2$ complex. Using the β_2 value from this work, we arrived at the tabulated value. [b] Values stated without reference are from this work.

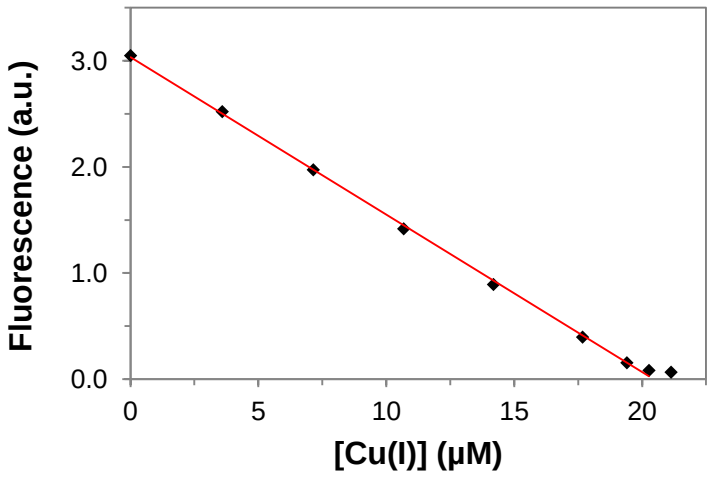

Figure 2.26. *Determination of Protein Concentration of CusF*. Mole-ratio titration of CusF with Cu(I) (provided by in-situ reduction of Cu(II)SO_4 with 100 μM sodium ascorbate) at pH 7 (50 mM MOPS, 150 mM NaCl).

2.2.3.1. Stability Constant of Cu(I) binding to CusF

In this work, Cu(I) binding affinity of CusF was determined by competition titrations using the two affinity standards, MCL-3 and BCA (Table 2.6).

a) Cu(I) Affinity of CusF from Competition with MCL-3

Fluorescence emission of CusF at 343 nm decreases linearly with addition of Cu(I) and quenches almost completely at 1:1 Cu(I)-protein stoichiometry. The metal induced quenching is due to the close proximity of the Cu(I) ion to the indole side chain of the tryptophan residue. Therefore, the concentration of CusF can be measured directly from the saturation point of the anaerobic titration of Cu(I) (provided by in-situ reduction of Cu(II)SO4 with 100 μM sodium ascorbate) with the apo-protein (Figure 2.26). Cu(I)-bound protein (holo-protein) prepared in situ can then be titrated with the ligand MCL-3, such that the metal will equilibrate between the apo-protein and the free ligand (Figure 2.27). The binding affinity of the protein ($\log K_{Cu(I)L}$ = 14.29±0.11) was calculated by

non-linear least-squares fitting of the fluorescence response over the entire spectral range using the SPECFIT software package.

Cu(I) binding affinities of proteins are usually pH-dependent due to variability in the protonation of the amino acid side chains in and around the metal binding sites with the alteration in pH. However, there is no reliable method to determine the protonation constant of a protein, thus binding affinities of proteins are always reported as apparent affinities (See Section 2.1.3) at a given pH.

b) Cu(I) Affinity of CusF from Competition with BCA

The binding affinity of CusF was previously estimated by Xue et al. by competition titration with BCA (57). However, in the absence of a cohesive value for $\log\beta_2^{Cu(I)}$ of BCA, these authors reported only a relative affinity of $K_d \times \beta_2 = 7.3 \times 10^3$, where K_d is the dissociation constant of the protein and β_2 is the overall stability constant of $Cu(I)(BCA)_2$ complex. Substituting the β_2 value of BCA from our work ($\log\beta_2^{Cu(I)} = 17.66$) into the above relationship, we calculated the $\log K_{Cu(I)L}$ of 13.8 for CusF, which is 0.5 log units lower than the value ($\log K_{Cu(I)L} = 14.29$) determined by the competition titration with MCL-3. Due to this discrepancy, we reexamined the Cu(I)-affinity of CusF by direct competition with BCA under spectrophotometric monitoring.. Cu(I) was added to a solution of BCA in 1:3 molar ratio to ensure 2:1 binding. The absorption of the purple colored $Cu(I)(BCA)_2$ complex at 562 nm decreases as the apo-protein being titrated (Figure 2.28). This is because of the shift in the initial metal binding equilibrium of BCA in presence of protein where both the ligand and the protein compete for the Cu(I) ions.

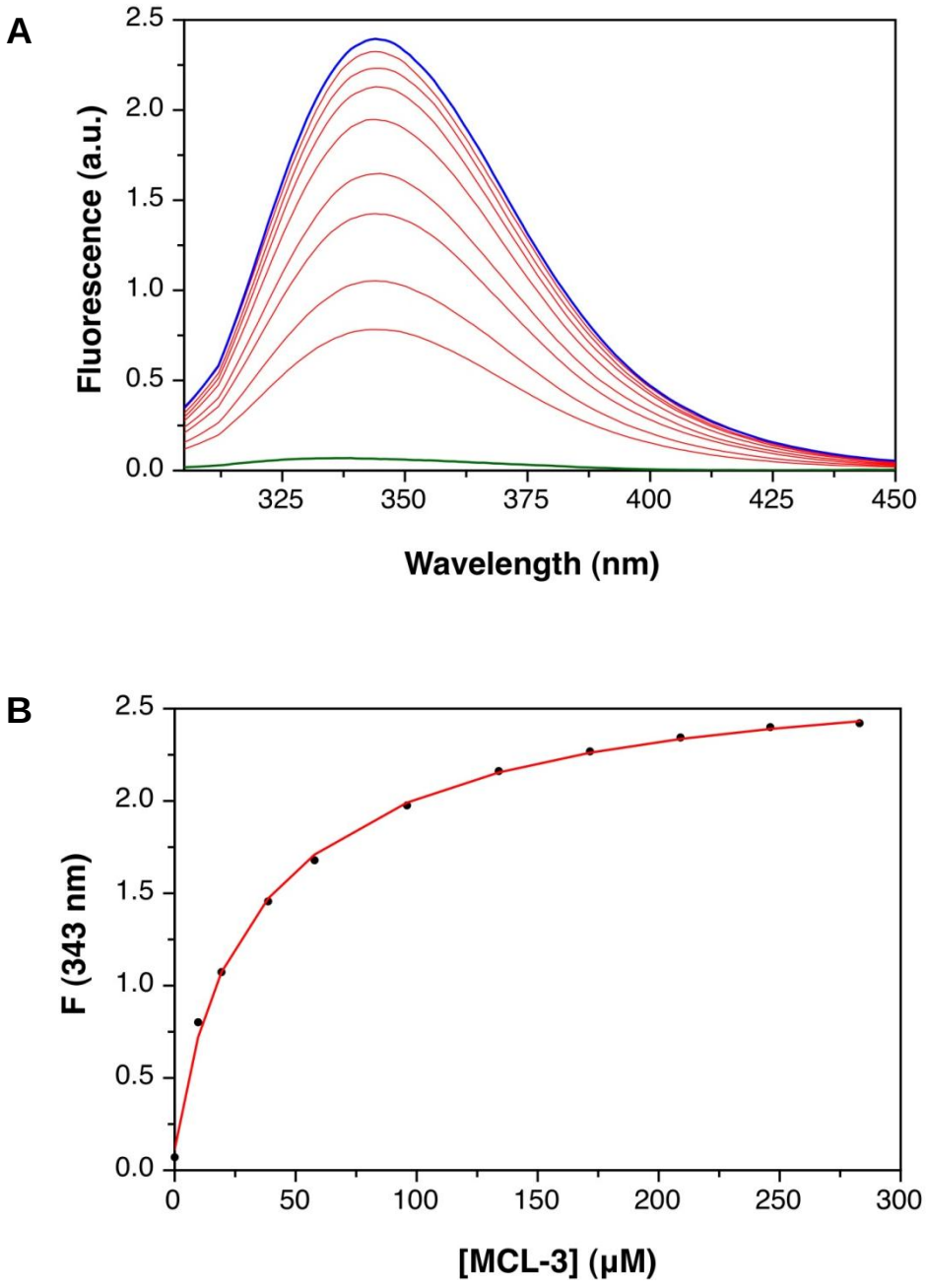

Figure 2.27. *Determination of Cu(I) Stability Constant of CusF: Titration of Cu(I)-complex of CusF with MCL-3.* **A.** Green trace and blue trace correspond to the fluorescence spectra at [MCL-3] = 0 and 283 μM, respectively. **B.** Absorbance change (black points) and curve fit (solid trace) for the titration. 20 μM of Cu(I)-complex of CusF (Cu(I) was provided by the in-situ reduction of $Cu(II)SO_4$ with sodium ascorbate) was titrated with the competing ligand MCL-3 at pH 7 (50 mM MOPS, 150 mM NaCl, 25 °C). Finally, Cu(I) stability constant value of CusF was determined by non-linear least-squares fitting over the entire spectral range using the SPECFIT software package (36). Average fitted value: $\log K_{Cu(I)L} = 14.29 \pm 0.11$.

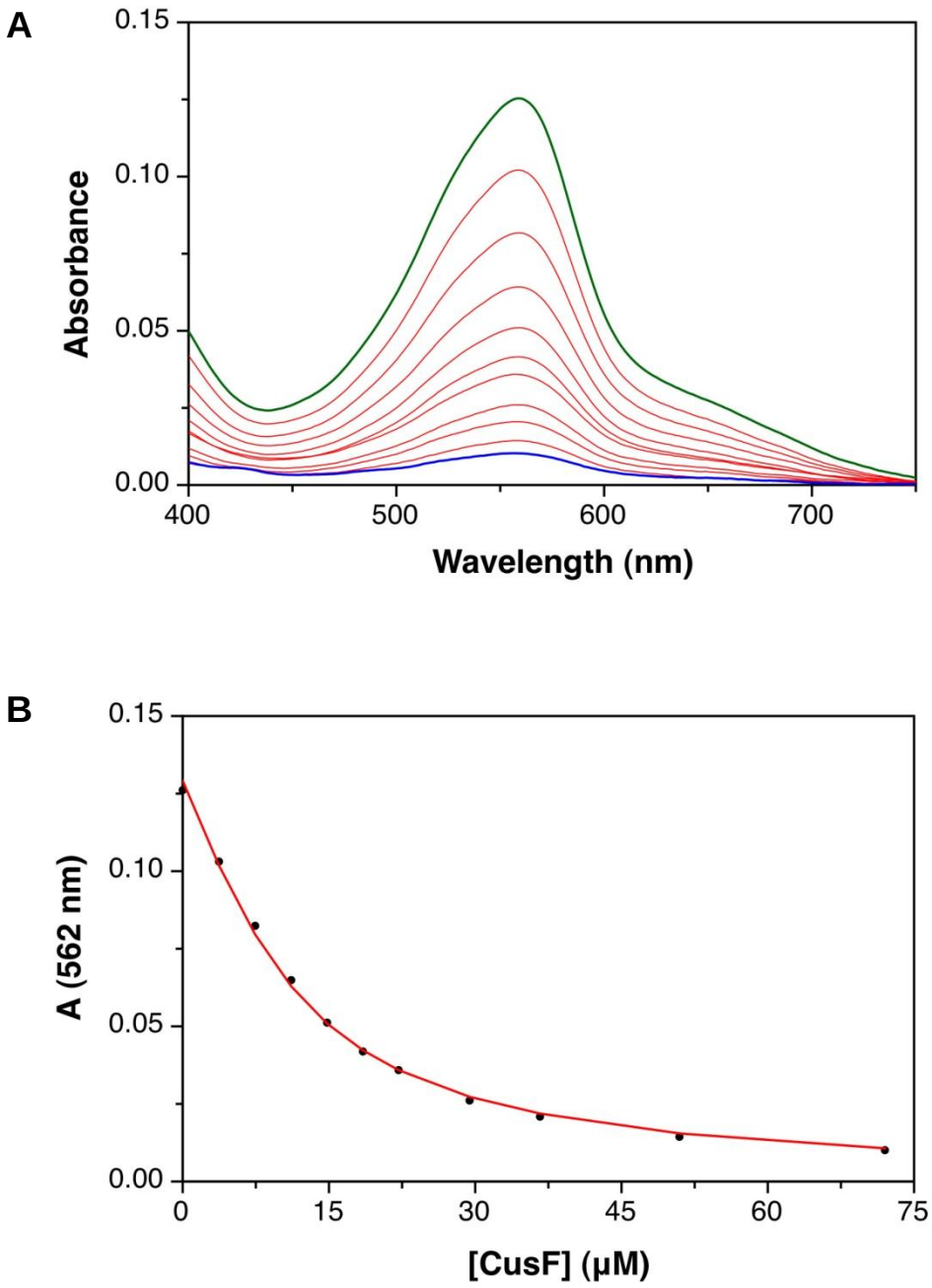

Figure 2.28. *Determination of Cu(I) Stability Constant of CusF: Titration of Cu(I)-complex of BCA with CusF.* **A.** Green trace and blue trace correspond to the UV-visible spectra at [CusF] = 0 and 72 µM, respectively. **B.** Absorbance change (black points) and curve fit (solid trace) for the titration. Cu(I)-complex of BCA was initially formed by the addition of 16 µM $[Cu(I)(CH_3CN)_4]PF_6$ to 50 µM of BCA. Cu(I)-complex of BCA was then titrated with CusF at pH 7 (50 mM MOPS, 150 mM NaCl, 25 °C). Finally, Cu(I) stability constant value of CusF was determined by non-linear least-squares fitting over the spectral range 450-700 nm using the SPECFIT software package (36). Average fitted value: $\log K_{Cu(I)L} = 14.21 \pm 0.01$.

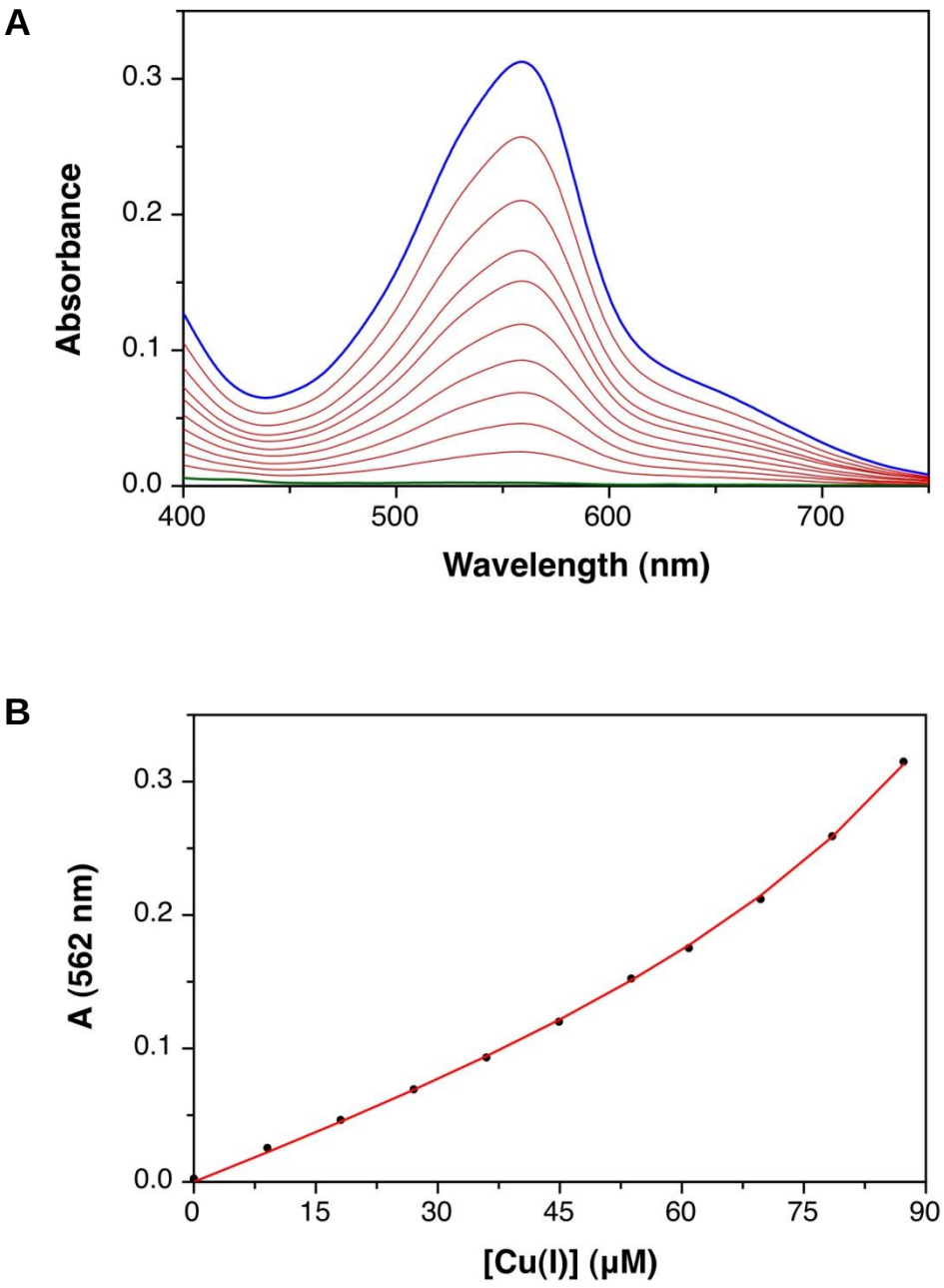

Figure 2.29. *Determination of Cu(I) Stability Constant of CusF: Titration of CusF with Cu(I) in Presence of BCA.* **A.** Green trace and blue trace correspond to the UV-visible spectra at [Cu(I)] = 0 and 87 μM, respectively. **B.** Absorbance change (black points) and curve fit (solid trace) for the titration. CusF (65 μM) was titrated with $[Cu(I)(CH_3CN)_4]PF_6$ in the presence of 80 μM BCA acting as a competing ligand at at pH 7 (50 mM MOPS, 150 mM NaCl, 25 °C). Cu(I) stability constant value of CusF was then determined by non-linear least-squares fitting over the spectral range 450-700 nm using the SPECFIT software package (36). Average fitted value: $\log K_{Cu(I)L} = 14.21 \pm 0.01$.

CusF can be easily expressed and purified in milligram quantities, but the yield of the purified proteins is often limited by reduced solubility or complex multi-step purification process. The titration strategy discussed above requires millimolar stock concentrations of the protein to avoid excessive dilution of the titration medium. Therefore, to determine binding affinities for proteins with limited yield, a modification of the above mentioned approach was examined in this work, where aqueous Cu(I) ions were added to a mixture of the apo-CusF and BCA. Since both BCA and CusF bind Cu(I) strongly, the concentration of free Cu^+ ion is negligible under this condition. The distribution of the Cu^+ ions between BCA and the protein can be followed by the increase in the absorption of $Cu(I)(BCA)_2$ complex at 562 nm (Figure 2.29). Cu(I) was added until ~70% of BCA was bound to copper to ensure 1:2 stoichiometry of $Cu(I)(BCA)_2$ complex throughout the titration. Acetonitrile addition was confined to < 2% of the total volume to prevent any protein denaturation. The binding affinity values obtained by both methods converged at $\log K_{Cu(I)L} = 14.21 \pm 0.03$.

2.3. Conclusion

Knowledge of Cu(I) stability constants of proteins is important to elucidate the mechanisms of cellular copper homeostasis. This information provides a guideline in tailoring the Cu(I)-affinities of synthetic fluorescent sensors to an optimum value which would be suitable for the detection of labile cellular copper. Furthermore, alteration in the original copper affinity of a protein is often associated with impaired copper transport resulting in a pathological condition. For example, a fatal neonatal hepatopathy can be linked to the P174L mutation in Sco1, where the substitution of a proline with a leucine reduces the Cu(I) binding affinity of the protein by a five orders of magnitude (60). The mutated Sco1 thus becomes unsuitable for copper exchange with the chaperone Cox17 which ultimately impairs the cascade of copper transfer reactions required for the CCO assembly in the mitochondria.

Accurate determination of Cu(I) stability constants of proteins critically depend on the Cu(I) affinity standards. This is because majority of the proteins bind the Cu(I) ions too tightly negating the measurement of their stability constants by direct titrations of proteins with Cu^{+} (aq) ions. Instead, the stability constants are determined from the equilibrium competitions between the proteins and the affinity standards for the same Cu^{+} (aq) ions. However, the previously reported binding affinity values of the frequently used Cu(I) affinity standards are largely inconsistent impeding reliable data acquisition for the Cu(I) stability constants of proteins. In this chapter, we developed a set of affinity standards which included three new sulfonated thioether-based ligands that form colorless, water-soluble, and air-stable copper complexes and three previously reported Cu(I) chelators. The Cu(I)-complex stability constants of each of these ligands were determined and cross-validated by independent methods, namely thermodynamic cycle and equilibrium competitions. The results from this work constitute a web of accurately cross-verified Cu(I)-affinity standards encompassing a wide range of affinities which will be useful in determining binding affinities of copper proteins unequivocally.

2.4. Experimental Methods

2.4.1. Determination of Protonation Constants

Protonation constants ($\log K_{Hn}$) of PEMEA and BCA were determined by spectrophotometric titrations as a function of $-\log [H_3O^{+}]$. For all other compounds, $\log K_{Hn}$ values were obtained from acid-base titrations. An ionic background of 0.1 M KCl was used in both methods. In all experiments, a combination glass electrode was calibrated for $-\log [H_3O^{+}]$ before and after the measurement of protonation constants. The calibration was done by acid-base titration of a 5 mM HCl solution (prepared from a volumetric standard) with 0.1 M KOH (volumetric standard added stepwise from a

motorized burette) at 0.1 M ionic strength (KCl). The endpoint, electrode potential, and slope were determined by Gran's method using GLEE software (61).

2.4.1.1. Acid-base Titrations

The measurements of protonation constants were carried out at 25 °C in a titration cell fitted with a temperature-controlled jacket. For BCS, MCL-1, and MCL-3, a known amount of standardized HCl was added to the ligand solution to protonate them completely. Ligand concentration of BCS was kept at 1 mM to avoid substantial complexation of the Ag^+ of the electrode, while 5 mM compounds were used for MCL-1 and MCL-2. DHEAMP was isolated as a hydrochloride salt, thus addition of HCl was unnecessary and 5 mM of the compound was used for the titration. Solutions containing fully protonated compounds were then titrated with a standardized KOH solution (added stepwise from a motorized burette). The Hyperquad software (35) was used to analyze the potentiometric data to obtain the protonation constant values.

2.4.1.2. Spectrophotometric Titrations

Spectrophotometric titrations with PEMEA at 55 μM ligand concentrations were carried out by varying $-\log[H_3O^+]$ from 4 to 3 with the addition of HCl and from 4 to 8.2 with the addition of KOH. Both data sets were combined by normalizing the spectra against the absorbance of the PEMEA at pH 4. The combined data were analyzed by nonlinear least-squares fitting over the entire spectral range using the Specfit software package (36).

2.4.2. Determination of Formal Potentials of Cu(II/I) Redox Couple

Cyclic voltammograms were acquired in 10 mM PIPBS buffer, pH 5, containing 0.1 M $KClO_4$ as the electrolyte using a CH-Instruments potentiostat (model 600A). Experiments were carried out in a single compartment cell with a glassy carbon working electrode, a Pt counter electrode, and an aqueous Ag/AgCl reference electrode (1 M

KCl). The half-wave potentials were referenced to ferrocenium (0.40 vs. SHE (62)) or ferroin (1.112 vs. SHE (8)) as external standards. Measurements were typically performed with a scan rate of 20 - 50 mV s^{-1}.

Table 2.7. *Experimental Details of Stability Constant Measurements*

Ligand	Competing Ligand	Copper Source	Buffer Composition	Conc. of Ligand	Conc. of Competing Ligand	Conc. of Copper
PEMEA	-	$CuSO_4$	10 mM PIPBS, 100 mM $KClO_4$, pH 5 (Buffer **A**)	96 µM	-	0 - 247 µM
	Acetonitrile	Cu(I)-Acetonitrile	14 mM $HClO_4$, 100 mM $KClO_4$, pH 2 (Buffer **B**)	100 µM	958 mM	0 - 236 µM
MCL-1	-	$CuSO_4$	Buffer **A**	50 µM	-	0 - 971 µM
	PEMEA	Cu(I)-MCL-1	Buffer **A**	200 – 978 µM	96 µM	200 µM
BCA	MCL-1	Cu(I)-MCL-1	Buffer **A**	100 µM	100 - 394 µM	100 µM
	PEMEA	Cu(I)-Acetonitrile	Buffer **A**	100 µM	0 - 227 µM	40 µM
MCL-2	BCA	Cu(I)-MCL-2	50 mM PIPES, 60 mM $KClO_4$, pH 7 (Buffer **C**)	0.04 – 4.97 mM	100 µM	40 µM
DHEAMP	-	$CuSO_4$	10 mM $HClO_4$, 100 mM $KClO_4$, pH 2.11 (Buffer **D**)	100 µM	-	0 - 393 µM

Table 2.7. *Continued*

Ligand	Competing Ligand	Copper Source	Buffer Composition	Conc. of Ligand	Conc. of Competing Ligand	Conc. of Copper
BCS	DHEAMP	$CuSO_4$	10 mM MES, 100 mM $KClO_4$, pH 6 (Buffer **E**)	300 µM	300 µM	0 - 390 µM
	MCL-1	Cu(I)-MCL-1	10 mM PIPES, 100 mM $KClO_4$, pH 7 (Buffer **F**)	100 µM	50 - 978 µM	50 µM
	MCL-1	Cu(I)-MCL-2	Buffer **F**	50 µM	0 - 391 µM	5 µM
MCL-3	-	$CuSO_4$	Buffer **A**	100 µM	-	0 - 198 µM
	BCA	Cu(I)-MCL-3	Buffer **A**	100- 682 µM	200 µM	100 µM
	BCS	Cu(I)-MCL-3	Buffer **A**	0.05 - 1.02 mM	100 µM	50 µM
CusF Protein	MCL-3	$CuSO_4$ + ascorbate	50 mM MOPS, 150 mM NaCl, pH 7 (Buffer **G**)	20 µM	0 - 283 µM	20 µM
	BCA	Cu(I)-Acetonitrile	Buffer **G**	0 -72 µM	50 µM	16 µM
	BCA	Cu(I)-Acetonitrile	Buffer **G**	65 µM	80 µM	0 - 87 µM

2.4.3. Determination of Stability Constants of Copper Ligands

Table 2.7 summarizes the details of the experimental conditions used in the measurement of stability constants of copper ligands, namely the composition of the titration medium; nature of the competing ligand and the copper source; individual concentrations of the components including ligand being measured, the competing ligand, and the copper.

As a general consideration, spectrophotometric titrations were carried out under anaerobic condition in a septum-fitted air tight cuvette. All solutions including buffers, acetonitrile, and deionized water were thoroughly degassed before use. Usually reagent solutions, especially preformed copper-complexes, were prepared fresh inside a nitrogen tent; in case an old stock solution of free ligand was used, it was degassed thoroughly. All solutions were added with air-tight syringes. 50-100 μM sodium ascorbate was added as a reducing agent for competition titrations with Cu^{+} ions where the apparent affinity of one of the ligands is low, e.g., PEMEA-acetonitrile titration. Concentrations of reagents were corrected for dilution before fitting the experimental data with the Specfit software.

2.4.4. Expression and Purification of CusF

E. coli BL21(DE3) cells containing the pASK-IBA3 plasmid (a gift from Dr. M.M. McEvoy) with the gene encoding CusF residues 6-88, were grown in LB media containing 100 mg/L ampicillin with shaking at 37 °C. The cells were grown to an optical density at 600 nm of 0.6 - 1.1, and then protein expression was induced with 0.8 mg/L anhydrotetracycline (AHT). After 5 hours, the cells were harvested by centrifugation and the pellet was stored at –80 °C. The cell pellet was thawed and resuspended in buffer G and CusF was extracted by three rounds of freezing and thawing of the suspended cells followed by agitation for 1 h at 4 °C. The cell extract was centrifuged at 6000 g for 15 min at 4 °C and the supernatant was stored at –80 °C. Before purification, the supernatant was concentrated with a 3K microsep centrifugal device (Pall Life Sciences) and applied to a Superdex 75 gel filtration column equilibrated with Buffer G for purification. Fractions containing CusF were pooled, concentrated, and applied to the Superdex 75 column for another round of gel purification. Fractions containing pure protein were confirmed by Laemmli-SDS-PAGE, pooled, concentrated, and stored at –20 °C in the elution buffer. The protein was used within two days of purification.

2.4.5. Determination of Stability Constant of CusF

Protein concentration of CusF was determined from the absorbance of the solution at 280 nm with extinction coefficient of 5500 M^{-1} cm^{-1} as calculated by ExPASy software ProtParam (63). The concentration was verified from the mole-ratio titration of CusF with Cu(I) generated in situ by the reduction of $CuSO_4$ with sodium ascorbate. Concentrations of BCA and Cu(I) were verified from a separate mole-ration titration between BCA and Cu(I)-acetonitrile. Extinction coefficient of 7900 M^{-1} cm^{-1} was used for $Cu(I)(BCA)_2$ complex at 562 nm (10). The experimental conditions for the competition titrations between CusF and MCL-3 and CusF and BCA are compiled in Table 2.7.

2.5. References

1. Lutsenko S (2010) Human copper homeostasis: a network of interconnected pathways. *Current Opinion in Chemical Biology* 14(2):211-217.

2. Debye P & Huckel E (1923) The theory of electrolytes I. The lowering of the freezing point and related occurrences. *Physikalische Zeitschrift* 24:185-206.

3. Manov GG, Bates RG, Hamer WJ, & Acree SF (1943) Values of the constants in the Debye-Huckel equation for activity coefficients. *Journal of the American Chemical Society* 65:1765-1767.

4. Kielland J (1937) Individual activity coefficients of ions in aqueous solutions. *Journal of the American Chemical Society* 59:1675-1678.

5. Davies CW (1962) *Ion association* (Washington, Butterworths).

6. Schwarzenbach G (1957) *Complexometric titrations* (New York, Interscience Publishers).

7. Morgan MT, Bagchi P, & Fahrni CJ (2013) Fluorescent probes for monovalent copper. *Encyclopedia of Inorganic and Bioinorganic Chemistry*, (John Wiley & Sons, in press).

8. Ambundo EA, Deydier MV, Grall AJ, Aguera-Vega N, Dressel LT, Cooper TH, Heeg MJ, Ochrymowycz LA, & Rorabacher DB (1999) Influence of coordination geometry upon copper(II/I) redox potentials. Physical parameters for twelve copper tripodal ligand complexes. *Inorganic Chemistry* 38(19):4233-4242.

9. Rae TD, Schmidt PJ, Pufahl RA, Culotta VC, & O'Halloran TV (1999) Undetectable intracellular free copper: The requirement of a copper chaperone for superoxide dismutase. *Science* 284(5415):805-808.

10. Xiao ZG, Brose J, Schimo S, Ackland SM, La Fontaine S, & Wedd AG (2011) Unification of the copper(I) binding affinities of the metallo-chaperones Atx1, Atox1, and related proteins. Detection probes and affinity standards. *Journal of Biological Chemistry* 286(13):11047-11055.

11. Xiao ZG & Wedd AG (2010) The challenges of determining metal-protein affinities. *Natural Product Reports* 27(5):768-789.

12. Deranlea D (1969) Theory of measurement of weak molecular complexes .2. Consequences of multiple equilibria. *Journal of the American Chemical Society* 91(15):4050

13. Hawkins CJ & Perrin DD (1963) Oxidation-reduction potentials of metal complexes in water .2. Copper complexes with 2,9-Dimethyl- and 2-Chloro-1,10-Phenanthroline. *Journal of the Chemical Society* (MAY):2996

14. Bernardo MM, Heeg MJ, Schroeder RR, Ochrymowycz LA, & Rorabacher DB (1992) Comparison of the influence of saturated nitrogen and sulfur donor atoms on the properties of copper(II/I) macrocyclic polyamino polythiaether ligand complexes - redox potentials and protonation and stability-constants of cuil species and new structural data. *Inorganic Chemistry* 31(2):191-198.

15. Milazzo G & Caroli S (1978) *Tables of Standard Electrode Potentals* (Wiley, New York).

16. Cox JD (1982) Notation for states and processes, significance of the word standard in chemical thermodynamics, and remarks on commonly tabulated forms of thermodynamic functions. *Pure and Applied Chemistry* 54(6):1239-1250.

17. Davies CW (1938) The extent of dissociation of salts in water. Part VIII. An equation for the mean ionic activity coefficient of an electroltye in water, and a revision of the dissociation constants of some sulphates. *Journal of the Chemical Society*:2093-2098.

18. Banci L, Bertini I, Ciofi-Baffoni S, Kozyreva T, Zovo K, & Palumaa P (2010) Affinity gradients drive copper to cellular destinations. *Nature* 465(7298):645

19. Allen S, Badarau A, & Dennison C (2012) Cu(I) affinities of the domain 1 and 3 sites in the human metallochaperone for Cu,Zn-superoxide dismutase. *Biochemistry* 51(7):1439-1448.

20. Crow JP, Sampson JB, Zhuang YX, Thompson JA, & Beckman JS (1997) Decreased zinc affinity of amyotrophic lateral sclerosis-associated superoxide

dismutase mutants leads to enhanced catalysis of tyrosine nitration by peroxynitrite. *Journal of Neurochemistry* 69(5):1936-1944.

21. Badarau A & Dennison C (2011) Copper trafficking mechanism of CXXC-containing domains: Insight from the pH-dependence of their Cu(I) affinities. *Journal of the American Chemical Society* 133(9):2983-2988.

22. Yatsunyk LA & Rosenzweig AC (2007) Cu(I) binding and transfer by the N terminus of the Wilson disease protein. *Journal of Biological Chemistry* 282(12):8622-8631.

23. Wernimont AK, Yatsunyk LA, & Rosenzweig AC (2004) Binding of copper(I) by the Wilson disease protein and its copper chaperone. *Journal of Biological Chemistry* 279(13):12269-12276.

24. Jensen PY, Bonander N, Moller LB, & Farver O (1999) Cooperative binding of copper(I) to the metal binding domains in Menkes disease protein. *Biochimica Et Biophysica Acta-Protein Structure and Molecular Enzymology* 1434(1):103-113.

25. Changela A, Chen K, Xue Y, Holschen J, Outten CE, O'Halloran TV, & Mondragon A (2003) Molecular basis of metal-ion selectivity and zeptomolar sensitivity by CueR. *Science* 301(5638):1383-1387.

26. Zeng L, Miller EW, Pralle A, Isacoff EY, & Chang CJ (2006) A selective turn-on fluorescent sensor for imaging copper in living cells. *Journal of the American Chemical Society* 128(1):10-11.

27. Kamau P & Jordan RB (2001) Complex formation constants for the aqueous copper(I)-acetonitrile system by a simple general method. *Inorganic Chemistry* 40(16):3879-3883.

28. Pufahl RA, Singer CP, Peariso KL, Lin SJ, Schmidt PJ, Fahrni CJ, Culotta VC, PennerHahn JE, & Ohalloran TV (1997) Metal ion chaperone function of the soluble Cu(I) receptor Atx1. *Science* 278(5339):853-856.

29. Wernimont AK, Huffman DL, Lamb AL, O'Halloran TV, & Rosenzweig AC (2000) Structural basis for copper transfer by the metallochaperone for the Menkes/Wilson disease proteins. *Nature Structural Biology* 7(9):766-771.

30. Miras R, Morin I, Jacquin O, Cuillel M, Guillain F, & Mintz E (2008) Interplay between glutathione, Atx1 and copper. 1. Copper(I) glutathionate induced dimerization of Atx1. *Journal of Biological Inorganic Chemistry* 13(2):195-205.

31. Badarau A & Dennison C (2011) Thermodynamics of copper and zinc distribution in the cyanobacterium Synechocystis PCC 6803. *Proceedings of the National Academy of Sciences of the United States of America* 108(32):13007-13012.

32. Xiao Z, Donnelly PS, Zimmermann M, & Wedd AG (2008) Transfer of copper between bis(thiosemicarbazone) ligands and intracellular copper-binding proteins. Insights into mechanisms of copper uptake and hypoxia selectivity. *Inorganic Chemistry* 47(10):4338-4347.

33. Xiao ZG, Loughlin F, George GN, Howlett GJ, & Wedd AG (2004) C-terminal domain of the membrane copper transporter Ctr1 from Saccharomyces cerevisiae binds four Cu(I) ions as a cuprous-thiolate polynuclear cluster: Sub-femtomolar Cu(I) affinity of three proteins involved in copper trafficking. *Journal of the American Chemical Society* 126(10):3081-3090.

34. Bernardo MM, Schroeder RR, & Rorabacher DB (1991) Electrochemical properties of copper(II) copper(I) macrocyclic polythia ether complexes - determination of formal potential values and cyclic voltammetric behavior. *Inorganic Chemistry* 30(6):1241-1247.

35. Gans P, Sabatini A, & Vacca A (1996) Investigation of equilibria in solution. Determination of equilibrium constants with the HYPERQUAD suite of programs. *Talanta* 43(10):1739-1753.

36. Binstead RA & Zuberbühler AD (2001) SPECFIT Global Analysis System (Spectrum Software Associates, Marlborough MA 01752), 3.0.27.

37. Gershuns AL (1970) Spectrophotometric study of the acid-base properties of 2,2'-bicinchoninic acid and its derivatives. *Visnik Kharkivskogo* 46.

38. Damu KV, Shaikjee MS, Michael JP, Howard AS, & Hancock RD (1986) Control of metal-ion selectivity in ligands containing neutral oxygen and pyridyl groups. *Inorganic Chemistry* 25(22):3879-3883.

39. Martell AE (1974) *Critical stability constants* (New York, Plenum Press).

40. Cooper TH, Mayer MJ, Leung KH, Ochrymowycz LA, & Rorabacher DB (1992) Kinetic and thermodynamic measurements on branched amino polythiaether ligands - a family of complexing agents analogous to EDTA and NTA exhibiting enhanced selectivity for copper(II). *Inorganic Chemistry* 31(18):3796-3804.

41. Avdeef A, Sofen SR, Bregante TL, & Raymond KN (1978) Coordination chemistry of microbial iron transport compounds .9. Stability-constants for catechol models of enterobactin. *Journal of the American Chemical Society* 100(17):5362-5370.

42. Alderighi L, Gans P, Ienco A, Peters D, Sabatini A, & Vacca A (1999) Hyperquad simulation and speciation (HySS): a utility program for the investigation of equilibria involving soluble and partially soluble species. *Coordination Chemistry Reviews* 184:311-318.

43. Smith PK, Krohn RI, Hermanson GT, Mallia AK, Gartner FH, Provenzano MD, Fujimoto EK, Goeke NM, Olson BJ, & Klenk DC (1985) Measurement of protein using bicinchoninic acid. *Analytical Biochemistry* 150(1):76-85.

44. Gekko K, Ohmae E, Kameyama K, & Takagi T (1998) Acetonitrile-protein interactions: amino acid solubility and preferential solvation. *Biochimica Et Biophysica Acta-Protein Structure and Molecular Enzymology* 1387(1-2):195-205.

45. Lin X, Zhao WJ, & Wang X (2010) Characterization of conformational changes and noncovalent complexes of myoglobin by electrospray ionization mass spectrometry, circular dichroism and fluorescence spectroscopy. *Journal of Mass Spectrometry* 45(6):618-626.

46. Smith GF & Wilkins DH (1953) New colorimetric reagent specific for copper - determination of copper in iron. *Analytical Chemistry* 25(3):510-511.

47. Landers JW & Zak B (1958) Determination of serum copper and iron in a single small sample. *American Journal of Clinical Pathology* 29(6):590-592.

48. Bjerrum J (1957) *Metal amine formation in aqueous solution. Theory of the reversible step reactions* (P. Haase & Son, Copenhagen).

49. Ahmadi R, Kalateh K, Alizadeh R, Khoshtarkib Z, & Amani V (2009) Dichlorido (2,9- dimethyl- 4,7- diphenyl- 1,10- phenanthroline- kappa N-2,N') mercury(II) acetonitrile hemisolvate. *Acta Crystallographica Section E-Structure Reports Online* 65:M848-U263.

50. Alizadeh R (2009) (2,9-Dimethyl-4,7-diphenyl-1,10-phenanthroline-kappa N-2,N')bis(thiocyanato-kappa S)mercury(II). *Acta Crystallographica Section E-Structure Reports Online* 65:M817-U1225.

51. Dale JM & Banks CV (1963) Study of metal-1,10-phenanthroline complex equilibria by potentiometric measurement. *Inorganic Chemistry* 2(3):591

52. Hall JR, Plowman RA, & Preston HS (1965) Cordination compounds of substituted 1,10-phenanthrolines and related dipyridyls .8. Complexes of silver and 2,9-dimethyl-1,10-phenanthroline. *Australian Journal of Chemistry* 18(9):1345

53. Yao SG, Cherny RA, Bush AI, Masters CL, & Barnham KJ (2004) Characterizing bathocuproine self-association and subsequent binding to Alzheimer's disease amyloid beta-peptide by NMR. *Journal of Peptide Science* 10(4):210-217.

54. Bertini I, Cavallaro G, & McGreevy KS (2010) Cellular copper management-a draft user's guide. *Coordination Chemistry Reviews* 254(5-6):506-524.

55. Pace CN, Vajdos F, Fee L, Grimsley G, & Gray T (1995) How to measure and predict the molar absorption-coefficient of a protein. *Protein Science* 4(11):2411-2423.

56. Loftin IR, Franke S, Roberts SA, Weichsel A, Heroux A, Montfort WR, Rensing C, & McEvoy MM (2005) A novel copper-binding fold for the periplasmic copper resistance protein CusF. *Biochemistry* 44(31):10533-10540.

57. Xue Y, Davis AV, Balakrishnan G, Stasser JP, Staehlin BM, Focia P, Spiro TG, Penner-Hahn JE, & O'Halloran TV (2008) Cu(I) recognition via cation-pi and methionine interactions in CusF. *Nature Chemical Biology* 4(2):107-109.

58. Loftin IR, Blackburn NJ, & McEvoy MM (2009) Tryptophan Cu(I)-pi interaction fine-tunes the metal binding properties of the bacterial metallochaperone CusF. *Journal of Biological Inorganic Chemistry* 14(6):905-912.

59. Kittleson JT, Loftin IR, Hausrath AC, Engelhardt KP, Rensing C, & McEvoy MM (2006) Periplasmic metal-resistance protein CusF exhibits high affinity and specificity for both Cu-I and Ag-I. *Biochemistry* 45(37):11096-11102.

60. Banci L, Bertini I, Ciofi-Baffoni S, Leontari I, Martinelli M, Palumaa P, Sillard R, & Wang SL (2007) Human Sco1 functional studies and pathological implications of the P174L mutant. *Proceedings of the National Academy of Sciences of the United States of America* 104(1):15-20.

61. Gans P & O'Sullivan B (2000) GLEE, a new computer program for glass electrode calibration. *Talanta* 51(1):33-37.

62. Koepp HM, Wendt H, & Strehlow H (1960) *Zeitschrift Fur Elektrochemie* 64(4):483-491.

63. Gasteiger E, Hoogland C, A. G, Duvaud S, Wilkins MR, Appel RD, & Bairoch A (2005) *The proteomics protocols handbook* (Totowa, N.J., Humana Press).

CHAPTER 3

IN-SITU VISUALIZATION OF BIOLOGICAL COPPER WITH A WATER SOLUBLE FLUORESCENT PROBE: IN-GEL DETECTION OF A COPPER CHAPERONE

In this chapter, the thermodynamic properties of a water soluble, high contrast Cu(I)-selective fluorescent probe CTAP-2 were determined. This is the first fluorescent probe among Cu(I)-sensors found in the literature which dissolves completely in water without formation of colloidal nanoparticles. This probe was utilized to develop a novel in-gel detection method of a copper chaperone under non-denaturing conditions. This work was published in the Journal of the American Chemical Society (1).

3.1. Background

The identification of genes and proteins involved in copper homeostasis greatly facilitated our understanding of the mechanisms of copper regulation (2), however, the knowledge about cellular distribution of copper during normal physiological function and its alteration in diseases are still limited. For example, little is known about the subcellular organelles and biomolecules including proteins and small molecules that are involved in transiently storing copper ions prior to their incorporation into copper-proteins. Many efforts have been directed towards developing highly sensitive analytical techniques and instruments which will be useful for the in situ analysis of copper ions as well as for the understanding of copper speciation in biomolecules within the native physiological environment. This section will provide a brief overview of the key achievements in the rapidly evolving research area of detecting biological copper and then it will elaborate on the design principles of Cu-selective fluorophores.

3.1.1. In-Situ Detection of Cellular Copper

The analytical techniques that were developed to furnish information about cellular copper status can be broadly classified into three categories: a) bulk techniques, like ICP-MS and AAS, to examine the total copper ion content of a cell; b) imaging techniques, exemplified by XRF, LA-ICP-MS, and SIMS, that provide knowledge about spatial distribution of the copper ions; and c) histochemical dyes and Cu(I)-selective fluorescent probes which are useful to capture the kinetically labile copper ion pool. The three categories provide distinct, yet complementary, information regarding copper homeostasis. For example, quantification of the total copper ion content in a cell (as in a) can report the movement of the metal into or out of the cell under different physiological conditions. The analytical techniques that reveal the copper topography of a cell (as in b) does not distinguish between the protein-bound and labile copper and is therefore of particular value in elucidating the speciation of the total cellular copper pool. Conversely, copper indicators (as in c) rely on a competitive exchange of copper ions with native endogenous ligands and hence only the labile fraction of the total cellular copper can be probed by this method.

3.1.1.1. Methods to Probe Bulk Copper Concentration

Atomic absorption spectrometry (AAS) and inductively coupled plasma mass spectrometry (ICP-MS) are extensively employed for the determination of the total trace element concentration in biological samples. These methods are useful in those studies, where knowledge of the total trace element content is sufficient without the need for speciation. In most cases, trace elements are determined in the bulk of biological extracts obtained after homogenization of different cell types or tissues, and often, after acid digestion.

a) Atomic Absorption Spectroscopy (AAS)

Atomic-absorption spectroscopy (AAS) uses the absorption of light to measure the concentration of gas-phase atoms by following the Beer-Lambert law. The atoms absorb ultraviolet or visible light and make transitions to higher electronic energy levels. The amount of energy required and as such the wavelength of the absorbed radiation is specific to a particular electron transition in a particular element, which gives the technique its elemental selectivity. Concentration measurements are usually determined from a working curve after calibrating the instrument with standards of known analyte concentration. In order to analyze a liquid or solid sample for its atomic constituents, it has to be atomized. The techniques most widely used for this purpose include flames and electrothermal (graphite tube) atomizers.

AAS has a wide range of applications in determining copper content in a variety of biological substances including human serum, urine, saliva, tooth samples, bone tissue, and hair sample (3). This technique has also been successfully used to investigate role of copper ions in various diseased conditions. For example, high urinary copper is a diagnostic feature of Wilson's disease linked to liver malfunction (4, 5) and AAS is often employed to measure copper content of urine in clinical laboratories (6). Similarly, AAS revealed elevated copper concentration associated with other diseases, for example, breast cancer (7, 8), rheumatoid arthritis (9), bladder cancer (10), colorectal cancer (11), coronary heart disease (12), and alcoholic liver disease (13).

Atomic-absorption spectroscopy is a fast inexpensive detection method, and sample preparation and instrumentation are easy to handle without substantial technical training. However, the sensitivity of the technique is low with the detection limits commonly at the ppm level (14).

b) Inductively Coupled Plasma Mass Spectrometry (ICP-MS)

In ICP-MS, a high-temperature inductively coupled plasma source composed of ionized argon gas converts the atoms of the elements in the sample to ions. These ions are then separated and detected by the mass spectrometer. The ability to filter ions on their mass-to-charge ratio allows ICP-MS to supply isotopic information, since different isotopes of the same element have different masses. Because the ion signal received by the detector is proportional to the initial concentration in the sample, the technique can be used for quantitative trace element speciation through calibration with known standards. ICP-MS is one of the most widely used mass spectrometric techniques for the analysis of trace elements because of its isotope specificity, versatility, high sensitivity (detection limit down to ppt level), and a large linear dynamic range (10^5–10^6) (15, 16).

Although ICP-MS can be successfully used for trace element analysis in biological tissues and fluids (3, 17-19), the potential of this method is best harnessed as a hyphenated technique combined with chromatographic separation of metallobiomolecules including metalloproteins. One of the most favored methods for a rapid semi-quantitative screening for the presence of metal–protein complexes in biological samples has been the coupling of size exclusion chromatography (SEC) and ICP-MS. SEC allows the fractionation of the metalloproteins as a function of size prior to elemental detection. Several SEC-ICP-MS applications exploited the capability of ICP-MS to detect a single or multiple metals in separated protein fractions (20-22). However, the chromatographic purity of such fractions is usually low and the identity of the metal-binding species cannot be assigned by this method.

ICP-MS is sometimes coupled with high-performance liquid chromatography (HPLC) to identify metal containing protein fractions. This is often used as a second separation step after size exclusion chromatography to achieve a higher degree of purity of the fractionated metal species. For example, SEC followed by anion exchange (AE) HPLC was performed to study the Cu accumulation and turnover in marine animals (23).

Capillary electrophoresis (CE) combined with ICP-MS is becoming increasingly popular to analyze metalloproteins as CE is less susceptible than HPLC to generate artifacts due to the metal exchange by interaction with the stationary phase. CE also offers additional advantages that are attractive for biological research, such as a small sample size and very high-resolution. However, CE-ICP-MS applications, thus far, mainly involved studies of metal-binding to metallothioneins (24). The reason is that the proteins with higher molecular mass increases the risk of adsorption on the capillary wall and thus preventing the analysis of such proteins (25).

The major problem for the metal detection in biological systems is the low concentration of the trace metals present in a biological tissue. This is further complicated by the fact that these endogenous trace metals of already low concentrations are usually distributed among several biomolecules and thus demanding the development of instrumental techniques with high detection sensitivity. In that regard, inductively coupled plasma mass spectrometry coupled with a chromatographic separation mode is virtually the only technique for element-specific detection that is compatible with the trace element concentrations in bulk biological materials. The major limitation of these hyphenated techniques is the contamination from the adsorbed metal ion impurities on the stationary phase as they can exchange with the native metal ions in a protein or can be scavenged by ligands from the biological extract leading to ghost signals. Moreover, ICP-MS does not allow the identification of the metal-containing species, hence the fractions separated by liquid chromatography have to be analyzed with mass spectrometry and the faithfulness of such identification depends on the purity of the separated fractions.

3.1.1.2. Bioimaging to Reveal Copper Topography

The characterization of the copper biochemistry of a cell is not complete with the studies of its genome and proteome, but it is critically dependent on the distribution of the metal among the different species in various cellular compartments. Therefore,

bioimaging of copper, which produces spatially resolved concentration maps of the metal in the cell, provides valuable information about the intracellular metal speciation and in some cases also characterizes the copper coordination sites *in situ*. Several microanalytical techniques, such as X-ray fluorescence, SIMS, LA-ICP-MS, offer micron to sub-micron spatial resolution and have detection limit around 0.1 to 100 μg g^{-1} and thus have been suitable to probe trace metal speciation in a cell (26). The instrumentations of these imaging modes are continually progressing in order to improve the spatial resolution and detection sensitivity of metal analysis.

a) X-ray fluorescence (XRF)

In XRF-based imaging, the inner shell electrons of atoms are excited and ultimately relax to the ground state with the emission of photons which correspond to a measurable X-ray fluoresceence. Because the emitted X-ray energy depends on the nuclear charge, each element has unique emission energy, so this technique allows for multi-element analysis of a single sample. XRF provides qualitative and quantitative information on the topography, concentration and oxidation state of copper ions (27). Another advantage of the XRF imaging is that the sample is not ablated during the measurement. Depending on the mode of excitation, XRF analytical techniques can be categorized into three different classes: electron probe X-ray microanalysis (EPXMA) which uses an electron beam to excite the sample, proton or particle induced X-ray emission (PIXE) where a proton beam is the excitation source, and synchrotron X-ray fluorescence (SXRF) which is based on excitation with X-ray.

Among the above-mentioned X-ray-based techniques, SXRF has the highest elemental sensitivity and together with submicron resolution and high penetration depth this technique has been proven to be useful for analyzing biological samples (28, 29). SXRF microscopy can also provide information regarding the oxidation state and coordination environment of metals by scanning the incident X-ray energy across the

absorption edge of an element of interest and by measuring the photons transmitted through the sample, this method is known as X-ray absorption near-edge structure (XANES) spectroscopy. In a study where SXRF microscopy was employed to explore the subcellular localization of copper in NIH 3T3 mouse fibroblast cells supplemented with 150 µM $CuCl_2$, XANES spectra showed a near-edge feature that is characteristic for low-coordinate monovalent copper ion, thus consistent with the reducing environment of the cytosol (30).

Synchrotron X-ray fluorescence microscopy was also applied to compare the cellular copper topology and concentration in disease states with the normal physiological conditions. Farquharson et al. applied SXRF to investigate the quantity and spatial distribution of trace metals in breast cancer cells (31, 32). The studies revealed an increase in all measured metal concentrations, particularly for Zn and Cu, in the tumor areas of the studied samples. Further analysis with XANES spectroscopy indicated that Cu is present as a mixture of its monovalent and divalent oxidation states, for both normal and cancerous tissue.

The major shortcoming of the SXRF technique is the radiation damage of the biological sample because of the use of the high energy excitation source. To control the effects of radiation damage which includes decrease in spatial resolution, freeze-drying is the method of choice to preserve the elemental content. However, this method is not optimum to preserve the innate three dimensional structure of the specimen or its substructure. Therefore, it is challenging to colocalize the elemental speciation with subcellular organelles which are typically visualized by organelle-specific fluorescent markers or immunofluorescence prior to the freeze-drying. In order to circumvent this problem, SXRF has to use appropriate organelle-specific markers labeled with a heavy xenobiotic element which could be directly measured by SXRF at the time of elemental analysis (33).

b) Secondary Ion Mass Spectrometry (SIMS)

In this technique, the surface of the solid specimen is sputtered during bombardment with a focused primary ion beam. The secondary ions generated from the surface of the sample are separated using their mass to charge ratio measured with a mass spectrometer. Therefore, SIMS imaging is able to determine the elemental, isotopic, and molecular composition of the specimen surface. SIMS is multielemental with isotopic capability, characterized by detection limits of 0.1–1 μg/g, and spatial resolution of 50 nm, and thus making it suitable for cellular imaging. For example, SIMS was used to develop an improved diagnostic tool for Wilson's disease by detecting copper in micro-scale biopsies (34). This study was done with a murine model of Wilson's disease and as expected a 40–50 times higher Cu concentration was measured in the disease tissue as compared to the control mouse.

Since the surface of the specimen is sputtered by a primary ion beam, SIMS is destructive to the specimen. SIMS experiments can also be difficult to perform because the technique requires specimens to be compatible with the use of ultra-high vacuum as encountered during the analysis. Furthermore, due to considerable matrix effects SIMS can only provide qualitative images of elements from the top atomic layer of biological tissues.

c) Laser Ablation Inductively Coupled Plasma Mass Spectrometry (LA-ICPMS)

In LA-ICP-MS, the sample material can be directly ablated from the surface by using a focused laser beam. The evaporated material is then transported with a carrier gas into an ICP-MS instrument for trace element analysis. Mass spectrometer separates ions by their mass-to-charge ratio and hence isotopic information can be attained by this method. Furthermore, since the laser ablates only one area at a time, this technique results in high positional precision. Because of high sensitivity of LA-ICP-MS, this technique is emerging as a method of choice for soft tissue analysis and it has been primarily used in

neurological research where metal speciation in brains from patients with neurological diseases are compared with healthy individuals. Centering around LA-ICP-MS imaging, Becker laboratory developed highly sophisticated analytical BrainMet techniques (BrainMet – Bioimaging of Metals in Brain and Metallomics) (35, 36), which have been routinely used to study the distribution and quantity of trace metals (e.g., Cu, Zn, Fe, Mo, Na, K, and Mg) in thin tissue sections of brain samples (37-42). These techniques were applied to understand change in metal speciation in various disease conditions, such as brain tumor (38, 40, 43, 44), Alzheimer's disease (45), and Parkinson's disease (37).

Although new biological applications of LA-ICP-MS are evolving, this method is still not being used extensively. The limited application of LA-ICP-MS in biological and medical research can be explained by difficulties in the laser ablation of biological matrices, destructive nature of the technique unsuitable for live-cell imaging, the lack of convenient quantification procedures, and relatively high price of modern and powerful laser ablation systems with a good resolution power suitable for cellular imaging.

3.1.1.3. Detection of Kinetically Labile Copper

As discussed in Section 1.3, the intracellular environment is devoid of free copper ions of either valence state to protect cells from deleterious oxidative damage. However, the rapid exchange of cellular copper with the extracellular medium indicates that not all copper ions are strongly chelated by proteins. This kinetically labile pool is instrumental in visualizing the bioavailable copper as it can exchange between the endogenous protein ligands and synthetic copper indicators. Although the labile copper pool constitutes only a portion of the total cellular copper, the fluctuation in this pool may induce cellular response to copper depletion or over-supply.

a) Histochemical Dyes

Historically, imaging of kinetically labile copper has been accomplished by histochemical techniques where thin sections of tissue or cultured cells were stained with chromogenic indicators for the in situ visualization of copper ions. One of the most widely used indicators for Cu is rubeanic acid (dithiooxamide), which was developed by Okamoto et al. (46) in 1938. In alcoholic solution, rubeanic acid forms a dark green precipitate of polymeric copper rubeanate with Cu(II) ions. With a detection limit of approximately 6 μM for Cu(II), rubeanic acid is not sufficiently sensitive for visualizing labile copper levels present in normal tissue; however, it has been successfully applied to demonstrate elevated copper levels in various tissues of Wilson's disease patients, including the liver, central nervous system (CNS), and kidney (47-49). Over the times various research groups have explored the utility of additional stains for the detection of copper, including diphenylcarbazide and rhodanine (p-dimethylaminobenzylidene-rhodanine) introduced by Okamoto et al. (50, 51); sodium diethyldithiocarbamate (DEDTC) by Waterhouse et al. (52); and orcein by Shikata et al. (53). A brief review on the applications and the limitations of these histochemical dyes was provided by McRae et al. (28).

Because chromogenic indicators lack the sensitivity for detecting the low concentrations of copper in normal biological samples, their applications are mostly limited to the diagnosis of pathological conditions typically associated with excess copper accumulations. Moreover, because these dyes need to compete with the endogenous biological ligands, they are only suitable for the visualization of the histologically reactive fraction of loosely bound labile copper ions.

b) Cu(I)-Selective Fluorescent Probes

Compared to chromogenic histochemical dyes, fluorescent probes offer much greater detection sensitivity, metal specificity, and spatial resolution. Due to their small

molecular size, fluorescent sensors may passively diffuse across cell membranes and are thus well suited for the noninvasive imaging of kinetically labile metal pools in living cells (54). However, compared to redox-inactive cations such as Mg (II), Ca(II) and Zn(II) (55, 56), the design of fluorescent probes for Cu(I) is more challenging due to interfering quenching pathways. In order to overcome the Cu(I)-induced quenching, Fahrni lab pioneered a design strategy that relies on PET switching mechanism (Section 3.2.2) to develop the first Cu(I) turn-on sensor CTAP-1 (30) based on a 1,3-diaryl-2-pyrazoline fluorophore platform. Imaging experiments with mouse fibroblast cells supplemented with copper revealed that CTAP-1 fluorescence was localized in the mitochondria and Golgi apparatus, indicating the presence of labile copper in these regions. The cellular staining pattern of CTAP-1 also qualitatively colocalized with the elemental copper distribution as visualized by X-ray fluorescence microscopy (micro-XRF). However, the contrast ratio (f_e) of CTAP-1 i.e., the fold increase in fluorescence emission upon saturation with Cu(I) is relatively low (f_e = 4.6). This limits the applicability of this probe in bioimaging because it is difficult to distinguish between fluctuations of cellular Cu(I) availability and local variations in probe concentration.

In addition to CTAP-1, Chang laboratory also developed several Cu(I) turn-on probes based on the PET mechanism. The coppersensor 1 (CS 1) (57, 58), which utilizes a BODIPY fluorophore, exhibits a contrast ratio of 10 in HEPES buffer at pH 7. Replacement of the fluoro substituents on the BODIPY dye with methoxy groups yielded CS3 (59), which exhibits a much improved fluorescence contrast over CS1 (f_e = 75). Imaging studies with human embryonic kidney cells (HEK293T) revealed a decrease in the fluorescence intensity of CS3 in cells grown in media treated with the membrane-impermeable copper chelator bathocuproine disulfonate (BCS) when compared to basal media. Furthermore, combined micro-XRF and fluorescence imaging studies with CS3 indicated a calcium-dependent copper translocation in neuronal cells. Based on the same Cu(I)-binding moiety as CS1, a mitochondrial-targeted copper sensor, Mito-CS1, was

developed by conjugating a lipophilic triphenylphosphonium cation to the BODIPY fluorophore (60). Built upon a cyanine 7 (CY7) near-infrared (NIR) fluorophore platform, Chang group has recently reported a copper sensor CS790 with near-infrared emission at 790 nm (61). The probe was employed to monitor labile copper pools in Atp7b$^{-/-}$ mice, a murine model of Wilson's disease. A similar Cu(I)-responsive NIR probe was developed by Cao et al. where the CY7 NIR fluorophore was conjugated with a Cu(I)-binding moiety similar to CS1. Additionally, Lim et al. introduced a two-photon Cu(I) sensor, ACu1 (62), which showed high photostability in visualizing labile copper distribution in live cells and tissues.

3.1.2. In-Gel Detection of Copper Bound to Protein

Recently, detection of metals in protein gels has attracted considerable attention, the principal techniques including autoradiography, synchrotron radiation XRF, and LA-ICP-MS. However, it is worth mentioning that these techniques can only detect the presence of metal ions in a gel spot. The identification of proteins in a spot was accomplished after tryptic digestion followed by mass spectrometry (MS) which in most cases cannot detect the intact metal-protein complexes. This is even more complicated by the fact that several proteins can overlap in a single gel spot. Therefore, it is difficult to prove conclusively that the protein identified by MS was the same protein that was analyzed for the metal content. Accordingly, correlation of a metal with a particular protein has to be ultimately established by further experimentations with the purified protein. Another difficulty associated with in-gel metal imaging is the loss of the endogenous metal ion from the protein. This limitation is primarily attributed to several factors that influence the protein metallation state during gel electrophoresis, including native versus denaturing electrophoresis, choice of trailing ion in the running buffer, intensity of the current, gel staining, gel drying, and metal contamination (63).

a) X-ray Fluorescence

SXRF analysis is multielemental and quantitative; the surface of the fluorescence peaks is directly proportional to the concentration of the elements within the sample (64). The one-dimensional IEF protein separation under non-denaturing conditions followed by SXRF has been successfully applied for the differentiation of metalloprotein content between tumor cells and surrounding normal tissues from hepatocellular carcinoma patients (65). While the detected Cu-containing proteins were very similar to their surrounding tissues, a decrease of Fe and Zn metalloprotein content in tumors was suggested. Recently, Raimunda et al. utilized non-denaturing two-dimensional gel electrophoresis to separate proteins and to investigate the metalloproteome of two microbial systems, *Shewanella oneidensis* and *Pseudomonas aeruginosa*, by XRF (66). This group pioneered methods for the native 2D gel electrophoresis separation of complex biological samples that are compatible with XRF analysis. This is an important contribution in the study of metalloproteins by XRF because 2D gel traditionally provides better separation of protein spots compared to 1D gel.

One of the unique features of X-ray based imaging is that it can provide information about coordination geometry and oxidation state of the metal site by combining XRF with XANES spectroscopy (See 3.1.1.2.a). Chevreux et al. (67) used XANES on IEF gels to determine the coordination environment of copper and zinc in bovine and human copper zinc superoxide dismutase. This study showed that zinc is present in its Zn(II) oxidation state in all analyzed isoforms of SOD as expected. Copper is present in the Cu(II) oxidation state in the main acidic isoform, while it is found in both Cu(II) and Cu(I) states in the main basic isoform.

Synchrotron radiation based methods for metalloprotein studies offer the identification, quantification, and speciation of metals in protein bands simultaneously by combining SXRF and XANES on the same sample. However, the detection limit offered by SXRF, about 0.1 $\mu g\ g^{-1}$, is worse than autoradiography and LA-ICP-MS, which means

that only highly expressed proteins can be identified. This method is also time-consuming as proteins separated on a gel often have to be transferred on a blot and dried before XRF measurements. Moreover, another obvious limitation of synchrotron radiation based methods is the access to a synchrotron facility.

b) LA-ICP-MS

Laser-ablation ICP-MS offers an attractive tool for the in-gel scanning of the protein spots for the presence of metal ions. Because of its high positional accuracy, a plot is obtained in which the quantity of a given metal is related to its position in the gel. Detection by LA-ICP-MS is also high throughput, because no further treatment of the gel after protein separation is required, and the output signal is, theoretically, directly proportional to the quantity of the trace element in the gel.

LA-ICP-MS has been used extensively by Becker et al. (68-75) to detect metal-containing proteins in brain tissues, especially with respect to Cu, Zn, and Fe. The detection limits for P, S, Cu, and Zn were determined in singular protein spots with 0.0013, 1.29, 0.029, and 0.063 mg g^{-1} respectively (76). Following LA-ICP-MS the individual protein spot containing metal ions can be excised and digested by trypsin enzyme to form peptide fragments in order to identify the protein by MALDI-MS and database search.

The main advantage of LA-ICPMS for in-gel detection of metals is that the screening of separated protein spots in a two-dimensional gel and the qualitative measurements of a multitude of protein spots was performed in just a few hours. Moreover, LA-ICP-MS offers high sensitivity, multi-elemental capacity, and isotopic resolution. However, elemental analysis of the gels by LA-ICP-MS is far from routine, primarily because of its destructive mode of operation. LA-ICP-MS ablates a small spot of the protein gels which causes two problems, first, because of the small volume of the ablated spot less abundant proteins are difficult to analyze for their metal content, and

second, the remaining amount of protein on the gel after ablation may not be sufficient for MS analysis in case of proteins with low expression. Furthermore, quantification of metal content using LA-ICP-MS can sometimes be difficult due to matrix effects.

c) Autoradiography

A relatively new method in metalloproteomics involves in-gel autoradiographic detection of a radioactive metal ion to study the proteome associated with that particular ion (77). This method is known as Metal Isotope native RadioAutography in Gel Electrophoresis (MIRAGE), and this has been applied to investigate the soluble Cu, Zn, and Fe metalloproteomes of *Escherichia coli* using the radioisotopes ^{64}Cu, ^{69m}Zn, and ^{59}Fe respectively (78, 79). MIRAGE involves four steps: i) labelling of target proteins with a radioisotope by adding the radioactive metal in the culture medium; ii) separation of holo-proteins using two-dimensional gel electrophoresis, where native isoelectric focusing (1D) is combined with Blue Native PAGE (2D); iii) visualization and quantification of the radioactive metal using autoradiography; and iv) protein identification by mass spectrometry.

The advantage of MIRAGE is that all the proteins that contain a particular metal ion can be visualized on a single native gel in a non-destructive manner. MIRAGE records the radioactive signal of a particular metal ion which is not the natural isotope found in the environment, hence this method is less susceptible to contamination. The radioactive signal can also be quantified easily against commercially available standards. However, unlike LA-ICP-MS and XRF, MIRAGE is not multielemental. Moreover, this technique requires short-lived radioisotopes which may be difficult to obtain and work with in common laboratory settings.

3.2. Copper(I) Selective Fluorescent Probes

Copper is mostly present in its monovalent oxidation state (Cu^{+}) inside the reducing cellular environment. Therefore, copper(I) selective fluorescent probes can serve as an important analytical tool to detect cellular copper pool. Similar to other fluorescent sensors, they have several advantages in biological applications including high optical sensitivity, submicrometer spatial resolution, and non-invasive imaging modality. However, redox lability of Cu^{+} ion poses unique challenges in designing effective Cu(I)-selective fluorescent probes. This section will elaborate on the challenges and key strategies in developing fluorescent Cu(I) sensors.

3.2.1. Challenges in Designing Copper(I) Selective Fluorescent Probes

In order to comprehend the underlying challenges in designing Cu(I) selective fluorescent probes for biological applications, first we need to understand the key features of cellular copper regulation. The dietary copper predominantly exists in its +2 oxidation state (Cu^{2+}), but inside the reducing cytosolic environment (-260 mV) (80) copper is presumably present in form of Cu(I). However, free aqueous Cu^{+} is redox labile and hence is susceptible towards oxidation and disproportionation in presence of oxygen. Additionally, aqueous Cu^{2+} is also highly reactive toward the ubiquitous intracellular free thiol glutathione which would readily reduce Cu^{2+} to Cu^{+} in millisecond time scale (54). Therefore, free aqueous copper ions of either oxidation state are incompatible with the intracellular environment, which typically contains high concentrations of glutathione and molecular oxygen. Furthermore, free Cu^{+} ions are capable to induce oxidative damages inside the cell and hence are toxic. In contrast to the detrimental free aqueous Cu^{+} ions, complexation of the metal with suitable ligands, that increase Cu(II)/Cu(I) reduction potential, can suppress disproportionation and oxidation of Cu(I). Therefore, it is not surprising that nature has evolved sophisticated copper homeostatic machinery

where cellular copper is chelated by high affinity ligands to control oxidative damage, while still maintaining a kinetically labile pool for physiological functions.

In light of the picture portrayed in the preceding paragraph, it is now conceivable that a successful copper-selective fluorescent probe design not only involves the usual optimization of photophysical properties such as optical sensitivity, but it also has to meet the following criteria in order to use the probe to detect cellular copper. First, it is not sufficient for the fluorescent probe to selectively bind Cu(I) over all other biologically relevant metal ions, it is also imperative that the probe discriminates against Cu(II) to prevent redox cycling between the two oxidation states which would ultimately deplete the cellular reservoir of glutathione and other reductants. Second, due to the lack of the free intracellular aquated copper, the availability of the metal ion, that is required for the fluorescence response of the probe, is limited to the exchangeable copper pool. Therefore, the Cu(I) binding affinity of the probe should be tailored such that it can compete with the endogenous ligands for the metal ion without disturbing the normal cellular functions. Finally, the probe should offer a high fluorescence contrast between the free and Cu(I)-bound form to minimize undesirable background fluorescence.

3.2.2. Design of Fluorescent Copper(I) Sensors: PET Switching Mechanism

The basic framework of metal ion selective fluorescent probes is to combine a metal-binding moiety with a fluorophore that will respond to any fluctuation of the metal status. Because Cu(I) is an efficient fluorescence quencher (81, 82), the design of Cu(I)-responsive fluorescent probes is challenging. In some instances, although this fluorescence quenching can be correlated with the copper ion concentration (83), the overpowering fluorescence from the unbound probe decreases the detection sensitivity. Therefore, Cu(I) sensors are largely turn-on probes where the intensity increases upon metal binding.

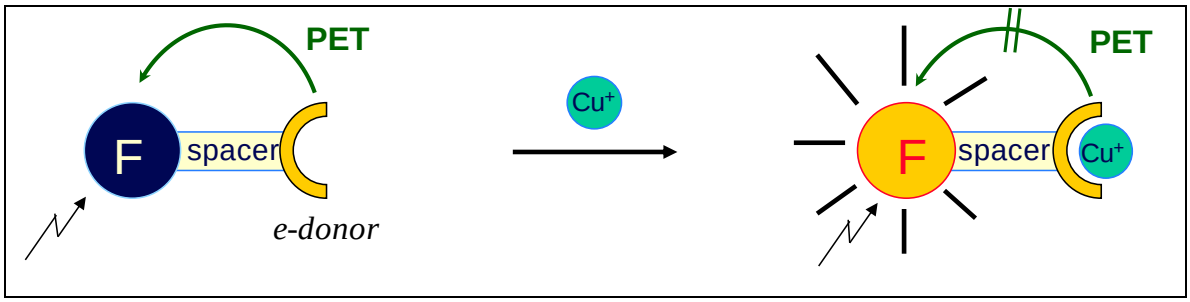

Figure 3.1. *A Cartoon of the Photoinduced Electron Transfer.*

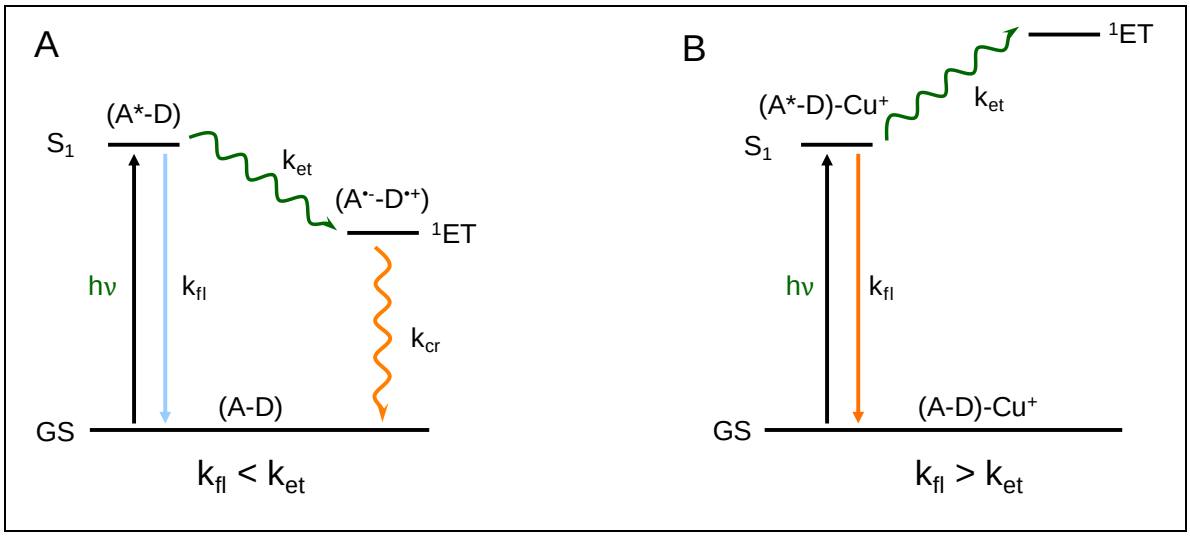

Figure 3.2. *Simplified Jablonski Diagram Illustrating the PET Process.* **A)** In absence of Cu^{+}, electron transfer from the donor (D) to the excited fluorophore (A*) is thermodynamically favorable. The rate of electron transfer (k_{et}) is faster than the rate of fluorescence (k_{fl}), resulting in emission quenching ($k_{fl} < k_{et}$). **B)** Cu^{+}-coordination to D decreases the driving force for PET, and slows down the electron transfer process. As a result, the fluorescence is switched on ($k_{fl} > k_{et}$). Diagram provided by Dr. C. J. Fahrni.

The fluorescence quenching due to Cu(I) can be reduced when the Cu(I)-binding site is decoupled from the fluorophore with a spacer. One way to obtain the metal induced turn-on response of the fluorophore of this architecture is to apply a photoinduced electron transfer (PET) switching mechanism. Generally, PET-based probes are composed of an acceptor-spacer-donor framework (Figure 3.1), where an electron-rich metal binding site functions as the electron donor (D) and the excited

fluorophore (A*) as the acceptor (Figure 3.2). In the absence of Cu(I), following the excitation of the fluorophore, an electron transfer occurs from the donor to the acceptor generating a radical ion pair ($A^{\bullet-}$–$D^{\bullet+}$). This undergoes a rapid non-radiative charge recombination process to return to the initial ground state resulting in fluorescence quenching. In the Cu(I)-bound form, the electron density of the donor is occupied to coordinate the metal ion, thus PET from the donor becomes thermodynamically less favorable. As a result, the fluorescence emission of the probe increases. CTAP-1 was the first probe reported to detect Cu(I) in aqueous solution which was developed by Fahrni group using the PET strategy (Figure 3.3).

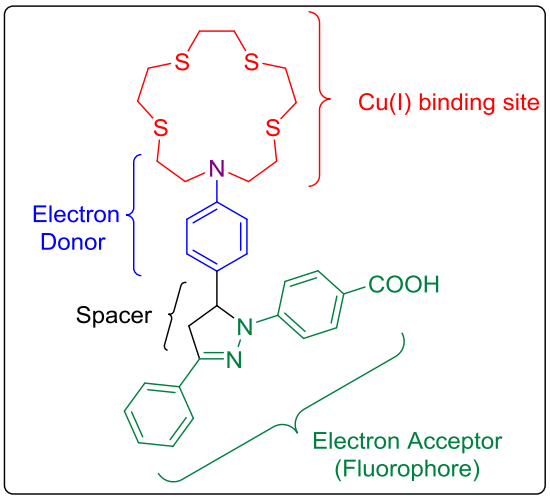

Figure 3.3. *Acceptor-Spacer-Donor Architecture of a PET-based Fluorophore* ***CTAP-1***. The nitrogen colored in purple is part of the Cu(I) binding site as well as the PET donor.

3.2.3. Photophysics of Photoinduced Electron Transfer

Typically, the cellular distribution of fluorescent probes is not homogeneous; it greatly depends on the chemical nature of the probe and the physiological environment of subcellular organelles. Thus, accumulation of free probe inside cellular compartments is

not unusual in bio-imaging. This can lead to staining artifacts especially when the fluorescence intensity of the free probe is very high and the enhancement upon metal binding is not sufficient to distinguish between background and copper-mediated response. Therefore, in detection of intracellular copper, the optimization of the fluorescence contrast between the free and the metal saturated probe is extremely important. This subsection will provide a background about photophysical parameters that drive the PET process as tuning of these properties will alter the fluorescence contrast (often given as fluorescence enhancement factor) of a probe.

3.2.3.1. Relationship between Fluorescence Enhancement and PET Rate

Since the copper ion does not directly interact with the fluorophore, in PET-based Cu(I) sensors, only the emission intensity but not the wavelength is altered upon metal binding. This change in intensity can be quantified by the fluorescence enhancement factor (f_e) which is defined as the ratio of the quantum yield of the Cu(I)-bound probe (Φ_f^b) to that of the free probe (Φ_f^0) by eqn. (3.1):

$$f_e = \frac{\Phi_f^b}{\Phi_f^0} \tag{3.1}$$

Fluorescence quantum yield of a fluorophore is defined by the ratio of the number of emitted photons to the number of photons absorbed. Therefore, in presence of non-radiative electron transfer process, the quantum yield of an unbound PET probe is given by,

$$\Phi_f^0 = \frac{k_{fl}}{k_{fl} + k_{nr} + k_{et}^0} \tag{3.2}$$

where k_{fl} = rate of fluorescence, k_{et}^0 = rate of the electron transfer process, and k_{nr} = rate of any other non-radiative deactivation pathways. Similar equation can be derived for the

quantum yield of the Cu(I)-bound probe where the rate of the electron transfer will be described by k_{et}^{b}.

Therefore, in terms of the rate constants, the fluorescence enhancement factor (as in eqn. (3.1)) can be given by eqn. (3.3) under the assumption that the rate constants of fluorescence and non-radiative deactivations other than electron transfer do not change upon metal binding,

$$f_e = \frac{k_{fl} + k_{nr} + k_{et}^{0}}{k_{fl} + k_{nr} + k_{et}^{b}} \tag{3.3}$$

3.2.3.2. Correlation between PET Rate Constant and Driving Force

For PET probes based on acceptor-spacer-donor architecture, the electron donor is separated from the fluorophore by a sigma bond spacer, and hence this electron transfer process can be rationalized as a nonadiabatic reaction according to the concept illustrated in semiclassical Marcus theory (84, 85). According to this theoretical model, the rate constant (k_{et}) and the thermodynamic driving force (ΔG_{et}) of PET can be related by eqn. (3.4),

$$k_{et} = \left(\frac{4\pi^3}{h^2 \lambda k_B T}\right)^{1/2} H_{DA}^2 \exp\left[-\frac{(\Delta G_{et} + \lambda)^2}{4\lambda k_B T}\right] \tag{3.4}$$

where h is Planck's constant, k_B is Boltzmann's constant, T is the absolute temperature, λ is the reorganization energy, and H_{DA} is the electronic coupling between the states before (A*-D) and after the electron transfer ($A^{\bullet-}$-$D^{\bullet+}$).

According to eqn. (3.4), it can be deduced that the rate of electron transfer (k_{et}) increases with increasing PET driving force (more negative ΔG_{et}) when ($-\Delta G_{et}$) < λ ("normal" region), the rate reaches maximum at ($-\Delta G_{et}$) = λ, and then decreases as the driving force increases under the condition ($-\Delta G_{et}$) > λ ("inverted" region) (Figure 3.4).

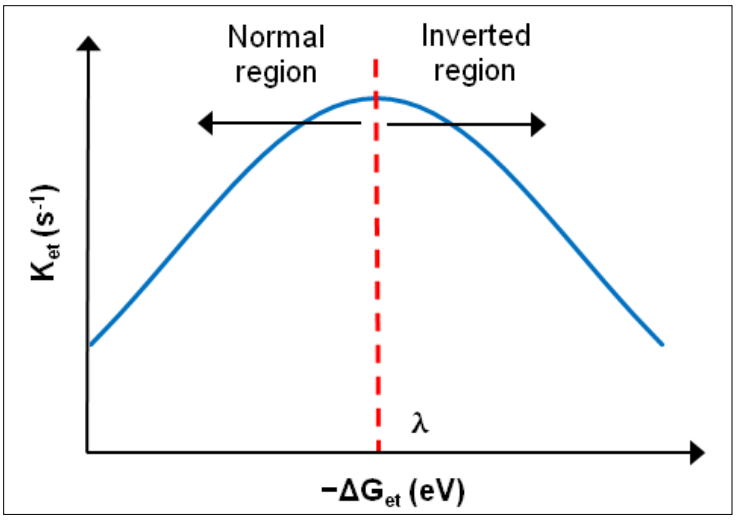

Figure 3.4. *Graphical Representation of the Relationship between Rate of Electron Transfer and PET Driving Force.*

3.2.3.3. Calculation of PET Driving Force

The driving force for the PET reaction (ΔG_{et}) can be estimated based on the Rehm-Weller equation (86) as given by eqn. (3.5),

$$\Delta G_{et} = E(D^+/D) - E(A/A^-) - \Delta E_{00} + w_p \qquad (3.5)$$

where $E(D^+/D)$ and $E(A/A^-)$ are the ground state reduction potentials of the electron donor and acceptor moieties, ΔE_{00} is the transition energy for the excitation of the fluorophore from the lowest vibrational state of S_0 to that of S_1, and w_p is the Coulombic stabilization energy of the radical ion pair ($A^{\bullet-}$-$D^{\bullet+}$) formed upon electron transfer. In aqueous environment, w_p is typically small due to solvation of the ion pair by surrounding water molecules.

During the electron transfer process, the donor is oxidized and the acceptor is reduced. Therefore, a more positive value of $E(D^+/D)$ will disfavor the oxidation of the donor corresponding to weaker driving force for PET (as ΔG_{et} becomes more positive).

On the other hand, a more positive value of $E(A/A^-)$ or increase in ΔE_{00} will result in a stronger PET driving force (as ΔG_{et} becomes more negative).

On the basis of the above discussion, it can be visualized that several factors can contribute to the tuning of fluorescence contrast of a PET probe by altering the PET driving force and in turn the rate of electron transfer. These photophysical parameters include the donor $E(D^+/D)$ and acceptor $E(A/A^-)$ potentials, the excited state energy ΔE_{00}, the electronic coupling (H_{AD}), and the reorganization energy (λ). The influence of these parameters in contrast optimization of PET-based fluorescence turn-on probes were investigated with a series of compounds built upon a tunable 1,3,5-triarylpyrazoline fluorophore platform (87-90) same as in CTAP-1 (Figure 3.3).

3.2.4. Problems Associated with Aggregation of Fluorescent Probes

Fluorescent probes applied for cellular imaging are usually lipophilic and poorly water soluble to facilitate their diffusion across the lipid bilayer membrane (91). Therefore, it is a common practice in cellular applications to dissolve these probes in organic solvents like DMSO followed by dilution of the stock solution in buffer to prepare the working solution. However, a systematic dynamic light scattering study with a large library of drug-like molecules showed evidence of colloidal aggregation when the working solution of these compounds were prepared by the above-mentioned method (92). Moreover, there is ample evidence in the literature showing effects of aggregation on the photophysical properties of fluorophores including spectral shift, quenching, and fluorescence enhancement (93-95). Spectroscopic properties of poorly soluble fluorescent molecules can further change in the biological membranes depending on their hydrophobicity, charge, and aggregation state (96). Therefore, the problems associated with applications of colloid forming fluorescent probes in cellular imaging are much more complicated than often perceived.

3.3. Results and Discussion

In the last decade, Fahrni group was invested in tuning the electronic properties of Cu(I)-selective fluorescent probes to optimize the fluorescence contrast. These efforts culminated in the development of several high contrast Cu(I) probes with the maximum fluorescence enhancement being 50 (89). However, these compounds were characterized in methanol due to their low solubility. Therefore, the natural progression of this work was to develop water soluble high-contrast Cu(I) sensors which can be useful to image kinetically labile cellular copper.

This work will discuss characterization of two such probes, CTAP-2 and **4.3** (Chapter 4), and application of CTAP-2 towards in-gel detection of a copper chaperone in non-denaturing condition. Both probes were synthesized by Dr. M. T. Morgan and the detail of the synthetic procedures can be found elsewhere (1, 97).

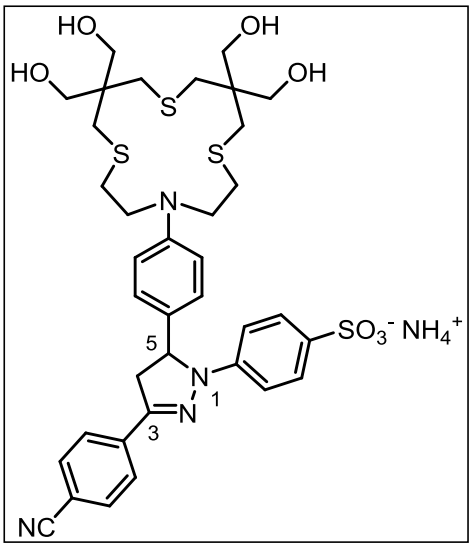

Figure 3.5. *Molecular Structure of **CTAP-2**.*

3.3.1. Characterization of CTAP-2

CTAP-2 is a highly water soluble Cu(I)-selective fluorescent probe designed on the triarylpyrazoline fluorophore platform (Figure 3.5). The turn-on response of this probe upon Cu(I) binding is based on photoinduced electron transfer (PET) switching mechanism as discussed in section 3.2.2. To solubilize this probe, the thioether-based Cu(I)-binding moiety was functionalized with four hydroxymethyl groups along with a sulfonic acid group attached to the fluorophore. Because of its very low pK_a the sulfonic acid primarily exists as a sulfonate ion, thus increasing the solubility of the probe as well as imparting the electron-withdrawing effect which is critical in designing high contrast probes (89). Although it had been previously shown that both 3,5-difluoro (89) and 4-cyano (90) substitution on the 3-aryl ring provide a suitable platform for electronic tuning to develop contrast optimized probes, the latter was chosen for CTAP-2 as 4-cyanophenyl group should be less lipophilic than 3,5-difluorophenyl moiety.

Table 3.1. *Photophysical Properties of CTAP-2*

Photophysical Property[a,f]	Value
Absorption maximum	396 nm
Emission maximum	508 nm
Quantum yield of the neutral free probe [b]	0.0015
Quantum yield of the acidic free probe [c]	0.25
Quantum yield of the Cu(I)-saturated probe [d]	0.083
Fluorescence enhancement factor [e]	65

[a] Data adapted with permission from Reference (1). © 2011 American Chemical Society; [b] 10 mM MOPS/K^+, pH 7.2; [c] 5 mM HCl; [d] Saturated with Cu(I) at pH 7.2 (10 mM MOPS); [e] Fluorescence enhancement factor of Cu(I)-saturated probe relative to the analyte-free probe at neutral pH (λ_{ex} = 380 nm, integrated emission from λ_{em}−10 to λ_{em} + 10 nm); [f] Data provided by Dr. M. T. Morgan.

3.3.1.1. Photophysical Properties

In aqueous buffer (10 mM MOPS/K^+, pH 7.2), upon excitation at 380 nm the fluorescence emission of analyte-free CTAP-2 was very weak but showed a strong fluorescence response upon Cu(I)-binding with an emission maximum at 508 nm. The fluorescence enhancement factor of Cu(I)-saturated probe relative to the free probe was estimated to be 65-fold with a quantum yield of 0.083 for the copper-bound probe (Table 3.1).

3.3.1.2. Water Solubility: Comparison with Previously Reported Cu(I)-Probes

The ammonium salt of CTAP-2 dissolves directly in water owing to the solubilization strategies employed in designing the probe. On the contrary, Cu(I) selective fluorescent probes usually tend to be lipophilic due to the thioether based cation binding sites typically employed to achieve selectivity for the soft Cu(I) cation. Because of their inadequate solubilities, the aqueous solutions of such probes cannot be prepared by direct dissolution in water. Instead, they are first dissolved in an organic solvent such as DMSO to form a concentrated stock solution, which is then diluted into water or aqueous buffer to give a final working concentration in the low micromolar range. However, as mentioned in section 3.2.4, the poorly soluble probes are prone to form colloidal aggregates under these conditions (92). Because the colloids are composed of nanoparticles with sizes below the diffraction limit, the aqueous solution remains optically clear. In absence of macroscopic precipitates, the UV-vis absorbance of such solutions usually changes linearly with the compound concentration. For this reason, UV-vis spectroscopy is not a suitable method to test for colloidal aggregation.

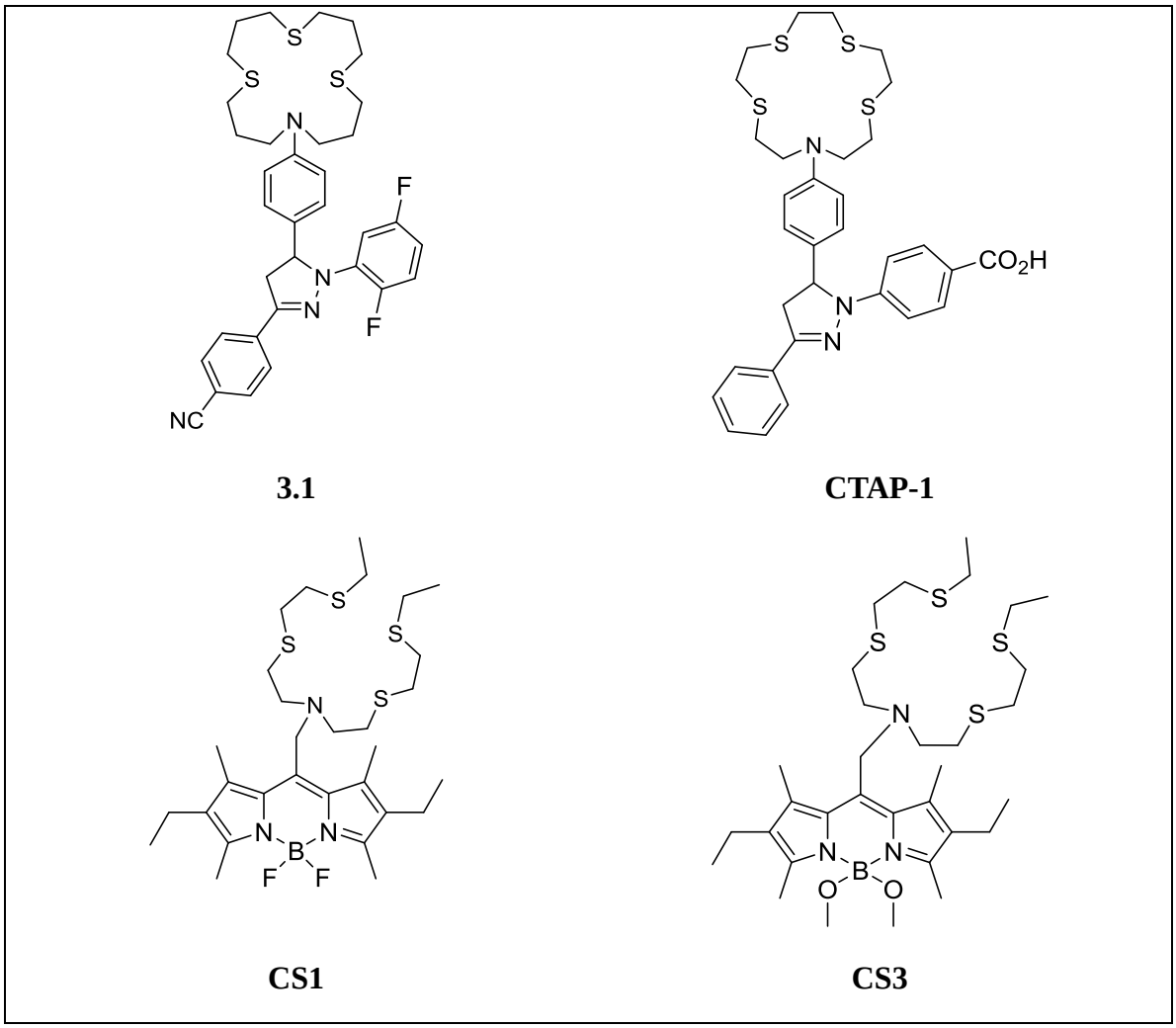

Figure 3.6. *Molecular Structures of Copper(I) Responsive Probes Studied by Dynamic Light Scattering.*

Dynamic light scattering (DLS), on the other hand, has been proven to be useful in characterizing colloidal aggregates. DLS measures fluctuations in the intensity of the light scattered by nanoparticles by comparing the intensity at time t to the intensity at a later time (t + τ). This intensity fluctuation, known as the autocorrelation function (C(t) in Figure 3.7), is due to the Brownian motion of the particles in solution where the scattered light continuously undergoes either constructive or destructive interference by the surrounding particles. These fluctuations can be linked to the fluctuations in the dielectric

constant of the scattering medium, from which it is possible to derive the diffusion coefficient of particles in colloidal suspensions. In sufficiently dilute systems, assuming that the particles are spherical, the Stokes-Einstein relation gives the radius of these particles from the diffusion coefficient data utilizing eqn. (3.6) ,

$$r = \frac{kT}{6\pi\eta D} \tag{3.6}$$

where k = Boltzmann constant, T = temperature, η = viscosity of the medium, and D = diffusion coefficient. Therefore, large particles diffuse slower than the small particles and as a result the correlation function also decays at a slower rate.

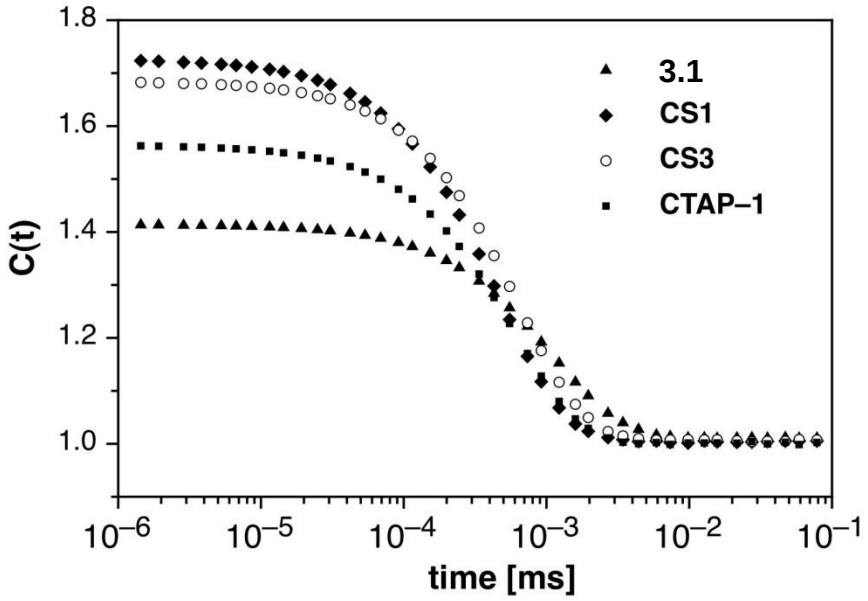

Figure 3.7. *Autocorrelation Curves from Dynamic Light Scattering of Fluorescent Probe Colloids.* Reproduced with permission from Reference (1). © 2011 American Chemical Society.

In order to examine the hypothesis of colloidal aggregation by lipophilic Cu(I)-sensors, previously reported Cu(I)-probes (Figure 3.6) were studied by dynamic light

scattering (DLS). Although the colloidal aggregation of lipophilic Cu(I)-probes in aqueous solution is expected based on their molecular structures, prior to this work the aggregation behavior of these probes had not been experimentally determined. To mimic the aggregation state associated with the dilution of organic stock solutions of poorly soluble dyes into aqueous buffer, a commonly used procedure for preparing aqueous solutions of lipophilic dyes, each of these probes was first dissolved in DMSO to a concentration of 1 mM. The stock solutions were then diluted in aqueous buffer (10 mM MOPS/K^+, pH 7.2) to prepare a working solution with a concentration of 5 μM. All of these probes formed clear homogeneous solutions when prepared this way, however, DLS experiments showed evidence of colloid formation. Following the light scattering principles laid out in the preceding paragraph, hydrodynamic radii of all compounds (Table 3.2) were determined from their autocorrelation curves (Figure 3.7). Increasing hydrodynamic radius resulted in slower diffusion and consequently decreased the rate of decay of the correlation function.

Table 3.2. *Hydrdynamic Radii of Cu(I)-selective Fluorescent Probes Measured by Dynamic Light Scattering.*

Probe [a]	Ref.	R_h (nm)[b]	SD (nm)[c]
3.1	(90)	100	12
CS1	(57)	49	6
CS3	(59)	67	9
CTAP-1	(30)	63	6

[a] DMSO stock solution (1 mM) of the probe diluted into aqueous buffer (10 mM MOPS/K^+, pH 7.2) to a final concentration of 5 μM. [b] Hydrodynamic radius; [c] Standard deviation. Data adapted with permission from Reference (1). © 2011 American Chemical Society.

For the Cu(I)-responsive probes **3.1**, CS1, and CS3, the lipophilic nature of these molecules was confirmed by the DLS measurements. Surprisingly, CTAP-1 which was functionalized with a carboxylic acid group to increase aqueous solubility also showed formation of colloidal aggregates with an average hydrodynamic radius comparable to CS3. In line with the concern of alteration of photophysical properties of fluorescent probes upon aggregation as expressed in section 3.2.4, a recent publication pointed towards potential misrepresentation of cellular imaging data acquired with copper sensor CS1. In this study, multiple evidences suggested that the fluorescence response of CS1 is not limited to the fluctuation in cellular copper, but this probe also responds to alteration in cellular pH, redox status, and lysosomal activity (98).

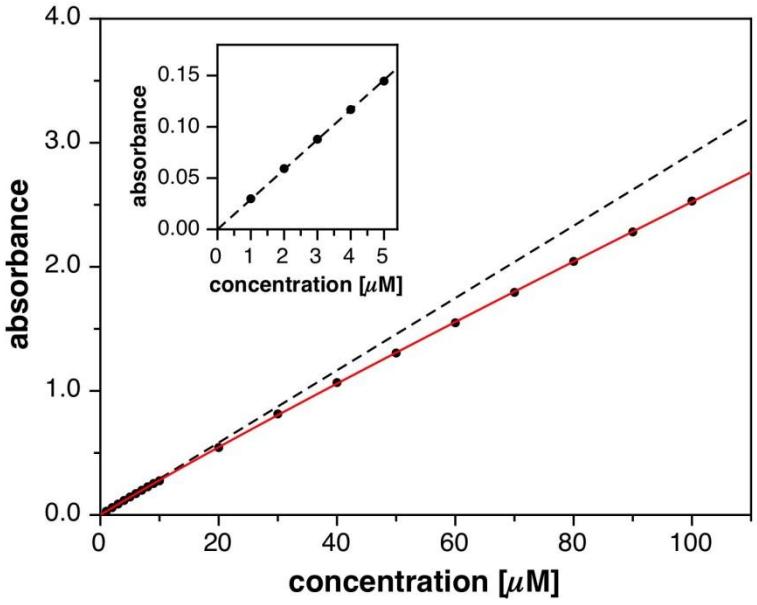

Figure 3.8. *Absorbance of CTAP-2 at 396 nm versus Concentration.* **Inset:** Expansion showing linearity within the 0-5 μM concentration range; **Dashed line:** the expected linear scaling based on the first five data points in 0-5 μM range; **Red curve:** non-linear least squares fitting using dimerization model. Reproduced with permission from Reference (1). © 2011 American Chemical Society. Data provided by Dr. M. T. Morgan.

In contrast to other probes, CTAP-2 gave no more DLS signal than the background count rate of the buffer, thus confirming the absence of colloidal aggregates. Furthermore, the absorption and emission intensity of Cu(I)-bound CTAP-2 scaled linearly with concentrations from 0 to 5 μM. Similarly, the absorbance of the free probe increased linearly in the same concentration range (Figure 3.8). At concentrations above 10 μM, deviation from linearity in the absorbance vs concentration plot is apparent, indicating the presence of self-association of CTAP-2. Nonlinear least-squares fitting of the experimental data assuming a simple dimerization equilibrium yielded an equilibrium constant of log$K$ = 3.98 ± 0.06 for the CTAP-2 dimer (1). While the presence of dimer formation is evident from this experiment, considerable self-association of CTAP-2 only occurs at concentrations that are substantially higher than the working concentration typically used for fluorescence measurements and especially cellular imaging.

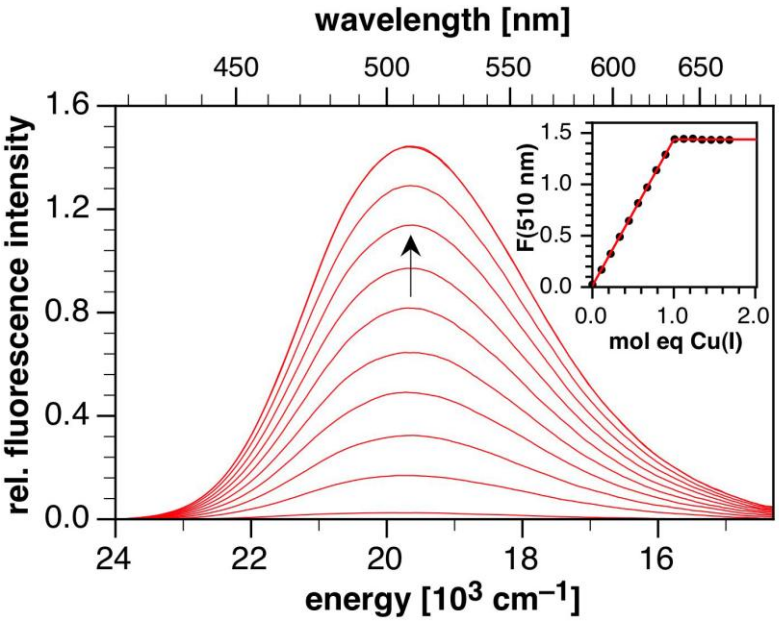

Figure 3.9. *Fluorescence Titration of CTAP-2 with Cu(I).* Reproduced with permission from Reference (1). © 2011 American Chemical Society. Data provided by Dr. M. T. Morgan.

3.3.1.3. Copper(I) Binding Stoichiometry

To determine the Cu(I)-binding stoichiometry of CTAP-2, a 4.5 μM solution of the probe in deoxygenated buffer (5 mM MOPS-K^+, pH 7.2) was titrated with Cu(I), supplied either from a 2.5 mM stock solution of $[Cu(I)(CH_3CN)_4]PF_6$ in CH_3CN or by in situ reduction of $CuSO_4$ with sodium ascorbate. Consistent with a 1:1 copper coordination stoichiometry, the fluorescence emission showed a linear increase with a sharp saturation at 1 molar equivalent of Cu(I), irrespective of the nature of the copper source (Figure 3.9).

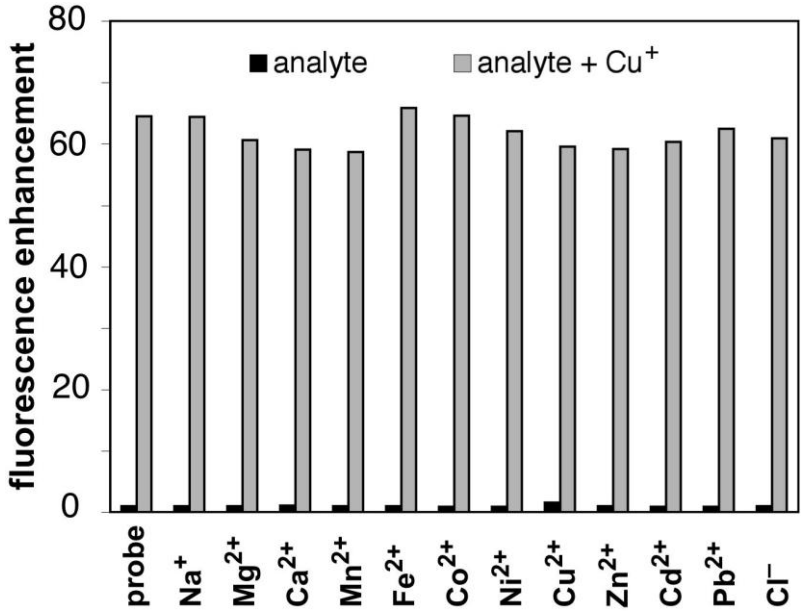

Figure 3.10. *Fluorescence Response of CTAP-2 to Various Cations.* **Black bars**, CTAP-2 in the presence of an excess of the indicated analyte (10 mM for Na^+, Mg^{2+}, Ca^{2+}; 10 μM for other cations); **gray bars**, addition of 5 μM Cu(I) to the solution of CTAP-2 and the indicated analyte. Cu(I) was supplied from 2.5 mM $[Cu(CH_3CN)_4]PF_6$ solution in CH_3CN. Reproduced with permission from Reference (1). © 2011 American Chemical Society. Data provided by Dr. M. T. Morgan.

3.3.1.4. Analyte Selectivity

To determine the selectivity of CTAP-2 for Cu(I) over other metal ions typically present in cellular environment, the fluorescence response of the probe was determined in presence of various cations. Furthermore, to assess the interference of these ions with the probe's response to Cu^+ ion, addition of each of these biologically relevant ions was also recorded in presence of Cu(I). As shown in Figure 3.10, no cation other than Cu(I) gave a significant fluorescence turn-on response, and none of the cations inhibited the response to Cu(I). It is also worth mentioning that CTAP-2 can successfully distinguish between Cu(I) and Cu(II) ions, which is an essential requirement of Cu(I) sensors to prevent cells from oxidative damages (see section 3.2.1).

3.3.1.5. Acid Dissociation Constant

As discussed in section 2.1.3, Cu(I) binding affinity of a ligand is pH-dependent. Depending on the pK_a value of the ligand, the ratio of the protonated and the deprotonated ligands changes with the variation of the pH. Consequently, apparent metal affinity of the ligand also varies as the extent of the competition between the protonation and the metal binding equilibria depends on the pH of the experimental medium. Furthermore, CTAP-2 gives a very strong fluorescence turn-on response upon protonation of the arylamine PET donor as implied by its relatively high fluorescence quantum yield under acidic conditions (Table 3.1). Therefore, the pK_a of CTAP-2 is not only important for binding affinity determination, but also for the susceptibility of the Cu(I) response to interference from environmental pH. To determine the pK_a, the fluorescence emission of CTAP-2 was recorded over a $-\log [H_3O^+]$ range from 2.4 to 5.0, and the data were analyzed using Specfit to yield a value of 3.97±0.01 at 0.1 M ionic strength (Figure 3.11).

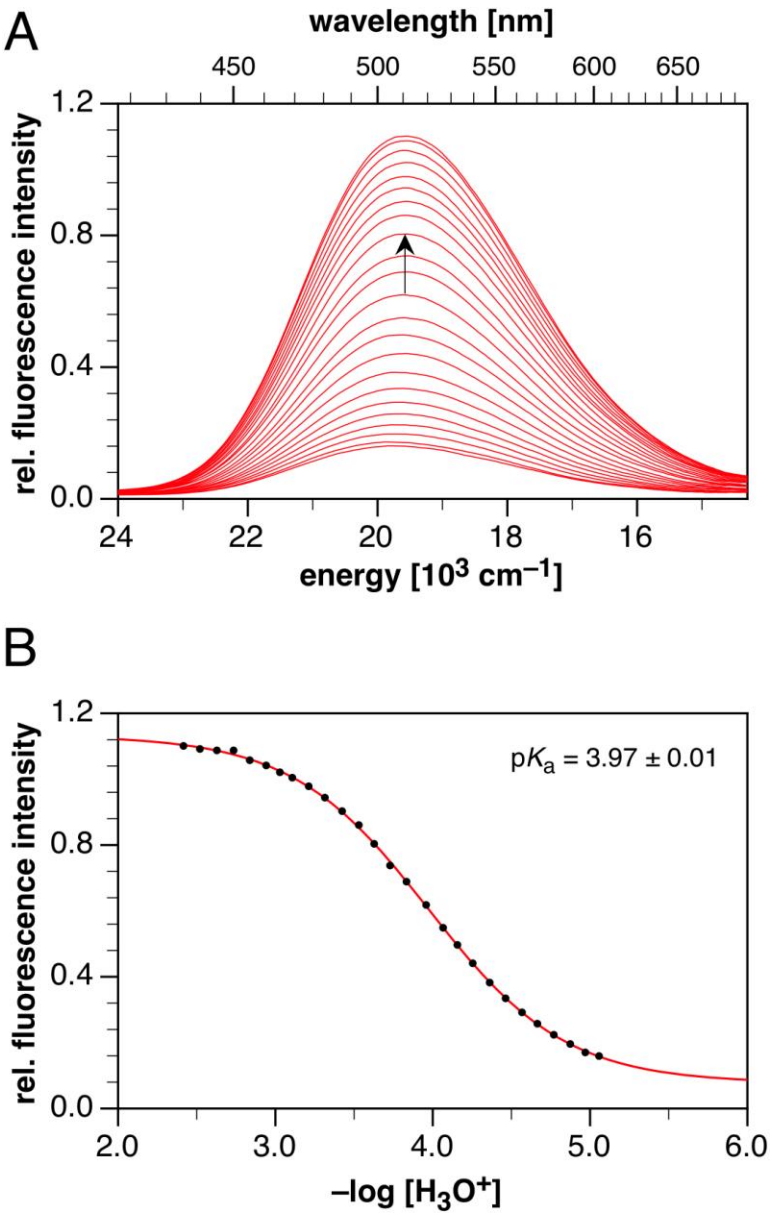

Figure 3.11. *Fluorimetric pH Titration of CTAP-2.* **A)** Fluorescence emission spectra as a function of proton concentration, –log [H_3O^+] ranging between 2.4 and 5.0. **B)** Curve fit of fluorescence intensity at 512 nm vs. –log [H_3O^+]. Average fitted value: pK_a = 3.97±0.03. Reproduced with permission from Reference (1). © 2011 American Chemical Society.

3.3.1.6. Cu(I) Stability Constant

Binding affinity of Cu(I)-responsive probes should ideally be tailored towards the bioavailability of the copper pools under study. An affinity that is too high will result in the probe sequestering copper ion from endogenous proteins perturbing the cellular homeostasis, while a probe with too low an affinity will not show any spectroscopic changes at physiological metal concentrations.

From the mole-ratio plot of CTAP-2 versus Cu(I) (Figure 3.9), it is evident that the probe saturates at exactly one molar equivalent of the metal. Under such condition, the ratio of the bound probe to the metal ion added is near unity i.e., all copper ions are essentially bound to the probe up to the saturation point. Therefore, the Cu(I) stability constant of the probe cannot be determined by direct titration with the copper ion, as for accurate measurement of this value, the fractional saturation of the probe should lie between 0.2-0.8 (see section 2.1.4). The Cu(I) stability constant of CTAP-2 was instead derived from its Cu(II) binding equilibrium as the interaction of the probe with Cu(II) is much more weaker. The two binding constants are related by eqn. (3.7),

$$E_{\mathrm{Cu(II/I)L}} = E^{0}_{\mathrm{Cu(II/I)aq}} - \frac{2.303\,RT}{F}\log\frac{K_{\mathrm{Cu(II)L}}}{K_{\mathrm{Cu(I)L}}} \qquad (3.7)$$

where $E_{\mathrm{Cu(II/I)L}}$ = formal potential of ligand bound Cu(II/I) couple; $E^{0}_{\mathrm{Cu(II/I)aq}}$ = standard reduction potential of the aqueous Cu(II/I) couple; F = Faraday constant; R = universal gas constant; T = temperature in Kelvin, $K_{\mathrm{Cu(II)L}}$ = Cu(II) stability constant, and $K_{\mathrm{Cu(I)L}}$ = Cu(I) stability constant. This method was described in detail in section 2.1.4.

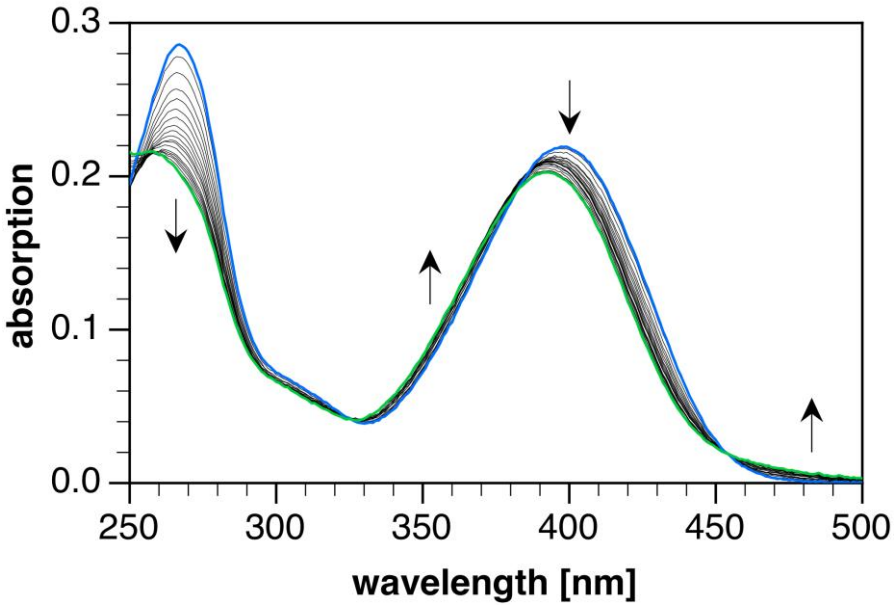

Figure 3.12. *UV-vis Titration of CTAP-2 with Cu(II).* Reproduced with permission from Reference (1). © 2011 American Chemical Society.

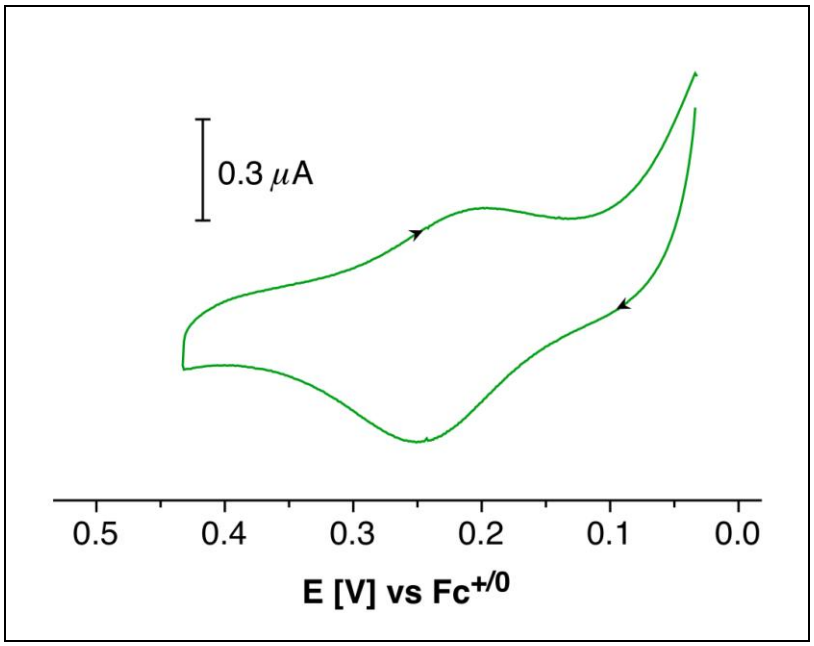

Figure 3.13. *Cyclic Voltammogram of CTAP-2.* Scan rate 50 mV s^{-1}. Reproduced with permission from Reference (1). © 2011 American Chemical Society.

The Cu(II)-binding of CTAP-2 was monitored by UV-vis spectroscopy where the probe was titrated with $CuSO_4$. The titration was done at pH 5 (10 mM PIPBS, 0.1 M $KClO_4$) to inhibit the precipitation of hydroxycopper(II) species which occurs in alkaline medium. The titration data shown in Figure 3.12 were fitted over 250-500 nm wavelength range using the Specfit software package to yield a value of $\log K_{Cu(II)L} = 2.97 \pm 0.07$ at pH 5. In presence of Cu(II), the formal potential of the probe-bound Cu(II/I) redox couple was determined by cyclic voltammetry (CV) in the same buffer (Figure 3.13). CV data showed a quasi-reversible one-electron redox process with a half-wave potential of 0.626 V (vs. SHE). On the basis of these data and a value of 0.13 V vs. SHE for $E^0_{Cu(II/I)aq}$ (99), the Cu(I) stability constant of CTAP-2 was estimated as $\log K_{Cu(I)L} = 11.4 \pm 0.1$ at pH 5. Given the low p*K*a of CTAP-2, these values are not significantly influenced by protonation under the conditions of measurement and thus are unchanged at pH 7.

3.3.2. Applications of CTAP-2

3.3.2.1. In-gel Detection of a Copper Chaperone

Copper homeostatic machinery in living organisms consists of several proteins with a broad range of functions including copper trafficking proteins or chaperones, cuproenzymes where copper acts as a redox cofactor, and copper storage proteins or peptides. Although detection of copper in whole cells and isolated from protein samples is being done routinely, there is a lack of simple and inexpensive methods to detect copper bound to the metalloproteins in their native state. Available technologies, namely laser ablation – inductively coupled plasma mass spectrometry (LA-ICP-MS) (74), autoradiography (100), and synchrotron X-ray fluorescence (66), either suffer from complex sample preparation or involve access to expensive specialized instruments (Section 3.1.2).

Encouraged by the high fluorescence contrast and selectivity toward Cu(I), the utility of CTAP-2 was explored as a reagent for the in-gel detection of copper proteins. For this purpose, hAtox1 was chosen which is a copper chaperone mediating the delivery of Cu(I) to ATP7A or ATP7B in the trans-Golgi network. The protein sample was separated by non-denaturing polyacrylamide gel electrophoresis (Native-PAGE). The only other example of fluorescence-based in-gel detection of copper proteins found in the literature employed quenching of fluorescence of BCS by Cu^{+} ions (101). Besides copper-dependent turn-on fluorescence response as in CTAP-2 is more sensitive that quenching based detection methods, in-gel detection by BCS utilized glacial acetic acid to denature the protein which could potentially mobilize the copper ions.

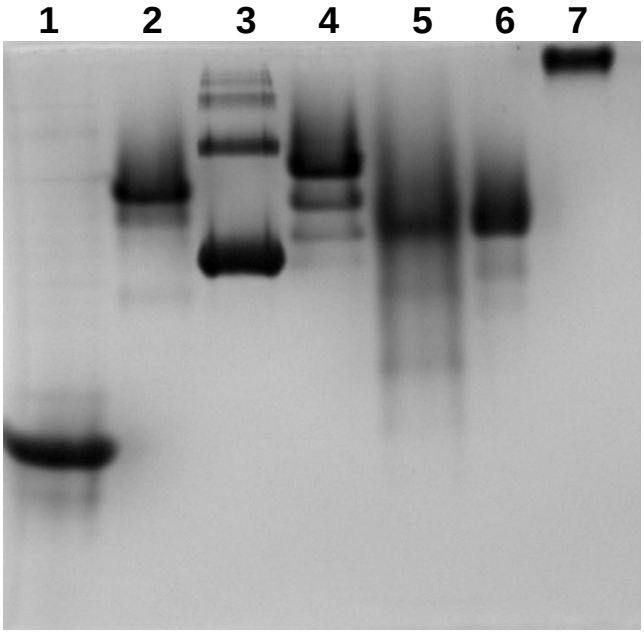

Figure 3.14. *Native-PAGE showing Relative Mobility of Proteins.* **Lane 1:** Thioredoxin, **Lane 2:** Superoxide Dismutase, **Lane 3:** Serum Albumin, **Lane 4:** Carbonic Anhydrase, **Lane 5:** hAtox1, **Lane 6:** Myoglobin, and **Lane 7:** Glyceraldehde-3-Phosphate Dehydrogenase. 36 µg of each of the proteins in native sample buffer were loaded on the gel, pH of the running buffer is 8.3, and the gel was stained with Coomassie blue.

Table 3.3. *Molar Masses and Isoelectric Points of Proteins.*

Lane	Protein	Organism	Molar Mass (kDa)[a]	pI [a]
1	Thioredoxin	Human	11.6	4.82
2	Superoxide Dismutase (Homodimer)	Bovine	31	5.86
3	Serum Albumin	Bovine	66.4	5.60
4	Carbonic Anhydrase	Bovine	29.0	6.40
5	hAtox1	Human	7.4	6.71
6	Myoglobin	Horse	16.9	7.36
7	Glyceraldehde – 3 - Phosphate Dehydrogenase	Rabbit	35.6	8.52

[a]. Molar mass and pI were calculated from the amino acid sequence of respective proteins (UniProt) using ExPASy software ProtParam (102).

In native gel electrophoresis, proteins maintain their native conformations as the samples are treated with neither SDS nor β-mercaptoethanol. While in SDS-PAGE the electrophoretic mobility of a protein depends primarily on its molecular mass, in native PAGE, the mobility depends on both the protein's hydrodynamic size and effective charge. The effective charge of a protein is governed by the intrinsic charge on the protein at the pH of the running buffer which can be predicted from the isoelectric point (pI) of the protein. Although there is a correlation between the molar mass and the hydrodynamic radius of a protein, the latter is also influenced by the actual conformation of the protein in solution. Figure 3.14 shows separation of seven proteins on a representative native-PAGE, their molecular masses and pI's are tabulated in Table 3.3. From these data it is evident that the relative mobility of proteins on a native gel is difficult to predict as this property is affected cumulatively by several factors including

hydrodynamic size, effective charge, conformation, presence of different isomers of the proteins, and the pH of the running buffer. However, unlike SDS-PAGE, native gel electrophoresis prevents the loss of metal ion from a metalloprotein as the protein remains folded in its native state during the electrophoresis (66).

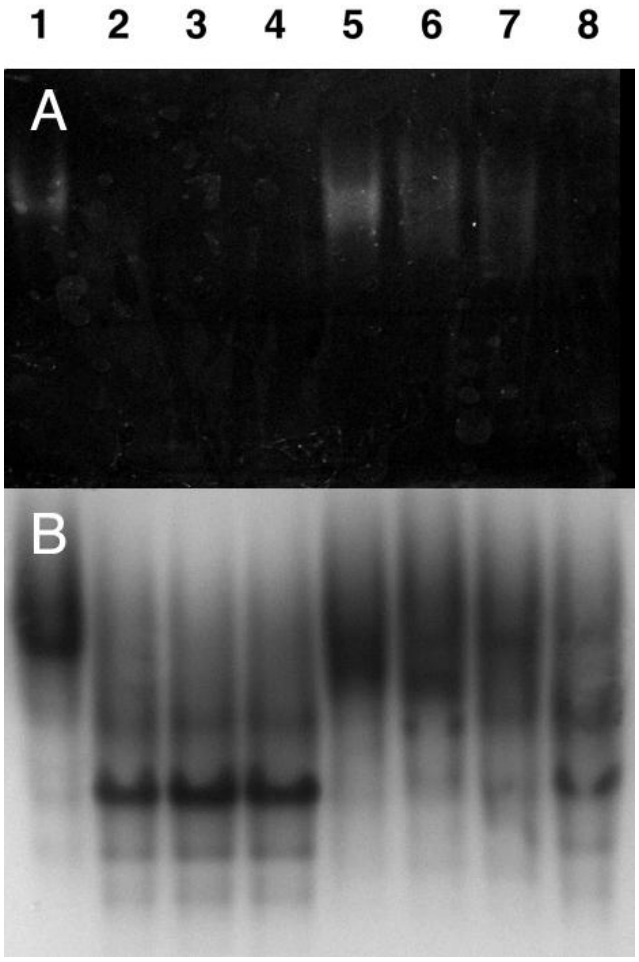

Figure 3.15. *In-gel Detection of a Copper Chaperone with CTAP-2: Response of the Fluorescent Probe with Increasing KCN.* **(A)** Native gel incubated with a 5 μM aqueous solution of CTAP-2 followed by visualization at 365 nm excitation (emission 537/BP 35 nm; UV transillumination mode). **(B)** Same gel after staining with Coomassie blue. **Lane 1:** untreated hAtox1; **Lane 2:** hAtox1, TCEP, 7.5 mM KCN; **Lane 3:** hAtox1, TCEP, 15 mM KCN; **Lane 4:** hAtox1, TCEP, 30 mM KCN; **Lane 5:** hAtox1, TCEP, $[Cu(I)(CH_3CN)_4]PF_6$; **Lane 6:** hAtox1, TCEP, $[Cu(I)(CH_3CN)_4]PF_6$, then 7.5 mM KCN; **Lane 7:** hAtox1, TCEP, $[Cu(I)(CH_3CN)_4]PF_6$, then 15 mM KCN; and **Lane 8:** hAtox1, TCEP, $[Cu(I)(CH_3CN)_4]PF_6$, then 30 mM KCN.

In order to evaluate the utility of CTAP-2 for the in-gel detection of copper proteins, hAtox1 was separated on a native gel with varying amount of apo:holo ratio of the protein (Figure 3.15). $[Cu(I)(CH_3CN)_4]PF_6$ was used to metallate the protein, whereas KCN was used to remove copper from the protein. After the incubation of the gel with CTAP-2, fluorescence signal was observed for the untreated protein (**Lane 1**), which disappeared with the treatment of the protein with KCN (**Lane 2-4**) even at the lowest concentration used in the experiment. Fluorescence signal of CTAP-2 intensified when exogenous copper was added to the protein as this treatment will result in majority of the protein being copper-bound (**Lane 5**). In contrast to **Lane 2-4**, when KCN was added to the copper-bound protein, the CTAP-2 fluorescence signal steadily decreases with increasing amount of KCN (**Lane 6-8**) and disappeared at the highest concentration added. Post-staining of the gel with Coomassie blue revealed the presence of the proteins in each lane and confirmed the removal of Cu(I) from hAtox1, based on the different mobilities of the apo and holo forms (103). Therefore, this study revealed that CTAP-2 can detect hAtox1 in a reversible copper-dependent manner.

Next we set out to determine the specificity of copper-dependent fluorescence response of CTAP-2. Similar to Figure 3.15, incubation of the native gel containing hAtox1 with CTAP-2 showed fluorescence signal only for the holo form (Cu(I)-bound) of the protein and not for the metal-free apo form obtained by removal of the metal by cyanide (Figure 3.16). CTAP-2 did not respond to carbonic anhydrase, a zinc protein, as expected, but interestingly the probe did not give any signal to Cu/Zn superoxide dismutase, which contains a copper site buried inside the protein (Figure 3.17). Therefore, CTAP-2 was successful to detect copper bound to a metallochaperone when the metal is readily accessible (Figure 3.17), however the mechanism of this response is uncertain. Given the high Cu(I) affinity of Atox1 ($\log K = 17.4$) (104), it is probable that CTAP-2 associates with the protein in a Cu(I)-dependent manner without actually removing the metal ion from the binding site. The hypothesis of the CTAP-2-Cu(I)-

Atox1 ternary complex formation is also supported by the fact that the fluorescence signal does not disappear with brief washing of the gel after incubation with the dye as might be expected for a water soluble probe like CTAP-2.

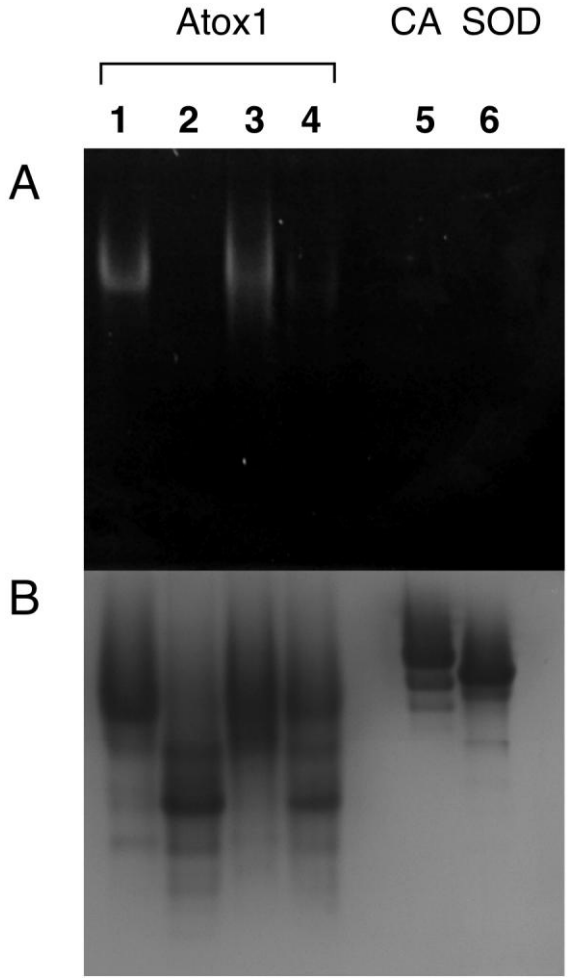

Figure 3.16. *Comparison of Fluorescence Response of CTAP-2 in hAtox1, Carbonic Anhydrase, and Superoxide Dismutase*. **(A)** Native gel incubated with a 5 μM aqueous solution of CTAP-2 followed by visualization at 365 nm excitation (emission 537/BP 35 nm; UV transillumination mode). **(B)** Same gel after staining with Coomassie blue. **Lane 1:** untreated hAtox1; **Lane 2:** hAtox1, TCEP, KCN; **Lane 3:** hAtox1, TCEP, $[Cu(I)(CH_3CN)_4]PF_6$; **Lane 4:** hAtox1, TCEP, $[Cu(I)(CH_3CN)_4]PF_6$, then KCN; **Lane 5:** carbonic anhydrase; and **Lane 6:**, superoxide dismutase (SOD1). Reproduced with permission from Reference (1). © 2011 American Chemical Society.

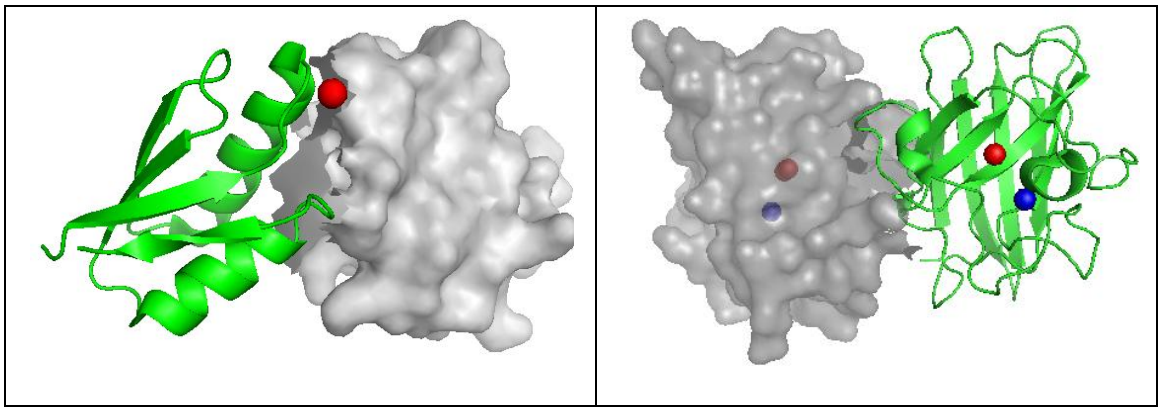

Figure 3.17. *Crystal Structures of Copper Proteins.* **Left:** Human Atox1 (PDB Code 1FEE (105)), **Right:** Bovine Superoxide Dismutase (PDB Code 1Q0E (106)), **Red sphere** and **blue sphere** represent Cu(I) and Zn(II) ions respectively.

Similar experiments were performed with probe **3.1** and CS3 (Figure 3.6). As illustrated in Figure 3.18, aqueous solution of probe **3.1**, prepared by the dilution of a DMSO stock solution, failed to detect hAtox1 on a native gel. Identical result was obtained with the probe CS3 (data not shown). Furthermore, incubation of the native gel with either **3.1** or CS3 resulted in high fluorescence background which was unsuitable for the further imaging. Therefore, after the incubation of the gel with the dye, a washing step had to be included before the imaging to reduce the background. These results are consistent with the fact that all of these compounds form colloidal aggregates in aqueous buffer. Although these lipophilic dyes will be highly soluble in methanolic solutions, we found that methanol is not a suitable solvent for staining native gels. Besides protein denaturation, which would result in loss of metal ions, the gel turned opaque and was rendered unsuitable for fluorescence imaging.

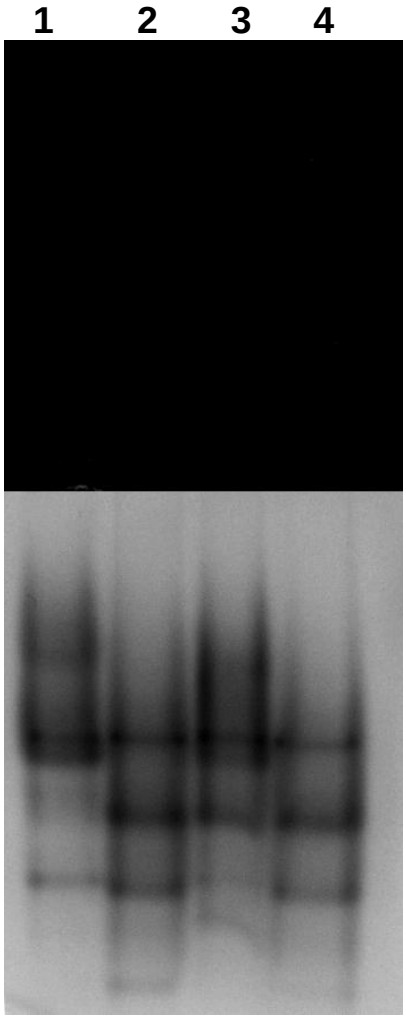

Figure 3.18. *Visualization of hAtox1 with Probe **3.1***. **(A)** Native gel incubated with a 5 μM aqueous solution of **3.1**, prepared by the dilution of a DMSO stock solution, followed by visualization at 365 nm excitation (emission 537/BP 35 nm; UV transillumination mode). **(B)** Same gel after staining with Coomassie blue. **Lane 1:** untreated hAtox1; **Lane 2:** hAtox1, TCEP, KCN; **Lane 3:** hAtox1, TCEP, $[Cu(I)(CH_3CN)_4]PF_6$; **Lane 4:** hAtox1, TCEP, $[Cu(I)(CH_3CN)_4]PF_6$, then KCN.

3.3.2.2. Preliminary Cellular Imaging

Despite its hydrophilic nature and the presence of an anionic sulfonate group, CTAP-2 proved to be cell permeant. The dye produced a perinuclear staining pattern in live NIH 3T3 cells under copper-supplemented conditions (Figure 3.19), the pattern is

consistent with the total subcellular copper distribution previously observed by synchrotron X-ray fluorescence microscopy (30). Although these preliminary results appear promising, given the low Cu(I)-binding affinity of CTAP-2 ($\log K_{Cu(I)L}$ = 11.4), it is unlikely to compete with endogenous proteins with affinities higher by at least two orders of magnitude and hence the significance of the observed staining pattern is not yet certain. Nevertheless, this experiment demonstrates that it is possible to design a Cu(I)-selective probe which is water soluble as well as cell permeable.

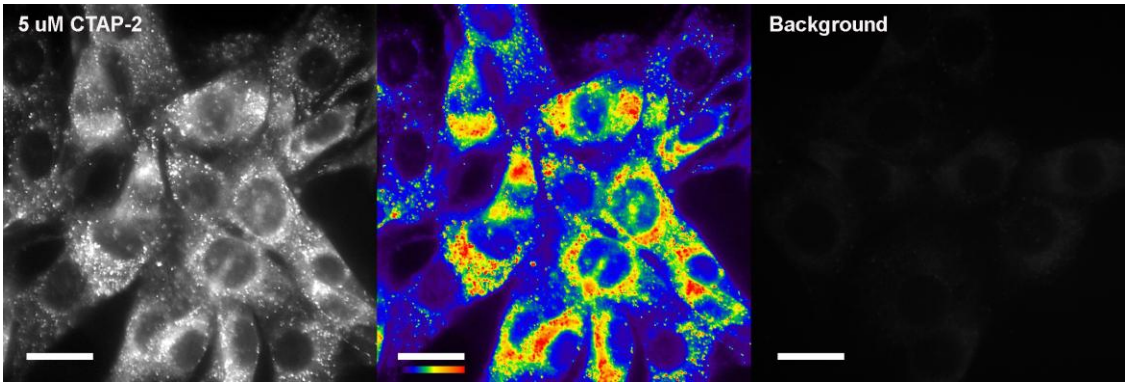

Figure 3.19. *Fluorescence Micrographs of Live Copper-supplemented NIH 3T3 cells with and without CTAP-2.* **Left:** Grayscale image of cells incubated with 5 µM CTAP-2 for 1 hour at 37°C. **Center:** False color image of the same cells (LUT shown as stripe below scale bar). **Right:** Micrograph of control cells in absence of CTAP-2 showing the cellular autofluorescence background under identical imaging conditions. Scale bar 20 µM. Reproduced with permission from Reference (1). © 2011 American Chemical Society.

3.4. Conclusion

This chapter elucidated the characterization of the thermodynamic properties, including Cu(I) stability constant, acid dissociation constant, and redox potential, of a highly water-soluble Cu(I)-probe CTAP-2. The probe which was developed by combining a polyhydroxylated thiazacrown ligand with a sulfonated triarylpyrazoline

fluorophore (by Dr. M. T. Morgan) did not exhibit any measurable aggregation effect at typical working concentrations of 1-5 μM in aqueous solution. In contrast, previously reported Cu(I)-selective fluorescence turn-on probes based on a thioether-rich Cu(I)-binding moiety coupled to an uncharged fluorophore are expected to have a strong tendency to aggregate in aqueous solution which can presumably alter the photophysical properties. The first ever proof of the formation of nanoparticles in aqueous solutions of such lipophilic fluorescent probes was provided by the dynamic light scattering experiments in this work. The exceptional aqueous solubility and high contrast ratio of the Cu(I)-selective probe allowed CTAP-2 to be used for the in-gel detection of a copper chaperone containing a solvent exposed Cu(I) site. The photophysical properties of CTAP-2 and the resolution of native gel are not optimum to detect proteins with labile Cu(I)-binding site from a complex mixture of proteins such as cellular extract. Nevertheless, in-gel detection of hAtox1 by CTAP-2 demonstrated a novel role of metal-responsive turn-on fluorescent probes that can be applied to identify labile metal-binding sites in a protein. This detection method also complements the existing techniques for in-gel metal profiling, including laser ablation inductively coupled plasma mass spectrometry (LA-ICP-MS) and synchrotron-based X-ray fluorescence mapping (Section 3.1.2), both of which measure the total metal content whereas the fluorescent probes can distinguish between the accessible metal-binding site and the one buried inside a protein. Furthermore, CTAP-2 proved to be cell permeant despite its hydrophilic nature. However, based on the Cu(I) stability constants of cellular copper proteins (10^{17}-10^{19}, (104)), it is improbable that CTAP-2, with Cu(I)-affinity several orders of magnitude lower, can be engaged in copper exchange with the endogenous proteins. Therefore, the interpretation of the observed cellular staining patterns is uncertain at present and will require further study, ideally with future Cu(I)-probes featuring higher binding affinities and improved contrast ratios.

3.5. Experimental Methods

3.5.1. Dynamic Light Scattering Experiments

To test for colloidal aggregate formation, the respective compounds were dissolved at a concentration of 1 mM in DMSO and directly diluted into aqueous buffer (MOPS/K^+, pH 7.2) to a final concentration of 5 μM. The hydrodynamic radii (R_h) of the formed colloidal particles were determined by dynamic light scattering (DLS) at a 90° angle using a DynaPro Protein Solutions DLS instrument (Wyatt Technology Corporation, Santa Barbara, CA). Particle size measurements represent an average value of 20 measurements with a 60 sec acquisition time each. All data analyses were performed using the Dynamic v.5.26 software (Wyatt Technology Corporation, Santa Barbara, CA). The R_h of the formed nanoparticles were determined from their respective diffusion coefficients according to the Stokes-Einstein relation.

3.5.2. Acid Dissociation Constant

Fluorescence spectra were acquired in 0.1 M KCl as ionic background. The excitation wavelength was set at 380 nm and the emission scan ranged from 410–700 nm. All solutions were filtered through 0.2 μm membrane filters to remove interfering dust particles or fibers. Three independent pK_a titrations were carried out at 2.3 μM concentration of CTAP-2 by adding HCl such that pH interval is 0.1 at each step. The data were analyzed by non-linear least-squares fitting using the Specfit software package (107).

3.5.3. Cu(II) Stability Constant

UV-vis absorption spectra were measured in 10 mM PIPBS buffer, pH 5, containing 0.1 M $KClO_4$. All solutions were filtered through 0.2 μm membrane filters to remove interfering dust particles or fibers. UV-Vis titrations with Cu(II) were carried out at 7 μM concentration of CTAP-2 (ammonium salt) by adding 100 μM aqueous

copper(II) sulfate in each step. The data were analyzed by non-linear leastsquares fitting using the Specfit software package (107).

3.5.4. Electrochemistry

The cyclic voltammograms were acquired in 10 mM PIPBS buffer, pH 5, containing 0.1M $KClO_4$ as the electrolyte using a CH-Instruments potentiostat (model 600A). The ammonium salt of CTAP-2 was measured at 14 μM concentration in a single compartment cell with a glassy carbon working electrode and a Pt counter electrode. An aqueous Ag/AgCl reference electrode (1 M KCl) was used. The half-wave potentials were referenced to ferrocenium as the external standard. Measurements were typically performed with a scan rate of 50 mV s^{-1} or 100 mV s^{-1}.

3.5.5. Cu(I) Stability Constant

The stability constant for binding of Cu(I) to CTAP-2 was estimated based on the Nernst equation (eqn. 3.7)**.** The formal potential of the aqueous Cu(II/I) redox couple ($E^0_{Cu(II/I)aq}$) was previously reported as 0.13 V (108). This value corresponds to a "formal concentration potential" which was obtained from the standard potential of the aquocopper(II) redox couple (E^0 = 0.153 V) by correcting for the activity of the aquated ions at an ionic strength of 0.10 M using the extended Debye-Hückel equation. This correction alters the calculated ratio of Cu(I) stability constants by a factor of 2. A reference potential of 0.40 V vs SHE was used for the $Fc^{+/0}$ redox couple in aqueous solution (109).

3.5.6. Atox1 Expression and Purification

E. coli BL21(DE3) cells containing pET11d with the gene encoding hATOX1 were grown at 37 °C to an optical density at 600 nm of 0.8-1.1, and then protein expression was induced with isopropyl β-D-1-thiogalactopyranoside (IPTG, 0.5 mM total concentration). After 4 hours, the cells were harvested and the pellet was stored at –80

°C. The cell pellet was thawed and resuspended in a buffer containing 20 mM MES, pH 6.0, 1 mM EDTA, and 5 mM DTT (added just before use) before purification. Purification of Atox1 was initiated by three rounds of freezing and thawing of the suspended cells followed by extraction for 1 h at 4 °C. The cell extract was centrifuged at 6000 x g for 15 min at 4 °C. The supernatant was then concentrated with a 3K microsep centrifugal device (Pall Life Sciences) and applied to a Superdex 75 gel filtration column equilibrated with 50 mM HEPES, pH 7.5, 200 mM NaCl for purification. Fractions containing pure protein were confirmed by Laemmli-SDS-PAGE, pooled, and stored at –80 °C in the elution buffer. Protein concentrations were quantified using Bradford protein assays using BSA as a standard (Pierce).

3.5.7. Electrophoresis of Purified Metalloproteins

Bovine superoxide dismutase (SOD1) and bovine carbonic anhydrase (CA) were purchased from Sigma-Aldrich. These proteins were subjected to native polyacrylamide gel electrophoresis (native-PAGE) without any prior treatment. In all experiments, a solution of hAtox1 (0.3 mM) in HEPES buffer (50 mM, pH 7.5, 0.2 M NaCl) was treated with tris(2-carboxyethyl)phosphine (TCEP, 3 mM final concentration) followed by addition of $[Cu(I)(CH_3CN)_4]PF_6$ (1.2 mM, diluted from a 25 mM stock solution in acetonitrile) to prepare Cu-Atox1. In combination with TCEP (3 mM final concentration), KCN (30 mM final concentration) was used to prepare reduced apo-Atox1 in experiments described in Figure 3.16 and Figure 3.18; variable concentrations of KCN were used as indicated as indicated in the legend of Figure 3.15 for each lane. A total amount of 25 μg protein in Tris-HCl sample buffer (pH 6.8) was loaded in each lane of a 4% stacking - 10% resolving Tris-HCl Native Gel, which was then subjected to electrophoresis at 200 V for 45 min using a Tris-glycine running buffer (25 mM Tris, 192 mM glycine, pH 8.3).

3.5.8. In-gel Visualization of Proteins with CTAP-2

After the electrophoresis run, the gel was immersed in a 5 μM aqueous solution of CTAP-2 for 15 minutes. Images were acquired with Alpha Imager (Cell Biosciences) using the UV transilluminator (excitation 365 nm) and Green Filter (537 nm, 35 nm Band Pass). Subsequently, protein content of the same gel was visualized by coomassie dye (GelCode Blue Stain Reagent, Pierce).

3.5.9. In-gel Visualization of Proteins with Probe 3.1

After the electrophoresis run, the gel was immersed in a 5 μM aqueous solution of **3.1** (prepared by dilution from a DMSO stock solution) for 15 minutes. The gel has to be washed for 5 minutes before the imaging to reduce the undesired fluorescence background. Images were acquired with Alpha Imager (Cell Biosciences) using the UV transilluminator (excitation 365 nm) and Green Filter (537 nm, 35 nm Band Pass). Subsequently, protein content of the same gel was visualized by coomassie dye (GelCode Blue Stain Reagent, Pierce).

3.5.10. Cell Permeability

NIH 3T3 mouse fibroblast cells were cultured at 37 ^{0}C (5% CO_2) in Dulbecco's modified Eagle's medium (DMEM, Invitrogen) supplemented with 10% bovine serum, 4 mM L-glutamine, 200 unit/ml penicillin, and 200 μg/ml streptomycin. For staining experiments cells were directly grown on cover slips in basal medium supplemented with 50 μM copper(II) chloride over a period of 16 hours. After removing the growth medium, the cells were gently washed with DMEM (prewarmed at 37 °C) and then incubated with CTAP-2 (5 μM in serum-free DMEM) for 1 hour at 37 °C (5% CO_2). After washing with prewarmed DMEM (supplemented with 25 mM HEPES), the cover slips were mounted on slides using Fluoromount-G (Southern Biotech). Fluorescence micrographs were acquired with a Zeiss inverted fluorescence microscope (Axiovert 200) equipped with a

cooled CCD camera (CoolSnap HQ, Photometrics) using a mercury lamp as excitation source combined with a 370-390 BP excitation filter, 400 nm dichroic mirror, and a 420 LP emission filter.

3.6. References

1. Morgan MT, Bagchi P, & Fahrni CJ (2011) Designed to dissolve: Suppression of colloidal aggregation of Cu(I)-selective fluorescent probes in aqueous buffer and in-gel detection of a metallochaperone. *Journal of the American Chemical Society* 133(40):15906-15909.

2. Nevitt T, Ohrvik H, & Thiele DJ (2012) Charting the travels of copper in eukaryotes from yeast to mammals. *Biochimica Et Biophysica Acta-Molecular Cell Research* 1823(9):1580-1593.

3. Taylor A, Day MP, Marshall J, Patriarca M, & White M (2012) Atomic spectrometry update. Clinical and biological materials, foods and beverages. *Journal of Analytical Atomic Spectrometry* 27(4):537-576.

4. Walshe JM (2011) The pattern of urinary copper excretion and its response to treatment in patients with Wilson's disease. *Qjm-an International Journal of Medicine* 104(9):775-778.

5. Gray LW, Peng FY, Molloy SA, Pendyala VS, Muchenditsi A, Muzik O, Lee J, Kaplan JH, & Lutsenko S (2012) Urinary copper elevation in a mouse model of wilson's disease is a regulated process to specifically decrease the hepatic copper load. *Plos One* 7(6).

6. McClatchey KD (2002) *Clinical laboratory medicine* (Philadelphia, Lippincott Wiliams & Wilkins) 2nd ed. Ed.

7. Dixon JM, McDonald C, Elton RA, Miller WR, & Edinburgh Breast G (1999) Risk of breast cancer in women with palpable breast cysts: a prospective study. *Lancet* 353(9166):1742-1745.

8. Sisman AR, Sis B, Canda T, & Onvural B (2009) Electrolytes and trace elements in human breast cyst fluid. *Biological Trace Element Research* 128(1):18-30.

9. Yazar M, Sarban S, Kocyigit A, & Isikan UE (2005) Synovial fluid and plasma selenium, copper, zinc, and iron concentrations in patients with rheumatoid arthritis and osteoarthritis. *Biological Trace Element Research* 106(2):123-132.

10. Mazdak H, Yazdekhasti F, Movahedian A, Mirkheshti N, & Shafieian M (2010) The comparative study of serum iron, copper, and zinc levels between bladder cancer patients and a control group. *International Urology and Nephrology* 42(1):89-93.

11. Melichar B, Jandik P, Malir F, Tichy M, Bures J, Mergancova J, & Voboril Z (1994) Increased urinary zinc and copper excretion in colorectal-cancer. *Journal of Trace Elements and Electrolytes in Health and Disease* 8(3-4):209-212.

12. Ford ES (2000) Serum copper concentration and coronary heart disease among US adults. *American Journal of Epidemiology* 151(12):1182-1188.

13. Kosch M, Schodjaian K, Nguyen SQ, Tokmak F, Westermann G, Hausberg M, Rahn KH, & Kisters K (1999) Trace element and electrolyte disturbances in alcoholic liver disease - role of zinc, cadmium, copper and magnesium metabolism. *Medical Science Research* 27(11):739-741.

14. Cantle JE (1982) *Atomic absorption spectrometry* (Amsterdam, Elsevier Scientific Pub. Co.).

15. Montaser A (1998) *Inductively coupled plasma mass spectrometry* (New York, J. Wiley).

16. Ha Y, Tsay OG, & Churchill DG (2011) A tutorial and mini-review of the ICP-MS technique for determinations of transition metal ion and main group element concentration in the neurodegenerative and brain sciences. *Monatshefte Fur Chemie* 142(4):385-398.

17. Ejima A, Watanabe C, Koyama H, & Satoh H (1996) Analysis of trace elements in the central nerve tissues with inductively coupled plasma-mass spectrometry. *Tohoku Journal of Experimental Medicine* 178(1):1-10.

18. Beauchemin D & Kisilevsky R (1998) A method based on ICP-MS for the analysis of Alzheimer's amyloid plaques. *Analytical Chemistry* 70(5):1026-1029.

19. Zhao T, Chen TL, Qiu YP, Zou XY, Li X, Su MM, Yan CH, Zhao AH, & Jia W (2009) Trace element profiling using inductively coupled plasma mass spectrometry and its application in an osteoarthritis study. *Analytical Chemistry* 81(9):3683-3692.

20. Richarz AN & Bratter P (2002) Speciation analysis of trace elements in the brains of individuals with Alzheimer's disease with special emphasis on metallothioneins. *Analytical and Bioanalytical Chemistry* 372(3):412-417.

21. Gonzalez-Fernandez M, Garcia-Barrera T, Arias-Borrego A, Jurado J, Pueyo C, Lopez-Barea J, & Gomez-Ariza JL (2009) Metallomics integrated with proteomics in deciphering metal-related environmental issues. *Biochimie* 91(10):1311-1317.

22. Cvetkovic A, Menon AL, Thorgersen MP, Scott JW, Poole FL, Jenney FE, Lancaster WA, Praissman JL, Shanmukh S, Vaccaro BJ, Trauger SA, Kalisiak E, Apon JV, Siuzdak G, Yannone SM, Tainer JA, & Adams MWW (2010)

Microbial metalloproteomes are largely uncharacterized. *Nature* 466(7307):779-U718.

23. Mason AZ & Borja MR (2002) A study of Cu turnover in proteins of the visceral complex of Littorina littorea by stable isotopic analysis using coupled HPLC-ICP-MS. *Marine Environmental Research* 54(3-5):351-355.

24. Polec-Pawlak K, Schaumloffel D, Szpunar J, Prange A, & Lobinski R (2002) Analysis for metal complexes with metallothionein in rat liver by capillary zone electrophoresis using ICP double-focussing sector-field isotope dilution MS and electrospray MS detection. *Journal of Analytical Atomic Spectrometry* 17(8):908-912.

25. Lobinski R, Schaumloffel D, & Szpunar J (2006) Mass spectrometry in bioinorganic analytical chemistry. *Mass Spectrometry Reviews* 25(2):255-289.

26. Qin ZY, Caruso JA, Lai B, Matusch A, & Becker JS (2011) Trace metal imaging with high spatial resolution: Applications in biomedicine. *Metallomics* 3(1):28-37.

27. Fahrni CJ (2007) Biological applications of X-ray fluorescence microscopy: exploring the subcellular topography and speciation of transition metals. *Current Opinion in Chemical Biology* 11(2):121-127.

28. McRae R, Bagchi P, Sumalekshmy S, & Fahrni CJ (2009) In situ imaging of metals in cells and tissues. *Chemical Reviews* 109(10):4780-4827.

29. McRae R, Lai B, & Fahrni CJ (2010) Copper redistribution in Atox1-deficient mouse fibroblast cells. *Journal of Biological Inorganic Chemistry* 15(1):99-105.

30. Yang LC, McRae R, Henary MM, Patel R, Lai B, Vogt S, & Fahrni CJ (2005) Imaging of the intracellular topography of copper with a fluorescent sensor and by synchrotron x-ray fluorescence microscopy. *Proceedings of the National Academy of Sciences of the United States of America* 102(32):11179-11184.

31. Farquharson MJ, Al-Ebraheem A, Falkenberg G, Leek R, Harris AL, & Bradley DA (2008) The distribution of trace elements Ca, Fe, Cu and Zn and the determination of copper oxidation state in breast tumour tissue using mu SRXRF and mu XANES. *Physics in Medicine and Biology* 53(11):3023-3037.

32. Farquharson MJ, Geraki K, Falkenberg G, Leek R, & Harris A (2007) The localisation and micro-mapping of copper and other trace elements in breast tumours using a synchrotron micro-XRF system. *Applied Radiation and Isotopes* 65(2):183-188.

33. McRae R, Lai B, Vogt S, & Fahrni CJ (2006) Correlative microXRF and optical immunofluorescence microscopy of adherent cells labeled with ultrasmall gold particles. *Journal of Structural Biology* 155(1):22-29.

34. Kriegeskotte C, Cantz T, Haberland J, Zibert A, Haier J, Kohler G, Scholer HR, Schmidt HHJ, & Arlinghaus HF (2009) Laser secondary neutral mass spectrometry for copper detection in micro-scale biopsies. *Journal of Mass Spectrometry* 44(10):1417-1422.

35. Becker JS, Matusch A, Becker JS, Wu B, Palm C, Becker AJ, & Salber D (2011) Mass spectrometric imaging (MSI) of metals using advanced BrainMet techniques for biomedical research. *International Journal of Mass Spectrometry* 307(1-3):3-15.

36. Wu B, Niehren S, & Becker JS (2011) Mass spectrometric imaging of elements in biological tissues by new BrainMet technique-laser microdissection inductively coupled plasma mass spectrometry (LMD-ICP-MS). *Journal of Analytical Atomic Spectrometry* 26(8):1653-1659.

37. Matusch A, Depboylu C, Palm C, Wu B, Hoeglinger GU, Schaefer MKH, & Becker JS (2010) Cerebral bioimaging of Cu, Fe, Zn, and Mn in the MPTP mouse model of Parkinson's disease using laser ablation inductively coupled plasma mass spectrometry (LA-ICP-MS). *Journal of the American Society for Mass Spectrometry* 21(1):161-171.

38. Zoriy MV, Dehnhardt M, Matusch A, & Becker JS (2008) Comparative imaging of P, S, Fe, Cu, Zn and C in thin sections of rat brain tumor as well as control tissues by laser ablation inductively coupled plasma mass spectrometry. *Spectrochimica Acta Part B-Atomic Spectroscopy* 63(3):375-382.

39. Becker JS, Zoriy MV, Pickhardt C, Palomero-Gallagher N, & Zilles K (2005) Imaging of copper, zinc, and other elements in thin section of human brain samples (Hippocampus) by laser ablation inductively coupled plasma mass spectrometry. *Analytical Chemistry* 77(10):3208-3216.

40. Becker JS, Zoriy MV, Pickhardta C, & Zilles K (2005) Copper, zinc, phosphorus and sulfur distribution in thin section of rat brain tissues measured by laser ablation inductively coupled plasma mass spectrometry: possibility for small-size tumor analysis. *Journal of Analytical Atomic Spectrometry* 20(9):912-917.

41. Dobrowolska J, Dehnhardt M, Matusch A, Zoriy M, Palomero-Gallagher N, Koscielniak P, Zilles K, & Becker JS (2008) Quantitative imaging of zinc, copper and lead in three distinct regions of the human brain by laser ablation inductively coupled plasma mass spectrometry. *Talanta* 74(4):717-723.

42. Zoriy MV & Becker JS (2007) Imaging of elements in thin cross sections of human brain samples by LA-ICP-MS: A study on reproducibility. *International Journal of Mass Spectrometry* 264(2-3):175-180.

43. Dehnhardt M, Zoriy MV, Khan Z, Reifenberger G, Ekstrom TJ, Becker JS, Zilles K, & Bauer A (2008) Element distribution is altered in a zone surrounding human

glioblastoma multiforme. *Journal of Trace Elements in Medicine and Biology* 22(1):17-23.

44. Zoriy MV, Dehnhardt M, Reifenberger G, Zilles K, & Becker JS (2006) Imaging of Cu, Zn, Pb and U in human brain tumor resections by laser ablation inductively coupled plasma mass spectrometry. *International Journal of Mass Spectrometry* 257(1-3):27-33.

45. Hutchinson RW, Cox AG, McLeod CW, Marshall PS, Harper A, Dawson EL, & Howlett DR (2005) Imaging and spatial distribution of beta-amyloid peptide and metal ions in Alzheimer's plaques by laser ablation-inductively coupled plasma-mass spectrometry. *Analytical Biochemistry* 346(2):225-233.

46. Okamoto K & Utamura M (1938) Biological investigations on copper. I. Histochemical detection of copper. *Acta Sch. Med. Univ. Imp. Kioto* 20:573-580.

47. Butt EM, Nusbaum RE, Gilmour TC, & Didio SL (1958) Trace metal patterns in disease states .2. Copper storage diseases, with consideration of juvenile cirrhosis, Wilsons disease, and hepatic copper of the newborn. *American Journal of Clinical Pathology* 30(6):479-497.

48. Green CL (1955) Histochemical demonstration of copper in a case of hepatolenticular degeneration. *American Journal of Pathology* 31(3):545-553.

49. Uzman LL (1956) Histochemical localization of copper with rubeanic acid. *Laboratory Investigation* 5(3):299-305.

50. Okamoto K, Utamura M, & Mikami G (1938) *Trans. Soc. Pathol. Jpn.* 22:348.

51. Okamoto K, Utamura M, & Mikami G (1939) *Trans. Soc. Pathol. Jpn.* 22:361.

52. Waterhouse DF (1945) *B COUNC SCI IND RES* 191:7.

53. Shikata T, Uzawa T, Yoshiwar.N, Akatsuka T, & Yamazaki S (1974) Staining methods of Australia-antigen in paraffin section - detection of cytoplasmic inclusion-bodies. *Japanese Journal of Experimental Medicine* 44(1):25-&.

54. Morgan MT, Bagchi P, & Fahrni CJ (2013) Fluorescent probes for monovalent copper. *Encyclopedia of Inorganic and Bioinorganic Chemistry*, (John Wiley & Sons, in press).

55. Dean KM, Qin Y, & Palmer AE (2012) Visualizing metal ions in cells: An overview of analytical techniques, approaches, and probes. *Biochimica Et Biophysica Acta-Molecular Cell Research* 1823(9):1406-1415.

56. Domaille DW, Que EL, & Chang CJ (2008) Synthetic fluorescent sensors for studying the cell biology of metals. *Nature Chemical Biology* 4(3):168-175.

57. Zeng L, Miller EW, Pralle A, Isacoff EY, & Chang CJ (2006) A selective turn-on fluorescent sensor for imaging copper in living cells. *Journal of the American Chemical Society* 128(1):10-11.

58. Miller EW, Zeng L, Domaille DW, & Chang CJ (2006) Preparation and use of Coppersensor-1, a synthetic fluorophore for live-cell copper imaging. *Nature Protocols* 1(2):824-827.

59. Dodani SC, Domaille DW, Nam CI, Miller EW, Finney LA, Vogt S, & Chang CJ (2011) Calcium-dependent copper redistributions in neuronal cells revealed by a fluorescent copper sensor and X-ray fluorescence microscopy. *Proceedings of the National Academy of Sciences of the United States of America* 108(15):5980-5985.

60. Dodani SC, Leary SC, Cobine PA, Winge DR, & Chang CJ (2011) A targetable fluorescent sensor reveals that copper-deficient SCO1 and SCO2 patient cells prioritize mitochondrial copper homeostasis. *Journal of the American Chemical Society* 133(22):8606-8616.

61. Hirayama T, Van de Bittner GC, Gray LW, Lutsenko S, & Chang CJ (2012) Near-infrared fluorescent sensor for in vivo copper imaging in a murine Wilson disease model. *Proceedings of the National Academy of Sciences of the United States of America* 109(7):2228-2233.

62. Lim CS, Han JH, Kim CW, Kang MY, Kang DW, & Cho BR (2011) A copper(I)-ion selective two-photon fluorescent probe for in vivo imaging. *Chemical Communications* 47(25):7146-7148.

63. Sussulini A & Becker JS (2011) Combination of PAGE and LA-ICP-MS as an analytical workflow in metallomics: state of the art, new quantification strategies, advantages and limitations. *Metallomics* 3(12):1271-1279.

64. Ortega R (2009) Synchrotron radiation for direct analysis of metalloproteins on electrophoresis gels. *Metallomics* 1(2):137-141.

65. Gao YX, Liu YB, Chen CY, Li B, He W, Huang YY, & Chai ZF (2005) Combination of synchrotron radiation X-ray fluorescence with isoelectric focusing for study of metalloprotein distribution in cytosol of hepatocellular carcinoma and surrounding normal tissues. *Journal of Analytical Atomic Spectrometry* 20(5):473-475.

66. Raimunda D, Khare T, Giometti C, Vogt S, Arguello JM, & Finney L (2012) Identifying metalloproteins through X-ray fluorescence mapping and mass spectrometry. *Metallomics* 4(9):921-927.

67. Chevreux S, Roudeau S, Fraysse A, Carmona A, Deves G, Solari PL, Weng TC, & Ortega R (2008) Direct speciation of metals in copper-zinc superoxide

dismutase isoforms on electrophoresis gels using X-ray absorption near edge structure. *Journal of Analytical Atomic Spectrometry* 23(8):1117-1120.

68. Becker JS, Lobinski R, & Becker JS (2009) Metal imaging in non-denaturating 2D electrophoresis gels by laser ablation inductively coupled plasma mass spectrometry (LA-ICP-MS) for the detection of metalloproteins. *Metallomics* 1(4):312-316.

69. Becker JS, Mounicou S, Zoriy MV, Becker JS, & Lobinski R (2008) Analysis of metal-binding proteins separated by non-denaturating gel electrophoresis using matrix-assisted laser desorption/ionization mass spectrometry (MALDI-MS) and laser ablation inductively coupled plasma mass spectrometry (LA-ICP-MS). *Talanta* 76(5):1183-1188.

70. Becker JS, Zoriy M, Becker JS, Pickhardt C, & Przybylski M (2004) Determination of phosphorus and metals in human brain proteins after isolation by gel electrophoresis by laser ablation inductively coupled plasma source mass spectrometry. *Journal of Analytical Atomic Spectrometry* 19(1):149-152.

71. Becker JS, Zoriy M, Dressler VL, Wu B, & Becker JS (2008) Imaging of metals and metal-containing species in biological tissues and on gels by laser ablation inductively coupled plasma mass spectrometry (LA-ICP-MS): A new analytical strategy for applications in life sciences. *Pure and Applied Chemistry* 80(12):2643-2655.

72. Becker JS, Zoriy M, Krause-Buchholz U, Becker JS, Pickhardt C, Przybylski M, Pompe W, & Rodel G (2004) In-gel screening of phosphorus and copper, zinc and iron in proteins of yeast mitochondria by LA-ICP-MS and identification of phosphorylated protein structures by MALDI-FT-ICR-MS after separation with two-dimensional gel electrophoresis. *Journal of Analytical Atomic Spectrometry* 19(9):1236-1243.

73. Becker JS, Zoriy M, Pickhardt C, Przybylski M, & Becker JS (2005) Investigation of Cu-, Zn- and Fe-containing human brain proteins using isotopic-enriched tracers by LA-ICP-MS and MALDI-FT-ICR-MS. *International Journal of Mass Spectrometry* 242(2-3):135-144.

74. Becker JS, Zoriy M, Przybylski M, & Becker JS (2007) High resolution mass spectrometric brain proteomics by MALDI-FTICR-MS combined with determination of P, S, Cu, Zn and Fe by LA-ICP-MS. *International Journal of Mass Spectrometry* 261(1):68-73.

75. Becker JS, Zoriy M, Przybylski M, & Becker JS (2007) Study of formation of Cu- and Zn-containing tau protein using isotopically-enriched tracers by LA-ICP-MS and MALDI-FTICR-MS. *Journal of Analytical Atomic Spectrometry* 22(1):63-68.

76. Becker JS, Zoriy M, Becker JS, Pickhardt C, Damoc E, Juhacz G, Palkovits M, & Przybylski M (2005) Determination of phosphorus-, copper-, and zinc-containing

human brain proteins by LA-ICPMS and MALDI-FTICR-MS. *Analytical Chemistry* 77(18):5851-5860.

77. Sevcenco AM, Hagen WR, & Hagedoorn PL (2012) Microbial metalloproteomes explored using MIRAGE. *Chemistry & Biodiversity* 9(9):1967-1980.

78. Sevcenco A-M, Krijger GC, Pinkse MWH, Verhaert PDEM, Hagen WR, & Hagedoorn P-L (2009) Development of a generic approach to native metalloproteomics: application to the quantitative identification of soluble copper proteins in Escherichia coli. *Journal of Biological Inorganic Chemistry* 14(4):631-640.

79. Sevcenco A-M, Pinkse MWH, Wolterbeek HT, Verhaert PDEM, Hagen WR, & Hagedoorn P-L (2011) Exploring the microbial metalloproteome using MIRAGE. *Metallomics* 3(12):1324-1330.

80. Go YM & Jones DP (2008) Redox compartmentalization in eukaryotic cells. *Biochimica Et Biophysica Acta-General Subjects* 1780(11):1271-1290.

81. Kim H-S & Ahner BA (2006) Calibration of Phen Green (TM) for use as a Cu(I)-selective fluorescent indicator. *Anal. Chim. Acta* 575(2):223-229.

82. Strambini GB & Gabellieri E (1991) Quenching of indole luminescence by copper ions - a distance dependence study. *Journal of Physical Chemistry* 95(11):4347-4352.

83. Rapisarda VA, Volentini SI, Farias RN, & Massa EM (2002) Quenching of bathocuproine disulfonate fluorescence by Cu(I) as a basis for copper quantification. *Analytical Biochemistry* 307(1):105-109.

84. Closs GL & Miller JR (1988) Intramolecular long-distance electron-transfer in organic-molecules. *Science* 240(4851):440-447.

85. Marcus RA & Sutin N (1985) Electron transfers in chemistry and biology. *Biochimica Et Biophysica Acta* 811(3):265-322.

86. Rehm D & Weller A (1970) Kinetics of fluorescence quenching by electron and H-atom transfer. *Israel Journal of Chemistry* 8(2):259-271.

87. Cody J, Mandal S, Yang L, & Fahrni CJ (2008) Differential tuning of the electron transfer parameters in 1,3,5-triarylpyrazolines: A rational design approach for optimizing the contrast ratio of fluorescent probes. *Journal of the American Chemical Society* 130(39):13023-13032.

88. Verma M, Chaudhry AF, & Fahrni CJ (2009) Predicting the photoinduced electron transfer thermodynamics in polyfluorinated 1,3,5-triarylpyrazolines based on multiple linear free energy relationships. *Organic & Biomolecular Chemistry* 7(8):1536-1546.

89. Verma M, Chaudhry AF, Morgan MT, & Fahrni CJ (2010) Electronically tuned 1,3,5-triarylpyrazolines as Cu(I)-selective fluorescent probes. *Organic & Biomolecular Chemistry* 8(2):363-370.

90. Chaudhry AF, Verma M, Morgan MT, Henary MM, Siegel N, Hales JM, Perry JW, & Fahrni CJ (2010) Kinetically controlled photoinduced electron transfer switching in Cu(I)-responsive fluorescent probes. *Journal of the American Chemical Society* 132(2):737-747.

91. Hyman LM & Franz KJ (2012) Probing oxidative stress: Small molecule fluorescent sensors of metal ions, reactive oxygen species, and thiols. *Coordination Chemistry Reviews* 256(19-20):2333-2356.

92. Feng BY, Shelat A, Doman TN, Guy RK, & Shoichet BK (2005) High-throughput assays for promiscuous inhibitors. *Nature Chemical Biology* 1(3):146-148.

93. Hong YN, Lam JWY, & Tang BZ (2011) Aggregation-induced emission. *Chemical Society Reviews* 40(11):5361-5388.

94. Kamino S, Muranaka A, Murakami M, Tatsumi A, Nagaoka N, Shirasaki Y, Watanabe K, Yoshida K, Horigome J, Komeda S, Uchiyama M, & Enomoto S (2013) A red-emissive aminobenzopyrano-xanthene dye: elucidation of fluorescence emission mechanisms in solution and in the aggregate state. *Physical Chemistry Chemical Physics* 15(6):2131-2140.

95. Chen CT (2004) Evolution of red organic light-emitting diodes: Materials and devices. *Chemistry of Materials* 16(23):4389-4400.

96. Ricchelli F (1995) Photophysical properties of porphyrins in biological-membranes. *Journal of Photochemistry and Photobiology B-Biology* 29(2-3):109-118.

97. Morgan MT, Bagchi P, & Fahrni CJ (2013) High-contrast fluorescence sensing of aqueous Cu(I) with triarylpyrazoline probes: dissecting the roles of ligand donor strength and excited state proton transfer. *Dalton Transactions* 42(9):3240-3248.

98. Price KA, Hickey JL, Xiao Z, Wedd AG, James SA, Liddell JR, Crouch PJ, White AR, & Donnelly PS (2012) The challenges of using a copper fluorescent sensor (CS1) to track intracellular distributions of copper in neuronal and glial cells. *Chemical Science* 3(9):2748-2759.

99. Bernardo MM, Heeg MJ, Schroeder RR, Ochrymowycz LA, & Rorabacher DB (1992) Comparison of the influence of saturated nitrogen and sulfur donor atoms on the properties of copper(II/I) macrocyclic polyamino polythiaether ligand complexes - redox potentials and protonation and stability-constants of Cu(l)L species and new structural data. *Inorganic Chemistry* 31(2):191-198.

100. Sevcenco AM, Pinkse MWH, Wolterbeek HT, Verhaert P, Hagen WR, & Hagedoorn PL (2011) Exploring the microbial metalloproteome using MIRAGE. *Metallomics* 3(12):1324-1330.

101. Bruyninckx WJ, Gutteridge S, & Mason HS (1978) Detection of copper on polyacrylamide gels. *Analytical Biochemistry* 89(1):174-177.

102. Gasteiger E, Hoogland C, A. G, Duvaud S, Wilkins MR, Appel RD, & Bairoch A (2005) *The proteomics protocols handbook* (Totowa, N.J., Humana Press).

103. Narindrasorasak S, Zhang XF, Roberts EA, & Sarkar B (2004) Comparative analysis of metal binding characteristics of copper chaperone proteins, Atx1 and Atox1. *Bioinorganic Chemistry and Applications* 2(1-2):105-123.

104. Xiao ZG, Brose J, Schimo S, Ackland SM, La Fontaine S, & Wedd AG (2011) Unification of the copper(I) binding affinities of the metallo-chaperones Atx1, Atox1, and related proteins. Detection probes and affinity standards. *Journal of Biological Chemistry* 286(13):11047-11055.

105. Wernimont AK, Huffman DL, Lamb AL, O'Halloran TV, & Rosenzweig AC (2000) Structural basis for copper transfer by the metallochaperone for the Menkes/Wilson disease proteins. *Nature Structural Biology* 7(9):766-771.

106. Hough MA & Hasnain SS (2003) Structure of fully reduced bovine copper zinc superoxide dismutase at 1.15 angstrom. *Structure* 11(8):937-946.

107. Binstead RA & Zuberbühler AD (2001) SPECFIT Global Analysis System (Spectrum Software Associates, Marlborough MA 01752), 3.0.27.

108. Bernardo MM, Schroeder RR, & Rorabacher DB (1991) Electrochemical properties of copper(II) copper(I) macrocyclic polythia ether complexes - determination of formal potential values and cyclic voltammetric behavior. *Inorganic Chemistry* 30(6):1241-1247.

109. Koepp HM, Wendt H, & Strehlow H (1960) *Zeitschrift Fur Elektrochemie* 64(4):483-491.

CHAPTER 4

DESIGNING HIGH CONTRAST COPPER(I)-SELECTIVE AQUEOUS FLUORESCENT PROBES: IMPORTANCE OF LIGAND DONOR STRENGTH AND EXCITED STATE PROTON TRANSFER

In this chapter, coordination properties of a water soluble, high contrast Cu(I)-selective fluorescent probe **4.3** were determined. With the ultimate goal of designing a fluorescent probe suitable for biological applications, this probe was originally developed to improve the photophysical parameters of CTAP-2 by modifying the ligand design. However, this work eventually provided plausible mechanisms for the incomplete fluorescence recovery and the low intrinsic fluorophore quantum yield often observed for the triarylpyrazoline-based aqueous Cu(I)-probes. This work was published in the Dalton Transactions (1).

4.1. Background

CTAP-1 was the first synthetic fluorescence turn-on probe reported for the detection of aqueous Cu(I) ions (2). This probe was designed on a 1,3-diaryl-2-pyrazoline fluorophore platform (Figure 3.3) using PET switching mechanism. Although CTAP-1 was used in detection of cellular copper, the contrast ratio (f_e) of the probe was relatively low (f_e = 4.6) limiting its applicability in bioimaging. Moreover, aqueous solution of CTAP-1, even with an ionizable carboxylic acid moiety attached to the fluorophore, showed evidence of colloid formation by dynamic light scattering. In contrast, CTAP-2 with an improved contrast ration of 65, was highly water soluble and at the same time cell permeable. The fluorescence quantum yield of Cu(I)-saturated CTAP-2, however, remained relatively low at 8.3% which was even lower than CTAP-1 (14%). Interestingly, protonation of the metal-free N-arylthiazacrown PET donor of CTAP-2

under acidic conditions increased the quantum yield by 3-fold to 25% (Table 3.1). Similar behavior was previously observed for the N-arylthiazacrown-based methanolic Cu(I)-probes **4.1a-d** (Figure 4.1). For example, probe **4.1b** (where R = 2,5-F_2) **(**Table 4.1**)**, which provided the highest contrast ratio of 29, gave a fluorescence quantum yield of only 9.5% upon saturation with Cu(I). However, protonation of the aniline nitrogen of the free probe yielded a more than 5-fold higher quantum yield of 54% (3).

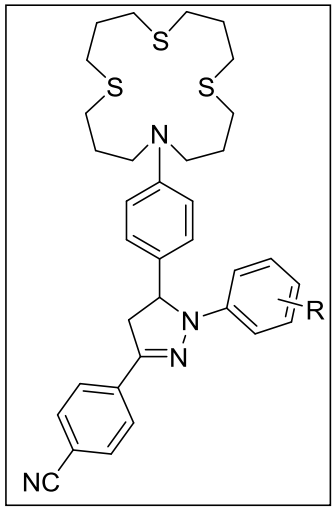

Figure 4.1. *Generalized Molecular Structure of Pyrazoline Probes **4.1a-d**.*

There could be potentially two contributing factors that can explain this incomplete fluorescence recovery of the PET probes. First, protonation of the aniline nitrogen renders it inactive towards oxidation, thereby completely blocking the PET process. In contrast, coordination to a soft cation like Cu^+ will increase the $E(D^+/D)$ to a smaller extent, thus under this condition the PET-induced fluorescence quenching observed for the free probe is not entirely inhibited. This residual fluorescence

quenching of the Cu(I)-bound form will decrease its quantum yield and hence reduce the fluorescence enhancement.

Table 4.1. *Comparison of Fluorescence Recoveries upon Cu(I) Binding and Protonation of Aniline Nitrogen*

Compound [a]	R	Φ_f Neutral [c]	Φ_f Acidic [d]	Φ_f Cu(I) [e]	f_e [b] Acidic [d]	f_e [b] Cu(I) [e]
4.1a	3-F	0.0072	0.53	0.15	74	21
4.1b	2,5-F_2	0.0033	0.54	0.095	164	29
4.1c	2,3,5-F_3	0.0024	0.6	0.048	250	20
4.1d	2,3,5,6-F_4	0.0010	0.55	0.02	550	20

[a] Data adapted with permission from Reference (3). © 2010 American Chemical Society; [b] $f_e = \Phi_f / \Phi_f$(neutral); [c] Probe in methanol alone; [d] 180 mM TFA in methanol; [e] 10 μM $[Cu(I)(CH_3CN)_4]PF_6$ in methanol (0.1% acetonitrile)

Second, it can be presumed that a competing photoinduced electron transfer from the probe-bound Cu(I) to form a Cu(II) complex can contribute towards incomplete fluorescence recovery. However, femtosecond time-resolved pump-probe experiments with the probe **4.1a** (where R = 3F) provided no evidence of the formation of a Cu(II) complex thus negating the above possibility (3). On the other hand, this data along with the time-resolved fluorescence decay measurements of the same probe showed evidence of at least three distinct emissive species. Furthermore, variable temperature NMR studies in deuterated methanol revealed a dynamic equilibrium between two types of Cu(I) coordinated species. One is the expected tetradentate NS_3-coordinated Cu(I)-complex and the other is a ternary complex formed by Cu(I)-coordination of a solvent molecule replacing the Cu-N bond. Because the ternary complex with the solvent weakens the interaction between Cu(I) and the aniline nitrogen, the photoinduced

electron transfer by the arylamine donor is not completely inhibited upon Cu(I) binding leading to incomplete fluorescence recovery.

The weakening of the Cu-N bond and the ternary complex formation with solvent molecule can be reasoned as an effect of steric hindrance between the ortho-hydrogens of the N-aryl ring and the thiaza crown backbone upon Cu(I) binding to the probes **4.1**. Binding to the solvent molecule reduces this strain and thus driving the equilibrium towards thermodynamically stable ternary complexes. This hypothesis was indeed confirmed with probe **4.2** where the aniline ring was fused with the ligand backbone to reduce the unfavorable steric interactions. Upon saturation with Cu(I), probe **4.2** offered a fluorescence enhancement of 210 and a quantum yield of 49% in methanol (4).

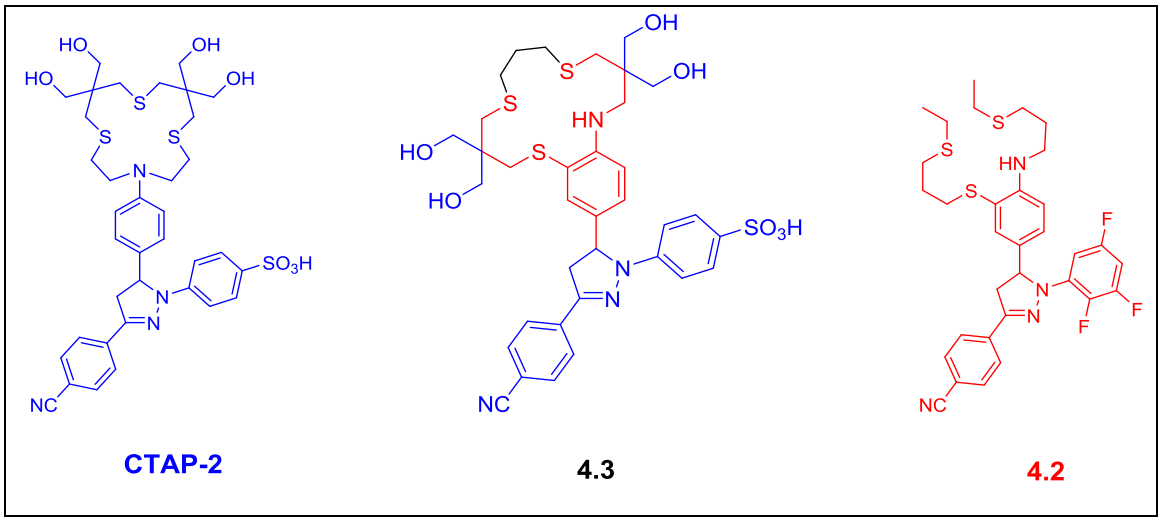

Figure 4.2. *Design Strategy of Water Soluble Cu(I)-probe **4.3**.* Part of the fluorophore that is derived from **CTAP-2** is colored **blue** and that derived from **4.2** is colored **red**.

4.2. Results and Discussion

This work will discuss characterization of thermodynamic properties of probe **4.3** which was synthesized by Dr. M. T. Morgan. The detail of the synthetic procedures can be found elsewhere (1).

With the objective of improving the fluorescence quantum yield of CTAP-2 utilizing a similar design strategy described for **4.2**, the probe **4.3** was conceived where the arylamine ring was integrated with the ligand backbone, the solubilization groups were similar to CTAP-2 including functionalization of the thioether-based Cu(I)-binding moiety with four hydroxymethyl groups along with the sulfonated fluorophore (Figure 4.2).

Table 4.2. *Comparison of Photophysical Properties of CTAP-2 and Probe **4.3***

Compound[a,d]	Medium	Abs max (nm)	Em max (nm)	Φ_f
4.3	pH 7.2[b]	394	506	0.0014
4.3	0.1 M HCl	391	504	0.070
4.3-Cu(I)	pH 7.2 [b]	388	506	0.074
CTAP-2	pH 7.2 [b]	396	512	0.0015
CTAP-2	5 mM HCl	388	512	0.25
CTAP-2-Cu(I)	pH 7.2 [b]	392	512	0.083[c]

[a] Data adapted with permission from Reference (1). © 2012, Royal Society of Chemistry; [b] 10 mM MOPS/K^+, pH 7.2; [c] 65-fold enhancement over Cu(I)-free CTAP-2 at 380 nm; [d] Data acquired by Dr. M. T. Morgan.

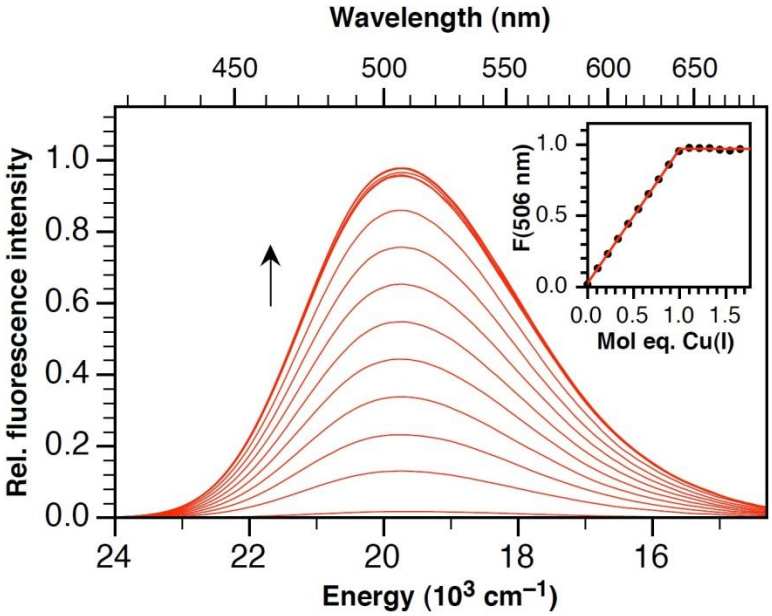

Figure 4.3. *Fluorescence Titration of Probe **4.3** with Cu(I).* Fluorescence response of probe **4.3** (4.6 μM) to Cu(I) (provided by in-situ reduction of Cu(II) with 100 μM ascorbate) in aqueous buffer at pH 7.2 (10 mM MOPS/K^+, 22 °C, λ_{ex} = 380 nm). Reproduced with permission from Reference (1). © 2012, Royal Society of Chemistry. Data acquired by Dr. M. T. Morgan.

4.2.1. Photophysical Characterization

Similar to CTAP-2, the ammonium salt of probe **4.3** was found to dissolve in water at millimolar concentrations. In aqueous buffer (10 mM MOPS/K^+, pH 7.2), upon excitation at 380 nm **4.3** gave a strong fluorescence turn-on response to Cu(I) with an emission maximum at 506 nm. As expected for a 1:1 metal-ligand binding, the fluorescence emission saturated sharply at 1 molar equivalent of the metal under deoxygenated conditions (Figure 4.3). However, contrary to our expectations, the fluorescence quantum yield (Φ_f = 0.074) and contrast ratio (f_e = 57) of **4.3** upon saturation with Cu(I) did not show an improvement over CTAP-2, which gave a fluorescence quantum yield and contrast ratio of 0.083 and 65, respectively (Table 4.2). The response of **4.3** to acidification was also surprisingly weak, reaching a maximum

fluorescence quantum yield of only 0.070 at 100 mM HCl versus 0.25 at 5 mM HCl for CTAP-2. Altogether these photophysical data pointed towards the possibility of additional fluorescence quenching pathways in probe **4.3** which would be responsible for lowering the intrinsic quantum yield of the probe.

4.2.2. Analyte Selectivity

The fluorescence response of probe **4.3** showed high selectivity for Cu(I) over all other cations tested, including Cu(II), Cd(II), and Hg(II) (Figure 4.4). Furthermore, identical fluorescence enhancements were obtained for Cu(I) regardless of whether supplied as the acetonitrile complex (*) or by in situ reduction of Cu(II) with excess ascorbate (**).

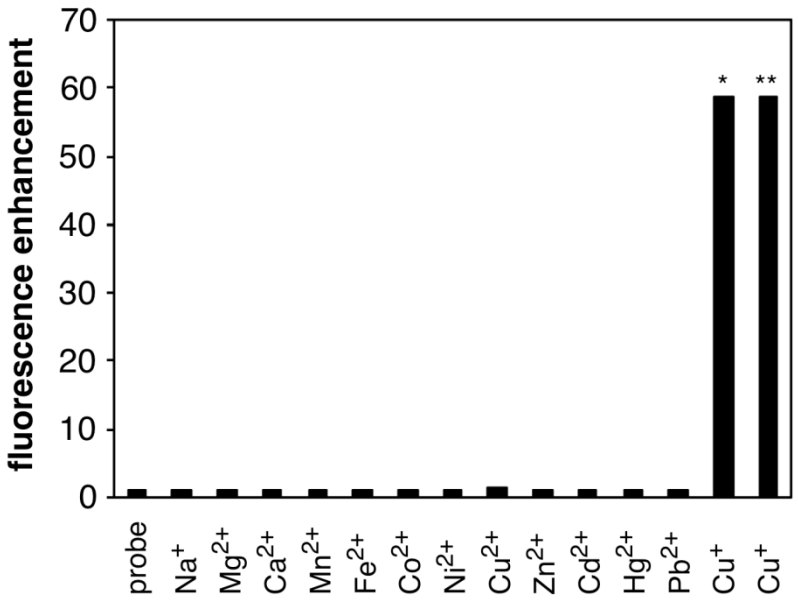

Figure 4.4. *Fluorescence Response of Probe **4.3** to Various Cations.* *$Cu^{I}(CH_3CN)_4PF_6$; **$Cu^{II}SO_4$ reduced in situ with 150 µM ascorbate. Reproduced with permission from Reference (1). © 2012, Royal Society of Chemistry. Data acquired by Dr. M. T. Morgan.

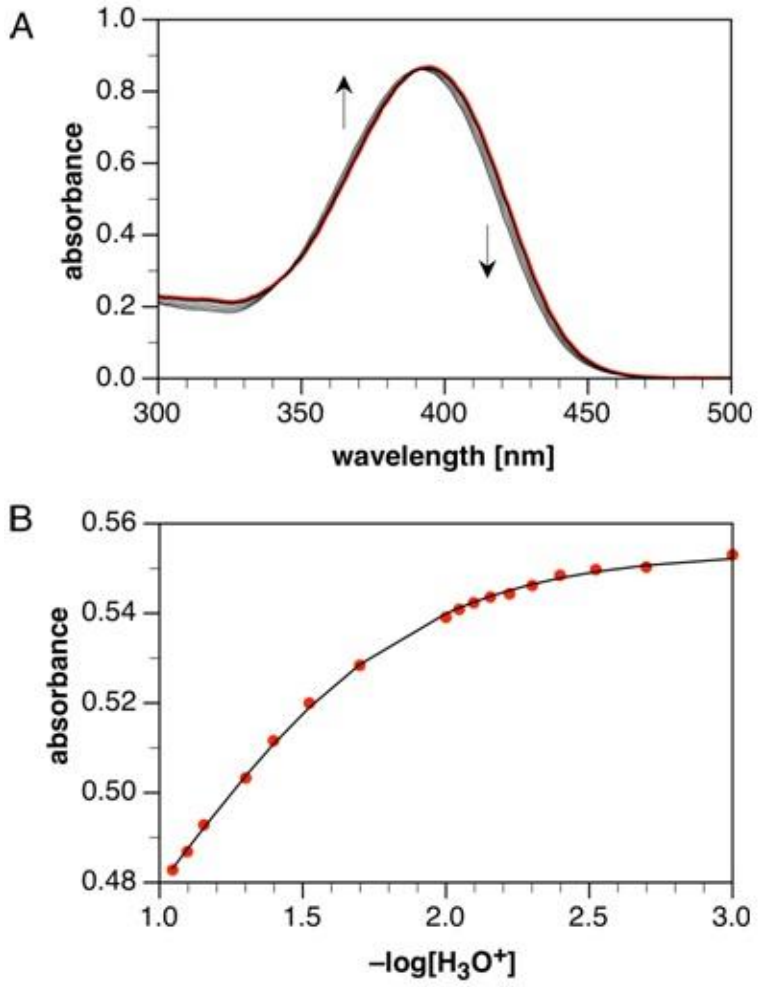

Figure 4.5. *Determination of Acid Dissociation Constant of Probe **4.3***. **A)** UV-vis spectra acquired for c(HCl) ranging between 1 mM to 100 mM. The red trace corresponds to the UV-vis absorption spectrum at $-\log[H_3O]^+ = 3.0$. **B)** Absorbance change (red points) and curve fit (solid trace) for the titration (A) at a wavelength of 419 nm ($pK_a = 1.0 \pm 0.05$). Reproduced with permission from Reference (1). © 2012, Royal Society of Chemistry.

4.2.3. Incomplete Fluorescence Recovery: Clues from Cu(I)-coordination Study

4.2.3.1. Acid Dissociation Constant

Initial experiments to understand the influence of acidification of the probe **4.3** on its spectral properties revealed an estimation of pK_a near 1. Protonation of the arylamine

nitrogen presumably results in spectral shift as observed previously with the absorption maximum of CTAP-2 which shifted from 396 to 388 nm upon protonation with 5 mM HCl (Table 4.2). Similarly, upon acidification probe **4.3** showed a significant shift in absorption maximum from 394 nm in 1 M KCl to 388 nm in 1M HCl. In 100 mM HCl, probe **4.3** gave an absorption maximum of 391 nm, exactly halfway between the values observed in 1 M HCl and neutral solution, suggesting a pK_a near 1 for protonation of the arylamine moiety.

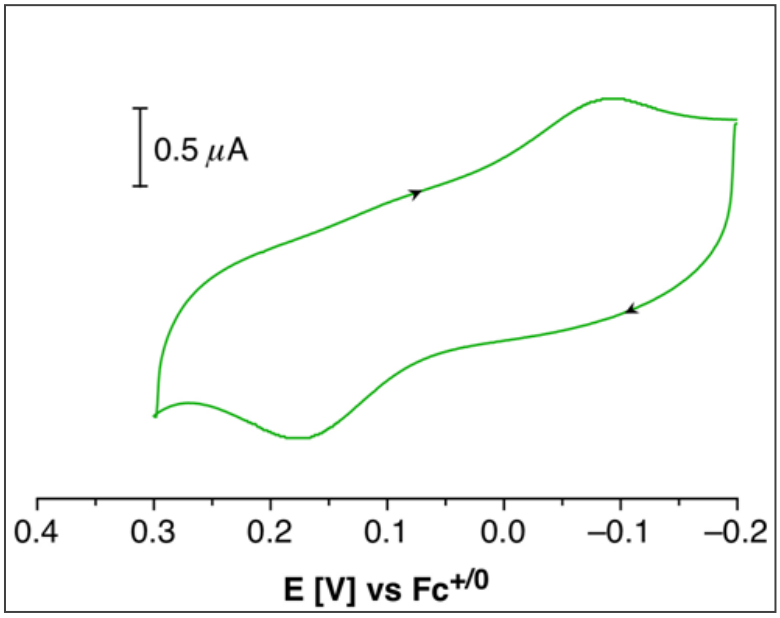

Figure 4.6. *Determination of Formal Potential of **4.3***. Cyclic voltammogram of **4.3** (70 μM) in the presence of 30 μM $[Cu(I)(CH_3CN)_4]PF_6$ at pH 5.0 under deoxygenated condition (10 mM PIPBS, 0.1 M $KClO_4$, glassy carbon working electrode, Pt counter electrode, aqueous Ag/AgCl/1 M KCl reference electrode, scan rate 50 mV/s, direction indicated by black arrows). The voltammogram was referenced against the external $Fc^{+/0}$ potential measured under the same conditions. Reproduced with permission from Reference (1). © 2012, Royal Society of Chemistry.

With this initial estimation of pK_a, spectrophotometric titrations with probe **4.3** were carried out by varying $-\log[H_3O^+]$ from 3 to 2 with the addition of 0.1M HCl. In the

–log[H_3O^+] range from 2 to 1, aqueous HCl-KCl mixtures of varying [H_3O^+] but constant ionic strength were used. The data were analyzed by non-linear least-squares fitting using the Specfit software package (5), yielding an extrapolated pK_a value of 1.0 at 0.1 M ionic background (Figure 4.5).

4.2.3.2. Cu(I) Stability Constant

Unlike CTAP-2, Cu(I) stability constant of probe **4.3** could not be determined from its Cu(II) affinity and redox potential of probe bound Cu(II/I) couple using Nernst eqn. (eqn. 3.7). One of the problems was a slow redox reaction between Cu(II) and the probe itself prohibiting the determination of its Cu(II)-affinity. Because of this additional redox process, with addition of each aliquot of $CuSO_4$, the absorption spectrum of the probe continued to change in a time-dependent fashion without reaching equilibrium. Furthermore, cyclic voltammetry experiments with Cu(I)-saturated **4.3** at pH 5 (50 mV/s scan rate) revealed a one-electron process with a peak separation of 266 mV and a formal potential of 0.480 V vs. SHE (Figure 4.6). Such a large peak separation indicates that large structural changes are associated with the conversion from Cu(I) to Cu(II). Given the large peak separation, the measured potential is not suitable to determine a reliable Cu(I) affinity based on eqn. 3.7.

Instead, the Cu(I)-affinity of **4.3** was determined via direct fluorescence titration using acetonitrile (2, 6). This gave a uniform apparent Cu(I) affinity of log$K_{Cu(I)L}$ = 9.72±0.03 at pH 7.2, irrespective of whether the titration was conducted by varying the Cu(I) concentration and keeping acetonitrile constant (Figure 4.7) or vice versa (**Figure 4.8**). This binding affinity is 50 fold weaker than that of CTAP-2 (log$K_{Cu(I)L}$ = 11.4) (7). This weak copper binding to the probe **4.3** is consistent with the unusually low pK_a of the arylamine nitrogen of the probe (Section 4.2.3.1), which is nearly 1000-fold lower than that of CTAP-2 (pK_a = 3.97) (7). Such a poorly basic nitrogen in the Cu(I)-binding moiety is expected to coordinate Cu(I) very feebly. Therefore, the low acid dissociation

constant together with a small value of Cu(I) binding affinity confirm an unusually low donor ability of the arylamine nitrogen compromising the fluorescence enhancement of the probe **4.3**.

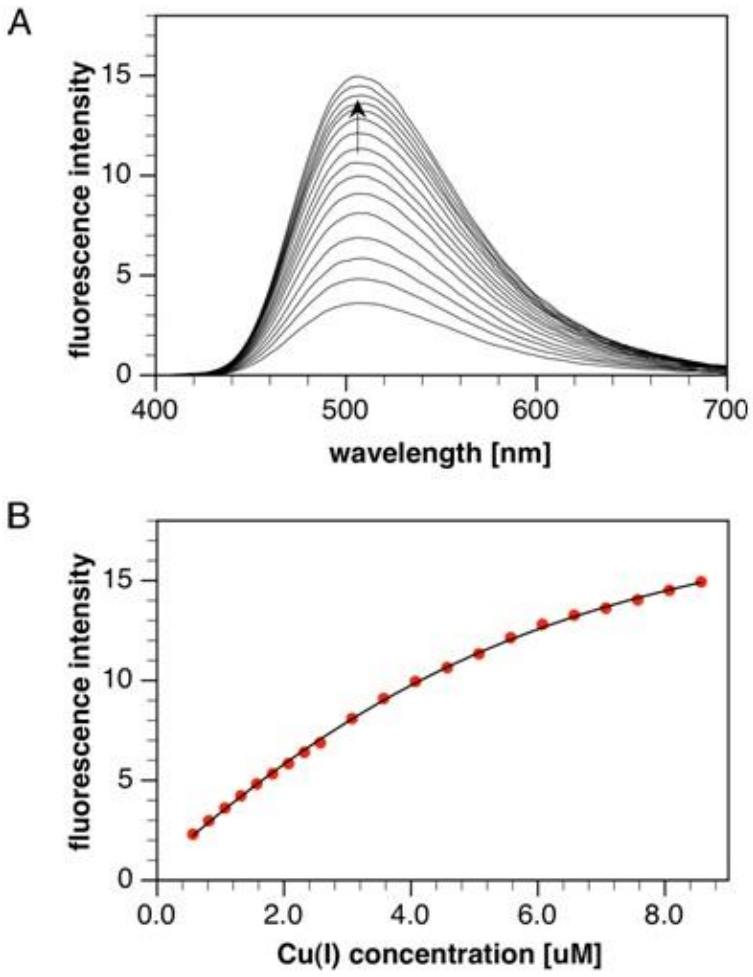

Figure 4.7. *Determination of Cu(I) Stability Constant of **4.3**: Titration with Cu(I).* Fluorescence titration of pyrazoline **4.3** (5 μM) with $CuSO_4$ in the presence of 100 μM sodium ascorbate and constant CH_3CN concentration of 0.70 M under deoxygenated condition in PIPBS buffer (50 mM, pH 5.0, 60 mM $KClO_4$, 22 °C). **A)** Fluroescence spectra acquired for c(Cu(II)) ranging between 0.56 to 8.56 μM. **B)** Fluorescence intensity change (red points) and curve fit (solid trace) for the titration (A) at a wavelength of 508 nm ($\log K^{Cu(I)}$ = 9.74±0.03). Reproduced with permission from Reference (1). © 2012, Royal Society of Chemistry.

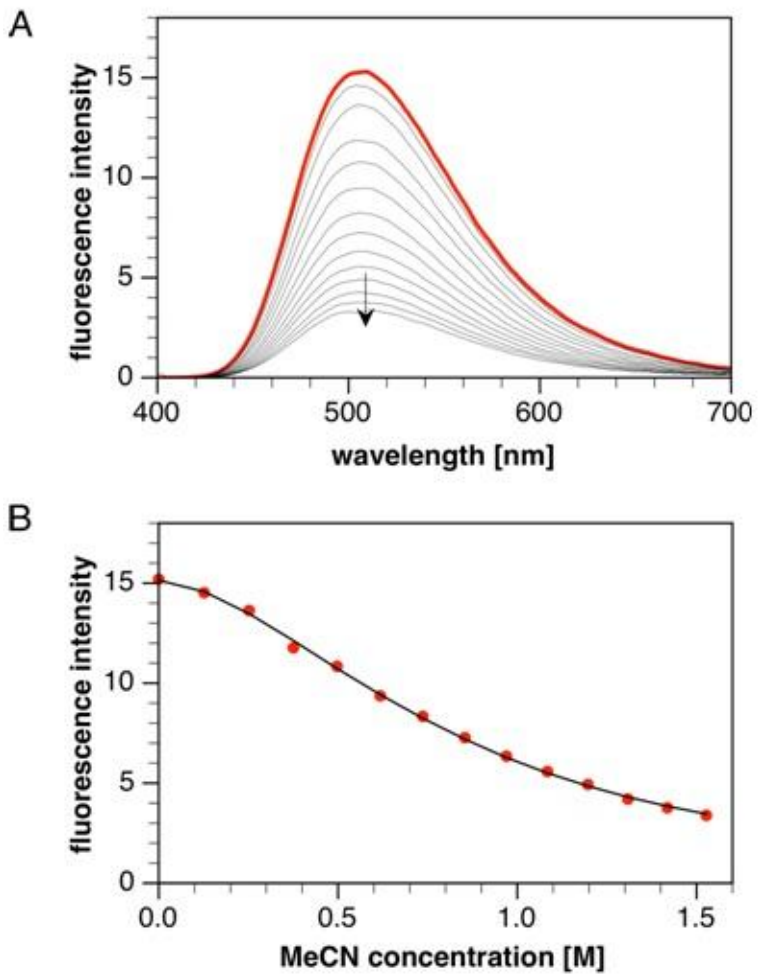

Figure 4.8. *Determination of Cu(I) Stability Constant of **4.3**: Titration with Acetonitrile.* Fluorescence titration of pyrazoline **4.3** (5μM) with CH_3CN in the presence of 3.6 μM $CuSO_4$ and 50 μM sodium ascorbate under deoxygenated condition in PIPBS buffer (50 mM, pH 5.0, 60 mM $KClO_4$, 22 °C). **A)** Fluorescence spectra acquired for c(CH_3CN) ranging between 0 to 1.60 M. The red trace corresponds to the emission spectrum prior to addition of CH_3CN. **B)** Fluorescence intensity change (red points) and curve fit (solid trace) for the titration (A) at a wavelength of 508 nm ($\log K^{Cu(I)} = 9.71 \pm 0.02$).Reproduced with permission from Reference (1). © 2012, Royal Society of Chemistry.

4.2.4. Incomplete Fluorescence Recovery: Clues from Photophysical Study

Photophysical studies done by Dr. M. T. Morgan uncovered possible factors that would be responsible for the incomplete fluorescence recovery of the probe **4.3** and CTAP-2. The detail of the experimental data can be found elsewhere (1).

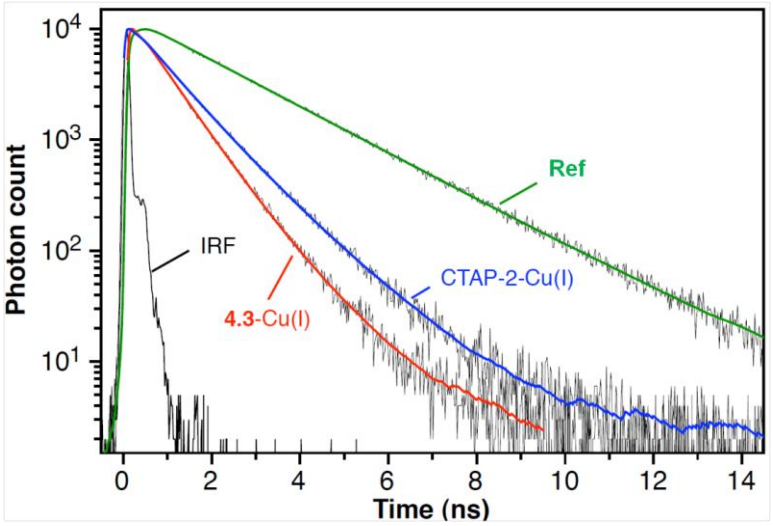

Figure 4.9. *Fluorescence Decay Profile of CTAP-2 and **4.3** Saturated with Cu(I) in Aqueous Buffer at pH 7.2 (10 mM MOPS/K^+, 22 °C).* Each sample was excited at 372 nm (80 ps fwhm), and the emission signal was detected at 506 nm by single photon counting. Non-linear least squares fitted traces are shown as solid lines (see Table 4.3 for the data; IRF = instrument response function).Reproduced with permission from Reference (1). © 2012, Royal Society of Chemistry. Data acquired by Dr. M. T. Morgan.

Table 4.3. *Time-resolved Fluorescence Decay Data in Aqueous Solution at 22 °C.*

Compound[e]	Medium	τ_F (ns)
4.3	pH 7.2[a]	0.72 (0.93)[d]
		1.44 (0.07)[d]
CTAP-2	pH 7.2[a]	0.82 (0.67)[d]
		1.36 (0.33)[d]
Ref	H_2O[b,c]	2.07

[a] Deoxygenated conditions. [b] Air saturated conditions. [c] Deoxygenation had no effect on the observed lifetime within experimental error. [d] Normalized pre-exponential factors from fitted biexponential decay function. [e] Data acquired by Dr. M. T. Morgan. Reproduced with permission from Reference (1). © 2012, Royal Society of Chemistry.

Time-resolved fluorescence spectroscopy data (Figure 4.9) showed that both CTAP-2-Cu(I) and **4.3**-Cu(I) gave multiexponential fluorescence decay profiles that were consistent with the presence of multiple coordination species. In contrast, the reference compound which was known to be composed of a single emissive species gave clean monoexponential decay. Deconvolution of the decay profiles of CTAP-2 and **4.3** with a biexponential model produced the lifetime components tabulated in Table 4.3. In contrast to CTAP-2 which showed two lifetime components of 0.82 ns (67%) and 1.36 ns (33%), the probe **4.3** exhibited a short-lived (0.72 ns) dominant component (93%) and a minor one (7%) with a longer lifetime (1.44 ns). The predominance of a single component in the decay profile of **4.3**-Cu(I) suggested that the modified ligand design of **4.3** effectively inhibited the formation of multiple coordination species which was the original aim of this work in order to improve the performance of CTAP-2. However, the rather short fluorescence lifetime (0.72 ns) of the Cu(I)-probe coupled with a low quantum yield (7.4%) implies a weak or absent interaction between the arylamine nitrogen and the Cu(I)-center as also inferred from the coordination properties of the probe (Section 4.2.3). Furthermore, concluding from the solvent isotope effects on the fluorescence quantum yield and lifetime of the Cu(I)-probes and the responses of the free probes to acidification (data not shown), it can be derived that two distinct excited state proton transfer (ESPT) pathways are operative under neutral and acidic conditions that reduce the intrinsic fluorophore quantum yield of the probe **4.3** and also CTAP-2.

4.3. Conclusion

In an attempt to design a Cu(I)-selective fluorescent probe with quantum yield and contrast ratio improved over CTAP-2 (Chapter 3), aqueous solubilization strategy of CTAP-2 was combined with a new ligand design where the PET donor aryl ring was integration into the ligand backbone. Based on previous results obtained in methanolic solution (4), we expected that the new ligand design would improve the fluorescence

performance of the new probe by eliminating the propensity of the ternary complex formation between the copper-bound probe and the solvent molecule which was proven to be responsible for incomplete fluorescence recovery of the triarylpyrazoline probes.

The new probe **4.3** gave a strong fluorescence turn-on response with high selectivity for Cu(I), however, the contrast ratio and quantum yield did not improve over CTAP-2. Further studies on the thermodynamic and photophysical properties of the probe uncovered two separate effects that limit the fluorescence contrast of the Cu(I)-probe as well as the intrinsic fluorophore quantum yield. One of the effects is the inadequate coordination of Cu(I) to the weakly basic arylamine nitrogen as concluded from the coordination properties and the fluorescence decay profile of the probes. The other effect is the fluorescence quenching via two distinct excited state proton transfer pathways operating under neutral and acidic conditions as deduced from the solvent isotope effects and responses of the probe to acidification.

4.4. Experimental Methods

4.4.1. Acid Dissociation Constant

To determine the pK_a of probe **4.3**, spectrophotometric titrations (10 cm path length) were carried out at a 2.8 μM ligand concentration and 0.1 M KCl as ionic background by varying $-\log[H_3O^+]$ from 3 to 2 with the addition of 0.1M HCl. In the $-\log[H_3O^+]$ range from 2 to 1, the amount of KCl present was adjusted downward such that the ionic strength of the solution remained constant at 0.1 M. The data were analyzed by nonlinear least-squares fitting using the Specfit software package (5).

4.4.2. Cu(I) Stability Constant

For the determination of the Cu(I) stability constant of probe **4.3** we used acetonitrile as competing ligand. Titrations were carried out at 5 μM concentration of **4.3** in deoxygenated PIPBS buffer (50 mM, 60 pH 5.0, 60 mM $KClO_4$ ionic background) by

either (a) adding aliquots of 0.25 μM $CuSO_4$ at constant acetonitrile concentration (0.7 M) and 100 μM sodium ascorbate (for in situ reduction to Cu(I)) or (b) varying the acetonitrile concentration from 0 to 1.6 M while keeping the Cu(I) concentration constant at 3.6 μM 65 (formed again by in situ by reduction of copper(II) sulfate with 50 μM sodium ascorbate). The data were analyzed by non-linear least squares fitting with Specfit using published Cu(I)/CH_3CN stability constants ($\log\beta_1$ = 2.63, $\log\beta_2$ = 4.02, and $\log\beta_3$ = 4.29) (8). In method (b), the data were corrected for volume changes with each acetonitrile addition.

4.4.3. Electrochemistry

Cyclic voltammograms were acquired in deoxygenated 10 mM PIPBS buffer, pH 5, containing 0.1M $KClO_4$ as the electrolyte using a CH-Instruments potentiostat. Compound **4.3** was analyzed at a concentration of 70 μM in a single compartment cell with a glassy carbon working electrode, a Pt counter electrode, and an aqueous Ag/AgCl reference electrode (1 M KCl). The potentials were referenced to ferrocenium (0.40 vs. SHE) (9) or ferroin (1.112 vs. SHE) (10) as external standards. Measurements were performed with a scan rate of 50 mV s^{-1}.

4.5. References

1. Morgan MT, Bagchi P, & Fahrni CJ (2013) High-contrast fluorescence sensing of aqueous Cu(I) with triarylpyrazoline probes: dissecting the roles of ligand donor strength and excited state proton transfer. *Dalton Transactions* 42(9):3240-3248.

2. Yang LC, McRae R, Henary MM, Patel R, Lai B, Vogt S, & Fahrni CJ (2005) Imaging of the intracellular topography of copper with a fluorescent sensor and by synchrotron x-ray fluorescence microscopy. *Proceedings of the National Academy of Sciences of the United States of America* 102(32):11179-11184.

3. Chaudhry AF, Verma M, Morgan MT, Henary MM, Siegel N, Hales JM, Perry JW, & Fahrni CJ (2010) Kinetically controlled photoinduced electron transfer switching in Cu(I)-responsive fluorescent probes. *Journal of the American Chemical Society* 132(2):737-747.

4. Chaudhry AF, Mandal S, Hardcastle KI, & Fahrni CJ (2011) High-contrast Cu(I)-selective fluorescent probes based on synergistic electronic and conformational switching. *Chemical Science* 2(6):1016-1024.

5. Binstead RA & Zuberbühler AD (2001) SPECFIT Global Analysis System (Spectrum Software Associates, Marlborough MA 01752), 3.0.27.

6. Balakrishnan KP, Kaden TA, Siegfried L, & Zuberbuhler AD (1984) Stabilities and redox properties of Cu(I) and Cu(II) complexes with macrocyclic ligands containing the N_2S_2 donor set. *Helvetica Chimica Acta* 67(4):1060-1069.

7. Morgan MT, Bagchi P, & Fahrni CJ (2011) Designed to dissolve: Suppression of colloidal aggregation of Cu(I)-selective fluorescent probes in aqueous buffer and in-gel detection of a metallochaperone. *Journal of the American Chemical Society* 133(40):15906-15909.

8. Kamau P & Jordan RB (2001) Complex formation constants for the aqueous copper(I)-acetonitrile system by a simple general method. *Inorganic Chemistry* 40(16):3879-3883.

9. Koepp HM, Wendt H, & Strehlow H (1960) *Zeitschrift Fur Elektrochemie* 64(4):483-491.

10. Ambundo EA, Deydier MV, Grall AJ, Aguera-Vega N, Dressel LT, Cooper TH, Heeg MJ, Ochrymowycz LA, & Rorabacher DB (1999) Influence of coordination geometry upon copper(II/I) redox potentials. Physical parameters for twelve copper tripodal ligand complexes. *Inorganic Chemistry* 38(19):4233-4242.

CHAPTER 5

PROTEOMIC IDENTIFICATION OF COPPER PROTEINS BY SELECTIVE LABELING OF COPPER(I) BINDING CYSTEINES

Proteomic profiling is gaining increased attention in cancer research as this method offers not only better understanding of the disease states, but also provides valuable insights in detecting putative biomarkers and in improving treatments (1-4). In contrast, despite copper imbalance being related to various diseases including Menkes disease, Wilson's disease, Parkinson's disease, and Alzheimer's disease (5, 6), the changes in copper proteome in these disease states are still poorly understood. In metalloproteins, cysteine is a ubiquitous ligand for Cu(I) coordination (7). Therefore, to develop methods for systematic proteomic profiling suitable for the copper proteome, several proteomics-based methods were developed in this chapter to identify copper(I) binding proteins in which the amino acid cysteine serves as the metal binding site. Moreover, this work will also lay a foundation for the identification of new copper proteins that are yet to be discovered.

5.1. Background

Copper is an essential trace element and required for various biological processes such as cellular respiration, connective tissue cross-linking, pigment formation, and antioxidant defense (8). Several copper binding proteins are an integral part of the copper homeostatic machinery and work in conjunction to regulate copper uptake, distribution, and excretion (9). However, identification of these copper binding proteins is often challenging due to lack of specification associated with copper-induced genetic screening, limitation of bioinformatics approach, and a dearth of reliable biochemical data.

5.1.1. Identification of Copper-binding Proteins

This subsection offers a brief overview of previously developed methods utilized to discover the proteins in mammalian copper proteome that regulate copper transport inside the cell.

5.1.1.1. Genetics-based Methods

Copper-dependent genetic screening, which is done by either copper overload or starvation, is not specific to genes involved in copper metabolism. Such screening will also identify genes involved in different cellular processes like copper-induced oxidative stress, which are under the influence of change in cellular copper status, even though they are not directly connected to copper metabolism. For example, a study for gene expression profiling in liver cells of copper-treated mice revealed significant upregulation of a set of 22 genes involved in immunity, iron, and cholesterol metabolism (10).

The yeast complementation assay provides a different approach in the identification of genes encoding proteins associated with copper metabolism. The human homolog of Cox17 (11), hAtox1 (12), hCTR1 (13), and CCS (14) are examples of proteins identified or functionally characterized by this method. The assay analyzes the rescue of the phenotypes of a yeast deletion mutant in the presence of a functionally conserved gene cloned from higher eukaryotes. Some of the properties that make yeast particularly suitable for biological studies include rapid growth, the ease of mutant isolation, and a well-defined genetic system. These properties allow the rapid identification of the phenotypic consequences of a mutation in any cloned gene, a technique generally unavailable in higher eukaryotes. However, successful recovery of the activities in yeast can be prevented even if the cloned gene has a conserved function. For example, the expressed protein may need to be part of a multi-protein complex to function properly but the key components of such a complex might not be present in

yeast, or the endogenous structure of the expressed protein may differ from the inherent one to render the resultant protein functionally inactive.

Furthermore, some copper transport proteins were discovered from their respective genes which were isolated by studying the disease phenotypes caused by the mutations of these genes. This is a rigorous genetic approach that led to the identification of genes encoding ATP7A (15-17), ATP7B (18-20), Sco1, and Sco2 proteins. However, some genes are indispensable to embryonic function, so that their deleterious mutations result in embryonic lethality precluding further studies. For example, the copper importer CTR1 is essential for embryonic development in mammals, as *Ctr1*$^{-/-}$ mice die *in utero* mid-way through gestation (21, 22). A similar effect was observed with mice lacking copper chaperone Cox17 (23). In other cases, abolition of a gene function may not have any prominent effect on the phenotype because of genetic redundancy where other nonallelic genes supply the same function (24), as a result, such genes are difficult to identify from disease states.

5.1.1.2. Bioinformatics- based Methods

The striking similarities between yeast and mammalian copper homeostasis have permitted the characterization of mammalian orthologues using *S. cerevisiae* gene sequences (12, 14), hence underscoring the importance of this genetically tractable organism in order to understand copper metabolism in mammals (25). Advances in genome sequencing led to the discovery of copper-binding proteins based on sequence homology. For example, the human CTR1 sequence has been used for homology screening, giving rise to a putative copper importer hCTR2 (13). However, identification of a gene encoding a putative copper-binding protein should be confirmed by biochemical studies proving the dependence of the function of the proteins of interest on the presence of the metal.

In recent years, development of several protein data repositories including PDB, UniProt, Pfam, and InterPro has opened another avenue for identifying novel copper proteins based on their amino acid sequences and three dimensional structures. For example, human COMMD proteins, a family of proteins structurally and functionally related to MURR1, were identified by searching human protein databases for sequences homologous to MURR1 (26). The function of MURR1 is to regulate the transcription factor NF-kappa-B and presumably to control copper metabolism (27).

Protein-based bioinformatics can also be utilized to identify novel copper proteins that are yet to be characterized, based on already known copper-binding motifs. In this approach, metalloproteins are identified through the searches of the whole ensemble of the sequences of proteins in the PDB using local sequence similarity to either known copper binding motif (28) or known copper-binding domains (29). Besides finding putative Cu-binding proteins, these studies also provide valuable information about the correlations between the copper coordination sphere and protein function. However, the bioinformatic approaches rely on the data stored in the protein databases which is largely gathered by experimental characterization of proteins, thus limiting the searchable number of potential candidates. Moreover, the predicted copper proteome suffers from other limitations questioning the reliability of the method. First, the searches based on known copper binding motifs often retrieve a significant number of metalloproteins which are known to bind metals other than copper to carry out their physiological functions (28). Second, the analysis done using copper-binding domains as an input suffer from the opposite problem, i.e., underestimation of the copper proteome, because there are a number of domains that are not yet recognized as copper-binding sites because of the lack of experimental data (29).

Both genetics and bioinformatics-based methods are high-throughput and hence can provide valuable support to experimental methods which often can be quite challenging. However, such screening results can be anomalous in assigning a metal to

the functionality of a protein, even though the protein does not bind the metal ion. For instance, Dancis et al. (30, 31) identified the copper importer CTRl by a genetic selection for mutants defective in iron uptake in yeast cells. Surprisingly, this protein had no affinity for iron, but rather transported copper. Accordingly, development of experimental analytical methods is required to verify the results of bioinformatics studies. Furthermore, copper sensing in mammals primarily occurs post-translationally, by adjusting intracellular protein trafficking or degradation (8, 32, 33). For example, copper-responsive degradation is presumably a strategy to regulate intracellular copper concentration that applies to the copper chaperone CCS (34, 35) and to the copper importer CTR1 (36, 37). Another mechanism adopted by copper-homeostasis proteins is metal dependent trafficking (38). This phenomenon was first observed for copper-transporting P-type ATPase ATP7A, which redistributes from *trans*-Golgi membranes to the plasma membrane when exposed to high cellular copper concentrations (39). Under basal conditions ATP7A supplies metal to copper proteins in the biosynthetic pathways inside *trans*-Golgi network, whereas under high-copper conditions it facilitates efflux of the metal. An analogous protein (ATP7B) is expressed primarily in the liver, where it relocates to apical hepatocyte membranes under high-copper conditions to aid biliary excretion of the metal (40). These post-translational modifications cannot be captured by genetic or transcriptional analysis as demonstrated by a study where CCS protein, but not its mRNA, was shown to be consistently elevated in copper deficiency (41). Therefore, development of proteomics-based methods not only complements the genetics and bioinformatics studies, but this area of research is imperative to fully comprehend the copper homeostasis at a molecular level.

5.1.2. Copper-proteomics: Detection of Proteins that Bind Copper

Copper-proteomics is a collection of bioanalytical approaches for the identification and quantification of copper-binding proteins as well as protein-bound

metal ions. The general workflow, which is usually known as top-down proteomics, follows two key steps: a) fractionation of samples, by sequential chromatographic or 2D gel separations, and b) metal and protein identification in individual fractions by different techniques. Detection of protein-bound copper ions was covered in chapter 2 and this subsection will, therefore, focus on the current methodological approaches undertaken in protein fractionation in connection with copper proteome and overall limitations of top-down technologies.

The major challenge in copper-proteomics is the preservation of the native metal-ligand interactions during sample preparation. In that regard, the first and foremost consideration is to avoid denaturation of the protein, as unfolding of protein usually leads to loss of the metal ions (42-44). Second, exposure to oxidizing environment should be limited because both copper ions and thiols of cysteine ligands are susceptible towards oxidation resulting in disruption of the metal binding. Third, copper-ligand interactions in proteins are pH-sensitive because metal ions and protons, both being positively charged, compete for the same binding sites (45). Accordingly, to identify copper binding proteins that are yet to be characterized or to verify metal binding capacity of a putative protein outside cellular environment as often encountered in working with cell lysates, the experimental setup should mimic the native physiological conditions as close as possible.

5.1.2.1. Two-dimensional (2D) Gel Electrophoresis

In two-dimensional (2D) gel electrophoresis, proteins are separated in the first dimension by isoelectric focusing (IEF) which takes advantage of varied net charges of the proteins determined by their isoelectric points (pI). In the second dimension, the mobility of a protein is determined solely by their molecular mass in denaturing SDS-PAGE, or mass and effective charge in non-denaturing native-PAGE. The protein spots are then analyzed for their metal content by a suitable technique, such as LA-ICP-MS (Laser Ablation Inductively Coupled Plasma Mass Spectrometry) (46), autoradiography

(47), or X-ray fluorescence (48). Subsequently, the protein spots are excised and in-gel digestion is carried out with a site-specific cleavage enzyme, normally trypsin, into peptide fragments. The resulting products are then identified by peptide mass fingerprinting using MALDI-MS (Matrix-Assisted Laser-Desorption Ionization-Mass Spectrometry) and peptide sequencing with tandem mass spectrometry. As mentioned in the preceding paragraph, to identify copper-proteins where the metal ion is non-covalently bound to the ligand, 2D gel electrophoresis has to be performed under non-denaturing condition. The problem with unfolding of metalloproteins during gel electrophoresis is not only limited to loss of the endogenous metal ion and thereby missing the putative metal-binding protein in the analysis (42-44), but the liberated metal coordination site of the protein can bind to other metals adventitiously which are not physiologically relevant. For example, a study was conducted with proteins from yeast mitochondria where metal ions bound to proteins were probed by Laser Ablation Inductively Coupled Plasma Mass Spectrometry (LA-ICP-MS). In this work, the proteins were first separated by blue-native gel electrophoresis (BN-PAGE) followed by SDS-PAGE and thereby revealing nonspecific accumulation of metal ions by LA-ICPMS (49). Consequently, this precludes the use of chaotropic agents, such as urea and thiourea, and detergents including CHAPS and SDS in 2D gel electrophoresis, all of which increases the solubility of the proteins during isoelectric focusing as the proteins tend to precipitate at isoelectric points. As a result, non-denaturing gels preserve the native metal-protein interactions but at the expense of resolution of the separated protein spots (48).

Isoelectric focusing is sometimes combined with blue-native gel electrophoresis (BN-PAGE) to separate proteins in the second dimension (47, 50). This technique involves addition of the anionic dye Coomassie blue G-250 to the protein sample prior to electrophoretic separation. Binding a large number of dye molecules imposes an overall negative charge even for basic proteins such that they migrate to the anode during electrophoresis according to their size (51). Although there is evidence in the literature

that shows loss of protein-bound metal during the post-separation staining of a gel by Coomassie blue (44), Jimenez et al. successfully used blue-native PAGE to identify Cu and Zn-binding proteins in the plankton extracts after LA–ICP–MS measurements (43). However, blue-native PAGE also suffers from poor resolution of the protein bands.

The major drawback of 2D gel electrophoresis is the limited dynamic range associated with the detection of copper and protein as individual 2D gel spot may only contain very small amounts of protein especially for the ones with low abundance. In order to improve the sensitivity of the method Pioselli et al. (52) explored the compatibility of a pre-fractionation technique, microsolution isoelectric focusing, with downstream proteome analysis. Pre-fractionation is a typical strategy for enriching low abundance proteins in biological samples. Following the same principle of isoelectric focusing, solution IEF (sIEF) traps the proteins at their pI values in liquid phase. In this study, metal retention of proteins including Cu/Zn-superoxide dismutase was evaluated under denaturing and non-denaturing conditions. While non-denaturing sIEF preserved the endogenous metal-protein interaction, precipitation of proteins under this condition resulted in low recovery, thus decreasing the overall utility of the method.

In summary, 2D gel electrophoresis is capable of resolving a large number of proteins in a single experiment However, because of time-consuming processes in gel electrophoresis and subsequent in-gel enzymatic digestion, 2D gel electrophoresis coupled with MS is a fairly low-throughput detection method. It also requires relatively large amount of biological samples in order to increase the detection sensitivity, especially for low abundance proteins. Furthermore, this technique is often unsuitable for proteins that are highly acidic or basic and large membrane proteins as they are more likely to precipitate during isoelectric focussing. This problem poses difficulties to detect membrane associated copper-proteins as exemplified by the ATPases, ATP7A and ATP7B.

5.1.2.2. Liquid Chromatography

The shortcomings of 2D gel electrophoresis have paved the path for developing gel-free technologies for proteomics analysis. In principle, biological samples can be separated using multidimensional liquid chromatography followed by identification and quantification of proteins by MALDI-MS and ESI-MS (Electrospray Ionization Mass Spectrometry), and metals by ICP-MS (Inductively Coupled Plasma Mass Spectrometry) and AAS (atomic absorption spectrometry). In the literature, several examples can be found where fractionation of biological samples were performed to identify copper-binding proteins using liquid chromatographic techniques including reversed-phase high-performance liquid chromatography (RP-HPLC) (53), ion-exchange (IE) chromatography (54), size-exclusion chromatography (SEC) (54, 55), capillary liquid chromatography (56), and capillary electrophoresis (57). RP-HPLC seems to be superior to SE and IE chromatography for the separation of metal–protein complexes because the stationary phase of the column is devoid of free ligands that can potentially bind metal ions. However, use of HPLC is largely limited to small proteins, such as metallothioneins, leaving a still unexplored potential for the separation of metalloproteins with high molecular weight. Recently, multi-step liquid chromatography has been used to fractionate microbial metalloproteomes (58). Although this work was not directed towards the copper proteome, the large scale sample preparation in this detailed study brought out many advantages and disadvantages associated with liquid chromatographic separations followed by metal speciation.

The main advantage of this approach is that the careful selection of appropriate separation conditions enables the isolation of metalloproteins in near-native environment. The metal-containing fraction can be readily collected for further proteomics analysis to identify the metal-containing protein. Moreover, chromatographic separation can be performed in shorter time compared to gel electrophoresis and this can be combined efficiently with metal-detection devices such as ICP-MS or protein-detection instrument

like ESI-MS offering the most promising tool for the identification of metal–protein complexes at the sub-nanomolar levels. A major disadvantage of the liquid chromatographic approach is the very low resolution; often one separated fraction contains multiple proteins with varied metal contents. Further resolution up to the level of one protein per fraction can be achieved by multi-step fractionations as demonstrated by Cvetkovic et al. (58), but the yield of the protein is seriously compromised during the process. Additionally, loss of endogenous metal-protein interaction and misincorporation of non-native metal ions in proteins are a few potential problems with liquid chromatographic separations.

5.1.2.3. Immobilized Metal-affinity Chromatography

Immobilized-metal affinity chromatography (IMAC) is another fractionation technique in metalloproteomics which is based on the differential binding affinities of the surface exposed amino acids towards immobilized metal ion (59). In application to copper-proteomics, usually unfolded metal depleted samples are loaded on an IMAC column saturated with $CuSO_4$, and proteins with affinity to Cu^{2+} ion are recovered and subsequently analyzed by 2D gels coupled with MALDI-MS (60, 61) or surface enhanced laser desorption ionization (SELDI) MS (62).

IMAC detects proteins with copper-binding affinity in the sample but does not provide information on the presence of such copper–protein complexes in vivo. Moreover, the reliability of IMAC in detection of copper-proteins is dubious primarily due to the use of Cu(II) as the immobilized metal ion. As presented in chapter 1, majority of the proteins involved in copper-trafficking bind to Cu(I) by sulfur ligands as found in cysteine and methionine residues, whereas the enzymes where copper being used as a redox cofactor, the metal is bound to histidine residues. Following the hard soft acid base principle, soft ligands like sulfur preferentially bind to Cu^{+} ions and hard acids like Cu^{2+} ion is primarily bound to bases like nitrogen of an imidazole group. Therefore, it is not

surprising that Cu-IMAC separation often results in enrichment of proteins containing histidine groups, because the amino acid residues that bind to the Cu-IMAC column follow the order of histidine > methionine > cysteine. Accordingly, IMAC is insufficient to detect a major group of copper-binding proteins containing CXXC motifs. Moreover, non-native metal-protein interaction and non-specific adsorption of proteins in the column matrix resulting in false-positive is another inevitable problem when isolating copper-proteins by IMAC.

In summary, the necessity for the development of proteomics-based methods in characterizing copper-proteome is two-fold: one is to identify novel putative copper-binding proteins for complete understanding of copper trafficking pathways, and the other is to compare protein expressions between normal physiology and disease states resulting from impaired copper metabolism in order to develop biomarkers and targeted therapy for various diseases. Evaluation of the current methodologies in this field reveals one common problem which is the loss of the copper ion during sample preparation and protein separation. Although native gel electrophoresis has been shown to maintain the integrity of the endogenous copper-protein complex, it is also noteworthy that there is evidence in the literature which shows the influence of other factors that can cause release of metal ions from proteins even under non-denaturing conditions. These factors include components of protein extraction, e.g., buffer composition, presence of protease inhibitor and reducing agents (43); choice of trailing ions, for example, tricine vs. glycine, and the current applied in the electrophoretic methods (63); and choice of mobile phase buffers in chromatographic separation (64). Another important problem is the contamination of non-native metal ions in protein samples during protein separation or metal analysis. This is often due to the loss of the endogenous copper ion from the protein followed by adventitious metal binding to the liberated coordination sites. Therefore, an ideal protocol for the detection of copper-binding proteins should involve a "metal-free" method where copper coordination to a protein will be translated to a

measurable response without the metal being actually present during the assay. The aim of this work was to develop such proteomics methods for copper-binding proteins rendering them suitable for identification of the copper-proteome.

5.2. Results and Discussion

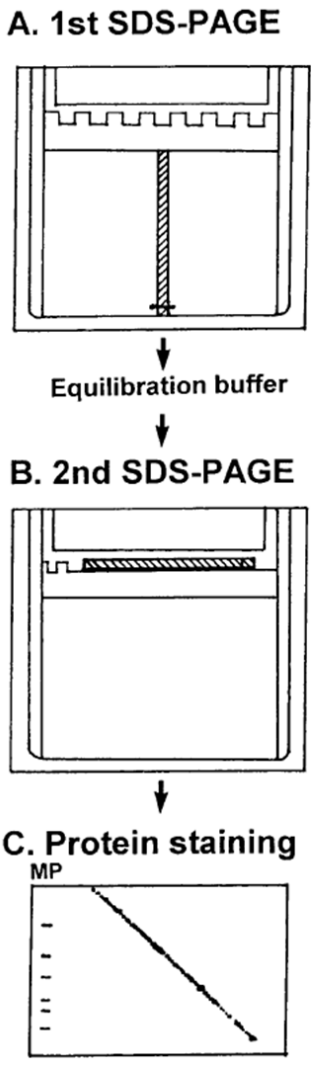

Scheme 5.1. *Key Steps of the Two-dimensional Diagonal Polyacrylamide Gel Electrophoresis* (shown for SDS–PAGE; see text for details). Reproduced with permission from (65), copyright © 1997, Elsevier.

5.2.1. Two-dimensional Diagonal Native PAGE: Mobility Shift assay

Metalloproteins can exhibit different electrophoretic mobilities in the presence and absence of metal ion cofactors when the binding of the metal ions induces changes in conformations or effective charges of the proteins. This property was exploited to develop mobility shift assay, which is based on two-dimensional (2D) polyacrylamide gel electrophoresis (PAGE), to identify metalloproteins from cellular extracts. The method was originally developed to detect calcium-binding proteins (65, 66) on SDS-PAGE; the major steps of this assay are shown in Scheme 5.1.

The general protocol of the mobility shift assay is as follows: **(A)** proteins isolated from cellular extract are separated by gel electrophoresis. Following the electrophoresis, the lane of the gel containing the protein sample is cut out longitudinally. The gel strip is then soaked in an appropriate equilibration buffer whose role is to alter the mobilities of the proteins in the second dimension. For metalloproteins, this can be achieved either by the addition of a ligand in the equilibration buffer in order to remove the metal ion under study from the holo-protein, or addition of the specific metal ion to the apo-protein before the second dimension electrophoresis. **(B)** Afterwards, the gel strip is placed horizontally on top of another gel and a second electrophoresis is carried out. **(C)** Finally, the gel is stained to visualize the proteins.

Scheme 5.2 shows the diagram of a representative 2D diagonal gel. Proteins, whose electrophoretic mobilities are the same in both dimensions, align along a diagonal, and hence the name “diagonal” gel is given by the author of this work to differentiate this method from the traditional 2D gel electrophoresis. Proteins containing a specific metal ion under study might migrate differently compared to their apo-forms owing to metal-induced changes in their conformations or effective charges. These proteins of interest constitute the off-diagonal spots. Moreover, an off-diagonal spot left to the diagonal (shown in red) means that the protein migrated less in the second dimension, whereas an

off-diagonal spot right to the diagonal (shown in black) means that the protein migrated more in the second dimension in comparison to the first dimension.

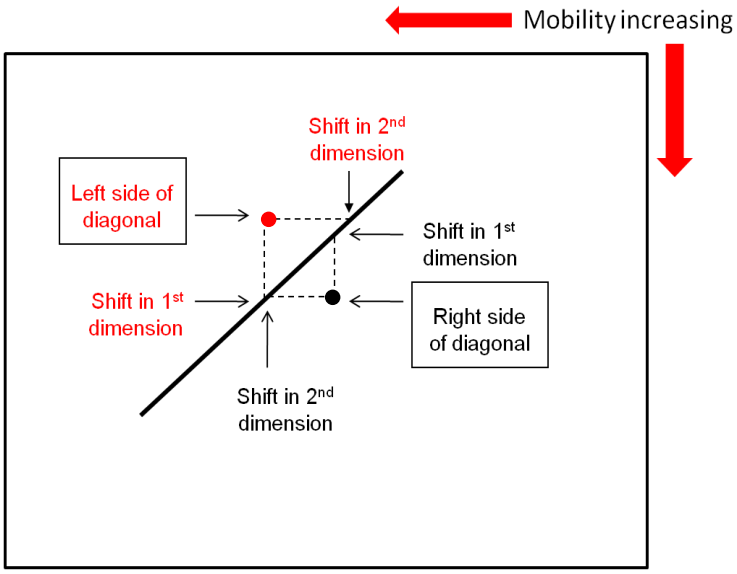

Scheme 5.2. *Analysis of a Representative 2D Diagonal Polyacrylamide Gel.*

In order to screen for periplasmic proteins with readily exchangeable copper sites of the cyanobacterium *Synechocystis* PCC 6803, Waldron et al. showed that the mobility shift assay can also be adapted to proteins separated under non-denaturing conditions (67). In 2D diagonal SDS-PAGE, the anionic surfactant SDS denatures the proteins and thus exposes even those metal-binding sites that are buried in the core of the proteins, whereas 2D diagonal native-PAGE is only applicable for proteins with solvent exposed metal-binding sites. Besides, as delineated in section 5.1.2, addition of SDS to protein samples will most likely result in loss of the endogenous non-covalently bound metal ions, while native-PAGE will preserve the innate metal-protein binding. Therefore, in an attempt to identify copper-binding proteins present in mammalian cells, the native 2D diagonal PAGE was adopted in this work. The previously published method by Waldron

et al. utilized acrylamide tube gels, frequently used in isoelectric focusing, for the first dimension, whereas the author of this work standardized the original protocol shown in Scheme 5.1 for copper-binding proteins. This is because, in our hands, the reproducibility of the first dimension slab gel proved to be much better than the tube gels.

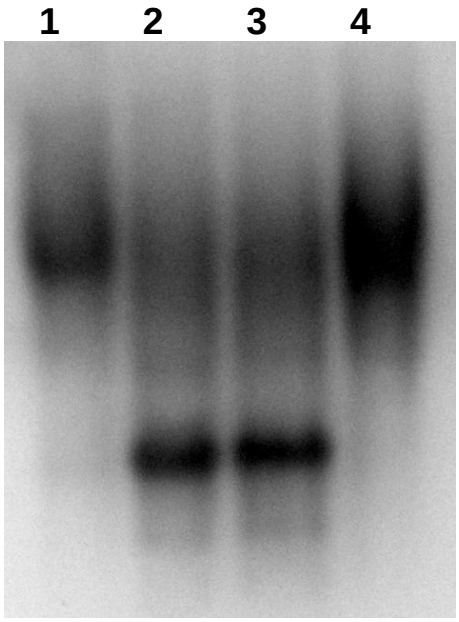

Figure 5.1. *Differential Mobility of hAtox1 under Non-denaturing Condition.* **Lane 1:** untreated hAtox1; **Lane 2:** hAtox1 and reducing agent TCEP; **Lane 3:** hAtox1, TCEP, and copper chelator BCS; **Lane 4:** hAtox1, TCEP, and $[Cu(I)(CH_3CN)_4]PF_6$. 24 µg of the protein in native sample buffer was loaded in each lane of the gel, pH of the running buffer is 8.3, and the gel was stained with Coomassie blue.

hAtox1 is a copper chaperone with solvent exposed metal-binding site (12, 68) and it binds Cu(I) with a cysteine-containing motif, CXXC. This protein has been shown to migrate differently during gel electrophoresis under non-denaturing conditions depending on the copper status (69, 70). This is presumably due to copper-dependent dimerization of the protein (71) or the change in overall charge of the protein upon copper-binding. As shown in Figure 5.1, untreated purified hAtox1 (Lane 1), probably a

combination of the oxidized apo-protein and Cu(I)-bound (holo) form, migrates differently than the protein reduced by tris(2-carboxyethyl) phosphine (TCEP) (Lane 2), or the metal-free (apo) form prepared by adding the copper chelator BCS (Lane 3). Holo-protein formed by addition of exogenous Cu(I) (Lane 4) migrates similar compared to untreated hAtox1 (Lane 1), but the Coomassie stained band in lane 4 is much more intense showing that the majority of the protein is concentrated in that region.

Encouraged by the copper-dependent differential mobility of purified hAtox1, the standardization of the native 2D diagonal PAGE for this work was accomplished with *E. coli* extract overexpressing hAtox1 (the expression of the correct protein was confirmed by Western blot using hAtox1 antibody, data not shown). The *E. coli* extract was used to provide a number of proteins whose mobilities will not be altered in a copper-dependent manner and hence these proteins will form the diagonal.

Native (without SDS and β-mercaptoethanol) polyacrylamide gel electrophoresis (PAGE) was performed according to the method of Laemmli (72). Slab gels were prepared consisting of a 10% acrylamide resolving gel and a 4% stacking gel. The protein samples were equilibrated in appropriate solutions (1^{st} equilibration, Figure 5.2) before they were resolved by electrophoresis in tris/glycine buffer. Following the first dimension electrophoresis, the lane of the gel containing the protein sample was cut out longitudinally (Scheme 5.1). The gel strip was then soaked in the 2^{nd} equilibration buffer (native sample buffer containing additives where necessary, Figure 5.2) at room temperature for 1 hour. Then the gel strip was placed horizontally on top of another slab gel (composition same as above) and electrophoresis in the second dimension was performed (Scheme 5.1). In experiments A and C, the resolving gels and the running buffer contained 1 mM and 250 μM BCS, a bidentate copper(I) chelator, respectively.

1st Equilibration	2nd Equilibration	1st Equilibration	2nd Equilibration
A: Experimental Gel		**B: Control Gel**	
2mM TCEP + 0.2 mM Cu(I)	2 mM BCS	2mM TCEP + 0.2 mM Cu(I)	–

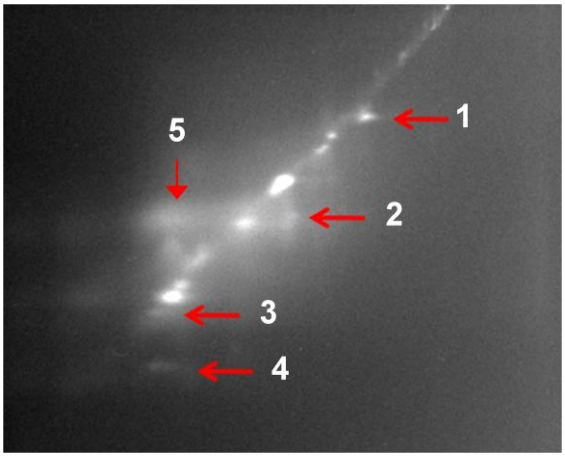

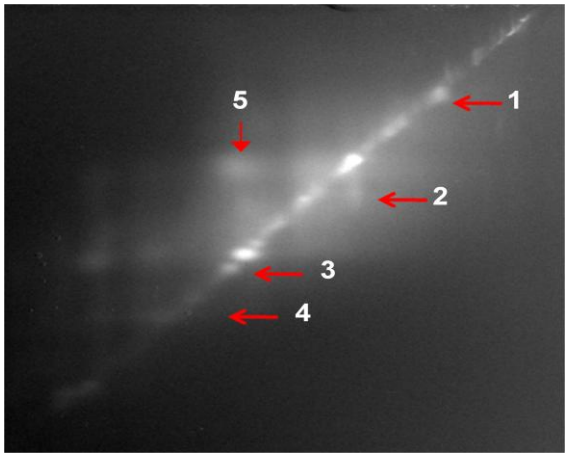

C: Experimental Gel		D: Control Gel	
2mM TCEP + 0.2 mM Cu(I)	2mM TCEP + 2 mM BCS	2mM TCEP + 0.2 mM Cu(I)	2mM TCEP

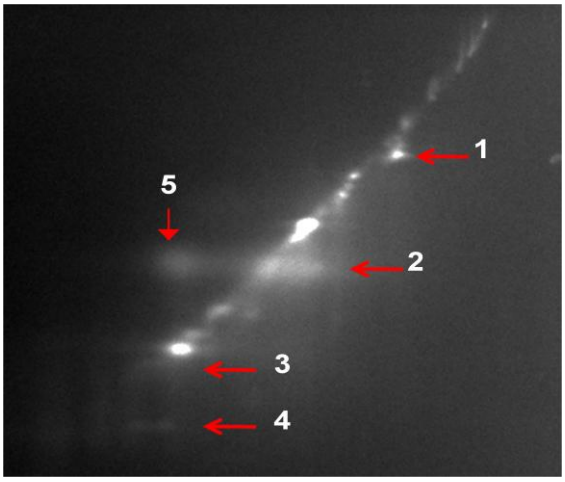

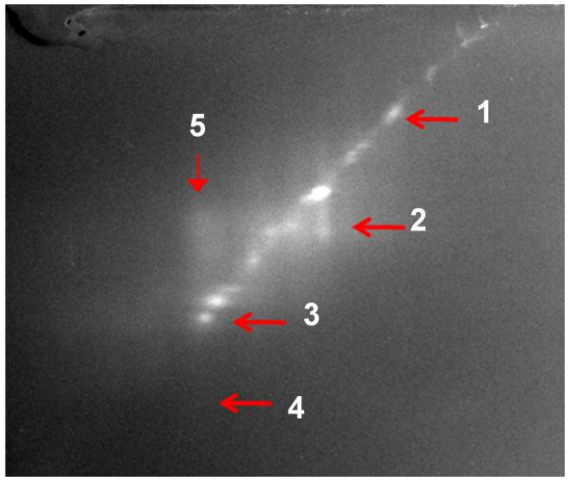

Figure 5.2. *Two-dimensional Diagonal Native Polyacrylamide Gel Electrophoresis under Different Copper Conditions.* Proteins were visualized by Coomassie staining; the gels were shown as inverted images for better visualization. See text for the experimental descriptions and results.

In experiment **A** (Figure 5.2), first the protein sample was equilibrated with the reducing agent TCEP to reduce the Cu(I)-binding cysteines and with $[Cu(I)(CH_3CN)_4]PF_6$ to supply the metal ion to the Cu(I)-proteins (1^{st} equilibration). In the second dimension, the equilibration buffer contained the copper chelator BCS (2^{nd} equilibration). Therefore, the copper-proteins that were metal-bound in the first dimension lost their metal ion in the second and hence were expected to migrate differently during the second electrophoresis step. Four distinct off-diagonal protein spots, **1**, **2**, **4**, and **5**, were identified which showed differential electrophoretic mobilities in experiment **A**.

It is noteworthy at this point, that the mobility shift assay can capture changes in electrophoretic migrations of proteins due to any factor that is different in the second dimension compared to the first one. These factors are not limited to the metal ion loss, for example, change in oxidation state can also cause a protein to migrate differently. Therefore, to identify the subset of proteins whose mobility shifts are caused only due to copper removal by BCS, a control gel was run. In control gel **B**, the same equilibration condition (TCEP + Cu(I)) was used in the first dimension as in experiment **A**, but no BCS was added in the second dimension. Consequently, copper proteins will remain metal-bound in both dimensions and thus were expected to have same electrophoretic mobilities. When control gel **B** was compared with the gel **A**, protein spot **1** was indeed found to lie on the diagonal. Interestingly, off-diagonal protein spot **4** disappeared from the control gel, while the intensity of the Coomassie stained spot **3** increased. However, two off-diagonal protein spots, **2** and **5**, were still present in the control gel **B** at the same position as in gel **A**. Therefore, the cause of the mobility shift of these proteins was not due to the copper removal by BCS, but it had originated from a different source.

The equilibration buffers used in the experiments **A** and **B** were very similar to those previously reported in the literature (67), where a mobility shift assay was used to screen proteins with readily exchangeable copper sites in the cyanobacterium

Synechocystis PCC 6803, and this protocol was used as a starting point for this work. Nevertheless, the reducing agent TCEP was used only in the first dimension both for the experimental gel **A** and control **B**. Therefore, it could be possible that in the equilibration step following the first dimension electrophoresis, the reduced proteins were air-oxidized in absence of a reductant, resulting in the differential migrations of the proteins in the second dimension. In order to investigate further whether this is indeed the reason for the mobility shifts of protein spots, **2** and **5**, another set of experiments (**C** and **D**) were designed.

In experiment **C**, the sample was first equilibrated in the same solution as in experiment **A**, i.e., TCEP and Cu(I). However, during the second equilibration, the buffer contained both BCS and TCEP. Because TCEP was added in both dimensions, it was expected that the proteins, which do not bind Cu(I), will remain in the reduced states. In control **D**, the same condition as in experiment **C** was used except that the copper chelator BCS was omitted. Interestingly, protein spots **2** and **5** did not disappear in either experiment **C** or control **D** and thus it can be concluded that the redox reversibility was not causing the differential electrophoretic mobilities in these spots. Moreover, there was no significant difference observed between the results of two experimental gels **A** and **B** and control gels **C** and **D**.

In the above experiments the occurrence and position of spots **3** and **4** were particularly interesting. In control gels **B** and **D**, the sample was treated with Cu(I) during the first equilibration and BCS was not added during the second equilibration such that the proteins that bind copper will be metal-bound in both dimensions. Under this condition the spot **3** was observed on the diagonal as expected for proteins with unchanged electrophoretic mobilities. However, in case of the experimental gels **A** and **C**, where the sample was treated with Cu(I) in the first dimension and BCS was added to remove the metal ion in the second dimension, spot **3** mostly disappeared and a new spot **4** was observed, shifted to the right of the diagonal. As explained with Scheme 5.2,

this means that the protein constituting spot **4** has a higher electrophoretic mobility in the second dimension than in the first. The differences in spots **3** and **4** between the experimental and control gels in Figure 5.2 can be explained on the basis of the native PAGE in Figure 5.1. It is evident from Figure 5.1, that the migration of the reduced apo-hAtox1 (lane 3) was increased compared to the copper-bound protein (lane 4). Accordingly, the spot **3** might be the copper bound form of a protein which lost its metal ion to BCS in the second dimension to form the corresponding reduced apo-protein. This resulted in higher mobility during the second dimension and thus the spot **4** appeared on the right side of the diagonal with concomitant decrease in the intensity of the spot **3**. Because of the diffuse spot appearance and insufficient quantities of the proteins in spots **3** and **4**, in-gel digestion followed by peptide mass fingerprinting to identify the proteins was not attempted. Nevertheless, a similar 2D diagonal gel with purified hAtox1 showed the same differential migration pattern and thus it is possible that the spots **3** and **4** were associated with hAtox1.

Although the mobility shift assay showed promises in identifying proteins with solvent-exposed copper-binding sites as exemplified with hAtox1 in this work, the method suffers from the low resolution in protein separation, an inherent limitation of native gel electrophoresis, and hence is not suitable to analyze complex protein mixtures. Moreover, the amount of protein that can be loaded on the gel was limiting as any overload in the first dimension resulted in non-specific diffusion of protein spots from the diagonal impeding the spot analysis on the gel.

5.2.2. Selective Labeling of Cu(I)-binding Cysteines with Biotin-conjugated Iodoacetamide

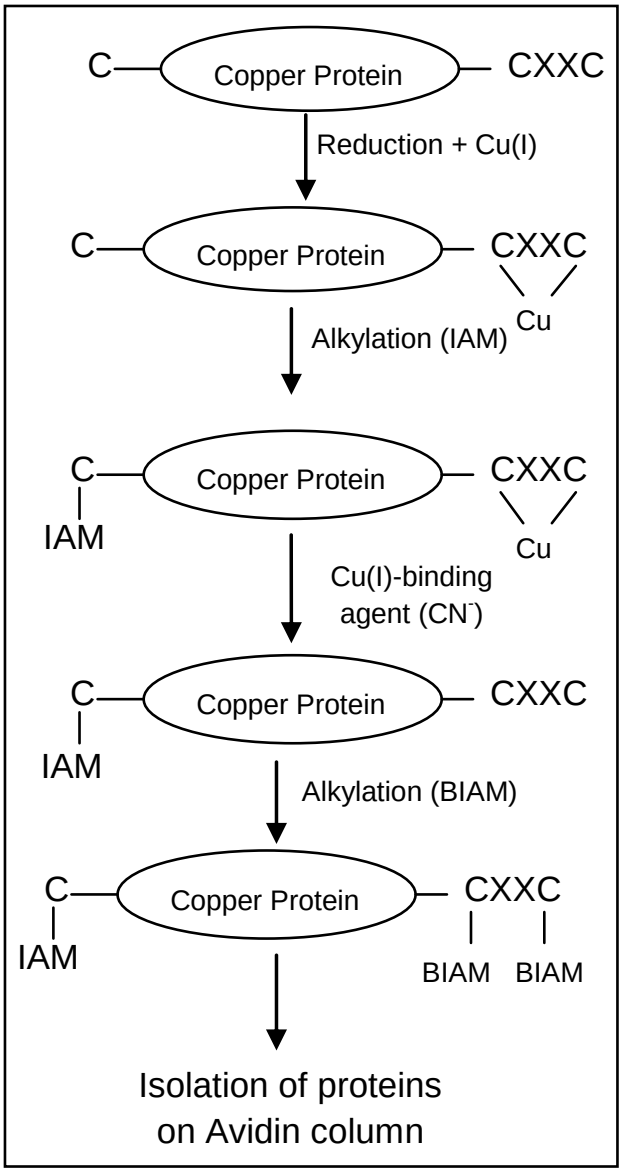

Scheme 5.3. *Key Steps of the Metal-dependent Labeling of Cu(I)-binding Cysteines with Biotin-conjugated Iodoacetamide.*

As discussed in Section 1.2, the amino acid cysteine dominates the Cu(I) binding sites in proteins (Table 1.2). Cysteine thiols in their reduced form are chemically reactive towards maleimide and iodoacetamide derivatives, and this technique is routinely used for covalent labeling of antibodies with fluorescent dyes (73). However, upon Cu(I) binding these thiols become less reactive as they are occupied in coordinating the metal ions. Therefore, thiol-specific labeling strategies can be employed to differentiate between the metal-free apo and the bound holo forms of copper-binding proteins. This metal-dependent labeling of copper-coordinating cysteines was exploited by Walker et al. (74) to monitor copper transfer from holo-WNDP (Wilson's disease protein) to apo-Atox1. In this study, the accessible cysteines in WNDP after the removal of copper by apo-Atox1 were labeled with the residue specific fluorescent reagent 7-diethylamino-3-(4′-maleimidylphenyl)-4-methylcoumarin (CPM). The addition of the increasing amounts of apo-Atox1 to copper-bound WNDP facilitated the copper transfer from holo-WNDP to apo-Atox1 which was observed by the increasing amount of fluorescent labeling of WNDP.

Labeling of cysteines with biotin-conjugated iodoacetamide (BIAM) was used to identify proteins containing redox active cysteine residues (75). Similar to loss of thiol reactivity upon Cu(I) binding, oxidized cysteins are also unable to react to iodoacetamide derivatives. The previously published protocol was modified for the copper-binding proteins in this work as shown in Scheme 5.3.

The method in Scheme 5.3 is described for a hypothetical protein with a CXXC motif that binds Cu(I) ion plus a third cysteine that does not bind the metal ion as encountered in the copper chaperone hAtox1. The third cysteine also represents the large population of cysteine-containing proteins that do not bind copper ions under normal physiological conditions, e.g., thioredoxin, zinc finger proteins, etc. First, exogenous Cu(I) was added to the TCEP-reduced apo protein to metallate the CXXC motif. Second, the free accessible cysteine(s) was alkylated with iodoacetamide (IAM) in order to block

the residue(s) from reacting with the biotinylated alkylating reagent in the following step. Third, potassium cyanide (KCN) was used to remove the Cu(I) ion from the protein. Fourth, the newly liberated cysteines were then reacted with N-(biotinoyl)-N′-(iodoacetyl)ethylenediamine to alkylate the cysteine residues with the biotin-conjugated iodoacetamide (BIAM). Finally, the biotin-labeled proteins were isolated from an avidin column and were identified by mass spectrometry. The major advantage of this method is that it has the potential to simultaneously identify the copper-binding proteins as well as the biotin-tagged cysteines that are involved in copper binding.

Although at a first glance the selective labeling of Cu(I)-binding cysteines with BIAM using reversible metal protection approach appears to be a suitable method to identify copper containing proteins, we found several limitations of this approach. First, TCEP proved to be reactive towards iodoacetamide derivatives as confirmed by NMR spectroscopy. Consequently, the alkylation could not be performed in presence of the reducing agent. This problem can be circumvented by the use of immobilized TCEP gel (Thermo Scientific Pierce) where the reducing agent is covalently immobilized to beaded agarose resin. The one limitation of the immobilized TCEP gel is that the small proteins could get trapped in the resin, thus resulting in poor recovery.

Second, the accessible cysteines, that do not bind copper ions, could not be alkylated exhaustively with iodoacetamide which was a key step in this method. A human copper chaperone hAtox1 was used in this work as a prototype of Cu(I)-binding proteins which have at least one additional cysteine that does not bind copper. Control experiments and mass spectrometric analysis with hAtox1 showed that even after labeling of the third cysteine with IAM, the amino acid residue still could react with BIAM resulting in biotinylation of the cysteine(s) that does not bind copper. Different iodoacetamide concentrations and equilibration time were used to optimize the first alkylation step, however, IAM concentrations can only be varied within a certain range as at higher concentration IAM started to displace Cu(I). Furthermore, another common

thiol-reactive reagent N-ethyl maleimide (NEM) was used to alkylate the accessible cysteines in presence of the copper ions, which showed even lower reactivity than iodoacetamide.

Incomplete labeling of unbound cysteine(s) with IAM would create a two-fold problem. One is the undesired biotinylation of cysteines in various proteins that do not bind copper ions, which will evidently increase the false positives while working with cellular extracts. The other problem is that the recovered copper-containing proteins will have biotin-labeled cysteines other than the ones that bind the metal ion, therefore specific identification of the copper-binding cysteines would not be possible.

5.2.3. Copper-dependent Labeling of Cysteines with Heavy and Light Isotopes

Differential stable isotope labeling is a common proteomics method to quantify the relative abundance of proteins between different biological samples (76). The method involves covalent labeling of proteins in two samples with chemically identical reagents containing "light" or "heavy" isotopes. Since the different isotopes have identical chemical properties, a set of isotopically labeled and unlabeled proteins usually provide an accurate measure of their relative abundance when analyzed by mass spectrometry.

The first example of isotopic labeling of cysteine in proteins employed acrylamide and its D^3-isoform to improve the identification of cysteine peptides during mass spectrometry (77). Later on, Isotope Coded Affinity Tag (ICAT) was developed by combining a biotin affinity tag and isotope coding in a single alkylating agent (78), which made it possible to both isotopically code and affinity select cysteine-containing peptides. Cysteines labeled with light and heavy isotopes have been proven to be a useful strategy to identify and quantify redox-active protein thiols (79-82).

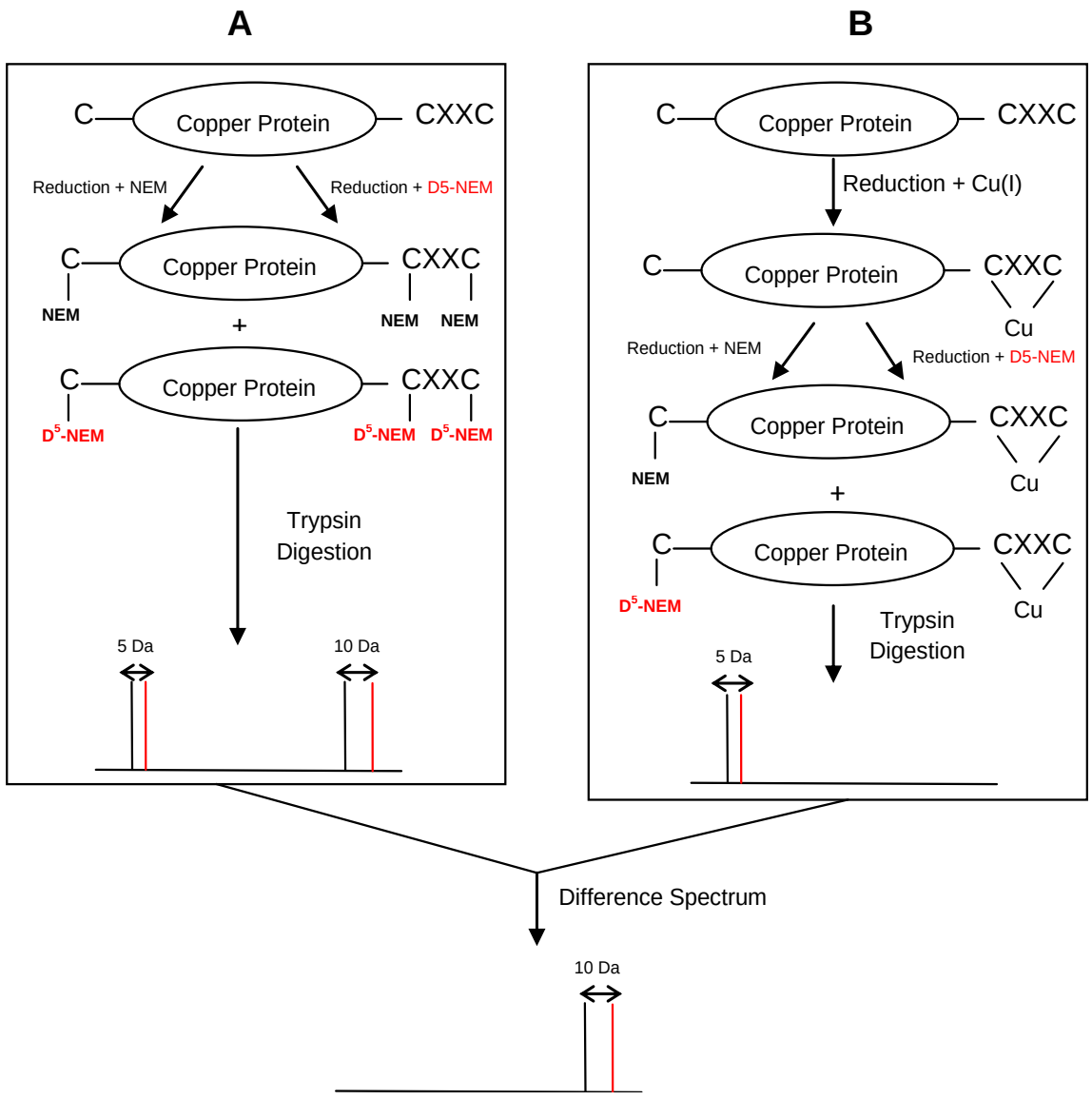

Scheme 5.4. *Key Steps of the Metal-dpendent Labeling of Cysteines with Heavy and Light Isotopes.*

In this work, we have developed a differential isotopic labeling approach for identification of copper-binding proteins. This method as described in Scheme 5.4, enabled us to differentiate between copper-bound and unbound cysteines in a protein. Similar to section 5.2.2, we will describe the method for a hypothetical protein that contains two types of cysteine residues: one binds Cu(I) ions and the other one does not. The protein sample was first divided into two equal portions, **A** and **B** and reduced with TCEP. Cu(I) was added to the reduced sample **B**. Next, both samples **A** and copper-loaded **B** were individually divided into two pools and one pool from each sample was reacted with N-ethyl maleimide (NEM) while the other was reacted with D^5-N-ethyl maleimide (D^5-NEM). After the alkylation step, NEM and D^5-NEM-labeled samples from a single pool were mixed at a 1:1 ratio. Finally, the maleimide-treated protein samples, **A** and **B**, were individually trypsin digested and the resultant peptides were subjected to MALDI mass spectrometry. The difference spectrum of sample **A** and **B** revealed the peptide fragment containing Cu(I)-binding cysteines. Mass difference between NEM and D^5-NEM is equal to 5, therefore in peptide fragments where one cysteine was isotopically labeled, a doublet separated by 5 mass units would be observed, whereas in fragments where two cysteines were labeled, such as CXXC motif, a doublet would be observed that was separated by 10 mass units.

The above method was tested for overexpressed hAtox1 as isolated from *E.coli* culture, with the ultimate goal to identify copper-binding proteins from cellular extracts. With that goal in mind, the protein was not purified for the standardization procedure as the native *E.coli* proteins would provide the complex background as normally encountered in cellular extracts. Following Scheme 5.4, *E.coli* extract overexpressing hAtox1 was labeled with NEM and D^5-NEM and the result is shown in Figure 5.3.

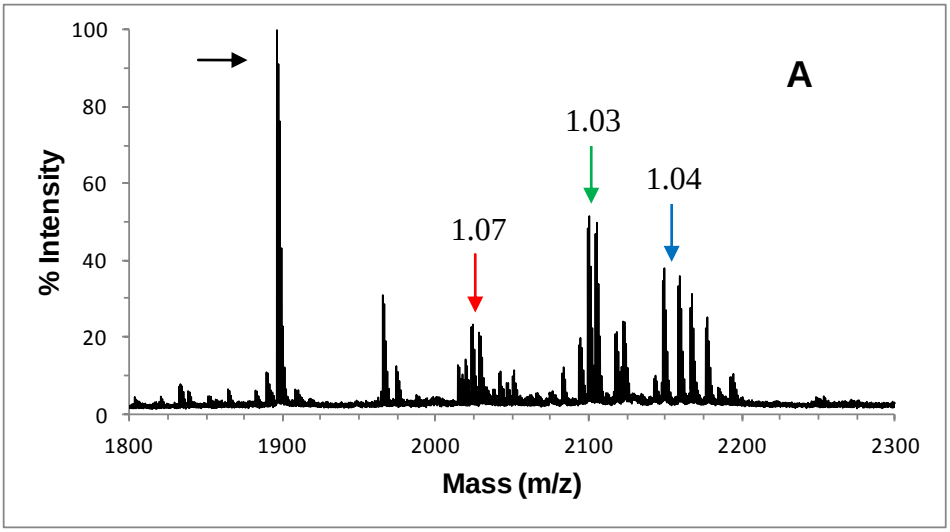
A
% Intensity
Mass (m/z)
1.07
1.03
1.04
100
80
60
40
20
0
1800
1900
2000
2100
2200
2300

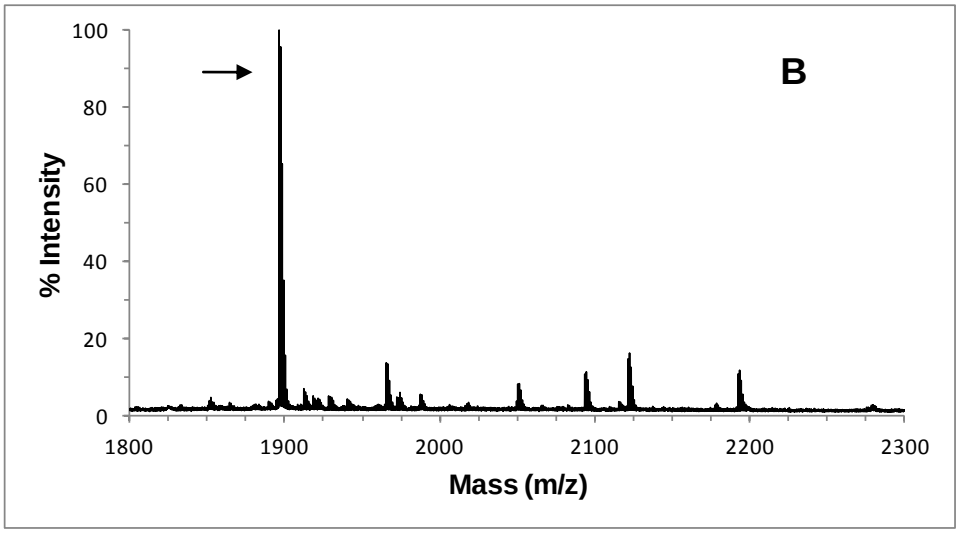
B
% Intensity
Mass (m/z)
100
80
60
40
20
0
1800
1900
2000
2100
2200
2300

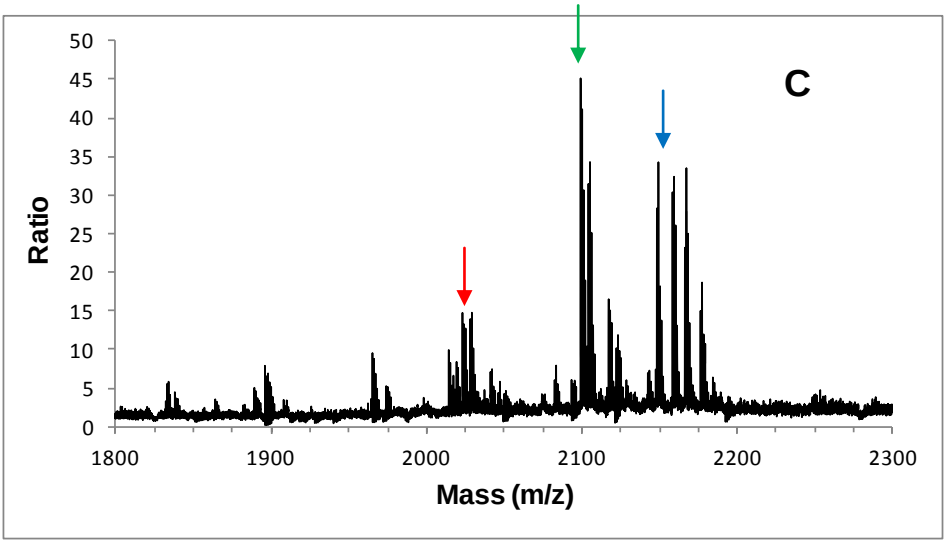
C
Ratio
Mass (m/z)
50
45
40
35
30
25
20
15
10
5
0
1800
1900
2000
2100
2200
2300

Figure 5.3. *Differential Labeling of hAtox1 with N-ethyl Maleimide and D^5-N-ethyl Maleimide.* **A)** Cysteines in CXXC motif were isotopically labeled in reduced apo-hAtox1; black arrow: unlabeled parent peak containing the CXXC motif, red arrow: one of the cysteines in the CXXC motif was isotopically labeled and the other one was unlabeled, green arrow: one cysteine was conjugated with β-mercaptoethanol while the other cysteine was labeled with the maleimides, blue arrow: both cysteines were isotopically labeled. The number over each arrow represented the ratio of NEM vs. D^5-NEM labeled peptides which would be ideally 1. **B)** cysteines in CXXC motif were protected in copper bound hAtox1 and thus were unable to react with the isotopic reagents; **C)** the difference spectrum between **A** and **B** revealing the peptide fragments that bound Cu(I) ions.

First of all, the isotopic labeling was incomplete as a significant amount of the parent peak corresponding to the unlabeled peptide fragment containing the CXXC motif was still present in Figure 5.3.**A** (black arrow). A similar observation was made by Kurono et al. which showed incomplete reactivity of maleimide towards thiols irrespective of the reaction time and temperature (83). The fragment containing the single cysteine, that did not bind copper ion, was not observed in the mass spectrum. It is noteworthy that this peptide fragment also did not appear in trypsin digested hAtox1 prior to the labeling. Nevertheless, as expected for sample **A**, the cysteines from CXXC motif were isotopically labeled with NEM and D^5-NEM resulting in a doublet separated by 10 mass units (Figure 5.3.**A**, blue arrow). These peaks at 2148.7 and 2158.7 were not present in sample **B**, where CXXC was copper-bound and thus blocking the thiols towards labeling (Figure 5.3.**B**). Interestingly, two additional doublets, each of them contained two peaks separated by 5 mass units, were observed in Figure 5.3.**A**; one of them corresponded to the isotopic labeling of one of the cysteines of the CXXC motif leaving the second cysteine unlabeled (red arrow). Another doublet was comprised of one cysteine of the CXXC motif conjugated with β-mercaptoethanol, while the other cysteine of the same motif was labeled with the maleimides (green arrow). β-Mercaptoethanol was used to quench the thiol maleimide reaction, and thus a hetero disulfide bond was presumably formed between the reagent and the protein. Neither of these additional

doublets was present in sample **B**, where the copper ion was added. The difference spectrum (Figure 5.3.**C**) between Figure 5.3.**A** and **B** showed all of the three doublets observed for the reduced apo-protein (blue, red, and green arrow). Furthermore, for each doublet, a second set of doublet was observed at a distance of M + 18, where M represents the mass value at which the original doublet appeared. Finally, as shown by the number over each arrow in Figure 5.3.**A**, the ratios of NEM vs. D^5-NEM labeled peptides were close to 1 showing the equal reactivity of the reagents toward cysteine thiols.

In place of β-mercaptoethanol, dithiothreitol (DTT) can also be used to quench the thiol maleimide reaction. Upon oxidation, DTT forms a stable six-membered ring with an intra-molecular disulfide bond, whereas β-mercaptoethanol forms an inter-molecular disulfide bond. Therefore, DTT might inhibit the conjugation of the reagent with the cysteine of the peptide fragments as encountered in the previous experiment with β-mercaptoethanol (Figure 5.3.**A**, green arrow). Use of DTT indeed prohibited the heterodimerization between the peptide fragments and the reagent; however, in comparison to Figure 5.3.**A**, the peaks corresponding to the unlabeled parent CXXC-containing peptide and the isotopically labeled peptide fragments were shifted by 429.2 mass units towards higher values. Moreover, similar to the previous experiment, the second set of doublets was also detected at a distance of M + 18 from the original ones even when DTT was utilized.

As evident from the differential isotopic labeling of hAtox1, the major advantage of this method is that the copper binding cysteines can be conveniently detected even in the presence of other peptide signals of much higher intensity. Therefore, this method is suitable to identify copper-binding proteins from complex cellular extract where a small fraction of the total proteins will bind copper. However, typical copper-binding proteins have one metal-binding motif in their entire amino acid sequence, and the proteins where Cu(I) is bound by the CXXC motif the two cysteines are separated by two amino acids.

Therefore it is expected that only one peptide fragment per protein containing the copper-binding cysteines can be identified by this method. Although there is evidence in the literature where a protein was assigned based on MS/MS spectrum of a single peptide fragment (79, 84), however, the confident identification of proteins by such procedure is often challenging. Nevertheless, the metal-dependent isotopic labeling can be reliably used to confirm copper-binding sites of proteins as illustrated with hAtox1.

5.2.4. Difference Gel Electrophoresis with Cy3 and Cy5 Meleimide Dyes

Since its introduction in 1975 (85), two-dimensional gel electrophoresis has become one of the fundamental methods in proteomic analyses due to its high resolution and sensitivity. However, in 2D electrophoresis no two gels are identical, and hence reliable detection of protein differences between two samples using traditional post-electrophoretic staining methods, e.g. coomassie blue and silver staining, is challenging. In order to circumvent the problem of gel-to-gel variability, difference gel electrophoresis (DIGE) was developed (86), which enabled the analysis of multiple protein samples within one gel. This method is based on covalent modification of proteins in different samples with structurally similar but spectroscopically distinct fluorophores. Therefore, the post-electrophoretic fluorescent images from different samples separated on the same gel can be directly compared and hence this method increases the confidence with which differences in protein abundance can be detected.

The first commercially available 2D DIGE reagents utilize mass and charge-matched cyanine dyes with N-hydroxy-succinimidyl ester groups to modify lysine residues of proteins (87). These are known as minimal labeling dyes as the dye to protein ratio is kept deliberately low (approximately 5%). Owing to the typically high lysine content of most proteins, the minimal labeling approach was employed in order to avoid multiple dye additions on each protein molecule which would generate multiple spots per

protein on a 2-D gel and also interfere with the solubility of the protein. As a result of the minimal labeling approach, the sensitivity of these techniques is low.

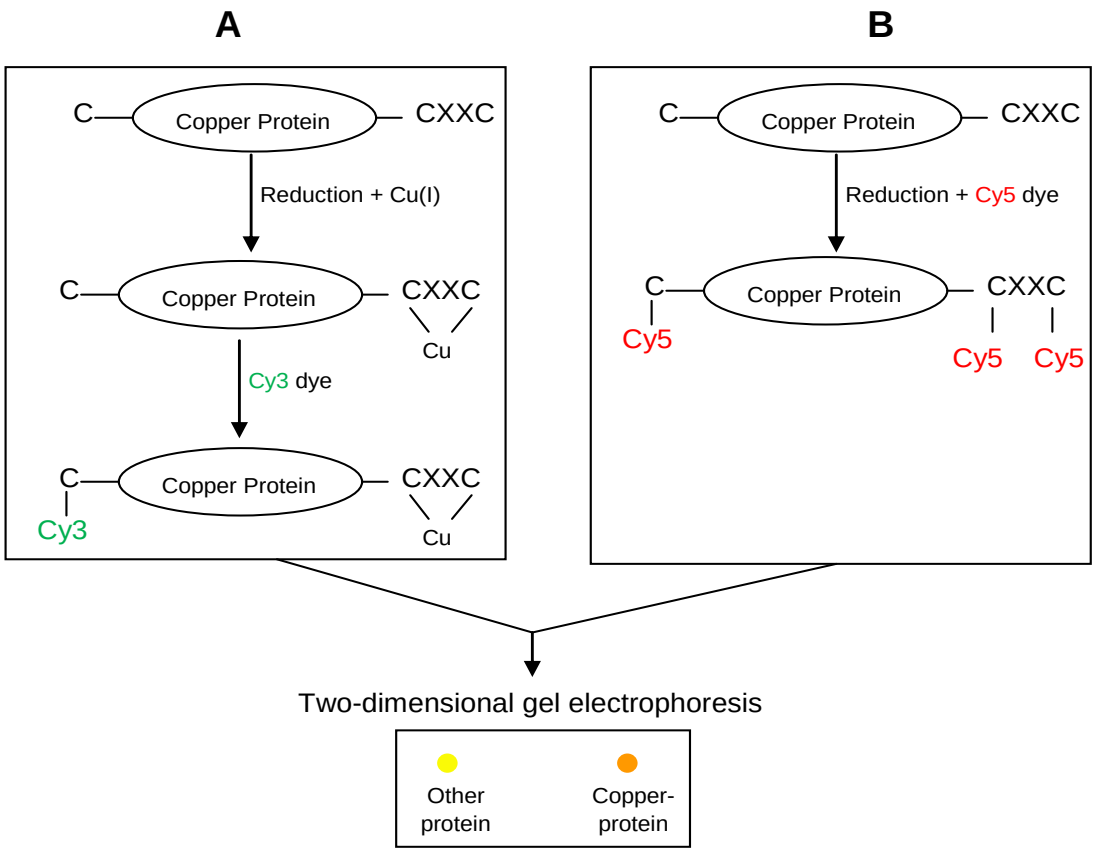

Scheme 5.5. *Key Steps of the Difference Gel Electrophoresis with Cy3 and Cy5 Meleimide Dyes*

One way to improve sensitivity of the 2-D DIGE technology is to exhaustively label an alternative less prevalent amino acid, such as cysteine. The maleimide group reacts with cysteine thiols through nucleophilic Michael addition to form a thioether and thus can serve as a platform to produce cysteine-reactive DIGE dyes. Although a variety of other maleimide-containing dyes have been described in the literature for labeling

cysteines in proteins with 2D gel applications (88-91), the CyDye DIGE Fluors (Cy3 and Cy5) by Amersham Biosciences are by far the most popular ones (92).

Encouraged by the use of 2-D DIGE technology in measuring redox changes in protein thiols (93-96), we devised a strategy to identify copper-binding proteins using 2D DIGE as shown in Scheme 5.5. Here the CXXC motif signifies the cysteine-containing copper-binding site of a protein, while the single cysteine represents both the additional cysteine in the same copper protein and other cysteine -containing proteins that do not bind copper ions under normal physiological conditions. Copper-free apo-protein samples would be first divided into two equal portions, **A** and **B**. Upon reduction, the copper ion would be added to the sample **A**. Each sample would then be reacted with a different DIGE dye, for example, Cy3 for the metallated sample **A** and Cy5 for the other sample **B**. The two differentially labeled samples with equal protein concentrations would be mixed together and separated on a 2D gel followed by imaging with a fluorescence scanner. Since Cy3 and Cy5 maleimides have similar chemical reactivity towards thiols, under this experimental condition the proteins that do not bind copper ions would show up as a yellow-colored spot due to equal intensities of green and red fluorescences of the Cy3 and Cy5 dyes, respectively. On the other hand, in this example, copper-binding proteins would show a 3-fold higher fluorescence intensity for the Cy5 dye compared to Cy3 making it possible to identify the copper proteins.

In this work, we first optimized our protocol to differentially label copper proteins in a metal-dependent manner with Cy3 and Cy5 dyes. For this purpose, we used a known copper chaperone hAtox1 and the labeling was evaluated in a one-dimensional SDS-PAGE. Furthermore, during this work, MCL-1 and MCL-2 (Figure 2.1) have already been characterized as water-soluble, air-stable copper ligands with stability constants ($\log K_{Cu(I)L}$) of 16.33 and 13.08 respectively (Table 2.5). MCL-2 is slightly basic (pK_a = 8.98) and hence has a lower apparent affinity ($\log K'_{Cu(I)L}$) at pH lower than its pK_a (Section 2.1.3). As a consequence, the pre-formed copper complex of MCL-2 has been

successfully used to metallate a variety of small molecule ligands of higher affinities (Table 2.4). Since most Cu(I)-binding proteins would have comparable or higher affinities than MCL-2 at biological pH (97, 98), in this work we further set out to examine the applicability of the copper complex of this ligand as a copper source to metallate proteins. This will eliminate the use of by far the most common copper supplying reagent Cu(I)-acetonitrile complex. Aqueous solution of Cu(I)-MCL-2 is much more stable towards oxidation and disproportionation compared to Cu(I)-acetonitrile complex dissolved in water. Although Cu(I)-acetonitrile complex is reasonably stable in acetonitrile-water mixture, presence of acetonitrile can alter the metal binding property of a protein by destabilizing its tertiary structure (99, 100).

a) Effect of TCEP on Protein Labeling

A critical step for the effective labeling of cysteine residues is reduction of the disulfide bonds. This is typically achieved by the use of reducing agents, such as dithiothreitol (DTT), β-mercaptoethanol (BME), tris(2-carboxyethyl) phosphine (TCEP), or tributylphosphine (TBP). TCEP is water-soluble, nonvolatile, and reduces disulfide bonds more efficiently at a wider pH range (101) and hence this has become a popular choice to reduce disulfide bonds in proteins. While it is obvious that thiol-containing reductants, including BME and DTT, would react with maleimides, it is generally thought that phosphines such as TCEP are nonreactive. However, in an earlier attempt by the author of this work to label proteins with fluorescein-5-maleimide, it was found that TCEP interfered with the protein labeling (data not shown). Similar observation was made by other groups which showed that TCEP inhibits labeling of proteins with both iodoacetamide and maleimide dyes (102, 103). In order to circumvent this problem, we utilized the immobilized TCEP gel in the reduction step as mentioned in Section 5.2.2.

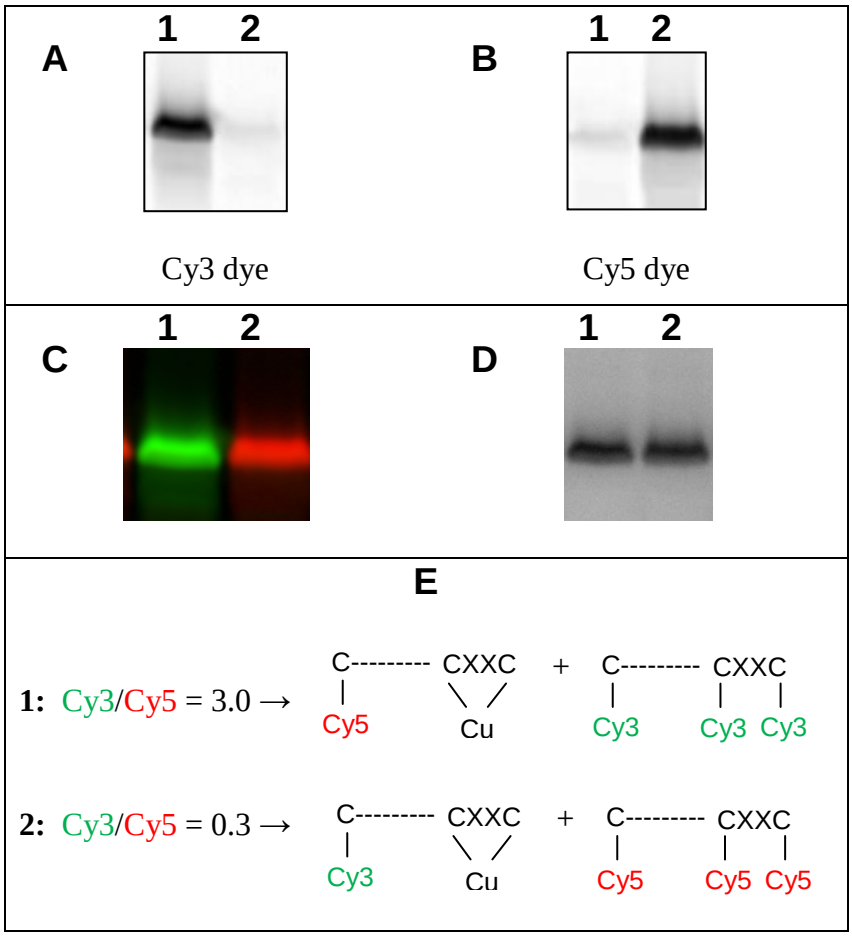

Figure 5.4. *Effect of MCL-2 on Protein Labeling.* **Lane 1:** Copper-bound hAtox1 was conjugated with Cy5 dye and mixed with Cy3-labeled apo-protein at equal concentrations; **Lane 2:** Copper-bound hAtox1 was conjugated with Cy3 dye and mixed with Cy5-labeled apo-protein at equal concentrations. **A**) Gray-scale Cy3 image showing the relative fluorescent signals of proteins labeled with Cy3 maleimide dye; **B**) Gray-scale Cy5 image showing the relative fluorescent signals of proteins labeled with Cy5 maleimide dye; **C**) Overlay of Cy3 and Cy5 fluorescent signals; **D**) Gel stained with Coomassie blue; **E**) Expected cysteine labeling of hAtox1 with Cy3 and Cy5 dyes in **Lane 1** and **2**.

b) Effect of MCL-2 on Protein Labeling

Next we evaluated the influence of MCL-2 in protein labeling and surprisingly we observed that the copper complex interfered with the labeling efficacy. hAtox1 was labeled with both Cy3 and Cy5 dyes in the presence and absence of Cu(I) ions, where Cu(I) was supplied by Cu(I)-MCL-2 complex (Figure 5.4). In one sample (**Lane 1**), copper(I)-bound hAtox1was reacted with the Cy5 dye and this was mixed with a Cy3-labeled reduced sample. In another sample (**Lane 2**), the Cu(I)-bound protein was labeled with Cy3 and the apo sample was labeled with Cy5 dyes. hAtox1 contains a CXXC copper-binding motif and a third cysteine that normally does not bind copper. Therefore, as evident from Figure 5.4.**E**, when Cy5 dye was added to Cu(I)-bound hAtox1 (**Lane 1**), the CXXC would not be labeled as the cysteine thiols were engaged in metal coordination, however, the third cysteine would be labeled with the Cy5 dye. Conversely, all three cysteines would be labeled with the Cy3 dye when added to the apo-sample (**Lane 1**). As a result, the expected ratio of the fluorescence intensities of Cy3 to Cy5 would be 3 in **Lane 1**. However, Figure 5.4.**B** (**Lane 1**) showed a Cy5 fluorescence signal of much lower (more than 3-fold) intensity compared to the Cy3 signal in Figure 5.4.**A** (**Lane 1**). Similar observation was made for the sample in **Lane 2** where the Cy3 fluorescence signal was much lower than the expectation. These results showed that whenever the labeling reaction was performed in the presence of the Cu-MCL-2 complex, the fluorescence output of the labeled protein was much lower than expected, indicating a probable interaction between the copper complex of MCL-2 and the DIGE dyes. Therefore, in future experiments excess Cu-MCL-2 complex was removed by gel filtration before labeling with Cy3 and Cy5 dyes.

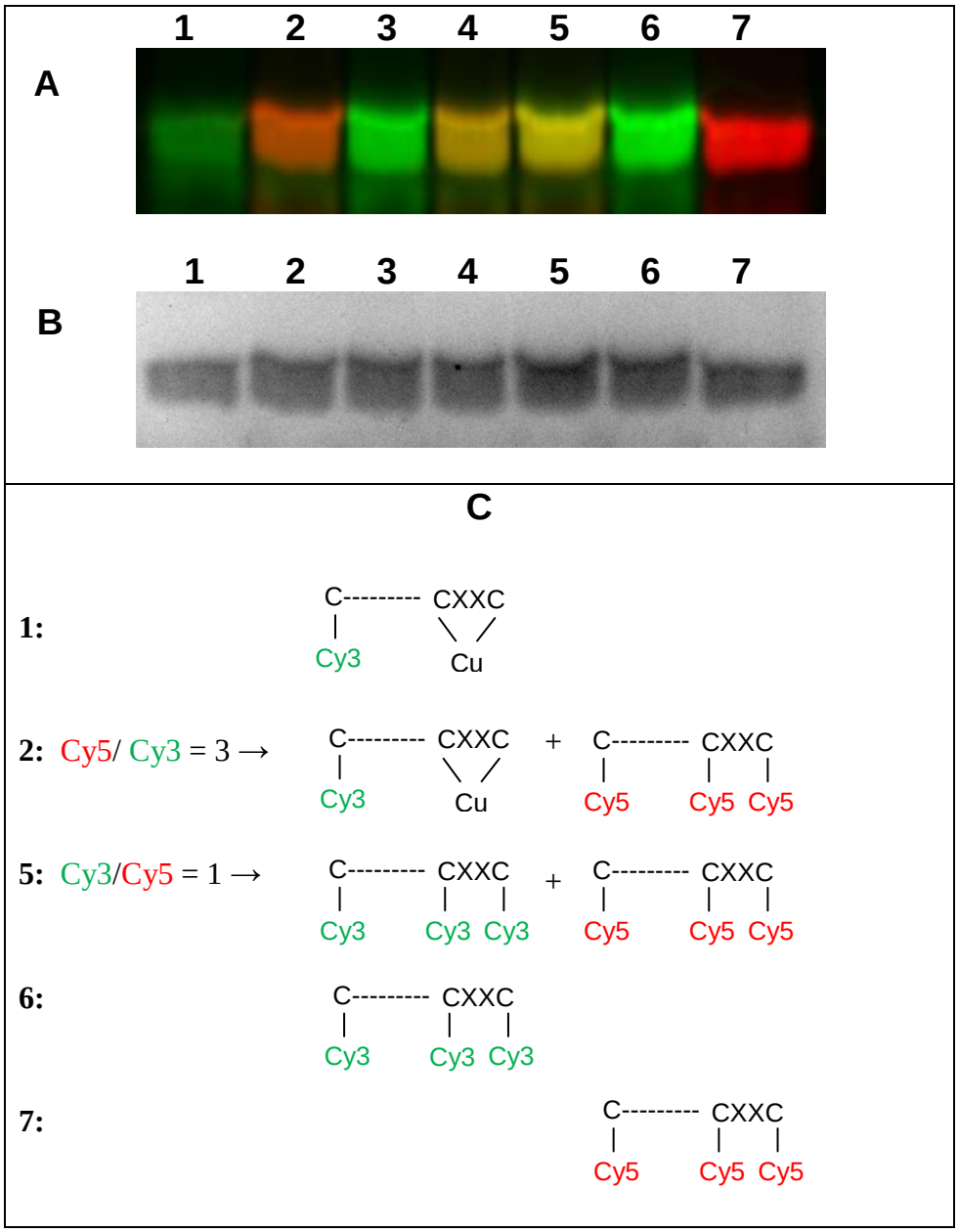

Figure 5.5. *Copper-dependent Labeling of hAtox1 with Cy3 and Cy5 Dyes.* **A**) Superimposed fluorescence scans of Cy3 and Cy5; **B**) Gel stained with Coomassie blue; **C**) Expected cysteine labeling of hAtox1 with Cy3 and Cy5 dyes in Lane **1**, **2**, **5**, **6**, and **7**. **Lane 1:** Following addition of Cu-MCL-2, hAtox1 was labeled with Cy3 dye only; **Lane 2:** Following addition of Cu-MCL-2, hAtox1 was conjugated with Cy3 dye and mixed with Cy5-labeled untreated protein at equal concentrations; **Lane 3:** Following addition of Cu-MCL-1, hAtox1 was labeled with Cy3 dye only; **Lane 4:** Following addition of Cu-MCL-1, hAtox1 was conjugated with Cy3 dye and mixed with Cy5-labeled untreated protein at equal concentrations; **Lane 5:** Untreated hAtox1 was labeled with both Cy3 and Cy5 dyes and mixed at equal concentrations; **Lane 6:** Untreated hAtox1 was labeled with Cy3 dye only; **Lane 7:** Untreated hAtox1 was labeled with Cy5 dye only.

c) Copper-dependent Labeling of hAtox1 and Fluorescence Quantification

The efficiency of the differential labeling of hAtox1 in the presence and absence of copper was examined and the results are shown in Figure 5.5. Pre-formed copper complexes of both MCL-1 and MCL-2 were used for this experiment. Based on the most recent literature value of the Cu(I)-binding affinity of hAtox1 ($\log K'_{Cu(I)L}$ = 17.4 at pH 7) (98), it was expected that Cu-MCL-1 ($\log K'_{Cu(I)L}$ = 15.97 at pH 7) would not be able to metallate hAtox1 as efficiently as Cu-MCL-2 ($\log K'_{Cu(I)L}$ = 10.99 at pH 7) complex. DIGE would also give an opportunity to compare directly the extent of copper incorporation into hAtox1 by Cu(I)-MCL-1 and Cu(I)-MCL-2 in a single experiment. Furthermore, Cu(I)-MCL-1 and Cu(I)-MCL-2 are structurally similar with identical donor atom sets (Figure 2.1); hence, any non-specific interaction between these copper complexes and the fluorophores of the DIGE dye should be comparable. Therefore, use of the both copper complexes in the same experiment would also enable us to assess whether these complexes could introduce any other factor, besides the metallation of the proteins, which might influence the experimental outcome.

The description of the samples in each lane of the gel shown in Figure 5.5 is given in the figure legend. As mentioned in the preceding paragraph, CXXC is the copper-binding motif in hAtox1 which also contains a third cysteine that normally does not bind copper. In order to compensate for any instrumental variation between the Cy3 and Cy5 channels (see experimental methods) of the Typhoon Imager, a control sample was run in **Lane 5**, where an equal amounts of Cy3 and Cy5-labeled apo-hAtox1 were mixed. As evident from Figure 5.5.C.**5**, this produced a Cy3/Cy5 ratio equal to 1.0. Therefore, all individual Cy3 and Cy5 fluorescent images in Figure 5.5.A were normalized against the respective signals in the **Lane 5**. The fluorescence signals were further normalized by the amount of protein in each lane, which was measured by densitometry of the Coomassie stain, to remove any difference from the protein loading especially when comparing fluorescence signals between two lanes. The accuracy of the normalization steps were

ascertained by measuring the Cy3/Cy5 ratio between **Lane 6** and **7**. As shown in Figure 5.5.C.**6** and Figure 5.5.C.**7**, the expected ratio was 1 which agreed very well with the normalized experimental Cy3/Cy5 ratio which was 0.95.

In **Lane 1**, Cu-MCL-2 was added to hAtox1 to metallate the protein, blocking the thiols from further covalent modification by Cy3 in the following step. Consequently, only the third cysteine was expected to be labeled by Cy3 in this sample (Figure 5.5.C.**1**). Conversely, in **Lane 6**, no copper ions were added to the sample, therefore, all three cysteines can be labeled by the Cy3 dye (Figure 5.5.C.**6**). Therefore, the expected ratio of Cy3 fluorescence intensities between **Lane 6** and **1** should be 3, whereas the experimental ratio was 2.4. Another way to measure the correlation of the DIGE labeling with the copper status of hAtox1 was to label the copper-bound protein with Cy3 while the unbound protein was reacted with Cy5. When these two samples were mixed at equal concentrations and loaded in the same lane of the gel (Figure 5.5; **Lane 2**), we found that the normalized Cy5/Cy3 ratio was 2.5 while the expected ratio was 3. This Cy5/Cy3 ratio in **Lane 2** is very similar to the Cy3 ratios between **Lane 6** and **1**, where both Cu-bound (**Lane 1**) and unbound (**Lane 6**) hAtox1 were labeled with the Cy3 dye.

In contrast, when Cu-MCL-1 was added to hAtox1 followed by labeling with the Cy3 dye (Figure 5.5; **Lane 3**), the normalized fluorescence intensity of Cy3 in **Lane 3** was comparable to the intensity in **Lane 6** (ratio of Cy3 in **Lane 6** vs. **Lane 3** = 1.2). In **Lane 4**, the Cu-MCL-1-treated hAtox1 was labeled with Cy3 and was mixed at equal concentrations with the Cy5-labeled untreated hAtox1. Similar to **Lane 3**, here we also found Cy5/Cy3 ratio to be 1.2 indicating that Cu-MCL-1 was not able to significantly metallate the protein.

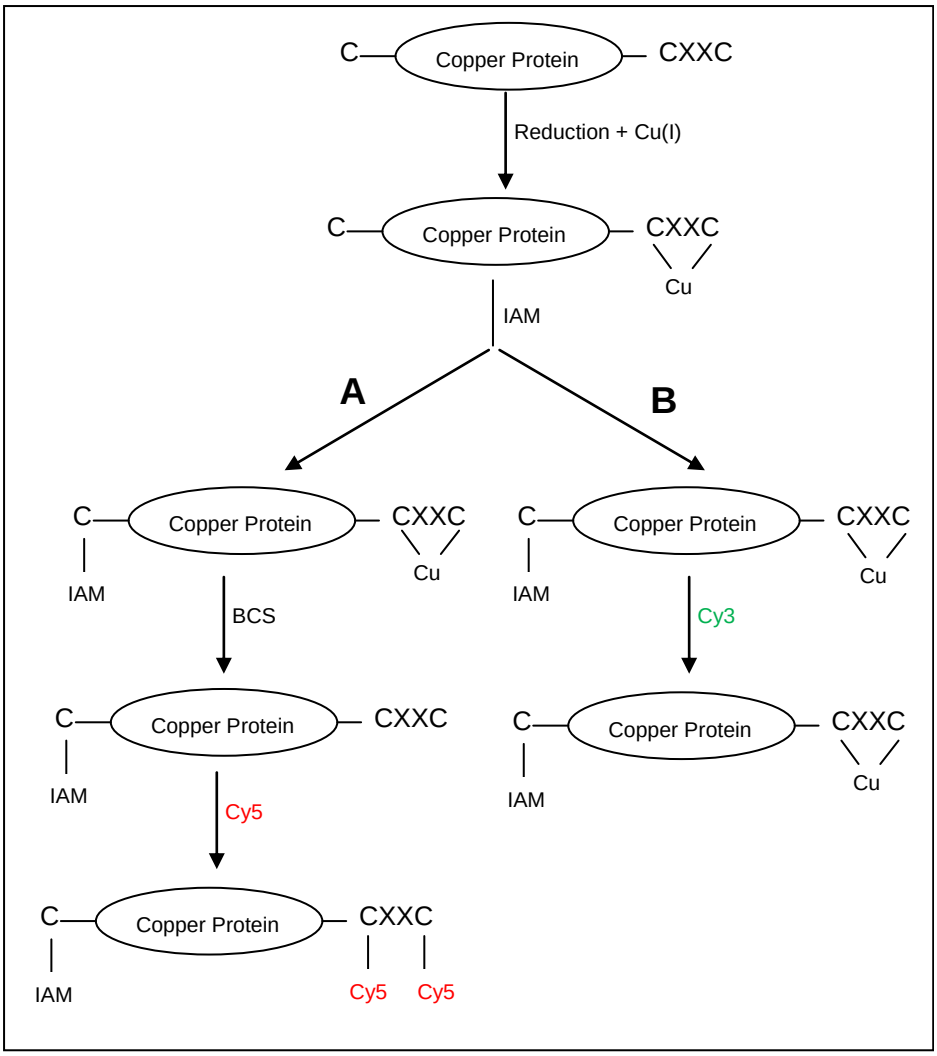

Scheme 5.6. *Key Steps in the Alkylation of Accessible Cysteines with Iodoacetamide prior to the Labeling with DIGE Dyes*

d) Alkylation of Accessible Cysteines with Iodoacetamide prior to the Labeling with DIGE Dyes

In the proposed experimental design in Scheme 5.5, the proteins that do not bind copper ions will be labeled equally with the Cy3 and Cy5 dyes and thus will appear as yellow spots on the 2D gel image. Since the majority of proteins in biological samples do not bind copper(I) ions (29), DIGE labeling of these proteins will result in a considerable background fluorescence which does not contain any information about the target copper-

proteins. One way to eliminate this problem is to alkylate the accessible cysteines with a non-fluorescent reagent prior to the labeling (95).

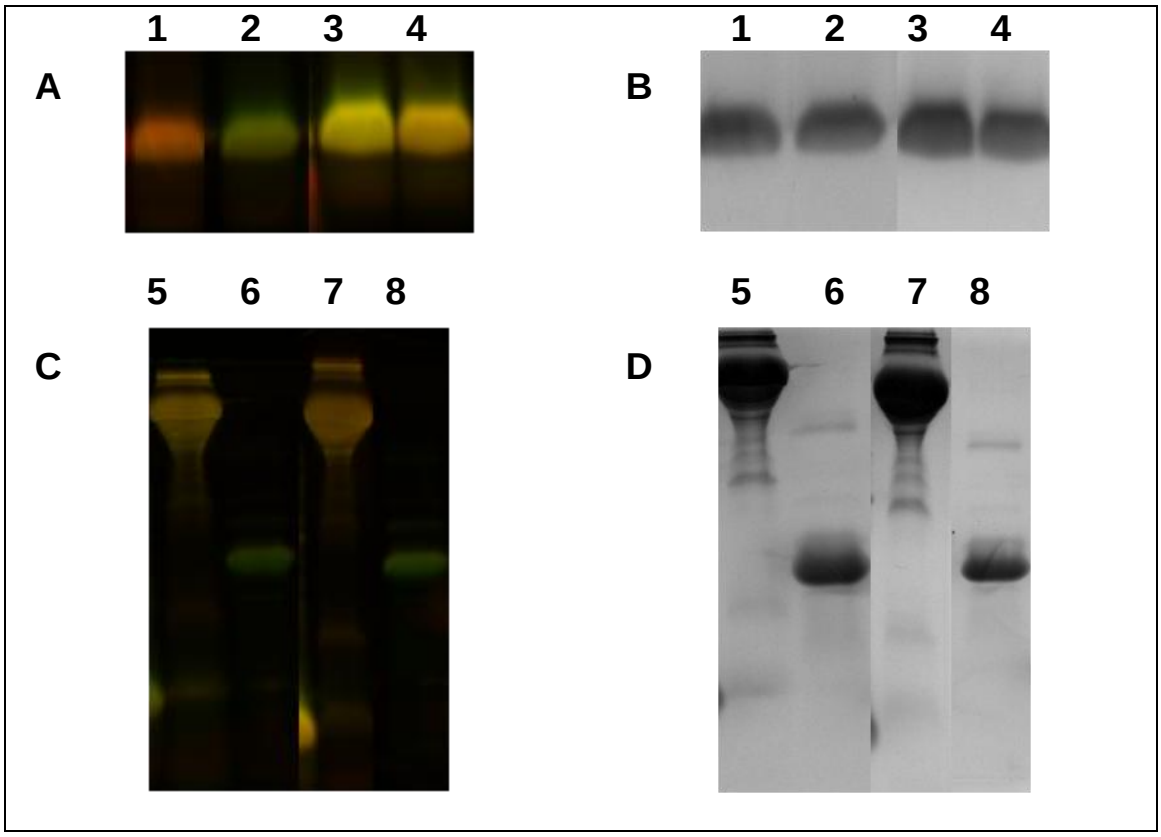

Figure 5.6. *Alkylation of Accessible Cysteines with Iodoacetamide prior to the Labeling with DIGE Dyes.* **A**) and **C**) Superimposed fluorescent scans of Cy3 and Cy5; **B**) and **D**) Gel stained with Coomassie blue. Panels **A** and **B** showed labeling of hATox1, while panels **C** and **D** showed that of BSA and Myoglobin. **Lane 1:** Following alkylation with IAM, Cu-hAtox1 was reacted with Cy3 dye and BCS-treated hatox1 was labeled with Cy5 dye (Scheme 5.6); Cu-MCL-2 was used as the copper source; **Lane 2:** Same experiment as in Lane **1** with the dye being swapped, i.e; Cu-hAtox1 was reacted with Cy5 dye and BCS-treated hatox1 was labeled with Cy3 dye; **Lane 3** and **4:** Same experiments as in Lane **2** and **1,** respectively, with the copper source being Cu-MCL-1; **Lane 5:** Same experiment as in Lane **1** with BSA acting as a control protein which has multiple cysteines that do not bind copper ions; Cu-MCL-2 was used as the copper source; **Lane 6:** Same experiment as in Lane **1** with myoglobin acting as a negative control which does not contain any cysteine residue; Cu-MCL-2 was used as the copper source; **Lane 7** and **8:** Same experiments as in Lane **5** and **6,** respectively, with the copper source being Cu-MCL-1. It is noteworthy that the experiments with Cu-MCL-2 (Lanes **1**, **2**, **5**, and **6**) and Cu-MCL-1 (Lanes **3**, **4**, **7**, and **8**) were done on two separate gels; however the results were combined in this figure for direct comparison.

As depicted in Scheme 5.6, first Cu(I) ions would be added to the protein sample. Second the free cysteines would be alkylated with iodoacetamide (IAM). Ideally, IAM should block all free cysteines that do not bind copper ions from further labeling; however, previously IAM failed to exhaustively alkylate available cysteines (Section 5.2.2). Therefore, in this experiment, following the addition of IAM the sample would be divided into two portions, **A** and **B**. Third, in sample **A**, copper chelator BCS would be added to remove the protein-bound copper ions followed by labeling of the resultant apo-proteins with Cy5. Simultaneously, in the other sample **B**, Cy3 was added to gauge the efficiency of the alkylation step by IAM.

For the sample in **Lane 1**, where the copper ion was supplied by Cu-MCL-2, Cy3 was reacted with Cu-bound hAtox1 while the apo-protein generated by BCS was labeled with Cy5. Following Scheme 5.6, the protein in **Lane 1** should ideally not be labeled with Cy3. However, as expected for incomplete alkylation of unprotected cysteines by iodoacetamide, Figure 5.6.**A** showed that the protein in **Lane 1** was labeled with Cy3 as well as Cy5 dyes with the fluorescence intensity of Cy5 being higher than that of Cy3 (Cy5/Cy3 ratio = 1.63). Similar results were obtained with the protein in **Lane 2** (Figure 5.6.**A)**. In contrast, for the samples in **Lane 3** and **4**, where the copper ion was supplied by Cu-MCL-1, the Cy5/Cy3 ratio was almost equal to 1, irrespective of what dye was reacted with Cu(I)-bound hAtox1. This correlated with the previous finding (Section 5.2.4.*c*) that showed Cu(I)-MCL-1 was inefficient in metallation of proteins. Therefore, in this case, even in the presence of copper ions the majority of the three cysteines in hAtox1 would be unprotected. If there were no difference of these cysteines towards alkylation with IAM, these groups would be expected to have an equal reactivity towards Cy3 and Cy5 dye, thus justifying the observed Cy5/Cy3 ratio of 1.

The equal reactivity of the Cy3 and Cy5 dyes towards available cysteines was further consolidated with the labeling of BSA in Figure 5.6.**C**. In this experiment, BSA furnished as an example of cysteine-containing proteins found in the biological sample

which physiologically do not bind copper ions. Therefore, this protein should not exhibit any copper-dependent differential labeling with Cy3 and Cy5 dyes. Moreover, the proteins like BSA would contribute to a considerable fluorescence background in a 2D DIGE gel where the proteins in a biological sample will be differentially labeled in presence and absence of copper ions following Scheme 5.5. Therefore, BSA would also allow us to assess the utility of IAA in order to reduce the fluorescence background as described in Scheme 5.6. The results in Figure 5.6.**C** (**Lanes 5** and **7**) showed that while IAA could not alkylate the cysteines completely, the reactivity of Cy3 and Cy5 dyes were still equal towards the unblocked cysteines, thus resulting in a ratio of 1. As expected, there was no difference in the labeling in the presence of either Cu(I)-MCL-1 or Cu(I)-MCL-2.

Additionally, in this experiment, myoglobin was used as a negative control as this protein does not have any cysteine. This would indicate the extent of non-specific interactions of proteins with the DIGE dyes. Surprisingly, myoglobin showed primarily a Cy3 fluorescence signal in Figure 5.6.**C** (**Lanes 6** and **8**) in the presence of both Cu-MCL-1 and Cu-MCL-2. Although maleimides preferentially react with cysteine thiols, it can also potentially react with lysine amines. Moreover, it had been shown that Cy3 maleimide reacts with amines at a greater rate than the Cy5 maleimide (95). In conclusion, these results (*a-d*) together showed that the DIGE labeling can be employed to differentiate between copper-bound and apo-proteins and therefore this technique has the potential to identify copper-binding proteins from biological samples separated on a 2D gel.

5.3. Conclusion

Proteomic profiling is gaining increased attention with the development of high-throughput proteomics techniques, including two-dimensional polyacrylamide gel electrophoresis (2D-PAGE) and difference gel electrophoresis (DIGE), along with the advancement in mass spectrometry-based quantitative proteomics which utilizes multi-dimensional chromatography for extensive separation of peptides and the incorporation of signature tags, such as ICAT, into proteins or peptides for quantitative analysis. Proteomic profiling in copper biology, which ideally constitutes the identification of the protein along with the metal ion cofactor, poses some unique challenges, including susceptibility of both the Cu(I)-binding sites in proteins and the metal ion itself towards oxidation and loss of metal ions during sample preparation and protein separation. In this work, we developed several "metal free" techniques which did not involve the imaging of protein bound copper ions but rather focused on translating the copper binding to a protein into a measurable and quantifiable signal that will distinguish a copper-binding protein from innumerable other proteins that do not bind copper. While the mobility shift assay based on 2D diagonal gel electrophoresis suffered from poor resolution in protein separation and selective labeling of Cu(I)-binding cysteines with biotin-conjugated iodoacetamide encountered technical difficulties, two other techniques including copper-dependent labeling of cysteines with heavy and light isotopes and difference gel electrophoresis with Cy3 and Cy5 meleimide dyes were able to differentiate between apo and copper-bound hAtox1. By combining the copper dependent labeling of proteins developed in this work with high-throughput technologies including ICAT and two-dimensional polyacrylamide gel electrophoresis, this work laid the foundation for proteomic profiling in copper biology.

5.4. Experimental Methods

5.4.1. Two-dimensional Diagonal Native PAGE

Native gels (w/o SDS and β-mercaptoethanol) were made consisting of a 10% (w/v) acrylamide resolving gel and a 3% (w/v) stacking gel. In all experiments, *E. coli* extract (1mg/ml) overexpressing hAtox1 in HEPES buffer (50 mM, pH 7.5, 0.2 M NaCl) was treated with tris(2-carboxyethyl)phosphine (TCEP, 2 mM final concentration) followed by addition of $[Cu(I)(CH_3CN)_4]PF_6$ (0.2 mM, diluted from a 10 mM stock solution in acetonitrile) to prepare Cu-bound proteins. Protein sample was then mixed with 2X native sample buffer (62.5 mM tris-HCl, pH 6.8, 25% glycerol, 0.01% bromophenol blue) before electrophoresis. Proteins were resolved by the first-dimension electrophoresis in tris/glycine running buffer (25 mM Tris and 192 mM glycine, pH 8.3). Just before the bromophenol blue dye front reached the bottom of the gel, electrophoresis was stopped, and the lane of the gel which resolved the protein sample was cut out longitudinally approximately 1.5 mm in width. The gel strip was soaked in 2 ml of equilibration buffer (0.125 M tris–HCl (pH 6.8), 20% glycerol, 0.002% bromophenol blue) for 30 minutes at room temperature comprising the additives as described for each experiment in Figure 5.2. Then, the gel was placed horizontally on top of a slab gel containing 1 mM BCS where necessary (Experimental gels **A** and **C**). In the second dimension, proteins were resolved by electrophoresis in the tris/glycine buffer containing 250 μM BCS where necessary (Experimental gels **A** and **C**). After electrophoresis, proteins were visualized using GelCode Blue Stain Reagent (Thermo Scientific).

5.4.2. Selective Labeling of Cu(I)-binding Cysteines with Biotin-conjugated Iodoacetamide

E. coli extracts (1mg/ml) overexpressing hAtox1 in HEPES buffer (50 mM, pH 7.5, 0.2 M NaCl) was reduced using immobilized TCEP gel (Thermo Scientific Pierce)

equilibrated with degassed HEPES buffer. $[Cu(I)(CH_3CN)_4]PF_6$ (1 mM, diluted from a 25 mM stock solution in acetonitrile) was immediately added to the reduced protein to prepare Cu-bound proteins. The sample was incubated with 5 mM iodoacetamide (IAM) for 3 hrs in the dark at room temperature to modify the accessible Cys residues with IAM. In order to avoid protein loss from multiple gel filtration steps, IAM was added in presence of copper ions. The experimental evidence suggested that $[Cu(I)(CH_3CN)_4]PF_6$ did not interfere with the IAM-mediated alkylation at least when IAM was added in large excess. The alkylation was quenched by incubating the sample with 10 mM β-mercaptoethanol for 1 hour at room temperature. The unreacted reagents were removed by gel filtration using Micro Bio-spin columns (Bio-Rad) equilibrated with degassed HEPES buffer. The alkylated Cu-bound sample was reacted with usually 10 mM KCN for 1 hour at room temperature to remove the protein bound copper (use of 50 mM KCN did not change the outcome of the experiment). The sample was the reduced by 1 mM TCEP reagent. The unreacted reagents were removed by gel filtration using Micro Bio-spin columns (Bio-Rad) equilibrated with degassed HEPES buffer. The sample was incubated with 1 mM BIAM for 1 hour in the dark at room temperature. The excess of BIAM was removed by PD-10 desalting column. The biotin-conjugated protein sample was purified with monomeric avidin column without any prior concentration step.

5.4.3. Metal-dependent Labeling of Cysteines with Heavy and Light Isotopes

E. coli extracts overexpressing hAtox1 (~1 mg/ml total protein concentration) in HEPES buffer (50 mM, pH 7.5, 0.2 M NaCl) was reduced with 1 mM TCEP. Sample was divided into two pools, **A** and **B**. In sample **B**, $[Cu(I)(CH_3CN)_4]PF_6$ (0.4 mM, diluted from a 10 mM stock solution in acetonitrile) was immediately added to the reduced protein to prepare Cu-bound proteins. Each of the samples **A** and **B** were divided into two parts, while one was reacted with N-ethyl maleimide (NEM, 2 mM final concentration), the other was reacted with D^5-N-ethyl maleimide (D^5-NEM, 2 mM final concentration),

ultimately generating four sample pools. In all four samples the alkylation was quenched with β-mercaptoethanol (BME, 20 mM final concentration). The two samples originating from **A**, one NEM-treated and another D^5-NEM-treated, were pooled and digested with trypsin in solution. Additionally, the two samples originating from **B** were treated identically. Finally, samples **A** and **B** were subjected to MALDI-MS. Immobilized TCEP gel (Thermo Scientific Pierce) and Micro Bio-spin columns (Bio-Rad) were not known to us at that time, therefore, we used twice as much maleimide reagent as TCEP to offset the interference of TCEP with maleimide reactivity. The available gel filtration method PD-10 desalting column greatly diluted the protein sample and even combination of a subsequent protein concentration step resulted in a significant protein loss and thus this step was avoided.

5.4.4. Difference Gel Electrophoresis with Cy3 and Cy5 Meleimide Dyes

E. coli extract overexpressing hAtox1 (~ 3 mg/ml) in HEPES buffer (50 mM, pH 7.5, 0.2 M NaCl) was incubated with the copper chelator BCS overnight at 4 °C. Considering hAtox1 as the predominant component of the *E. coli* extract, amount of BCS added was 10 molar equivalence to the protein. Next day, the protein was purified with Micro Bio-spin columns (Bio-Rad) equilibrated with degassed HEPES buffer to generate the apo-protein. The apo-protein sample was reduced using immobilized TCEP gel (Thermo Scientific Pierce) equilibrated with degassed HEPES buffer. To prepare Cu-bound protein, a 1:1 mix of MCL-2 and Cu-MCL-2 were added to the protein sample, where the total concentration of MCL-2 added was 4 molar equivalence with respect to the protein again, followed by gel filtration. Labeling of the apo-reduced sample and the Cu-bound protein sample with Cy dyes (Amersham Biosciences) were done at concentration of the dye being 250 nmol per mg of the protein. The protein samples with the Cy dyes were reacted for 1 hour at room temperature in the dark and purified by Micro Bio-spin columns (Bio-Rad). The fluorescent images were taken by the Typhoon

Imager using the green laser (532 nm) for the excitation of the Cy3 dye and the red laser (633 nm) for the Cy5 dye. The emission filter used for the Cy3 dye was 580 nm BP 30 and that for the Cy5 dye was 670 BP 30.

5.1. References

1. Chung LP & Baxter RC (2012) Breast cancer biomarkers: proteomic discovery and translation to clinically relevant assays. *Expert Review of Proteomics* 9(6):599-614.

2. Gjertsen BT & Wiig H (2012) Investigation of therapy resistance mechanisms in myeloid leukemia by protein profiling of bone marrow extracellular fluid. *Expert Review of Proteomics* 9(6):595-598.

3. Ma YL, Zhang P, Wang F, & Qin HL (2012) Searching for consistently reported up- and down-regulated biomarkers in colorectal cancer: a systematic review of proteomic studies. *Molecular Biology Reports* 39(8):8483-8490.

4. Martinez-Aguilar J, Chik J, Nicholson J, Semaan C, McKay MJ, & Molloy MP (2013) Quantitative mass spectrometry for colorectal cancer proteomics. *Proteomics Clinical Applications* 7(1-2):42-54.

5. Kozlowski H, Luczkowski M, Remelli M, & Valensin D (2012) Copper, zinc and iron in neurodegenerative diseases (Alzheimer's, Parkinson's and prion diseases). *Coordination Chemistry Reviews* 256(19-20):2129-2141.

6. McRae R, Bagchi P, Sumalekshmy S, & Fahrni CJ (2009) In situ imaging of metals in cells and tissues. *Chemical Reviews* 109(10):4780-4827.

7. Bertini I, Cavallaro G, & McGreevy KS (2010) Cellular copper management-a draft user's guide. *Coordination Chemistry Reviews* 254(5-6):506-524.

8. Kim BE, Nevitt T, & Thiele DJ (2008) Mechanisms for copper acquisition, distribution and regulation. *Nature Chemical Biology* 4(3):176-185.

9. Lutsenko S (2010) Human copper homeostasis: a network of interconnected pathways. *Current Opinion in Chemical Biology* 14(2):211-217.

10. Muller P, van Bakel H, van de Sluis B, Holstege F, Wijmenga C, & Klomp LWJ (2007) Gene expression profiling of liver cells after copper overload in vivo and in vitro reveals new copper-regulated genes. *Journal of Biological Inorganic Chemistry* 12(4):495-507.

11. Amaravadi R, Glerum DM, & Tzagoloff A (1997) Isolation of a cDNA encoding the human homolog of COX17, a yeast gene essential for mitochondrial copper recruitment. *Human Genetics* 99(3):329-333.

12. Klomp LWJ, Lin SJ, Yuan DS, Klausner RD, Culotta VC, & Gitlin JD (1997) Identification and functional expression of HAH1, a novel human gene involved in copper homeostasis. *Journal of Biological Chemistry* 272(14):9221-9226.

13. Zhou B & Gitschier J (1997) hCTR1: A human gene for copper uptake identified by complementation in yeast. *Proceedings of the National Academy of Sciences of the United States of America* 94(14):7481-7486.

14. Culotta VC, Klomp LWJ, Strain J, Casareno RLB, Krems B, & Gitlin JD (1997) The copper chaperone for superoxide dismutase. *Journal of Biological Chemistry* 272(38):23469-23472.

15. Chelly J, Tumer Z, Tonnesen T, Petterson A, Ishikawabrush Y, Tommerup N, Horn N, & Monaco AP (1993) Isolation of a candidate gene for Menkes disease that encodes a potential heavy-metal binding-protein. *Nature Genetics* 3(1):14-19.

16. Mercer JFB, Livingston J, Hall B, Paynter JA, Begy C, Chandrasekharappa S, Lockhart P, Grimes A, Bhave M, Siemieniak D, & Glover TW (1993) Isolation of a partial candidate gene for Menkes disease by positional cloning. *Nature Genetics* 3(1):20-25.

17. Vulpe C, Levinson B, Whitney S, Packman S, & Gitschier J (1993) Isolation of a candidate gene for Menkes disease and evidence that it encodes a copper-transporting ATPase. *Nature Genetics* 3(1):7-13.

18. Tanzi RE, Petrukhin K, Chernov I, Pellequer JL, Wasco W, Ross B, Romano DM, Parano E, Pavone L, Brzustowicz LM, Devoto M, Peppercorn J, Bush AI, Sternlieb I, Pirastu M, Gusella JF, Evgrafov O, Penchaszadeh GK, Honig B, Edelman IS, Soares MB, Scheinberg IH, & Gilliam TC (1993) The Wilson disease gene is a copper transporting ATPase with homology to the Menkes disease gene. *Nature Genetics* 5(4):344-350.

19. Yamaguchi Y, Heiny ME, & Gitlin JD (1993) Isolation and characterization of a human liver cDNA as a candidate gene for Wilson disease. *Biochemical and Biophysical Research Communications* 197(1):271-277.

20. Bull PC, Thomas GR, Rommens JM, Forbes JR, & Cox DW (1993) The Wilson disease gene is a putative copper transporting P-type ATPase similar to the Menkes gene. *Nature Genetics* 5(4):327-337.

21. Lee LW, Prohaska JR, & Thiele DJ (2001) Essential role for mammalian copper transporter Ctr1 in copper homeostasis and embryonic development. *Proceedings of the National Academy of Sciences of the United States of America* 98(12):6842-6847.

22. Kuo YM, Zhou B, Cosco D, & Gitschier J (2001) The copper transporter CTR1 provides an essential function in mammalian embryonic development.

Proceedings of the National Academy of Sciences of the United States of America 98(12):6836-6841.

23. Takahashi Y, Kako K, Kashiwabara S, Takehara A, Inada Y, Arai H, Nakada K, Kodama H, Hayashi J, Baba T, & Munekata E (2002) Mammalian copper chaperone Cox17p has an essential role in activation of cytochrome c oxidase and embryonic development. *Molecular and Cellular Biology* 22(21):7614-7621.

24. Kirby K, Jensen LT, Binnington J, Hilliker AJ, Ulloa J, Culotta VC, & Phillips JP (2008) Instability of superoxide dismutase 1 of drosophila in mutants deficient for its cognate copper chaperone. *Journal of Biological Chemistry* 283(51):35393-35401.

25. Nevitt T, Ohrvik H, & Thiele DJ (2012) Charting the travels of copper in eukaryotes from yeast to mammals. *Biochimica Et Biophysica Acta-Molecular Cell Research* 1823(9):1580-1593.

26. Burstein E, Hoberg JE, Wilkinson AS, Rumble JM, Csomos RA, Komarck CM, Maine GN, Wilkinson JC, Mayo MW, & Duckett CS (2005) COMMD proteins, a novel family of structural and functional homologs of MURR1. *Journal of Biological Chemistry* 280(23):22222-22232.

27. Greene WC (2004) How resting T cells deMURR HIV infection. *Nature Immunology* 5(1):18-19.

28. Andreini C, Bertini I, & Rosato A (2004) A hint to search for metalloproteins in gene banks. *Bioinformatics* 20(9):1373-1380.

29. Andreini C, Banci L, Bertini I, & Rosato A (2008) Occurrence of copper proteins through the three domains of life: A bioinformatic approach. *Journal of Proteome Research* 7(1):209-216.

30. Dancis A, Haile D, Yuan DS, & Klausner RD (1994) The *Saccharomyces-cerevisiae* copper transport protein (CTR1p) - biochemical, characterization, regulation by copper, and physiological-role in copper uptake. *Journal of Biological Chemistry* 269(41):25660-25667.

31. Dancis A, Yuan DS, Haile D, Askwith C, Eide D, Moehle C, Kaplan J, & Klausner RD (1994) Molecular characterization of a copper transport protein in *Saccharomyces-cerevisiae* - an unexpected role for copper in iron transport. *Cell* 76(2):393-402.

32. Waldron KJ, Rutherford JC, Ford D, & Robinson NJ (2009) Metalloproteins and metal sensing. *Nature* 460(7257):823-830.

33. van den Berghe PVE & Klomp L (2010) Posttranslational regulation of copper transporters. *Journal of Biological Inorganic Chemistry* 15(1):37-46.

34. Caruano-Yzermans AL, Bartnikas TB, & Gitlin JD (2006) Mechanisms of the copper-dependent turnover of the copper chaperone for superoxide dismutase. *Journal of Biological Chemistry* 281(19):13581-13587.

35. Bertinato J & L'Abbe MR (2003) Copper modulates the degradation of copper chaperone for Cu,Zn superoxide dismutase by the 26 S proteosome. *Journal of Biological Chemistry* 278(37):35071-35078.

36. Guo Y, Smith K, Lee J, Thiele DJ, & Petris MJ (2004) Identification of methionine-rich clusters that regulate copper-stimulated endocytosis of the human CTR1 copper transporter. *Journal of Biological Chemistry* 279(17):17428-17433.

37. Petris MJ, Smith K, Lee J, & Thiele DJ (2003) Copper-stimulated endocytosis and degradation of the human copper transporter, hCTR1. *Journal of Biological Chemistry* 278(11):9639-9646.

38. La Fontaine S & Mercer JFB (2007) Trafficking of the copper-ATPases, ATP7A and ATP7B: Role in copper homeostasis. *Archives of Biochemistry and Biophysics* 463(2):149-167.

39. Petris MJ, Mercer JFB, Culvenor JG, Lockhart P, Gleeson PA, & Camakaris J (1996) Ligand-regulated transport of the Menkes copper P-type ATPase efflux pump from the Golgi apparatus to the plasma membrane: A novel mechanism of regulated trafficking. *Embo Journal* 15(22):6084-6095.

40. Braiterman L, Nyasae L, Guo Y, Bustos R, Lutsenko S, & Hubbard A (2009) Apical targeting and Golgi retention signals reside within a 9-amino acid sequence in the copper-ATPase, ATP7B. *American Journal of Physiology-Gastrointestinal and Liver Physiology* 296(2):G433-G444.

41. Prohaska JR, Broderius M, & Brokate B (2003) Metallochaperone for Cu,Zn-superoxide dismutase (CCS) protein but not mRNA is higher in organs from copper-deficient mice and rats. *Archives of Biochemistry and Biophysics* 417(2):227-234.

42. Finney L, Chishti Y, Khare T, Giometti C, Levina A, Lay PA, & Vogt S (2010) Imaging metals in proteins by combining electrophoresis with rapid x-ray fluorescence mapping. *Acs Chemical Biology* 5(6):577-587.

43. Jimenez MS, Rodriguez L, Bertolin JR, Gomez MT, & Castillo JR (2013) Evaluation of gel electrophoresis techniques and laser ablation-inductively coupled plasma-mass spectrometry for screening analysis of Zn and Cu-binding proteins in plankton. *Analytical and Bioanalytical Chemistry* 405(1):359-368.

44. Raab A, Ploselli B, Munro C, Thomas-Oates J, & Feldmann J (2009) Evaluation of gel electrophoresis conditions for the separation of metal-tagged proteins with subsequent laser ablation ICP-MS detection. *Electrophoresis* 30(2):303-314.

45. Badarau A & Dennison C (2011) Copper trafficking mechanism of CXXC-containing domains: Insight from the pH-dependence of their Cu(I) affinities. *Journal of the American Chemical Society* 133(9):2983-2988.

46. Becker JS, Zoriy M, Przybylski M, & Becker JS (2007) High resolution mass spectrometric brain proteomics by MALDI-FTICR-MS combined with determination of P, S, Cu, Zn and Fe by LA-ICP-MS. *International Journal of Mass Spectrometry* 261(1):68-73.

47. Sevcenco AM, Krijger GC, Pinkse MWH, Verhaert P, Hagen WR, & Hagedoorn PL (2009) Development of a generic approach to native metalloproteomics: application to the quantitative identification of soluble copper proteins in Escherichia coli. *Journal of Biological Inorganic Chemistry* 14(4):631-640.

48. Raimunda D, Khare T, Giometti C, Vogt S, Arguello JM, & Finney L (2012) Identifying metalloproteins through X-ray fluorescence mapping and mass spectrometry. *Metallomics* 4(9):921-927.

49. Becker JS, Zoriy M, Krause-Buchholz U, Becker JS, Pickhardt C, Przybylski M, Pompe W, & Rodel G (2004) In-gel screening of phosphorus and copper, zinc and iron in proteins of yeast mitochondria by LA-ICP-MS and identification of phosphorylated protein structures by MALDI-FT-ICR-MS after separation with two-dimensional gel electrophoresis. *Journal of Analytical Atomic Spectrometry* 19(9):1236-1243.

50. Sevcenco AM, Pinkse MWH, Wolterbeek HT, Verhaert P, Hagen WR, & Hagedoorn PL (2011) Exploring the microbial metalloproteome using MIRAGE. *Metallomics* 3(12):1324-1330.

51. Schagger H & Vonjagow G (1991) Blue native electrophoresis for isolation of membrane-protein complexes in enzymatically active form. *Analytical Biochemistry* 199(2):223-231.

52. Pioselli B, Munro C, Raab A, Deitrich CL, Songsrirote K, Feldmann J, & Thomas-Oates J (2009) Denaturing and non-denaturing microsolution isoelectric focussing to mine the metalloproteome. *Metallomics* 1(6):501-510.

53. Polec K, Perez-Calvo M, Garcia-Arribas O, Szpunar J, Ribas-Ozonas B, & Lobinski R (2002) Investigation of metal complexes with metallothionein in rat tissues by hyphenated techniques. *Journal of Inorganic Biochemistry* 88(2):197-206.

54. Gonzalez-Fernandez M, Garcia-Barrera T, Arias-Borrego A, Jurado J, Pueyo C, Lopez-Barea J, & Gomez-Ariza JL (2009) Metallomics integrated with proteomics in deciphering metal-related environmental issues. *Biochimie* 91(10):1311-1317.

55. Manley SA & Gailer J (2009) Analysis of the plasma metalloproteome by SEC-ICP-AES: bridging proteomics and metabolomics. *Expert Review of Proteomics* 6(3):251-265.

56. Ellis J, Del Castillot E, Montes Bayon M, Grimm R, Clark JF, Pyne-Geithman G, Wilbur S, & Caruso JA (2008) A preliminary study of metalloproteins in CSF by CapLC-ICPMS and nanoLC-CHIP/ITMS. *Journal of Proteome Research* 7(9):3747-3754.

57. Mounicou S, Polec K, Chassaigne H, Potin-Gautier M, & Lobinski R (2000) Characterization of metal complexes with metallothioneins by capillary zone electrophoresis (CZE) with ICP-MS and electrospray (ES)-MS detection. *Journal of Analytical Atomic Spectrometry* 15(6):635-642.

58. Cvetkovic A, Menon AL, Thorgersen MP, Scott JW, Poole FL, Jenney FE, Lancaster WA, Praissman JL, Shanmukh S, Vaccaro BJ, Trauger SA, Kalisiak E, Apon JV, Siuzdak G, Yannone SM, Tainer JA, & Adams MWW (2010) Microbial metalloproteomes are largely uncharacterized. *Nature* 466(7307):779-U718.

59. Porath J, Carlsson J, Olsson I, & Belfrage G (1975) Metal chelate affinity chromatography, a new approach to protein fractionation. *Nature* 258(5536):598-599.

60. Smith SD, She YM, Roberts EA, & Sarkar B (2004) Using immobilized metal affinity chromatography, two-dimensional electrophoresis and mass spectrometry to identify hepatocellular proteins with copper-binding ability. *Journal of Proteome Research* 3(4):834-840.

61. Kung CCS, Huang WN, Huang YC, & Yeh KC (2006) Proteomic survey of copper-binding proteins in Arabidopsis roots by immobilized metal affinity chromatography and mass spectrometry. *Proteomics* 6(9):2746-2758.

62. Roelofsen H, Balgobind R, & Vonk RJ (2004) Proteomic analyzes of copper metabolism in an in vitro model of Wilson disease using surface enhanced laser desorption/ionization-time of flight-mass spectrometry. *Journal of Cellular Biochemistry* 93(4):732-740.

63. Jimenez MS, Rodriguez L, Gomez MT, & Castillo JR (2010) Metal-protein binding losses in proteomic studies by PAGE-LA-ICP-MS. *Talanta* 81(1-2):241-247.

64. Jahromi EZ, White W, Wu Q, Yamdagni R, & Gailer J (2010) Remarkable effect of mobile phase buffer on the SEC-ICP-AES derived Cu, Fe and Zn-metalloproteome pattern of rabbit blood plasma. *Metallomics* 2(7):460-468.

65. Kameshita I & Fujisawa H (1997) Detection of calcium binding proteins by two-dimensional sodium dodecyl sulfate-polyacrylamide gel electrophoresis. *Analytical Biochemistry* 249(2):252-255.

66. Gye MC, Park S, Kim YS, & Ahn HS (2001) Mobility shift assay of calcium-binding proteins of mouse epididymal spermatozoa. *Andrologia* 33(4):193-198.

67. Waldron KJ, Tottey S, Yanagisawa S, Dennison C, & Robinson NJ (2007) A periplasmic iron-binding protein contributes toward inward copper supply. *Journal of Biological Chemistry* 282(6):3837-3846.

68. Anastassopoulou I, Banci L, Bertini I, Cantini F, Katsari E, & Rosato A (2004) Solution structure of the apo and copper(I)-loaded human metallochaperone HAH1. *Biochemistry* 43(41):13046-13053.

69. Narindrasorasak S, Zhang XF, Roberts EA, & Sarkar B (2004) Comparative analysis of metal binding characteristics of copper chaperone proteins, Atx1 and Atox1. *Bioinorganic Chemistry and Applications* 2(1-2):105-123.

70. Morgan MT, Bagchi P, & Fahrni CJ (2011) Designed to dissolve: Suppression of colloidal aggregation of Cu(I)-selective fluorescent probes in aqueous buffer and in-gel detection of a metallochaperone. *Journal of the American Chemical Society* 133(40):15906-15909.

71. Wernimont AK, Huffman DL, Lamb AL, O'Halloran TV, & Rosenzweig AC (2000) Structural basis for copper transfer by the metallochaperone for the Menkes/Wilson disease proteins. *Nature Structural Biology* 7(9):766-771.

72. Laemmli UK (1970) Cleavage of Structural Proteins During Assembly of Head of Bacteriophage-T4. *Nature* 227(5259):680-&.

73. Hermanson GT (1996) *Bioconjugate techniques* (San Diego, Academic Press).

74. Walker JM, Tsivkovskii R, & Lutsenko S (2002) Metallochaperone Atox1 transfers copper to the NH2-terminal domain of the Wilson's disease protein and regulates its catalytic activity. *Journal of Biological Chemistry* 277(31):27953-27959.

75. Marino SM, Li YH, Fomenko DE, Agisheva N, Cerny RL, & Gladyshev VN (2010) Characterization of Surface-Exposed Reactive Cysteine Residues in Saccharomyces cerevisiae. *Biochemistry* 49(35):7709-7721.

76. Julka S & Regnier F (2004) Quantification in proteomics through stable isotope coding: A review. *Journal of Proteome Research* 3(3):350-363.

77. Sechi S & Chait BT (1998) Modification of cysteine residues by alkylation. A tool in peptide mapping and protein identification. *Analytical Chemistry* 70(24):5150-5158.

78. Gygi SP, Rist B, Gerber SA, Turecek F, Gelb MH, & Aebersold R (1999) Quantitative analysis of complex protein mixtures using isotope-coded affinity tags. *Nature Biotechnology* 17(10):994-999.

79. Hagglund P, Bunkenborg J, Maeda K, & Svensson B (2008) Identification of Thioredoxin Disulfide Targets Using a Quantitative Proteomics Approach Based on Isotope-Coded Affinity Tags. *Journal of Proteome Research* 7(12):5270-5276.

80. Sethuraman M, McComb ME, Heibeck T, Costello CE, & Cohen RA (2004) Isotope-coded affinity tag approach to identify and quantify oxidant-sensitive protein thiols. *Molecular & Cellular Proteomics* 3(3):273-278.

81. Sethuraman M, McComb ME, Huang H, Huang SQ, Heibeck T, Costello CE, & Cohen RA (2004) Isotope-coded affinity tag (ICAT) approach to redox proteomics: Identification and quantitation of oxidant-sensitive cysteine thiols in complex protein mixtures. *Journal of Proteome Research* 3(6):1228-1233.

82. Leichert LI, Gehrke F, Gudiseva HV, Blackwell T, Ilbert M, Walker AK, Strahler JR, Andrews PC, & Jakob U (2008) Quantifying changes in the thiol redox proteome upon oxidative stress in vivo. *Proceedings of the National Academy of Sciences of the United States of America* 105(24):8197-8202.

83. Kurono S, Kurono T, Komori N, Niwayama S, & Matsumoto H (2006) Quantitative proteome analysis and C-13-labeled iodoacetanilide using D-labeled N-ethylmaleimide by matrix-assisted laser desorption/ionization time-of-flight mass spectrometry. *Bioorganic & Medicinal Chemistry* 14(24):8197-8209.

84. Fu C, Hu J, Liu T, Ago T, Sadoshima J, & Li H (2008) Quantitative analysis of redox-sensitive proteome with DIGE and ICAT. *Journal of Proteome Research* 7(9):3789-3802.

85. Ofarrell PH (1975) High-resolution 2-dimensional electrophoresis of proteins. *Journal of Biological Chemistry* 250(10):4007-4021.

86. Unlu M, Morgan ME, & Minden JS (1997) Difference gel electrophoresis: A single gel method for detecting changes in protein extracts. *Electrophoresis* 18(11):2071-2077.

87. Tonge R, Shaw J, Middleton B, Rowlinson R, Rayner S, Young J, Pognan F, Hawkins E, Currie I, & Davison M (2001) Validation and development of fluorescence two-dimensional differential gel electrophoresis proteomics technology. *Proteomics* 1(3):377-396.

88. Riederer IM, Herrero RM, Leuba G, & Riederer BM (2008) Serial protein labeling with infrared maleimide dyes to identify cysteine modifications. *Journal of Proteomics* 71(2):222-230.

89. Riederer IM & Riederer BM (2007) Differential protein labeling with thiol-reactive infrared DY-680 and DY-780 maleimides and analysis by two-dimensional gel electrophoresis. *Proteomics* 7(11):1753-1756.

90. Pretzer E & Wiktorowicz JE (2008) Saturation fluorescence labeling of proteins for proteomic analyses. *Analytical Biochemistry* 374(2):250-262.

91. Dietz L, Bosque A, Pankert P, Ohnesorge S, Merz P, Anel A, Schnolzer M, & Thierse HJ (2009) Quantitative DY-maleimide-based proteomic 2-DE-labeling strategies using human skin proteins. *Proteomics* 9(18):4298-4308.

92. Shaw J, Rowlinson R, Nickson J, Stone T, Sweet A, Williams K, & Tonge R (2003) Evaluation of saturation labelling two-dimensional difference gel electrophoresis fluorescent dyes. *Proteomics* 3(7):1181-1195.

93. Chouchani ET, Hurd TR, Nadtochiy SM, Brookes PS, Fearnley IM, Lilley KS, Smith RAJ, & Murphy MP (2010) Identification of S-nitrosated mitochondrial proteins by S-nitrosothiol difference in gel electrophoresis (SNO-DIGE): implications for the regulation of mitochondrial function by reversible S-nitrosation. *Biochemical Journal* 430:49-59.

94. Hurd TR, James AM, Lilley KS, & Murphy MR (2009) Measuring redox changes to mitochondrial protein thiols with redox difference gel electrophoresis (REDOX-DIGE). *Methods in Enzymology, Vol 456: Mitochondrial Function, Part A: Mitochondrial Electron Transport Complexes and Reactive Oxygen Species*, Methods in Enzymology, ed Allison WS), Vol 456, pp 343-361.

95. Hurd TR, Prime TA, Harbour ME, Lilley KS, & Murphy MP (2007) Detection of reactive oxygen species-sensitive thiol proteins by redox difference gel electrophoresis - Implications for mitochondrial redox signaling. *Journal of Biological Chemistry* 282(30):22040-22051.

96. Requejo R, Chouchani ET, Hurd TR, Menger KE, Hampton MB, & Murphy MP (2010) Measuring mitochondrial protein thiol redox state. *Methods in Enzymology, Vol 474: Thiol Redox Transitions in Cell Signaling, Pt B: Cellular Localization and Signaling*, Methods in Enzymology, eds Cadenas E & Packer L), Vol 474, pp 123-147.

97. Xiao ZG, Brose J, Schimo S, Ackland SM, La Fontaine S, & Wedd AG (2011) Unification of the copper(I) binding affinities of the metallo-chaperones Atx1, Atox1, and related proteins. Detection probes and affinity standards. *Journal of Biological Chemistry* 286(13):11047-11055.

98. Xiao ZG & Wedd AG (2010) The challenges of determining metal-protein affinities. *Natural Product Reports* 27(5):768-789.

99. Gekko K, Ohmae E, Kameyama K, & Takagi T (1998) Acetonitrile-protein interactions: amino acid solubility and preferential solvation. *Biochimica Et*

Biophysica Acta-Protein Structure and Molecular Enzymology 1387(1-2):195-205.

100. Lin X, Zhao WJ, & Wang X (2010) Characterization of conformational changes and noncovalent complexes of myoglobin by electrospray ionization mass spectrometry, circular dichroism and fluorescence spectroscopy. *Journal of Mass Spectrometry* 45(6):618-626.

101. Han JC & Han GY (1994) A procedure for quantitative-determination of tris(2-carboxyethyl)phosphine, an odorless reducing agent more stable and effective than dithiothreitol. *Analytical Biochemistry* 220(1):5-10.

102. Tyagarajan K, Pretzer E, & Wiktorowicz JE (2003) Thiol-reactive dyes for fluorescence labeling of proteomic samples. *Electrophoresis* 24(14):2348-2358.

103. Getz EB, Xiao M, Chakrabarty T, Cooke R, & Selvin PR (1999) A comparison between the sulfhydryl reductants tris(2-carboxyethyl)phosphine and dithiothreitol for use in protein biochemistry. *Analytical Biochemistry* 273(1):73-80.

CHAPTER 6

CONCLUSION

The work in this dissertation was initiated with three key objectives in mind with the ultimate goal to improve our understanding of copper biochemistry: (1) development of a set of well-characterized copper(I) affinity standards which can be applied to determine the Cu(I) binding affinities of proteins and small-molecule ligands; (2) characterization of coordination properties of Cu(I)-selective fluorescent probes in order to develop Cu(I)-sensors suitable for cellular imaging; and (3) development of methods to selectively label Cu(I)-binding cysteines in copper-proteins which will facilitate the identification of putative copper-binding proteins.

a) Cu(I) Affinity Standards

Accurate binding affinity determination of Cu(I)-proteins has been challenging partly because of the lack of reliable affinity standards reported in the literature. In this work, a set of copper(I) affinity standards was developed which included three new sulfonated thioether-based ligands (synthesized by Dr. M. T. Morgan) that form colorless, water-soluble, and air-stable copper complexes and three previously reported Cu(I) chelators. The coordination properties, including Cu(I)-stability constants, protonation constants, redox potentials, were carefully determined for each of these ligands and were cross-validated by independent methods. The results from this work constitute a web of accurately cross-verified Cu(I)-affinity standards with a wide range of affinities. The applications of these ligands were demonstrated with the measurement of the binding affinity of a copper chaperone CusF. Since these six ligands encompass a varied range of affinities, this work can be extended to a multitude of proteins whose Cu(I)-stability constants can be determined unequivocally by competition titrations with these ligands. These ligands also have the prospective applications as therapeutic Cu(I)-chelating agents.

b) Cu(I) Selective Fluorescent Probes

Cu(I) selective turn-on fluorescent probes are useful in imaging kinetically labile cellular copper pool. While the development of Cu(I) sensors was primarily focused on improving their photophysical properties, including quantum yields and fluorescence contrast ratios, the importance of increasing the aqueous solubility of these probes was greatly overlooked. CTAP-2 (synthesized by Dr. M. T. Morgan) was the first Cu(I)-selective fluorescent indicator which readily dissolved in water. As demonstrated by the dynamic light scattering, aqueous solutions of several previously published Cu(I) probes contained nanoparticles, whereas CTAP-2 did not indicate any nanoparticle formation. Despite the water solubility of CTAP-2, the probe was surprisingly cell permeable. However, the Cu(I) binding affinity of CTAP-2 was several orders of magnitude lower than that required for the imaging of the endogenous intracellular copper pool. A novel biochemical application of CTAP was also developed in this work involving in-gel detection of a copper chaperone under non-denaturing condition. In future endeavors to develop water-soluble Cu(I)-selective fluorescent probes, synthetic efforts should focus on improving Cu(I)-affinity.

c) Selective Labeling of Cu(I)-binding Cysteines

In order to screen for putative copper-binding proteins from complex cellular extracts, several proteomics-based methods were developed in this work. Since cysteine acts as an ubiquitous ligand in Cu(I)-binding in proteins, the strategies were adopted to selectively label cysteines in a copper-dependent manner. The most promising method in this work involved copper-dependent labeling of cysteines with Cy3 and Cy5 dyes. Based on the work on one-dimensional gel electrophoresis, this method can successfully differentiate between copper-bound and unbound proteins in a quantitative fashion. This work can be extended to two-dimensional gel electrophoresis which can have several

applications, including identification of putative copper(I)-binding proteins, comparison of protein profiles between normal and disease conditions, and biomarker discovery.